厚生労働科学研究費補助金
化学物質リスク研究事業

発達期における総合的な
遅発性神経毒性試験法の開発
(H28-化学--一般-003)

平成 29 年度総括・分担研究報告書

研究代表者　諫田 泰成

平成 30（2018）年 5 月

目　　次

化学物質リスク研究事業　課題番号 H28-化学-一般-003

研究成果概要

発達期における統合的な遅発性神経毒性試験法の開発

研究代表者　　国立医薬品食品衛生研究所　薬理部長
諫田　泰成

＜全体要旨＞
近年、自閉症など発達障害が急速に増加し社会問題となっている。その原因の一つは発達期における化学物質の曝露とされる。発達期の神経系は成体と比較して感受性が高く、健康被害が長期間あるいは遅発性に生じることが考えられ、子どもの健康影響評価法の確立が強く望まれる。
現在、OECDやEPAによって、妊娠ラットを用いる発達神経毒性試験ガイドラインが制定されているが、試験方法が複雑で、試験期間は1年以上、動物数は720にも及び経費も膨大である。さらに、日本ではこのようなガイドラインは未整備である。そこで我々は、発達期における細胞機能異常と神経回路異常の毒性作用メカニズムに基づいて、新たにスループット性の高い発達神経毒性評価スキームを作製し、評価指標の選定やプロトコルの最適化を行うことにより統合的な発達神経毒性試験法の開発を行っている。
ヒトiPS細胞（神経発生モデル細胞の評価系）やラット小脳および海馬（生後初期における遅発性毒性評価系）を用いて、化学物質の影響評価に関する評価指標の最適化を行った。特に、ラット海馬ニューロンを用いた、スループット性の高いスクリーニング系の構築に着手し、新たにHESI NeuToxと国際バリデーション実験を開始した。また、バルプロ酸などのメカニズムを理解する上で、妊娠中の母親への摂取栄養の程度や栄養成分の偏りによって胎児のエピゲノムに影響し生後の発育や疾患の発症に寄与する、というDoHaDについて調査研究を行った。さらにバルプロ酸投与症例の胎盤のメチル化エピゲノム解析に着手した。
今後は、最適化された評価指標をもとに遅発性毒性評価系の統合化を行う。さらに、OECDやHESIとの国際連携のもと試験法の開発を目指す。

＜研究体制＞

・諫田泰成（国立医薬品食品衛生研究所）
「ヒト幹細胞の分化による評価法の開発」

・山崎大樹（国立医薬品食品衛生研究所）
「海馬ニューロンを用いた神経ネットワークによる評価法の開発」

・吉田祥子（豊橋技術科学大学）
「生後小脳の神経回路の機能的影響による評価法の開発」

・上野晋（産業医科大学）
「幼若期海馬の神経回路機能による評価法の開発」

・秦健一郎（成育医療研究センター）
「既存の毒性データおよびヒトデータとの検証」

A. 研究目的

本研究では、胎児期の神経発生モデル細胞を用いたスクリーニングを行い（細胞評価グループ）、さらに生後の成熟期における遅発性神経毒性の早期予測評価法（神経ネットワーク評価グループ）を検証し、統合的な新規試験法として開発を目指す。現在進行中のHESI NeuTo、OECD DNT 専門家グループとの国際連携をもとに、試験法の確立に向けて、科学的根拠を取得する。

上記 2 グループにヒト毒性データ検証グループを加えた 3 グループの密な連携により、これらの評価系やヒト試料の有用性を明らかにして、国際的に整備が進められつつある発達神経毒性の評価系にデータを提供して、化学物質の規制行政への応用に取り組みたい。

B. 研究方法

詳細は各分担報告書を参照のこと。

C. 研究結果

【①ヒト幹細胞の分化による評価法】

ヒト iPS 細胞を用いて、化学物質の影響評価に関する評価指標の最適化を行い、ATP 産生と分化能を確定した。遅発性神経毒性が懸念される化学物質の作用を検出でき、陰性対照物質は影響を与えなかった。従って、ヒト iPS 細胞におけるミトコンドリア機能を指標にして、成長期における化学物質の発達神経毒性を評価できる可能性が示唆された。さらに、OECD DNT 専門委員、HESI steering committee として国際連携を推進した。

【②神経ネットワークによる評価法】

HESI NeuTox の多点電極システムサブチームに参加し、プレバリデーションの議論を行い、プロトコルを決定した。これをもとに、バリデーション試験のデータ取得を開始した。

【③生後小脳の神経回路】

遅発性神経毒性が考えられる化学物質であるバルプロ酸、クロルピリホスを胎生期の動物に投与し、生後の神経回路発達の変化を小脳神経細胞の突起伸展と小脳構造の変化、動物の行動変化から定量化して示した。また、行動異常との相関も明らかにした。

【④幼若期海馬の神経回路機能】

遅発性神経毒性試験手法の妥当性を調べる目的で、発達神経毒性の懸念がある 1BP について検討した結果、神経回路興奮性の亢進をもたらすことを明らかにした。規制値との比較を行うことにより妥当性を評価し、評価指標の有用となる可能性を明らかにした。

【⑤既存毒性データ、ヒトデータとの検証】

陽性対照物質バルプロ酸などの作用メカニズムを明らかにするため、ヒトのエピゲノムデータに関して調査を開始した。調査研究により、胎児期あるいは新生児期に受けた影響により、ゲノムのメチル化が生じ生後長期に渡って継続し、疾患リスクとなる可能性が示唆され、バルプロ酸投与例の胎盤のエピゲノム解析に着手した。

D. 考察

本研究において、これまでに我々が構築した神経発生モデル細胞の評価系および生後初期における遅発性毒性評価系を用いて、化学物質の統合的な健康影響評価法のプロトコル、評価指標を確立し、新規試験法の提案に向けた取り組みを推進している。

現在 OECD で提案されている in vitro DNT と同様に、ヒト iPS 細胞の分化誘導能に基づく評価系およびラット神経細胞のプラットフォームを用いて化学物質の影響評価に関する評価指標の最適化を検討して、国際的な議論に資する科学的根拠の取得を行っている。諫田は OECD DNT の専門委員として参加しており、2018 年 3 月にキックオフ電話会議および WNT 会議で議論を行った。ヒト iPS 細胞は特に重要なツールであり、IATA の整備を進めることとなった。HESI に関して、Tim Shafer (EPA)らと議論を重ねてラット神経細胞の多点電極システムのプロトコルが決定し、現在、データ取得中である。

海馬及び小脳についても in vitro と in vivo をつなぐ評価系として重要であり、HESI NeuTox の steering committee (諫田が参加)においてもどのように両者を比較検証すべきなのか議論を行っている。日本としても科学的根拠となるデータを示す必要があり、引き続き取り組みたい。

化学物質の安全性評価においてはヒト試料の整備が必要不可欠である。我々は既存のデータベースの中で成育医療研究センターの胎盤の症例に着目し、発達神経が懸念される医薬品投与例の胎盤エピゲノム解析を行っており、発達との相関を検証中である。

E. 結論

胎児期、成熟期において陽性対照となる化学物質を用いて、試験法の確立に向けて安定な評価指標とプロトコルを選定した。ラット海馬ニューロンを用いた、スループット性の高いスクリーニング系を新たに構築し、国際バリデーション試験のデータ取得を開始し、OECD とも専門委員として連携している。また、新たにヒト胎盤試料の有用性を明らかにするため、エピゲノム解析に着手した。

F. 研究発表

各分担研究者の報告書に示すように、多数の論文発表および学会発表を行った。

厚生労働科学研究費補助金（化学物質リスク研究事業）
分担研究報告書

ヒト幹細胞の分化による評価法の開発

研究代表者　　国立医薬品食品衛生研究所薬理部第二室長
諫田　泰成

要旨
ヒト iPS 細胞を用いて、化学物質さらには医薬品についても影響評価に関する指標の最適化を行った。その結果、遅発性神経毒性が懸念される船底防汚剤であるトリブチルスズ（TBT）曝露により、ヒト iPS 細胞における神経分化の抑制が認められた。また分化抑制メカニズムとして、Mfn1 分解を介したミトコンドリア機能異常を見出した。さらに医薬品の中で、遅発性神経毒性が懸念されている抗がん剤 5 フルオロウラシル（5-FU）投与により同様のミトコンドリア異常及び神経分化抑制を見出した。以上より、ヒト iPS 細胞におけるミトコンドリア機能を指標にして、成長期における化学物質や医薬品の発達神経毒性を評価できる可能性が示唆された。

A. 研究目的

近年、子供の学習障害や自閉症などの発達障害が増加しているが、その原因の一つとして環境中の化学物質の影響や医薬品の副作用が指摘されている（Robaey et al., *Dev. Disabil. Res. Rev.*, 2008; Landrigan et al., *Environ. Health Perspect. Med.*, 2012; Ouzir et al., *Food Chem. Toxicol.*, 2016）。ヒト iPS 細胞はヒト発生過程を in vitro で模倣できることから、化学物質や医薬品の神経毒性を検出できる可能性が考えられる。しかし、評価系としての手法は確立されていない。

本研究では、化学物質や医薬品の発達期における毒性を評価するために、ヒト iPS 細胞を用いて分化に対する影響を調べた。評価系の構築には、HESI と共有している発達毒性が懸念される陽性対照物質のリストから、船底防汚剤であるトリブチルスズ（TBT）と抗がん剤である 5 フルオロウラシル（5-FU）を選択した。また陰性対照としてアスコルビン酸及びソルビトールを選択した。

B. 研究方法

1. 細胞

ヒト iPS 細胞株 253G1（Nakagawa et al., *Nat. Biotechnol.*, 2008）は、TeSR-E8 培地（Stem Cell Technologies）にてフィーダーフリー[マトリゲル（BD Biosciences）コート]の条件で培養した。

2. 三胚葉分化

外胚葉への分化は Dual smad 阻害法（Chambers et al., *Nat. Biotechnol.*, 2009）に従い、BMP シグナル阻害剤 LDN193189（Wako）及び Activin シグナル阻害剤 SB431542（Wako）を用いて iPS 細胞を 2 日間培養した。中胚葉への分化は GSK3 阻害剤 CHIR99021（Wako）を用いて iPS 細胞を 1 日培養した（Lian et al., *Nat. Protoc.*, 2013）。内胚葉への分化は activinA（R&D）、Wnt3a（R&D）、さらに HDAC 阻害剤 NaB（Sigma）を用いて iPS 細胞を 4 日間培養した（Kajiwara et al., *Proc. Natl. Acad. Sci. USA*, 2012）。

3. 神経分化誘導

上記 Dual smad 阻害法を用いて、LDN193189 及び SB431542 により iPS 細胞を外胚葉からさらに神経前駆細胞へと分化させた。

4. ATP 量

ルシフェラーゼ法に基づいて定量した。

5. qPCR

TRIzol 試薬（Life Technologies）を用いて RNA を抽出した。QuantiTect SYBR Green RT-PCR Kit（QIAGEN）、ABI PRISM 7900HT を用いて qPCR を行った。

6. 細胞染色

細胞を 4%PFA で固定後、抗 PAX6 抗体

（Biolegend）を用いて染色を行った。さらに核を DAPI 染色した後、蛍光顕微鏡で観察した。

7. shRNA を用いたノックダウン

shRNA 導入はレンチウイルス（SIGMA）を用いた。ヒト iPS 細胞にウイルスを moi 1 で感染させた。さらに 24 時間後にピューロマイシンを添加して感染細胞のセレクションを行った。

C. 研究結果

1. ヒト iPS 細胞の分化に対する TBT の作用

まず iPS 細胞の分化への影響を検討するために、三胚葉へ分化させ TBT の影響を調べた。TBT 曝露した iPS 細胞を三胚葉へ分化させた結果、Dual smad 阻害法で分化させた外胚葉においてマーカーの OTX2（Mortensen et al., *Hum. Mol. Genet.*, 2015）や IRX1（Houweling et al., *Mech. Dev.*, 2001）の発現低下が認められた（図 1）。一方、中胚葉や内胚葉分化では各々のマーカーに影響はなかった。したがって、TBT は iPS 細胞の外胚葉分化誘導を阻害することが明らかとなった。

TBT が iPS 細胞の外胚葉分化を阻害したので、さらに神経前駆細胞へと分化させて、TBT 曝露の影響を検討した。TBT 曝露した iPS 細胞に神経分化刺激を与えた結果、神経分化マーカーである PAX6（Manuel et al., *Front. Cell Neurosci.*, 2015）陽性細胞数の低下が認められた（図 2）。したがって、TBT は iPS 細胞の神経分化誘導を阻害することが明らかとなった。

我々はこれまでに TBT 曝露した iPS 細胞でミトコンドリア形態制御因子の発現を検討した結果、分裂因子（Drp1, Fis1）および融合因子（Mfn1, Mfn2, Opa1）の遺伝子発現には影響がなかったが、Mfn1 タンパク質が分解されることを見出している（Yamada et al., *Toxicol. In Vitro*, 2016）。さらに Mfn1 分解に伴い、細胞内 ATP 含量の低下やミトコンドリア膜電位の低下といったミトコンドリア機能異常が引き起こされることも見出している（Yamada et al., *Toxicol. In Vitro*, 2016）。そこで TBT による神経分化の阻害がミトコンドリア異常を介しているかを明らかにするために、Mfn1 をノックダウンした iPS 細胞（論文発表 3）を用いて、神経分化誘導を行った。その結果、Mfn1 ノックダウンにより、TBT 曝露と同様に、OTX2 の遺伝子発現や PAX6 陽性細胞数の低下が認められた（図 3）。したがって、TBT による神経分化の阻害は、Mfn1 分解を介したミトコンドリア異常により引き起こされることが示唆された。

2. TBT の神経分化阻害における Erk シグナルの関与

ミトコンドリア機能の破綻は Erk のリン酸化を引き起こすことが報告されている（Yu et al., *Toxicol. Appl. Pharmacol.*, 2012）。一方、Erk のリン酸化によって OTX2 の発現が抑制され神経分化が阻害されるという報告もある（Greber et al., *EMBO J.*, 2011）。したがって、TBT による神経分化阻害の経路として Erk シグナルの関与が考えられる。まず TBT の作用に対する Erk シグナルの関与を調べるために、ヒト iPS 細胞に TBT を曝露した結果、Erk のリン酸化レベルの亢進が認められた。またこのリン酸化は Erk 阻害剤 U0126 処理により消失した（図 4A, B）。さらに神経（外胚葉）分化時の TBT 曝露による OTX2 の低下は、U0126 処理により回復した（図 4C）。我々はこれまでに Mfn1 をノックダウンした iPS 細胞において Erk リン酸化レベルが亢進することを報告している（本リン酸化は U0126 処理で消失する）。さらに Mfn1 ノックダウンによる神経マーカーの低下が U0126 処理により回復することも見出している。したがって、TBT のミトコンドリア異常を介した神経分化阻害には Erk シグナルが関与していることが示唆された（図 5）。

3. ヒト iPS 細胞のミトコンドリア機能や神経分化に対する医薬品 5-FU の影響

発達神経毒性が懸念される抗がん剤 5-FU を用いて、これまで見出した iPS 細胞の評価指標への影響を検討した。まず 5-FU 曝露は細胞内 ATP 量の低下を引き起こした（図 6A）。さらに 5-FU 曝露した iPS 細胞に神経分化刺激を与えた結果、PAX6 遺伝子の発現

低下が認められた（図 6B）。一方、陰性対照であるアスコルビン酸及びソルビトール添加は ATP 量や PAX6 発現に影響を及ぼさなかった。したがって、5-FU は TBT と同様に、ミトコンドリア機能異常を引き起こし、神経分化を阻害する可能性が明らかとなった。

以上より、医薬品についても、iPS 細胞のミトコンドリア機能を指標にして発達神経毒性を評価できる可能性が示唆された。

D. 考察

本研究では、ヒト iPS 細胞を用いて、これまで見出したミトコンドリア指標（ATP 産生など）により発達神経毒性が懸念される化学物質や医薬品の影響を評価できることを明らかにした。特に、iPS 細胞で使用した TBT や 5-FU は各々血中に存在しうる濃度（Findlay et al., *Ann. Oncol.*, 1996; Whalen et al., *Environ. Res.*, 1999）をアッセイに使用しており、本アッセイ系は非常に好感度であると考えられる。

今回、iPS 細胞を用いて TBT の毒性作用点として、ミトコンドリア異常を介した神経分化の阻害を見出し、CPF と同様の神経毒性を示すことを明らかにした（論文発表 1, 3）。5-FU も同様のミトコンドリア異常や神経分化阻害を引き起こす（論文発表 2）ことから、発達神経毒性評価においてミトコンドリア機能は有効であり、医薬品など幅広く応用できる可能性が期待される。今後も iPS 細胞において、発達神経毒性が懸念される被験物質を増やすことで、ミトコンドリアを指標とした毒性マーカーの探索や評価法の検討を行い、簡便で再現性のある評価法の確立を目指す。

また、研究代表者として、HESI NeuTox の国際検証試験の議論を新たに開始して、連携を取りながら試験法の確立に取り組みたい。

E. 結論

ヒト iPS 細胞のミトコンドリア機能を指標にして、成長期における化学物質や医薬品の発達神経毒性を評価できる可能性が示唆された。

F. 研究発表

1. 論文発表

[1] Yamada S., Kubo Y., Yamazaki D., Sekino Y., Nomura Y., Yoshida S., Kanda Y. “Tributyltin Inhibits Neural Induction of Human Induced Pluripotent Stem Cells.” 論文投稿中

[2] Yamada S., Yamazaki D., Kanda Y. “5-Fluorouracil inhibits neural induction via Mfn1/2 reduction in human induced pluripotent stem cells.” 論文投稿中

[3] Yamada S., Kubo Y., Yamazaki D., Sekino Y. and Kanda Y. “Chlorpyrifos inhibits neural induction via Mfn1-mediated mitochondrial dysfunction in human induced pluripotent stem cells.” Sci Rep. (2017) 7:40925

2. 学会発表

[1] 山田茂、久保祐亮、山崎大樹、関野祐子、諫田泰成：ヒト iPS 細胞の神経分化におけるミトコンドリア因子 Mfn1 の機能、第 90 回日本薬理学会、2017 長崎

[2] 山田茂、山崎大樹、諫田泰成：ヒト iPS 細胞の神経分化に対するトリブチルスズの影響、第 44 回日本毒性学会、2017 横浜

[3] 山田茂、山崎大樹、諫田泰成：ヒト iPS 細胞の神経分化に対するクロルピリホス曝露の影響、第 136 回日本薬理学会関東部会、2017 東京

[4] 山田茂、山崎大樹、諫田泰成：ヒト iPS 細胞の神経分化能を指標にした発達神経毒性評価系の開発、第 3 回次世代を担う若手のためのレギュラトリーサイエンスフォーラム、2017 東京

[5] Yamada S., Yamazaki D., Kanda Y. : Development of human iPS cell-based platform for developmental neurotoxicity testing, SPS, 2017, Berlin

G. 知的財産権の出願・登録状況

該当なし

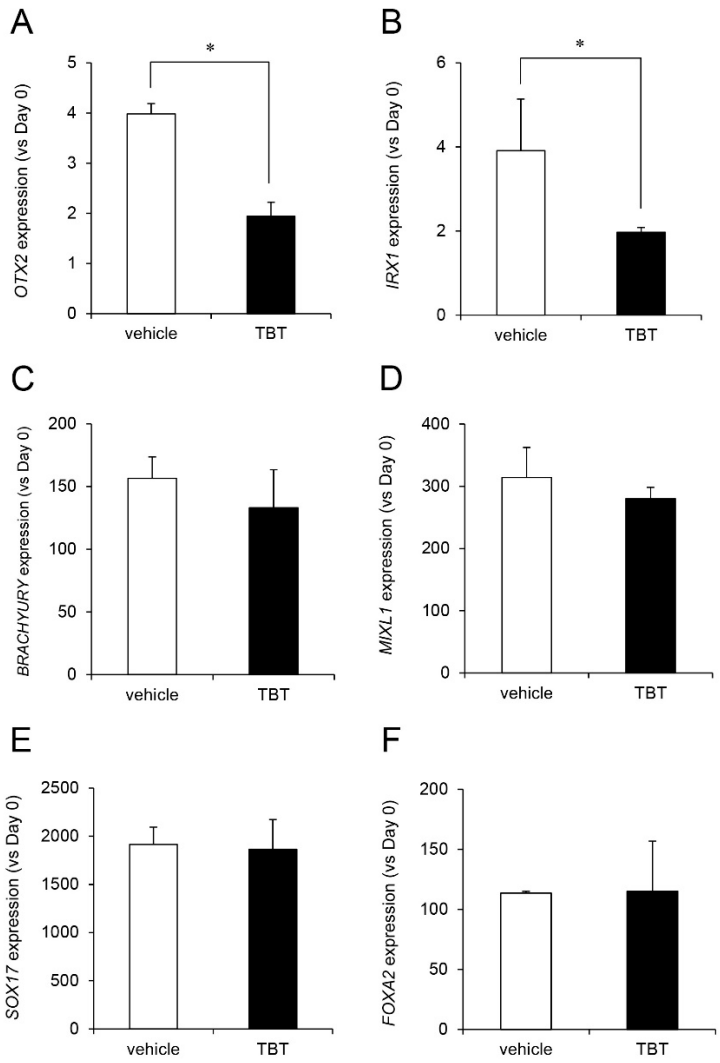

図 1　TBT による外胚葉分化阻害

50 nM の TBT を曝露したヒト iPS 細胞に外・中・内胚葉分化刺激を与えた後、各々の分化マーカーの遺伝子発現を qPCR で調べた。

(A) 外胚葉マーカーOTX2 遺伝子の発現変化
(B) 外胚葉マーカーIRX1 遺伝子の発現変化
(C) 中胚葉マーカーBRACHYURY 遺伝子の発現変化
(D) 中胚葉マーカーMIXL1 遺伝子の発現変化
(E) 内胚葉マーカーSOX17 遺伝子の発現変化
(F) 内胚葉マーカーFOXA2 遺伝子の発現変化

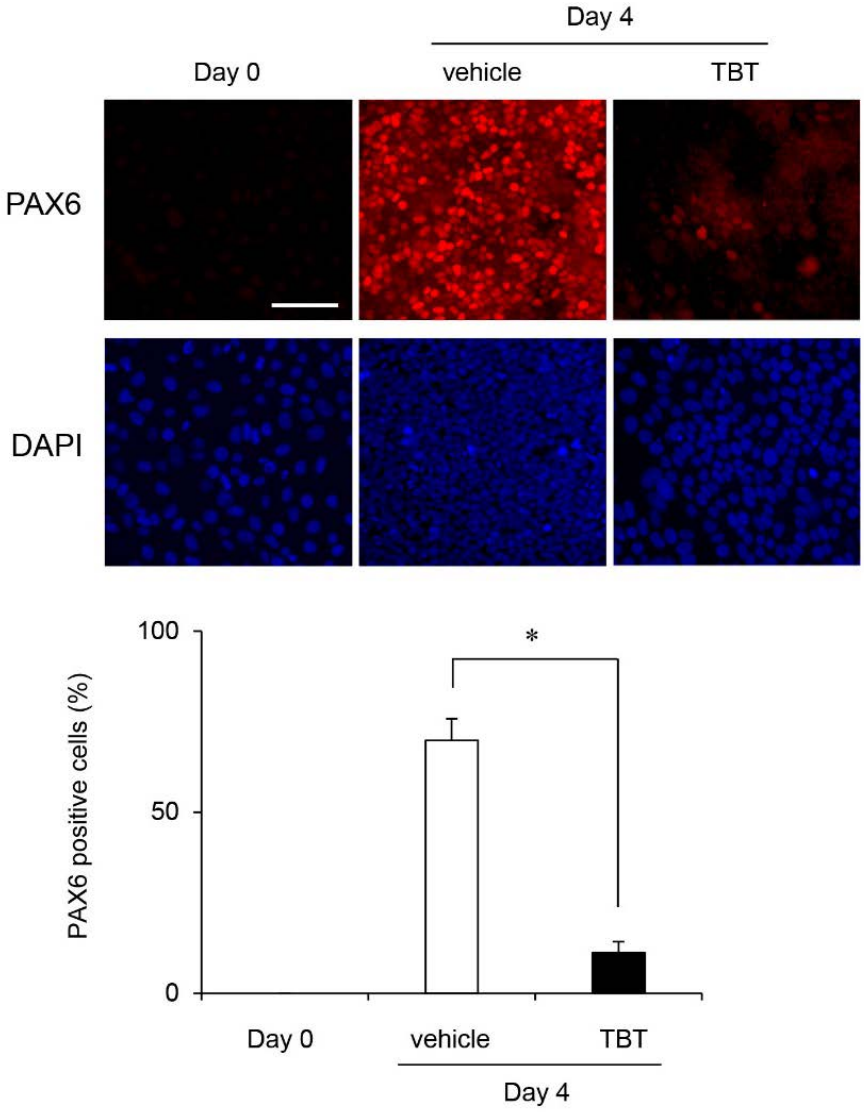

図 2　TBT による神経分化誘導の阻害

50 nM の TBT を曝露したヒト iPS 細胞に神経分化刺激を与えた後、4 日目に神経分化マーカーPAX6 の陽性細胞数を調べた。

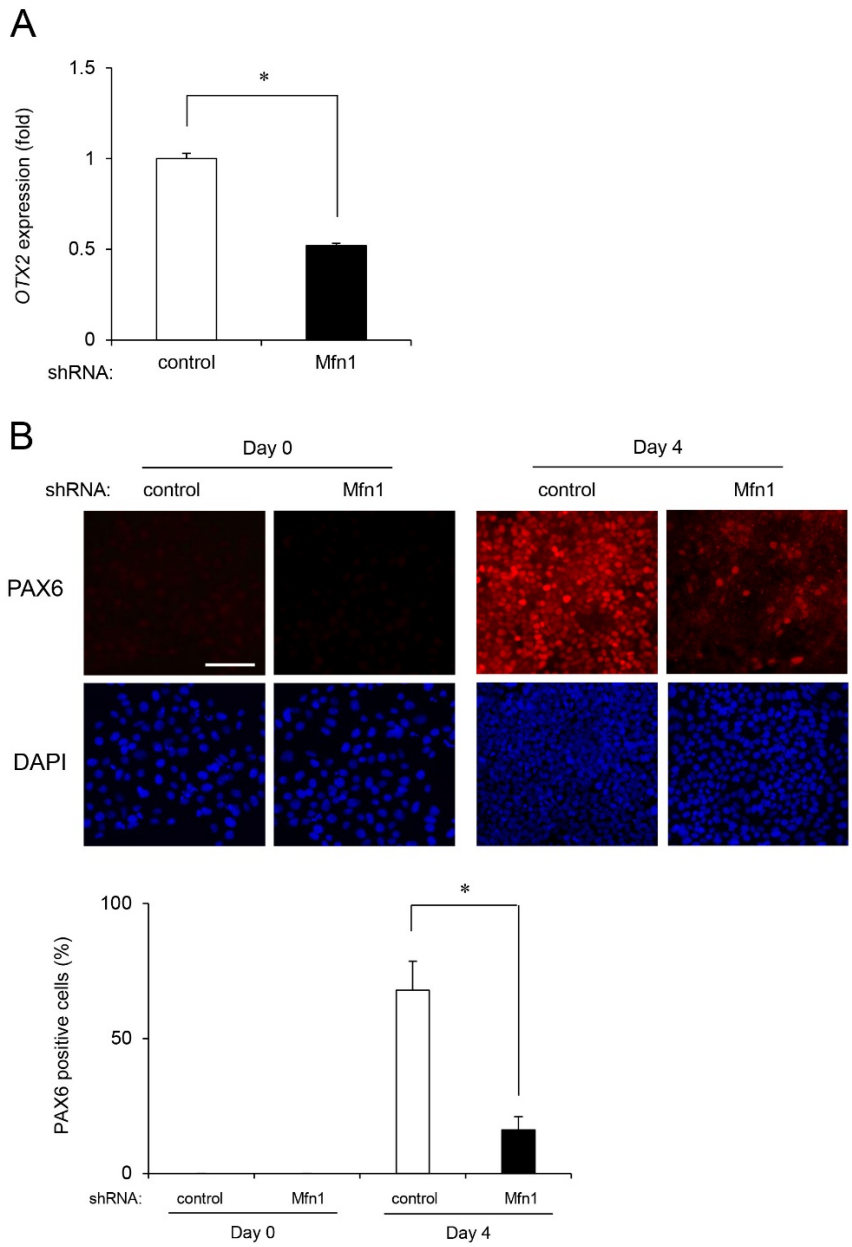

図 3　Mfn1 ノックダウンによる神経分化誘導の阻害

Mfn1 をノックダウンしたヒト iPS 細胞に神経分化刺激を与えた後、タイムコースをとって神経分化マーカーの発現を調べた。

(A) 神経分化 2 日目の外胚葉マーカーOTX2 遺伝子の発現変化

(B) 神経分化 4 日目の神経分化マーカーPAX6 陽性細胞数の変化

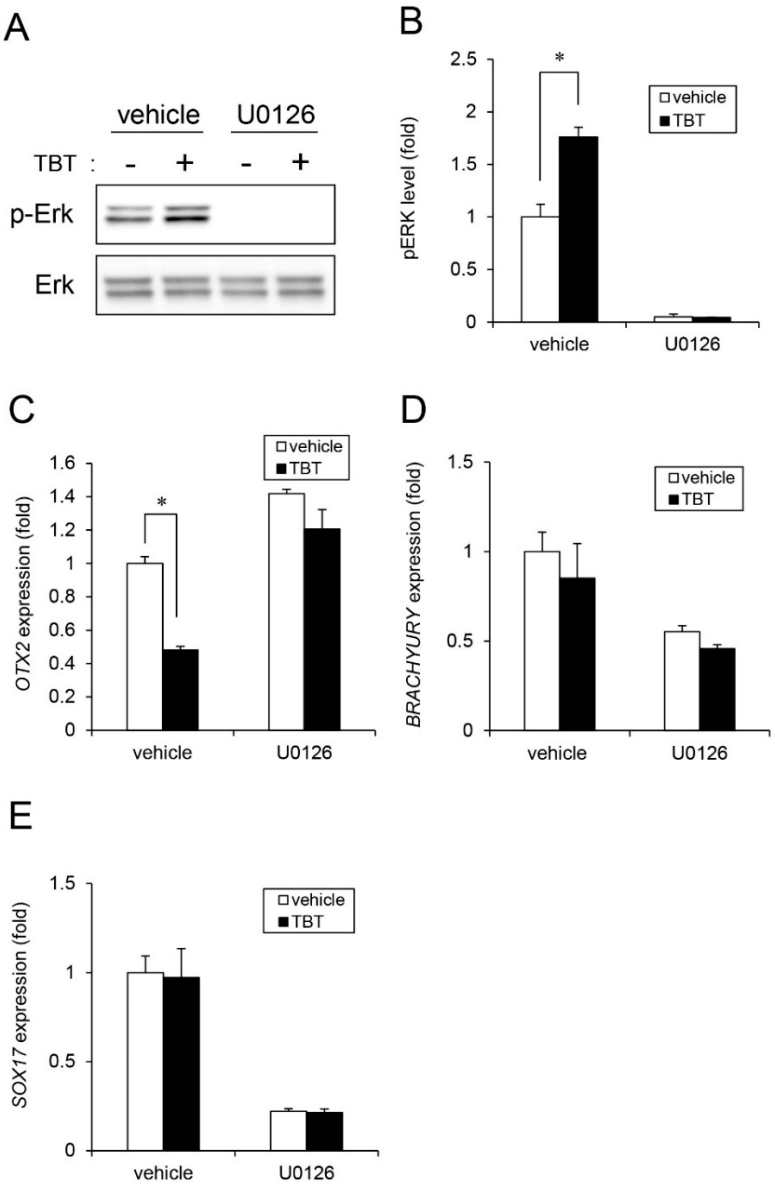

図 4　TBT の神経（外胚葉）誘導阻害における Erk シグナルの関与

(A) 50 nM の TBT を曝露したヒト iPS 細胞から cell lysate を作成し、Erk のリン酸化レベルをウエスタン法によって調べた結果、Erk リン酸化の亢進が認められた。このリン酸化レベルの亢進は Erk 阻害剤である U0126 処理により消失した。

(B) (A)の結果を定量的に評価した。

(C)ヒト iPS 細胞の神経（外胚葉）誘導において、TBT 曝露による OTX2 の発現低下は、U0126 処理により回復した。

(D)ヒト iPS 細胞の中胚葉誘導において、TBT 曝露による BRACHYURY の発現変化は認められなかった。

(E)ヒト iPS 細胞の内胚葉誘導において、TBT 曝露による SOX17 の発現変化は認められなかった。

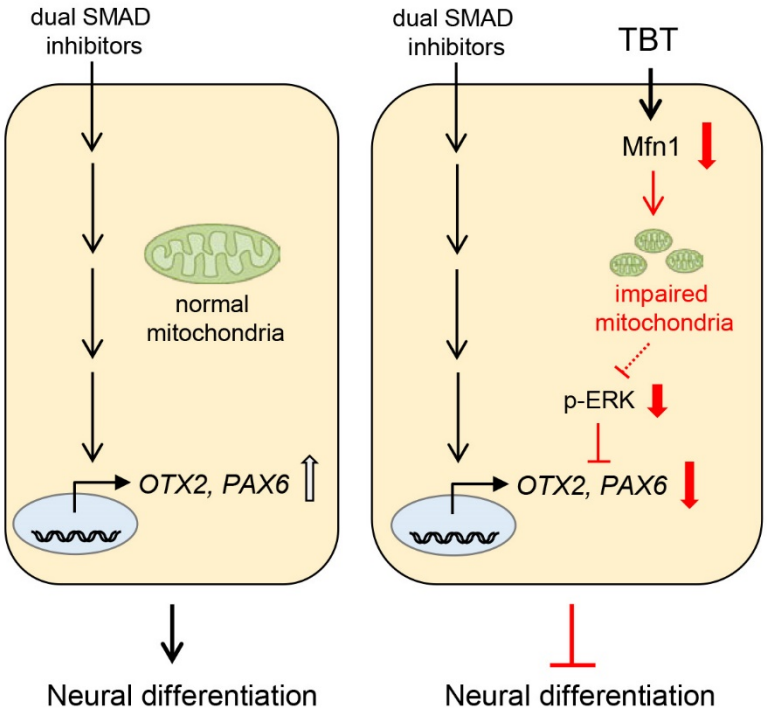

図 5　TBT の神経分化阻害作用（模式図）

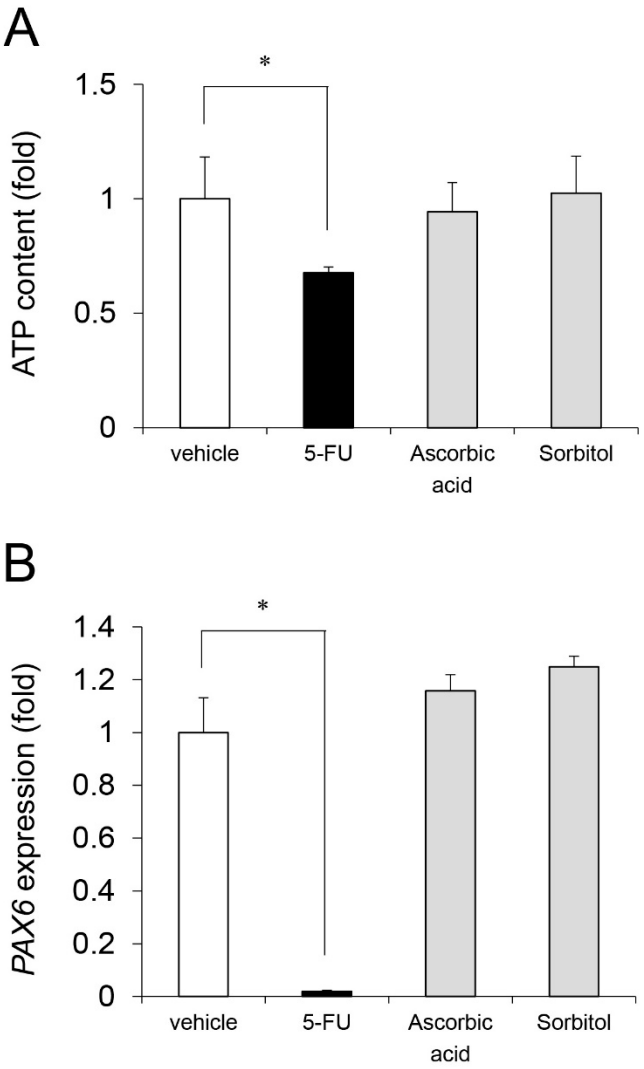

図 6　5-FU による ATP 産生及び神経分化誘導の阻害

(A) 1 μM の 5-FU を曝露したヒト iPS 細胞において細胞内 ATP 量を測定した。陰性対照としてアスコルビン酸及びソルビトール添加（各々100 μM）の影響も調べた。

(B) 1 μM の 5-FU を曝露したヒト iPS 細胞に神経分化刺激を与えた後、4 日目に神経分化マーカーPAX6 遺伝子の発現変化を調べた。陰性対照としてアスコルビン酸及びソルビトール添加（各々100 μM）の影響も調べた。

厚生労働科学研究費補助金（化学物質リスク研究事業）
分担研究報告書

海馬ニューロンを用いた神経ネットワークによる評価法の開発

研究分担者　国立医薬品食品衛生研究所薬理部　主任研究官
山崎　大樹
研究協力者　群馬大学大学院医学研究科　教授
白尾　智明

要旨

本研究では、ラット海馬神経細胞および HESI NeuTox バリデーション試験のためのラット大脳皮質神経細胞を用いて、多点電極システムにおける化合物の急性投与に対する評価系の構築を行った。両細胞において、最適化したネットワーク活動評価条件にて複数の化合物を評価した。今後、より多くの化合物を評価し、これまでの結果と比較することで試験法としての有用性や予測性について検証を行う。

A. 研究目的

近年、子供の学習障害や自閉症などの発達障害が増加しているが、その原因の一つとして環境中の化学物質の関与が指摘されている。現在の化学物質に対する発達神経毒性を評価するガイドライン（OECD: TG426 および EPA: OPPTS870.6300）は、妊娠ラットを用いた複雑な試験系であり、試験期間が１年以上、動物数も 700 以上に及び経費も膨大であるため、これまでにわずかな化学物質しか評価できていない。そこで本研究では、スループット性および再現性の高いラット神経細胞を用いた多点電極（MEA: Micro-electrode array）システム法による評価系の構築を目指した。

これまでに選定した評価指標をもとに、ラット海馬神経細胞を用いてネットワーク活動を評価するための条件を最適化した。次いで複数の化学物質を評価し、スループット性および再現性が高いスクリーニング系となるようプロトコルを確定した。また、HESI NeuTox 多点電極サブチームにおけるバリデーション試験の実施を見据えて、ラット大脳皮質神経細胞を用いた測定条件の最適化および予備試験を実施した。

B. 研究方法

1. 細胞

細胞はラット大脳皮質神経細胞（Lonza、スイス、バーゼル）および群馬大学・白尾教授の研究室で作製されたラット胎児凍結海馬神経細胞を用いた。

2. プレートコーティング

多点電極システムとして Maestro（Axion Biosystems 社）を用いて、神経活動を計測した。細胞播種前日までに Maestro 用 48 ウェルプレートを 0.1%ポリエチレンイミン（PEI）（0.1% PEI in 0.1 M Boric acid buffer solution（pH 8.5）でコーティングした。0.1% PEI 溶液を各ウェルに 100 µl ずつ添加後 CO_2 インキュベーター内に 1 時間静置した後、滅菌水で 3 回リン

スし、クリーンベンチ内で 1 時間乾燥させた。乾燥後、フタをしてアルミホイルで遮光し、4ºC に保管した。過去の検討により、PEI コート後 1 週間以上経過すると、神経活動の抑制が観察されたことから、PEI コートしたプレートは 1 週間以内に使用した。

3. 細胞播種、培地交換および神経活動測定

液体窒素から取り出した凍結細胞は 37ºC の温浴に 3 分間浸して解凍した。解凍した細胞懸濁液を 50 ml 遠沈管に入れ、そこへ播種用培地（海馬神経細胞: 10% FBS, 1.14 mM Pyruvic acid, 0.7% Glucose in Minimum Essential medium、大脳皮質神経細胞: 5% FBS, 2% B-27, 2 mM GlutaMax, 1% Penicillin-Streptomycin in Neurobasal medium-A）を細胞懸濁液と合わせて 10 ml になるまで少しずつ加えた。よく混合した後に細胞数を計測した。海馬神経細胞は 200 x g で、大脳皮質神経細胞は 370 x g で 5 分間遠心し、一定の細胞密度になるように 20 µg/ml ラミニンを含む播種用培地を添加し、10 µl/ウェルにて電極上に播種した。播種 2 時間後に、培養培地（海馬神経細胞: 0.25% GlutaMAX, 1% Penicillin-Streptomycin, 2% B27 in Neurobasal medium-A、大脳皮質神経細胞: 播種用培地と同じ組成）を添加した。必要に応じて 0.5 µM AraC を Day 5-7 で加えた。大脳皮質神経細胞について、Day 5 以降は播種用培地、血清除去培地（2% B-27, 2 mM GlutaMax, 1% Penicillin-Streptomycin in Neurobasal medium-A）、あるいは Brainphys neuronal medium（2% NeuroCult™ SM1 Neuronal Supplement）にて培養した。培養は 16-20 日目まで行い、定期的に培地交換および MEA による測定を行った。また、神経活動が安定して得られる培養 16-20 日後に、化合物を急性で添加し、その投与前後での神経活動の変化を解析した。

4. 解析

1 電極における 1 分間あたりのスパイク発生頻度（MFR: Mean firing rate）、活性化電極（AE: Active electrodes、1 分間に 5 回以上スパイクが発生した電極と定義する）、バースト頻度（Burst frequency、1 電極における 1 分間あたりのバースト発生頻度）や同期性（Synchrony index）等についても解析した。

C. 研究結果

1. ラット胎児凍結海馬神経細胞を用いた MEA による化学物質の毒性評価

ラット胎児凍結海馬神経細胞において、これまでに選定した評価指標のもと、ネットワーク活動評価の条件を以下のように定めた。1) プレートコーティング: 0.1% PEI、2) 細胞播種密度: 生細胞数 50,000 細胞／ウェル、3) AraC 濃度および投与期間: Day5-7 に 0.5 µM、4) 培地交換: 3-4 日ごとに全量交換、5) 化学物質の投与: Day 16～に 200 µl の培養液と混合後に細胞に添加。まず、各ウェルの MFR および AE の経時的変化について、観察を行った。その結果、いずれのパラメーターもウェル毎のバラツキが小さく、MFR は Day 14 をピークとして、Day 16 では少し減少傾向であった（図 1A）。一方、Day 9 の時点でほとんどすべての電極が活性化状態となり、Day 16 までそれは維持された（図 1B）。そこで、Day 17 において、陰性対照物質であるアセチルサリチル酸（ASA）を含む複数の化学物質（有機スズ化合物で船底塗料などに用いられているトリブチルスズ: TBT、有機リン系殺虫剤クロルピリホ

ス: CPF、抗てんかん薬として用いられているバルプロ酸: VPA)を急性で 4 濃度ずつ投与し、MFR への影響を調べた。その結果、陰性対照物質である ASA は 300 μM まで投与しても MFR に変化がなかったが、3 μM TBT、30 μM CPF、3 mM VPA にて有意に MFR が減少することを明らかにした(図 2A)。その他、$GABA_A$ 受容体アンタゴニストであるビククリン(BIC)および Ca^{2+}チャネル拮抗薬であるベラパミル(VER)についても実施したので、結果を掲載した(図 2B)。今後、発達神経毒性評価系として感受性や反応性等において、過去に本研究班で行った他の試験系と比較することで試験法としての有用性や予測性を検証する。

2. HESI NeuTox MEA サブチームにおけるバリデーション試験

我々は、痙攣誘発毒性評価を化合物のメカニズムに基づいて議論を行う HESI NeuTox MEA サブチームに昨年度より参加している。ここでは、電話会議および対面会議にてバリデーション試験に関する議論を行いながら、痙攣誘発毒性評価法の開発および国際協調を推進している。バリデーション試験に参加する施設および使用する細胞を表 1 にまとめた。

我々は、NeuTox のバリデーション試験に参加するにあたり予備試験を実施することとした。予備試験の実施にあたり、バリデーション試験に用いるラット大脳皮質神経細胞にて、測定条件の最適化を行った。バリデーションに参加する他の施設の実験条件等と比較・検討した。その結果、以下の条件にて測定を行うこととなった。1) プレートコーティング: 0.1%PEI、2) 細胞播種密度: 総細胞数 120,000 細胞／ウェル、3) AraC: 投与しない、4) 培地交換: 3-4 日ごとに全量交換、5) 化学物質の投与: およそ Day 20 に 200 μl の培養液と混合後に細胞に添加。海馬神経細胞における培養条件を用いて、測定条件の最適化を開始した当初、ピクロトキシン投与により MFR および Burst frequency がピクロトキシンの濃度依存的に減少した。この反応はピクロトキシンの作用機序からは考えにくいものであったため、3 種類(播種用培地、血清除去培地、および Brainphys neuronal medium)の培地条件にてピクロトキシンの反応性について検討を行うこととした。図 3A には、3 種類の培地における MFR の経時的変化を、図 3B には、AE の経時的変化を示した。MFR は 3 種類の培地でそれほど大きな違いはなかったが、活性化電極は Brainphys を用いた際には、Day 8 において半分以上が活性化し、その後緩やかに増加していった。また、播種用培地を用いた場合にも、Day 11 の時点で 3/4 の電極が活性化した。一方で、血清除去培地を用いた場合には、活性化電極の数は Day 19 まで緩やかに増加していった。逆に Burst frequency は血清除去培地を用いると他の 2 種類の培地よりも大きな値を示した(図 3C)。Day 20 において、$GABA_A$ 受容体アンタゴニストであるピクロトキシンおよびビククリンを急性投与した際の、MFR、Burst frequency および同期性(Synchrony index)についてそれぞれ図 4A-C にまとめた。ピクロトキシンおよびビククリンの作用機序は、神経活動に対して抑制的に寄与している $GABA_A$ 受容体を阻害し、興奮性を上昇させるとともにスパイクの同期性を上昇させる。これに類似した反応を示したのが血清除去培地であった。今後、再現性を確認するとともにバリデーション試験のデータ提出に向けて合計 12 化合物のデータ取得を行う。

D. 考察

本研究では、ラット海馬および大脳皮質神経細胞を用いて、MEA における化合物の急性投与に対する評価系の構築を行った。両細胞において、条件が最適化されたため複数の化合物を評価系した。ラット海馬神経細胞においては、過去に本研究班で実施済の他の評価系の結果との比較を行うことで試験法の有用性や予測性を検証する。一方で大脳皮質神経細胞においては、$GABA_A$ 受容体アンタゴニストであるピクロトキシンおよびビククリンを投与し、期待される結果が得られたことから、今後 12 化合物に対して評価を行い、有用性や予測性の検証を詳細に実施する。取得したデータについては、HESI NeuTox のバリデーション試験用データとして提出予定である。

E. 結論

2 種類のラット神経細胞を用いて、MEA によるスループット性および再現性の高い評価系の構築を行った。今後、試験法としての妥当性の検証を行う。

F. 研究発表

1. 論文発表

[1] Yamazaki D., Kanda Y., Sekino Y. “Field potential recording method using multi-electrode array system-Cellular responses in human iPSC-derived cardiomyocytes and rodent brain-derived neurons.” BUNSEKI (2017) 7:290-295

2. 学会発表

[1] 山田茂、山崎大樹、諫田泰成：ヒト iPS 細胞の神経分化に対するクロルピリホス曝露の影響、第 136 回日本薬理学会関東部会、2017 東京

[2] 山崎大樹、後藤和愛、小金澤紀子、花村健次、白尾智明、関野祐子、諫田泰成:海馬ニューロンを用いた神経活動ネットワークによる評価法の開発、第 44 回日本毒性学会、2017 横浜

[3] 山田茂、山崎大樹、諫田泰成：ヒト iPS 細胞の神経分化に対するトリブチルスズの影響、第 44 回日本毒性学会、2017 横浜

[4] Yamazaki D., Goto K., Koganezawa N., Hanamura K., Shirao T., Sekino Y., Kanda Y. : Development the assay of spontaneous activity in rat hippocampal neural networks, 10th world congress, Alternative and animal use in the life science, 2017, Seattle

[5] 山田茂、山崎大樹、諫田泰成：ヒト iPS 細胞の神経分化能を指標にした発達神経毒性評価系の開発、第 3 回次世代を担う若手のためのレギュラトリーサイエンスフォーラム、2017 東京

[6] Yamada S., Yamazaki D., Kanda Y. : Development of human iPS cell-based platform for developmental neurotoxicity testing, SPS, 2017, Berlin

G. 知的財産権の出願・登録状況

該当なし

表 1　HESI NeuTox バリデーション試験への参加施設の使用機器と細胞

施設	機器	細胞
Cyprotex	Axion Maestro	Glutaneurons
Janssen (JNJ)	Axion Maestro	Rat cortical neurons, hiPSC neurons (CNS4U)
Ncardia	Axion Maestro	iPS neurons + astro,
GlaxoSmithKline	Axion Maestro	Rat cortical neurons
NIHS	Axion Maestro	Rat cortical neurons
BMS	Axion Maestro	CDI GTN + Astrocyte
Axion	Axion Maestro	Rat cortical neurons
Tohoku Inst. of Tech	AlphaMed Presto	Rat Hippocampal Neurons, hiPSC Neurons
Eisai	Axion Maestro, AlphaMed Presto	Rat Hippocampal Neurons
NeuCyte	Axion Maestro APEX	SynFire Neural Cells
EPA	Axion Maestro	
BMS	Axion Maestro	CDI iPSC GlutaNeurons

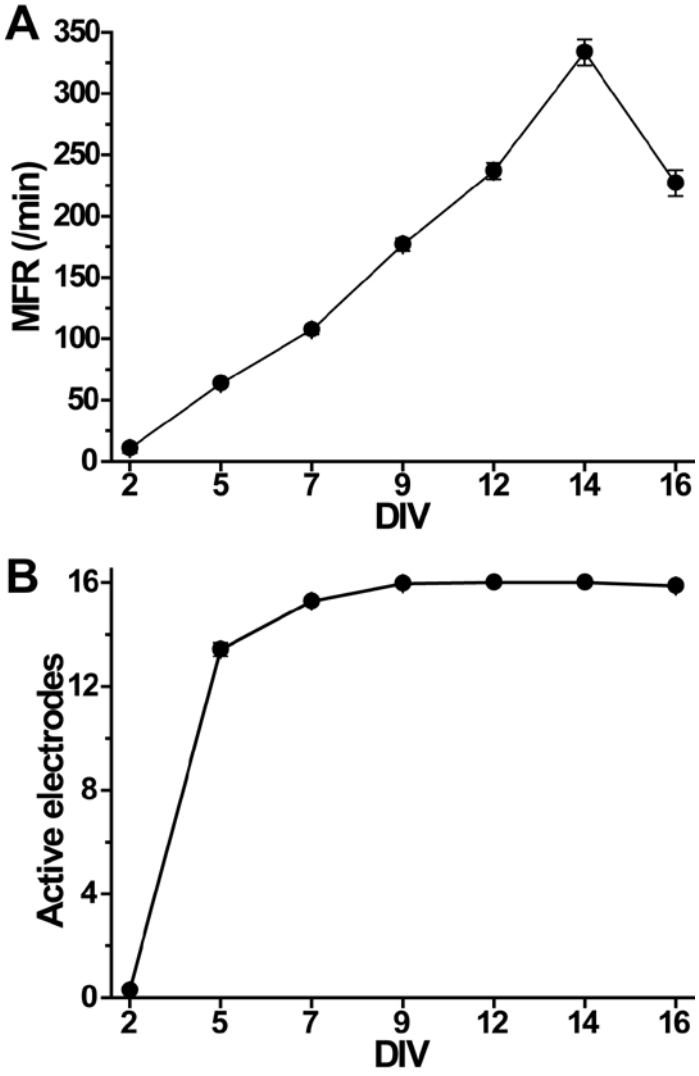

図 1　ラット海馬神経細胞における神経活動の経時的変化

1) プレートコーティング: 0.1% PEI、2) 細胞播種密度: 生細胞数 50,000 細胞／ウェル、3) AraC 濃度および投与期間: Day5-7 に 0.5 μM、4) 培地交換: 3-4 日ごとに全量交換の条件にてラット海馬神経細胞を培養した際の、MFR（A）および Active electrodes（B）の経時的変化を示した。MFR が Day 16 にて落ち込んでおることから、このタイミングで化学物質を急性投与した。いずれも 48 サンプルの平均値および平均誤差（SEM）を示した。

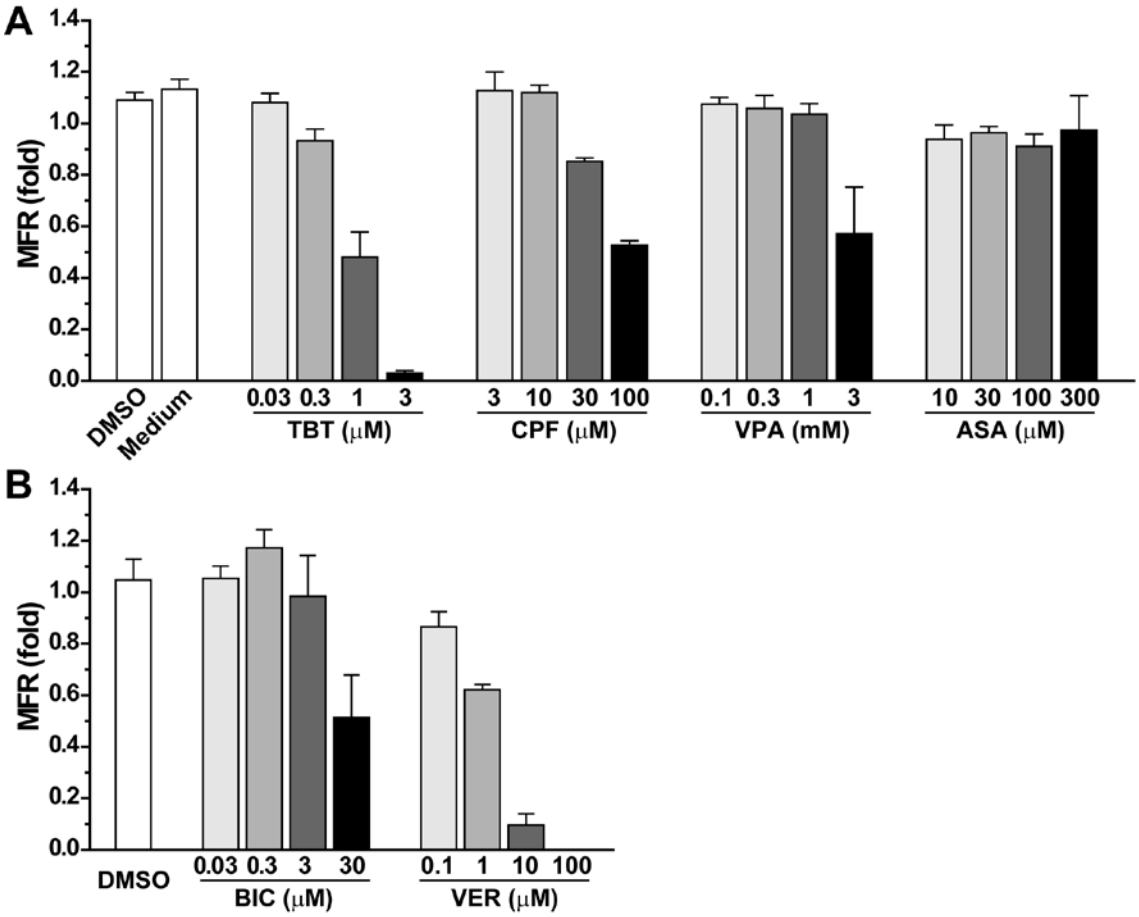

図 2　ラット海馬神経細胞における化学物質の急性投与に対する反応

（A）図 1 の Day 16 のタイミングにて、トリブチルスズ（TBT）、クロルピリホス（CPF）、バルプロ酸（VPA）、アセチルサリチル酸（ASA）を 4 濃度ずつ急性投与した。各化学物質の投与前の MFR の値（5 分間の平均値）を 1.0 として規格化し、投与 60 分後の MFR の値（5 分間の平均値）を算出した。（B）図 1 の Day 16 のタイミングにて、ビククリン（BIC）、ベラパミル（VER）を 4 濃度ずつ急性投与した。各化学物質の投与前の MFR の値（5 分間の平均値）を 1.0 として規格化し、投与 60 分後の MFR の値（5 分間の平均値）を算出した。例数はすべて 3 以上である。

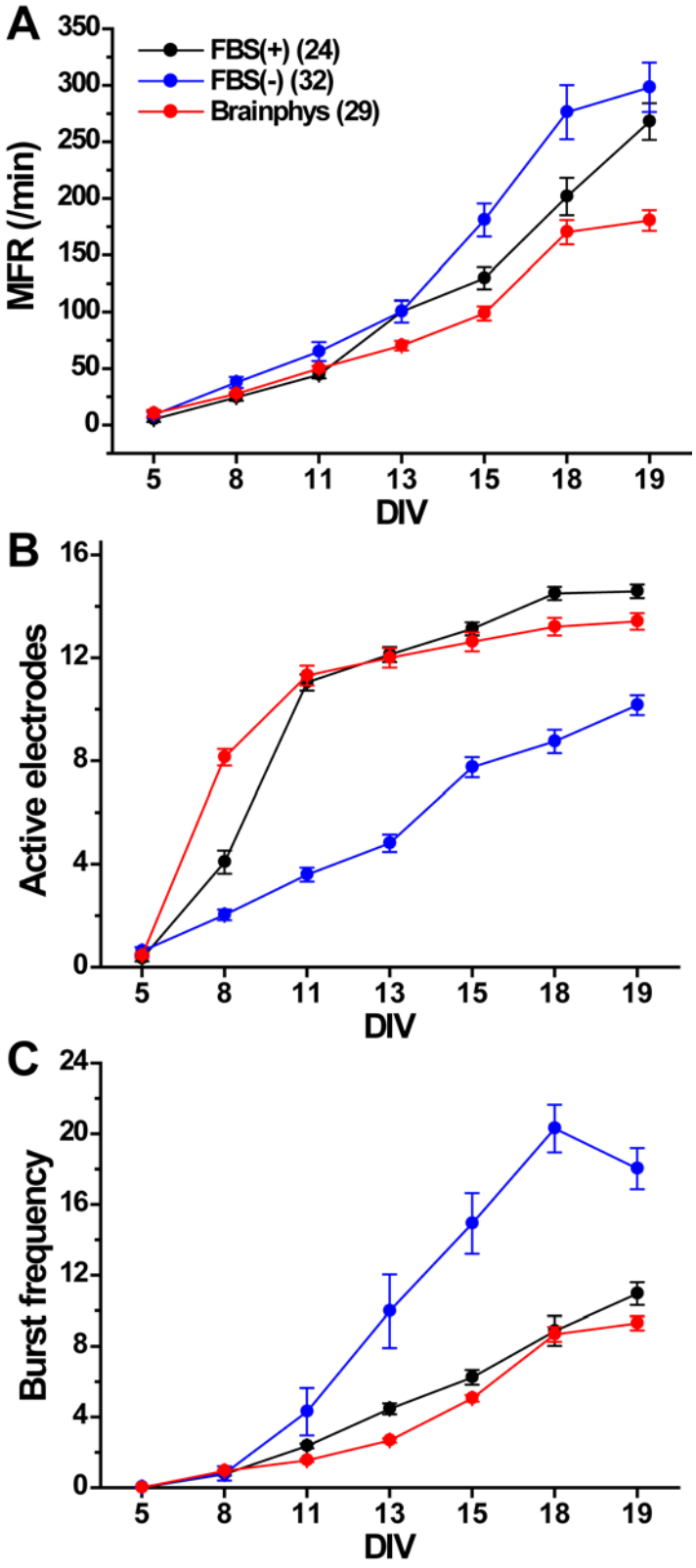

図 3　ラット大脳皮質神経細胞の神経活動に対する培地の検討

ラット大脳皮質神経細胞の神経活動に対する播種用培地（FBS+）、血清除去培地（FBS-、Day 5 までは播種用培地で培養し、Day 5 から FBS-に置換）および Brainphys の 3 種類の培地の影響を検討した。MFR（A）、Active electrodes（B）および Burst frequency（C）のそれぞれのパラメーターを Day 5 から Day 19 まで経時的変化を示した。括弧内は例数を示す。

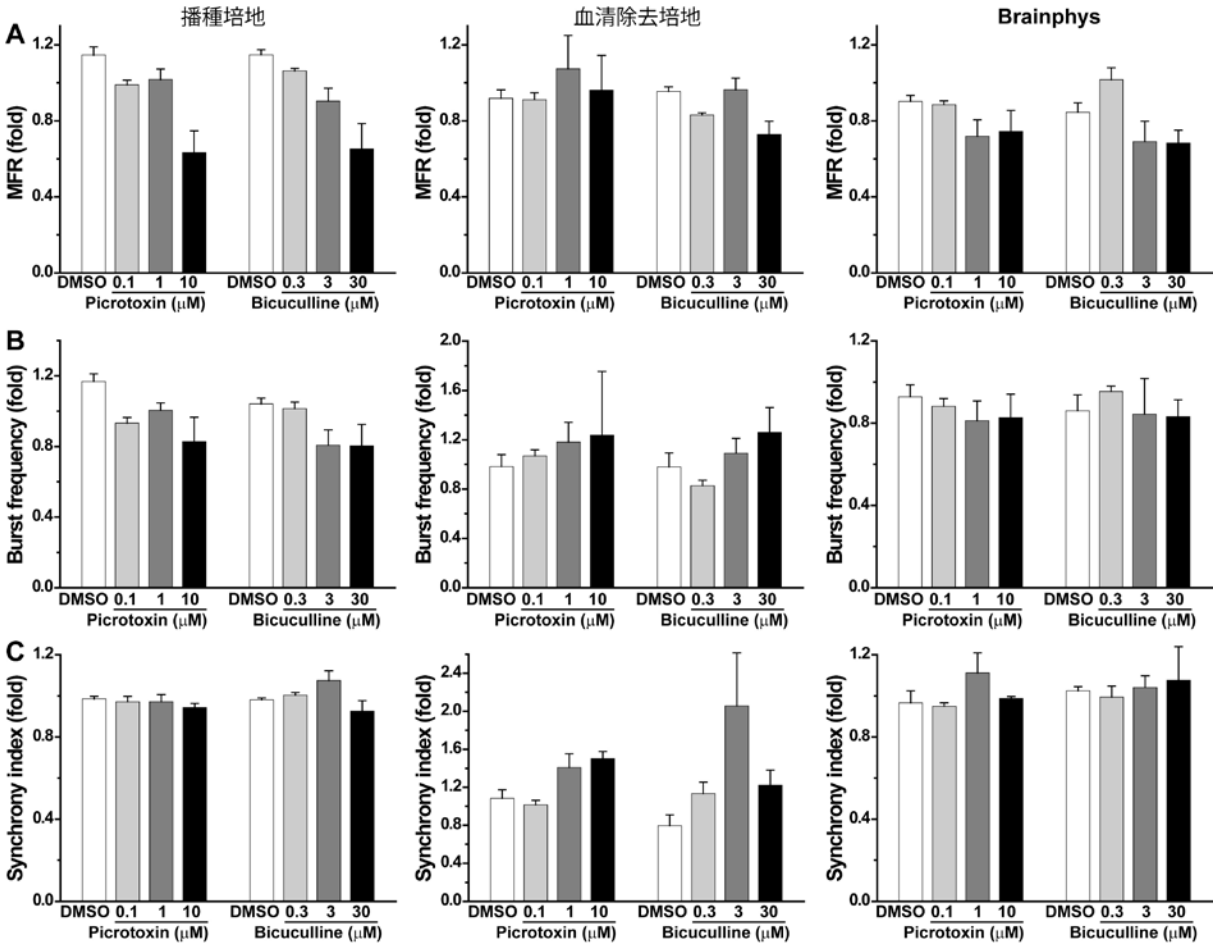

図4　ラット大脳皮質神経細胞の$GABA_A$受容体アンタゴニストによる反応性に対する培地の検討

$GABA_A$ 受容体アンタゴニストであるピクロトキシンおよびビククリンの急性投与に対する、MFR（A）、Burst frequency（B）および Synchrony index（C）の反応を検討した。左レーンが播種用培地、真ん中が血清除去培地、右レーンが Brainphys 培地である。Day 20 において、両化合物を急性投与し、各化学物質の投与前の各パラメーター値（5 分間の平均値）を 1.0 として規格化し、投与 60 分後の各パラメーター値（5 分間の平均値）を算出した。いずれも 3 例以上のデータを示す。

厚生労働科学研究費補助金（化学物質リスク研究事業）
分担研究報告書

生後小脳の神経回路の機能的影響による評価法の開発

研究分担者　豊橋技術科学大学　環境・生命工学系
吉田　祥子
研究協力者　東京大学　薬学部
関野　祐子

要旨
本年度は、化学物質に対して感受性の高いラット小脳皮質を用いて、化学物質曝露による神経突起進展、神経回路形成への影響を検討し、最も適切な定量化方法を決定することを目的として実施した。ヒト自閉症誘発が報告されているバルプロ酸、およびクロルピリホスに加え，同様の薬理作用機序が考えられる SAHA、MS-275、環境毒性物質の有機スズについて、神経細胞レベルおよび小脳組織レベルでの変化を観察し、定量化を試みた。さらにバルプロ酸について、投与時期と投与濃度を変化させその効果を検討した。本年度は、化学物質投与による神経伸長変化の定量化、小脳虫部第一裂の過剰な褶曲の定量化、行動観察の定量化を行った。その結果、遅発性神経毒性が考えられる化学物質であるバルプロ酸、クロルピリホスが、生後の神経回路発達の変化を小脳神経細胞の突起伸展と小脳構造の変化、動物の行動変化を引き起こすことを定量的に示した。これにより投与量依存性、投与時期依存性が明瞭になり、さらに遺伝子レベル、たんぱく質レベルでの発達期神経毒性の定量化につなげることが期待される。

A. 研究目的

ヒト自閉症誘発が報告されているバルプロ酸(VPA)、VPA と同様にヒストン脱アセチル化酵素(HDAC)阻害剤であるスベロイルアニリドヒドロキサム酸(SAHA)、MS-275、ヒト自閉症誘発が報告されているクロルピリホス(CPF)、および環境毒性物質のトリブチルスズ(TBT)投与による小脳発達への影響を、免疫組織化学的手法による神経の形態的変化、およびヘマトキシリン-エオシン染色(HE 染色)による小脳虫部全体の構造変化を観察した。さらに個体の行動に及ぼす変化を確認するために、光学測定法による伝達物質放出の変化の観察、および発達期と成熟期の個体の行動観察を行った。

B. 研究方法

近年自閉症の変異部位であることが報告されている小脳を研究試料として用いた。各化学物質を妊娠動物に投与し、出生動物の小脳を摘出してその効果を観察した。妊娠 16 日のラットに、600 mg/kgの VPA(経口)、50mg/kg の SAHA(腹腔内)、4mg/kg の MS-275(経口)、10mg/kg の CPF(経口)、20mg/kg の TBT(経口)をそれぞれ投与した。VPA については、妊娠 14 日、18 日にそれぞれ 600 mg/kgの投与することを試験した。また，妊娠 16 日に 200 mg/kg、300 mg/kg、400 mg/kgの VPA 投与を試験した。

各投与動物を生後２から３週で灌流固定後、小脳虫部の矢状面スライスを調整し、抗カルビンジン抗体染色によってプルキンエ細胞の樹状突起長を測定し，化学物質投与による神経伸長変化の定量化を行った。さらにスライス全体を HE 染色し、小脳虫部スライスの第 V/VI 小葉間にある primary fissure（第一裂）について、プルキンエ層の長さと裂の深さの比を計算し、投与動物と対照動物を比較して化学物質投与の影響の定量化を行った。また各投与動物の発達期（生後 4 日から 10 日）お

よび成熟期（生後６週から８週）で、発達期では震えのような不随意運動の出現率を計測、成熟期では新規環境での行動を計測し定量化を行った。さらに生後 10 日から 21 日の小脳皮質層からの伝達物質放出を、酵素光学測定法を用いて観察した。

C. 研究結果

VPA投与動物、SAHA投与動物では,プルキンエ細胞の樹状突起伸長が対照動物より早く著しく、生後２週で1.6倍、生後3週でも1.3倍の伸長を示した。これはCPF投与動物でも観察されたが、MS-275投与動物、TBT投与動物では観察されなかった（図１）。突起伸長の加速と同時に、プルキンエ細胞のプログラム細胞死が引き起こされず、単層化しないプルキンエ細胞層が観察された。樹状突起は複雑な網状の形状を示し、主たる垂直突起が識別できない状態を示した。

VPA投与動物では、小脳虫部第一裂（V葉-VI葉間）に過剰な褶曲が観察された。これにより、プルキンエ層が長くなり，対照動物の1.2倍の長さのプルキンエ層を持つに至った。CPF投与動物では1.05倍のプルキンエ層を示した。一方MS-275、TBT投与動物では観察されず、神経突起伸展異常と同様の傾向を示した。妊娠14日にVPAを投与した動物では1.25倍のプルキンエ層が観察されたが、妊娠18日投与動物は対照動物と差を示さなかった。この変化はVPAの投与量に正の相関を示した（図２）。

行動観察の結果、VPA投与動物では,初期に多くの不随意運動を確認したが、成長につれて減少する傾向があった。SAHA投与動物では,多くの不随意運動を確認し、且つ成長につれて増加する傾向が見られた。MS-275投与動物では若干の増加が確認されたが,著しい変化は確認できなかった。TBT投与動物では,多くの不随意運動を確認し、また，成長につれて不随意運動が増加する傾向にあった（図３）。成熟期の行動では、VPA投与動物は新規環境でも警戒が少なく、過活動の傾向を示した（図４）。移動速度は速く、躊躇なく中心部を通過し、対照動物との差異が見られた。

伝達物質放出では、発達期に過剰な伝達物質の放出が観察された（図５）。グルタミン酸誘発性のATP放出は、グリア細胞からのシナプス形成誘発因子と考えられており、ATP受容体の阻害によってシナプス形成は著しく抑制される。VPA投与動物、SAHA投与動物ではグルタミン酸誘発性ATP放出が発達初期から亢進しており、何らかのグリア細胞性の異常が起こっていることを示唆した。

D. 考察

研究結果を通じ、発達期小脳皮質の形成異常、プルキンエ細胞の形成異常、伝達物質放出の異常によって自閉症誘発が疑われる化学物質の神経毒性の定量化の可能性を示した。発達期神経系におけるこれらの変化は、成熟期では個体の行動異常につながることが確認できた。神経細胞の変化を引き起こす発生制御たんぱく質、神経栄養因子などの発現変異を示唆しているものと考えられる。これらの神経回路レベル、行動レベルでの変化を細胞レベルの変化につなげることが必要と考えられる。

E. 結論

本研究において、遅発性神経毒性が考えられる化学物質であるバルプロ酸、クロルピリホスを胎生期の動物に投与し、生後の神経回路発達の変化を小脳神経細胞の突起伸展と小脳構造の変化、動物の行動変化から定量化して示した。定量化により投与量依存性、投与時期依存性が明瞭になり、さらに遺伝子レベル、たんぱく質レベルでの発達期神経毒性の定量化につなげることが期待される。

F. 研究発表

1. 論文発表

[1] Mabuchi H., Ong HY., Watanabe K., Yoshida S., Hozumi N. “Visualization of Spatially Distributed Bioactive Molecules Using Enzyme-Linked Photo Assay.” IEEJ Trans FM. (2016) 136(2):99-104

[2] Takanashi K., Washiya M., Ota K., Yoshida S., Hozumi N., Kobayashi K. “Quantitative evaluation method for differentiation of C2C12 myoblasts by ultrasonic microscopy.” Jpn J

Appl Phys. (2017) 56:07JF11

[3] Tiong TKS., Chean TW., Yamada H., Takahashi K., Hozumi N., Kobayashi K., Yoshida S. “Effects of anticancer drugs on glia–glioma brain tumor model characterized by acoustic impedance microscopy.” Jpn J Appl Phys. (2017) 56:07JF15

[4] Fueta Y., Sekino Y., Yoshida S., KandaY., Ueno S. “Prenatal exposure to valproic acid alters the development of excitability in the postnatal rat hippocampus.” NeuroToxicology (2018) 65: 1-8

[5] Zhang W., Qian L., Lambertini L., Finik J., Huang Y., Tsuchiya K.J., Pehme P., Buthmann J., Yoshida S., Chen J., Nomura Y. “Timing of Prenatal Exposure to Trauma and Altered Placental Expressions of HPA-Axis Genes and Genes Driving Neurodevelopment.” J Neuroendocrinol. (2018) DOI: 10.1111/jne. 12581 in press

他 2件

2. 学会発表

[1] Yoshida S. Neuroscience meeting 2017, nano-symposium, 2017, Washington DC

［2］ Yoshida S. 第 60 回日本神経化学会大会 シンポジウム、2017 仙台

[3] Yoshida S., Fueta Y., Ueno S., Hozumi N., Sekino Y., Kanda Y. 10th DOHaD world congress, 2017, Rotterdam

[4] Yoshida S., Rahayu RH., Takanashi K., Kishikawa K., Kurita H., Takashima K., Hozumi N., Kobayashi K., Yamamoto S. 5th Joint Meeting of the Acoustical Society of America and the Acoustical Society of Japan, 2016, Waikiki

[5] Yoshida S., Hozumi N., Fueta Y., Ueno S., Sekino S. Society of Toxicology, 55th Annual Meeting, 2016, New Orleans

他 20 件

H. 知的財産権の出願・登録状況

［1］ 吉田祥子，穂積直裕，氏家雅彦，光学観察装置，特願 2016-221213

［2］ 吉田祥子、細胞放出物質検出装置、細胞放出物質検出方法及び細胞放出物質検出用固定化酵素基板
（ア）特許 5871224

他 1 件

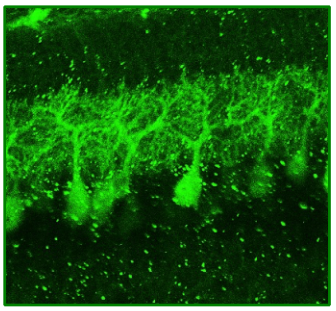

生後10日の対照　物のプルキンエ細胞

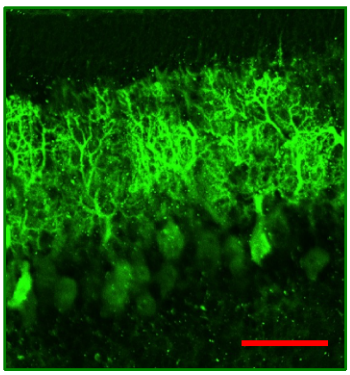

生後10日のVPA投与　物のプルキンエ細胞
（抗カルビンジン　D-28k染色）

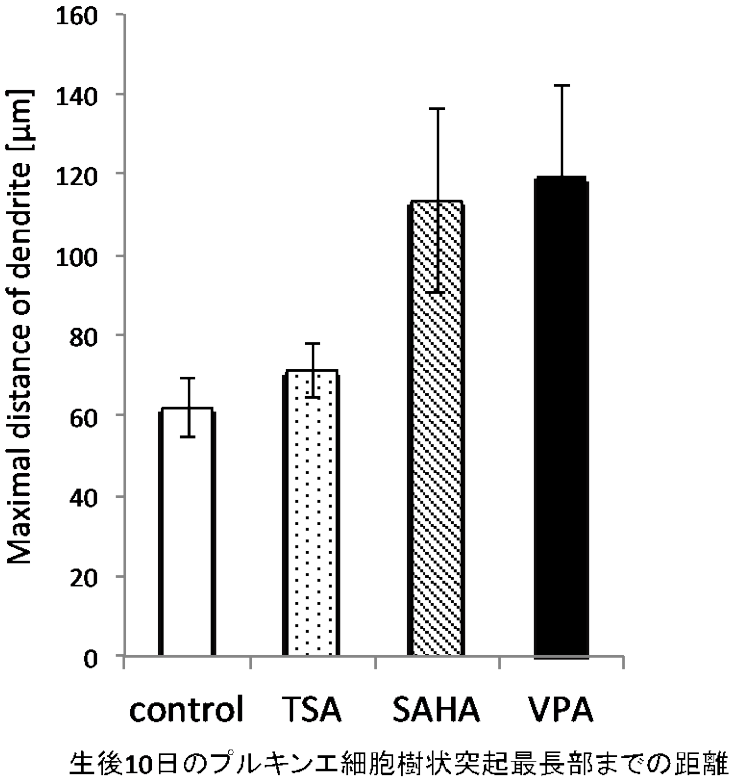

生後10日のプルキンエ細胞樹状突起最長部までの距離

図 1　化学物質を投与した生後 10 日目の動物のプルキンエ細胞

VPA 投与動物、SAHA 投与動物では, プルキンエ細胞の樹状突起伸長が対照動物より早く、より長くなる傾向が認められた。

A

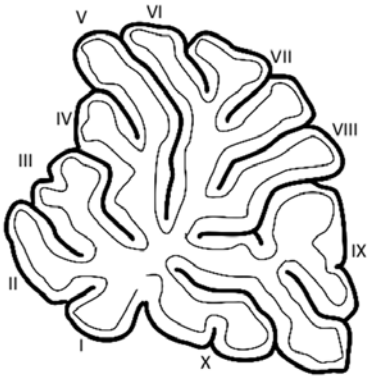

生後 16 日　対照動物小脳

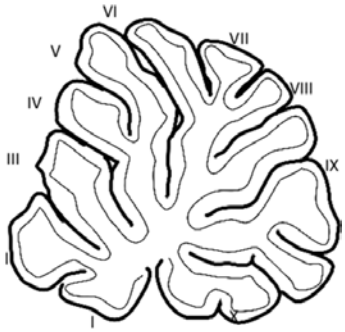

VPA 200 mg/kg 投与動物小脳　(P15)

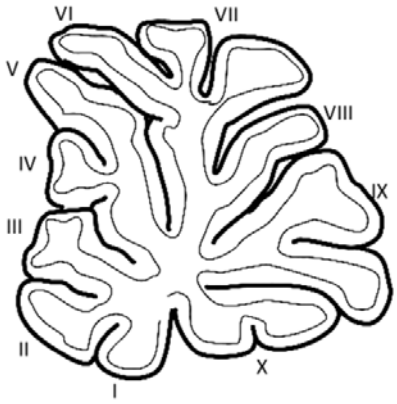

VPA 400 mg/kg 投与動物小脳　(P16)

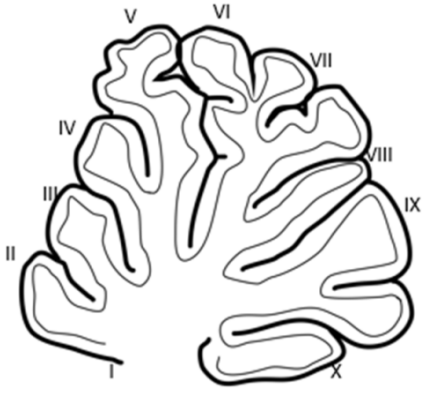

VPA 600 mg/kg 投与動物小脳　(P16)

B

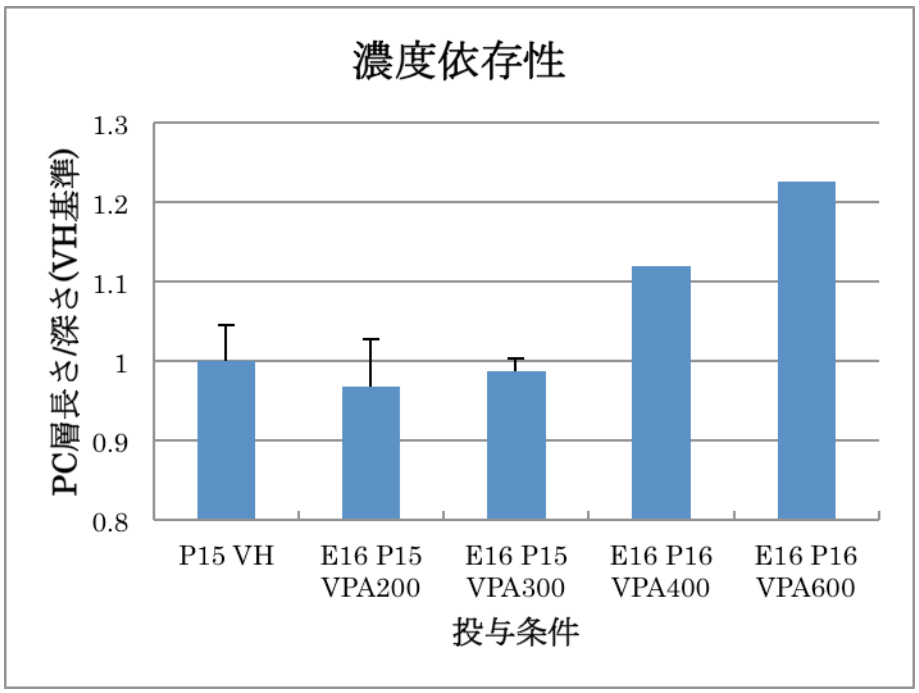

C

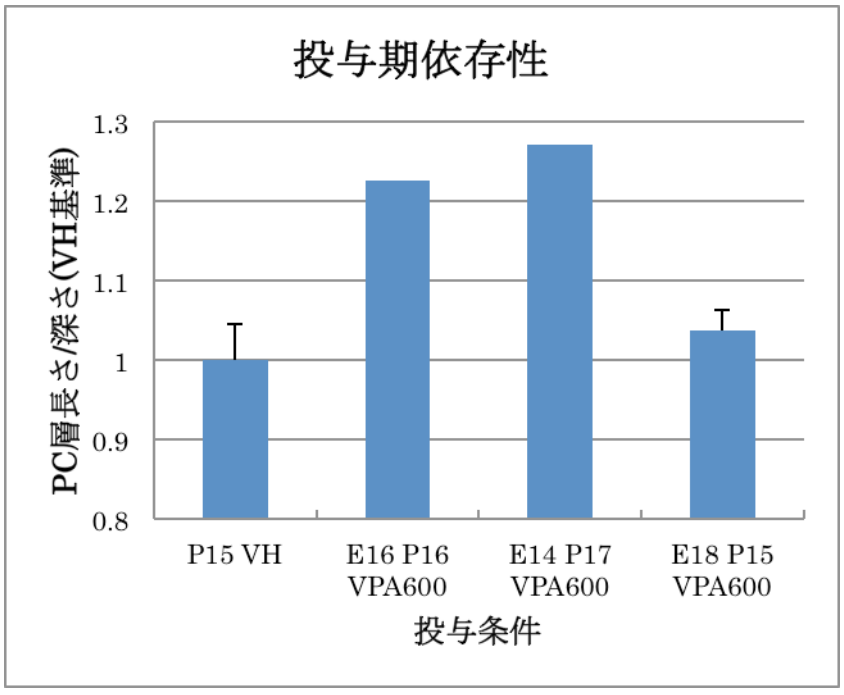

図 2　各条件で VPA を投与した動物の小脳虫部

(A)　小脳虫部褶曲構造の変化
(B)　VPA の投与濃度による小脳虫部の褶曲度の変化
(C)　VPA の投与時期による小脳虫部の褶曲度の変化

A

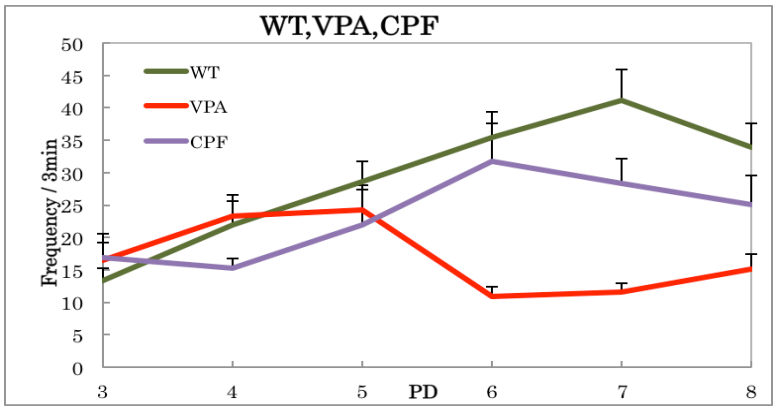

B

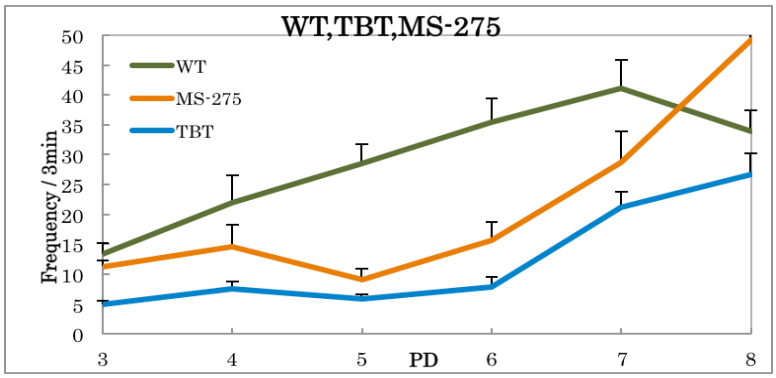

C

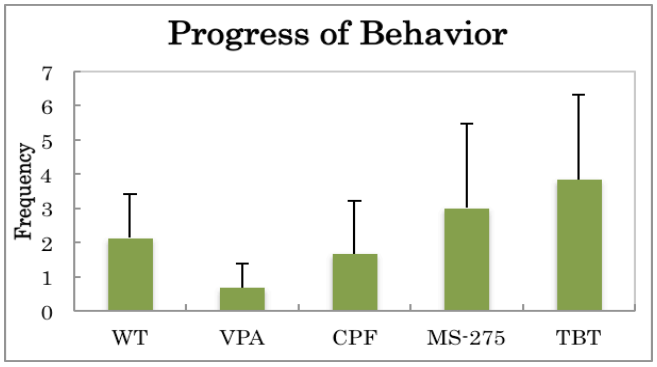

図 3　VPA, CPF, TBT, MS-275 投与動物の生後１０日程度の不随意運動の発生頻度

(A)VPA は対照動物よりも早く不随意運動の低下が見られる。
(B)TBT や MS-275 ではむしろ遅くなる。
(C)運動の頻度変化をしめす。

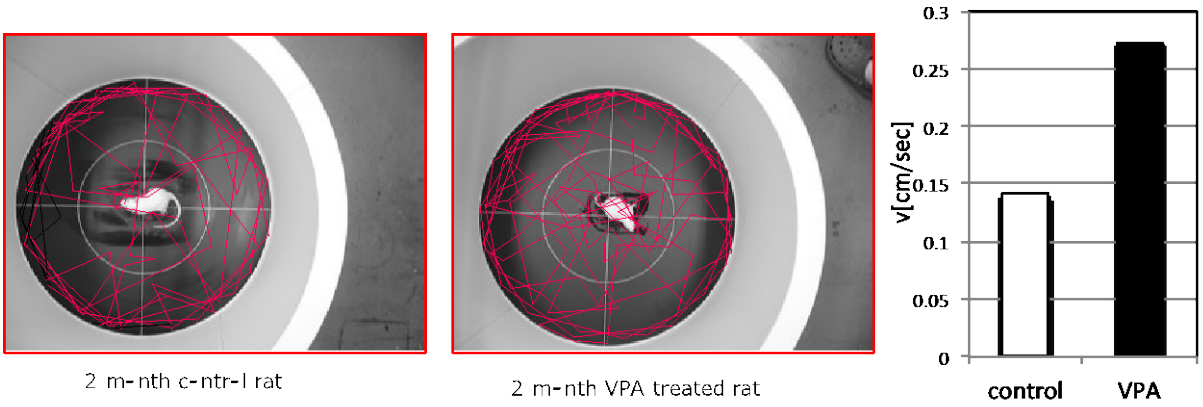

生後2ヶ月　物の3分間の移　軌跡と、移　の平均速度

図 4　　生後 2 ヶ月の動物の 3 分間の移動軌跡と移動の平均速度

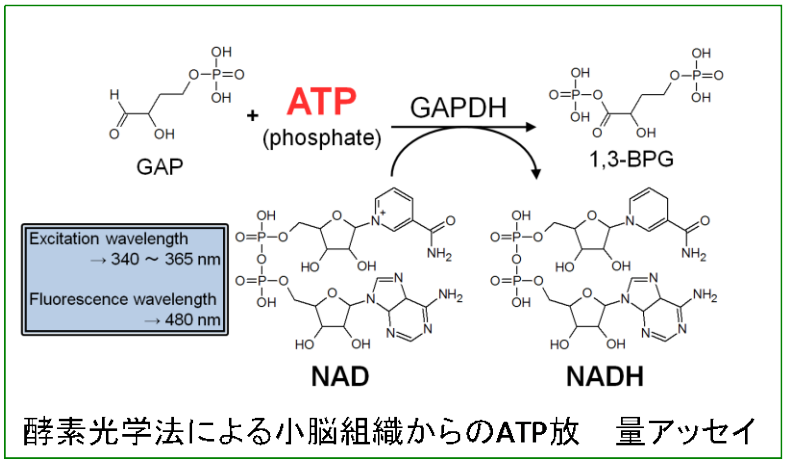

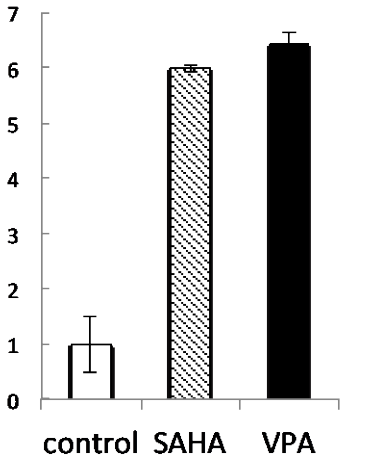

図 5　生後 11 日のグルタミン酸誘発性 ATP 放出

厚生労働科学研究費補助金（化学物質リスク研究事業）
分担研究報告書

幼若期海馬の神経回路機能による評価法の開発

研究分担者　産業医科大学　産業生態科学研究所　教授
上野　晋
研究協力者　産業医科大学　産業保健学部　講師
笛田　由紀子
研究協力者　豊橋技術科学大学　環境・生命工学系　講師
吉田　祥子

要旨
本研究班が提案してきた遅発性神経毒性試験手法の妥当性を調べる目的で、産業化学物質 1-ブロモプロパン（1BP）を検討した。1BP については生殖毒性や神経毒性などが報告されているが、発達神経毒性は未だ不明である。そこで妊娠ラットに対して 1BP の吸入曝露を行い、産まれた仔ラットの成長に伴う海馬神経回路機能の発達を検討した。その結果、1BP 胎生期曝露により神経回路機能の興奮性が授乳期に亢進すること、成長後にはその回路におけるフィードバック抑制機能が減弱することが判明した。特に前者については、神経細胞の入出力特性がロジスティック方程式を用いて総合的に評価できる可能性も見出した。これらの結果より、1BP が遅延性の神経毒性を有する可能性が示唆され、さらに産業化学物質についてもその遅延性神経毒性の評価指標として、生後早期の海馬神経回路機能評価が有用となる可能性が確認された。

A．研究目的

我々はこれまでに胎生期・神経発達期の化学物質曝露に起因する生後の遅発性神経毒性を評価する in vitro 試験法の開発を目指し、作用の異なる神経毒性物質（自閉症モデル動物作製に用いられるバルプロ酸、内分泌かく乱作用を示す有機スズ化合物、有機リン系農薬クロルピリホス）を用いて、海馬神経回路機能に対する影響を指標とした発達期の神経毒性評価を行ってきた。この知見をもとに、当分担研究班では発達神経毒性が不明な産業化学物質 1-ブロモプロパン（1BP）を妊娠ラットに吸入曝露させ、産まれた仔ラットから脳スライス標本を採取し、神経回路異常の有無について電気生理学的手法による検証を行った。

B．研究方法

1．1BP の吸入曝露（研究協力者　笛田由紀子）

Wistar 系妊娠ラットに対して、曝露チャンバー内で 1BP を濃度 400、700 ppm で 1 日 6 時間、妊娠 1～20 日目まで反復吸入曝露を行った。対照群には同様のチャンバーで新鮮空気を供与した。

2．刺激応答性とフィードバック抑制の電気生理学的評価法（研究協力者　笛田由紀子）

図 1 の実験プロトコルに示すように、反復吸入曝露を行った妊娠ラットより得られた雄性仔ラットの生後 2 週齢～13 週齢時に、深麻酔下断頭したのち速やかに海馬を取り出した。ティッシュチョッパー（McIlwain tissue chopper）を用いて、すべての日/週齢について厚さ 600 μm の海馬スライス標本を両側の背側海馬（海馬長軸の中央あたり）から作製した。

バルプロ酸投与実験と同様に、刺激電極と記録電極を海馬スライスに設置した後（図 2）、CA1 領野の錐体細胞層からは集合スパイク電位を、シナプス層から集合興奮性シナプス

後電位を記録して神経回路興奮性および興奮性シナプス強度を評価した（図 3）。

評価法は、10 μA～600 μA の電気刺激を与えた時の神経細胞の応答性の発達に伴う変化を、2 週齢（13～15 日齢）については対照群と 400/700 ppm 曝露群の間で、5 週齢、8 週齢および 13 週齢については対照群と 700 ppm 曝露群との間で比較した。2 週齢の神経細胞の入出力特性とは、神経細胞への入力を集合興奮性シナプス後電位の傾き（fEPSP slope）とし、出力をその神経細胞群が発生する集合スパイク電位（PS）の振幅とした。この入出力特性は、ES coupling と称されており、例えばシナプスの長期増強時には、ES coupling の亢進現象（ES potentiation）が観察される。本研究でもこの ES coupling を定量的に評価するために、後述するロジステイック方程式で回帰曲線を求めた（図 4）。

遅延性発達毒性評価には、刺激応答性に加えて、2 連続刺激で誘発される誘発電位から計算されるフィードバック抑制系の機能評価を指標とした。このフィードバック抑制系が形成されていれば、2 回目の刺激に対する応答は 1 回目の刺激に対する応答よりも小さくなる。つまり、2 回目の応答の大きさを 1 回目の応答の大きさで除した比（ペアパルス応答比）は 1 よりも小さい値となる。さらにペアパルス応答比が 1 よりも小さい場合には、この抑制系機能の強さをその比の大きさで定量的に評価できるという面もあり、簡便な評価指標ともいえる。そこで神経細胞層へのフィードバック抑制の強さを、2 回目の PS の振幅を 1 回目の PS の振幅で除して数値化して評価した。

3. ロジステイック方程式による ES coupling の解析

解析には GraphPad Prism 6（GraphPad Software, La Jolla, CA, USA）を用い、5 パラメーターロジステック式で非線形回帰を行った。最大値は 600 μA 電気刺激における PS 振幅値が最大値の 90%と仮定し（Top）、最小値は PS 振幅値を 0 mV（Bottom）として固定した。この最大値の半分の値を示す fEPSP slope 値（量反応曲線における EC_{50} に相当する）、傾斜因子（Hill Slope）、および非対称性を定量化するパラメータ S、の 5 種類のパラメータで解析をした。

（倫理面への配慮）

本研究の遂行にあたっては、産業医科大学に定められた、関係する遵守すべき指針等を把握して、十分な管理体制のもと、倫理面に万全の配慮をした。

C. 研究結果

これまで検討してきたバルプロ酸の胎生期曝露による神経発達への影響と類似して、1BP の胎生期曝露でも濃度 400 ppm から興奮性シナプス強度の増強、ならびに神経回路の刺激応答性の亢進が生後 2 週齢、特に 14 日齢で認められた。またこの亢進現象を評価するに当たり、集合興奮性シナプス後電位と集合スパイク電位とから得られるロジステイック曲線が有用であること可能性を見出した（図 5）。ところが授乳期に観察された刺激応答性の亢進は 5 週齢以降には観察されず、1BP 曝露群は対照群と同程度の刺激応答性を示していた。

ペアパルス応答比によるフィードバック抑制機能の評価において、1BP 胎生期曝露により性成熟後にフィードバック抑制機能が減弱することも判明した（図 6、7）。

D. 考察

バルプロ酸胎生期曝露ラットで見出した現象と類似した生後 2 週齢における海馬神経回路興奮性の亢進が、1BP の胎生期曝露ラットにおいても、曝露濃度 400 ppm から認められた。このことより、1BP も発達神経毒性を有する化学物質である可能性が示唆された。さらに、入出力特性の亢進は、ES coupling のデータをロジステイック曲線で回帰して得られるパラメータの比較によって定量化することができることが判明した。

性成熟後の海馬においては、刺激応答性が対照群と 1BP 曝露群とでは同程度であったが、フィードバック抑制機能が 1BP 曝露群で減弱していた。抑制系の減弱は中枢神経系の興奮性のバランスを不安定にすることから、てんかんのような中枢神経系の過剰興奮を病態とする疾患の素因となり得ることが動物やヒトでも報告されている。1BP の胎生期曝露により成熟後のフィードバック抑制系が減弱したことから、1BP が遅延性神経毒性を有する化学物質である可能性が示唆された。

成獣ラットを用いた 1BP の亜慢性曝露による中枢神経毒性の検討において、海馬神経回路のフィードバック抑制という指標についての NOAEL（無毒性量）は 200 ppm であり、LOAEL（最少毒性量）は 400 ppm であることが報告されている（Fueta et al, 2007）。これは成熟した脳に対しての NOAEL あるいは LOAEL ともいえる。一方、本研究は胎生期曝露という、化学物質曝露に対して一般的に脆弱であると考えられる時期での曝露を行っているが、今回得られた LOAEL は成熟脳と同程度の 400 ppm であった。ただし、亜慢性曝露の場合と胎生期曝露の場合とでは曝露期間が異なるため（前者は 6 時間/日、5 日/週、12 週間）、累積曝露量としては亜慢性曝露の場合が多いことが想定される。したがって、LOAEL が同程度であったとしても、1BP に対する感受性はやはり胎生期の脳が高いと考えられる。

1BP については、本邦で許容濃度（0.5 ppm）がすでに日本産業衛生学会により勧告されているものの、その提案理由の中に発達神経毒性は考慮されていない。一方、米国における曝露限界値（0.1 ppm）には、ヒトの事例は認められないものの動物実験データに基づく発達毒性が考慮されている (7th Edition *Documentation,* Product ID: 7DOC-730)。発達神経毒性が出現した 400 ppm を LOAEL として、ヒトへの推定を試みると種差、個体差、LOAEL から NOAEL の推定等の不確実係数をすべて 10 として考慮した場合には 0.4 ppm となり、上記の基準値とは大きく矛盾しない。不確実係数の値には議論の余地があるものの、産業化学物質の発達神経毒性評価にも本研究で用いた評価手法が応用できれば、新規化学物質の許容濃度の提案の際の情報提供はもちろんのこと、1BP のようにすでに勧告された許容濃度に対して、発達神経毒性を考慮した場合の妥当性の検証などに有用となることが期待される。

今回の曝露条件については、1BP の産業現場における曝露様式が主に吸入曝露であることを想定し、また曝露濃度および曝露期間については、先行研究（Fueta et al, 2007 ; Ishidao et al, 2016）を参考にした。バルプロ酸や有機スズ化合物の評価を行った時のように妊娠後期における単回曝露という様式でも産業化学物質が評価できるかどうかは今後の検討課題である。

また、授乳期の神経回路興奮性の亢進には抑制性神経伝達が関連している可能性があり、その分子メカニズムについては現在免疫組織化学的手法で検討中である。さらに、バルプロ酸の投与時期によって、授乳期の神経回路興奮性への影響が変化するのかどうかも現在検討中である。

E．結論

発達神経毒性の詳細が不明であった産業化学物質である 1BP について検討した結果、授乳期での神経回路興奮性に対して亢進作用を示したことから、1BP が発達神経毒性を有する可能性が示唆された。

F．研究発表

1．論文発表

[1] Fueta Y., Sekino Y., Yoshida S., Kanda Y., Ueno S. “Prenatal exposure to valproic acid alters the development of excitability in the postnatal rat hippocampus.” NeuroToxicology (2018) 65:1-8

[2] Fueta Y., Ishidao T., Ueno S., Yoshida Y., Kanda Y., Hori H. “Prenatal exposure to 1-bromopropane causes delayed adverse effects on hippocampal neuronal excitability in the CA1 subfield of rat offspring.” J Occup Health. (2018) 60:74-79

2．学会発表

[1] 笛田由紀子、石田尾徹、吉田祥子、保利一、諫田泰成、上野晋：産業化学物質 1-ブロモプロパンの遅発性発達神経毒性評価、第 44 回日本毒性学会学術年会、2017 横浜

[2] Iwamoto S., Tomida T., Nakajima S., Fueta Y., Ueno S., Sekino Y., Maev R., Hozumi N., Yoshida S. : Maturation-dependent alteration of cerebellar structure in maturated autistic model rat, 第 40 回日本神経科学大会、2017 千葉

[3] 笛田由紀子、石田尾徹、吉田祥子、関野祐子、諫田泰成、保利一、上野晋：化学物質の胎生期曝露がもたらす発達神経毒性の評価－授乳期ラット海馬スライスを用いた神経細胞の応答特性の検討、第 6 回日本 DOHaD 学会学術集会、2017 東京

[4] Ueno S., Fueta Y. : Developmental neurotoxicity evaluation: Studies on neural

network activity at synaptogenic period, 第60回日本神経化学会大会、2017 仙台

[5] Miyamoto K., Mikami T., Fueta Y., Ueno S., Sekino Y., Kanda Y., Hozumi N., Yoshida S. : Alteration of GABA release in developing cerebellar cortex of VPA-administrated autistic model rat, 第60回日本神経化学会大会、2017 仙台

[6] Mikami T., Fueta Y., Ueno S., Sekino Y., Kanda Y., Hozumi N., Yoshida S. : Alteration of neurotransmitter release in cerebellar cortex of Valproate-administrated Autistic model rat, 第60回日本神経化学会大会、2017 仙台

[7] Sato S., Fueta Y., Ueno S., Sekino Y., Kanda Y., Yoshida S. : Alteration of neural circuit with autism-inducing drug administration in developing rat cerebellum, 第60回日本神経化学会大会、2017 仙台

[8] Ikai K., Nakajima S., Tomida T., Ueno S., Sekino Y., Kanda Y., Yoshida S. : Recovery effects from chemical-induced autistic degeneration with bumetanide or oxytocin in developing rat cerebellum, 第60回日本神経化学会大会、2017 仙台

[9] Yoshida Y., Fueta Y., Ueno S., Hozumi N., Sekino Y., Kanda Y. : Structual and functional alteration of developing rat cerebellum by administration of autism-inducing drugs, 10th DOHaD world congress, 2017, Rotterdam

[10] 笛田由紀子、石田尾徹、上野晋、吉田祥子、諫田泰成、保利一：1-ブロモプロパンのラット胎生期曝露は遅延性発達神経毒性をひきおこす、第 91 回日本産業衛生学会、2018 熊本（発表予定）.

G. 知的財産権の出願・登録状況

該当なし

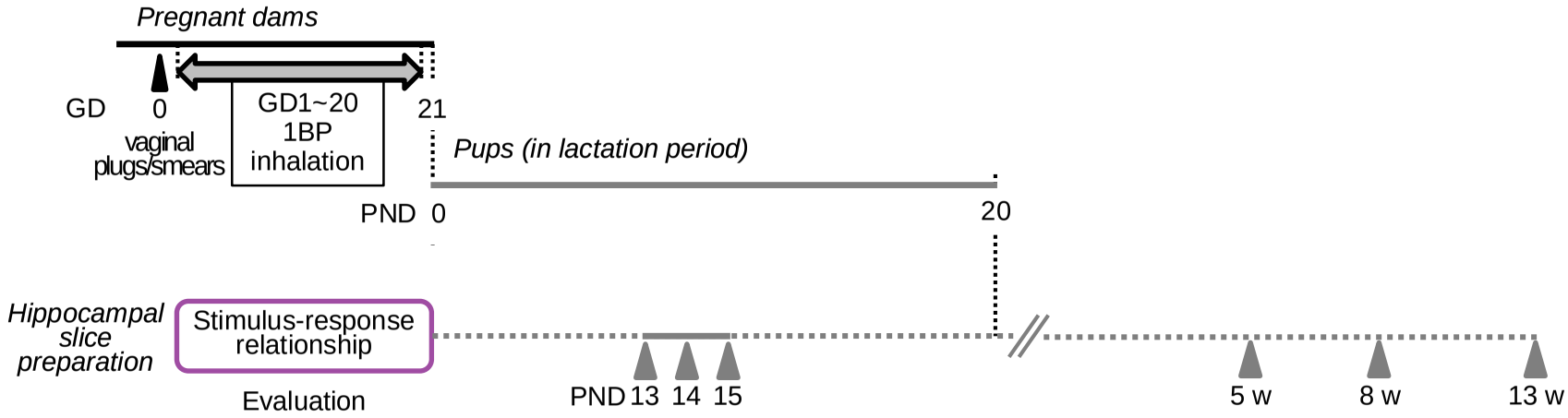

図 1　海馬スライスを用いた電気生理学的手法による発達神経毒性評価のためのプロトコル

ラットの妊娠 1 日目から 20 日目までの連続 20 日間、産業化学物質 1BP の吸入曝露（400/700 ppm、6 時間/日）を行った。開眼前の生後 13、14 日および開眼が始まる生後 15 日の 3 日間に、連続して海馬スライス標本を作製して発達神経毒性の評価を行った。さらに、成長後の影響を調べるために、離乳後の幼若期（5 週齢）、性成熟後（8 週齢）、 成獣期（13 週齢）の 3 点で遅延性の神経毒性の有無を調べた。

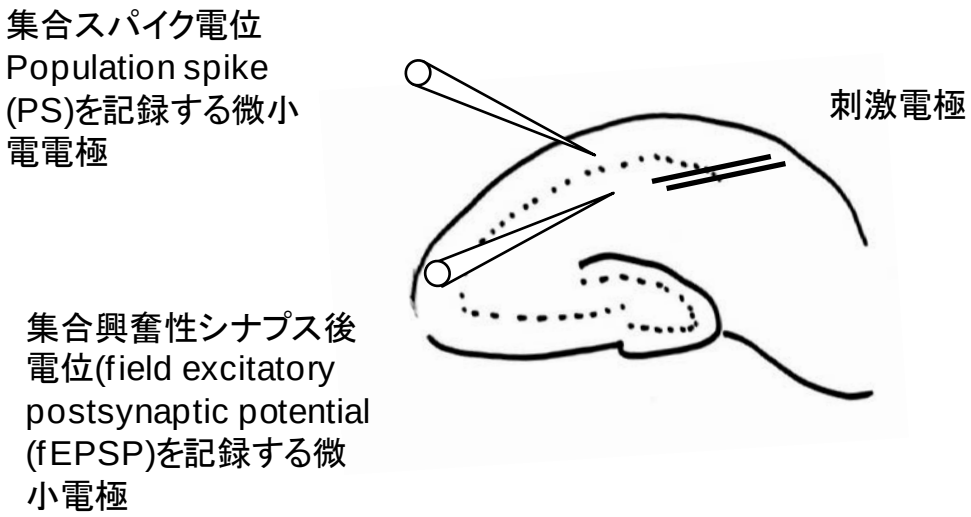

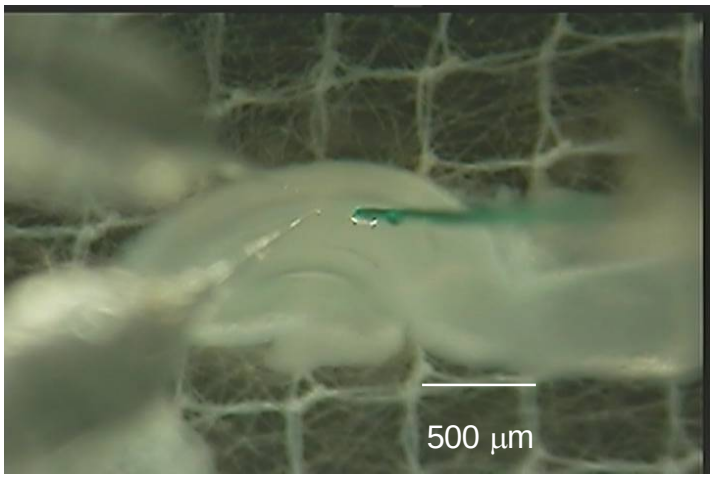

図２　発達神経毒性評価法のための海馬スライスを用いた電気生理学的手法

上図：海馬スライスにおける双極性電気刺激電極と２つの記録用ガラス微小電極の位置を示す。下図：実体顕微鏡下に撮影した生の海馬スライスと、刺激電極（左）および記録用ガラス微小電極（左）の配置。

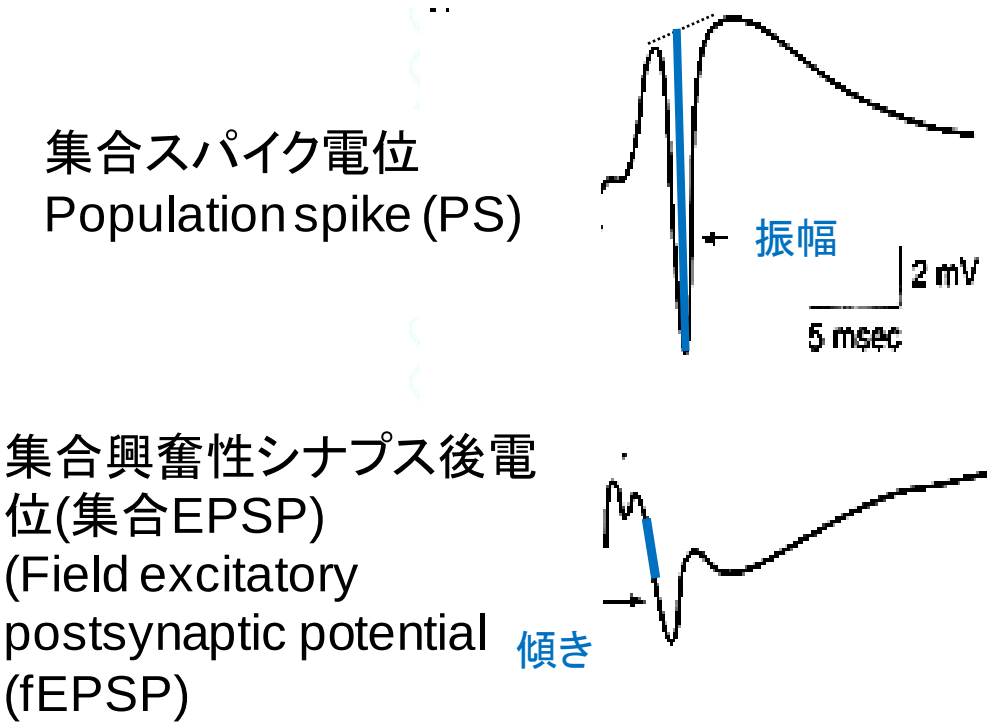

図 3　発達神経毒性評価の指標とする集合スパイク電位(PS)の振幅～回路興奮性を反映～と集合興奮性シナプス後電位の傾き(fEPSP slope)～興奮性シナプス強度を反映～の計測方法

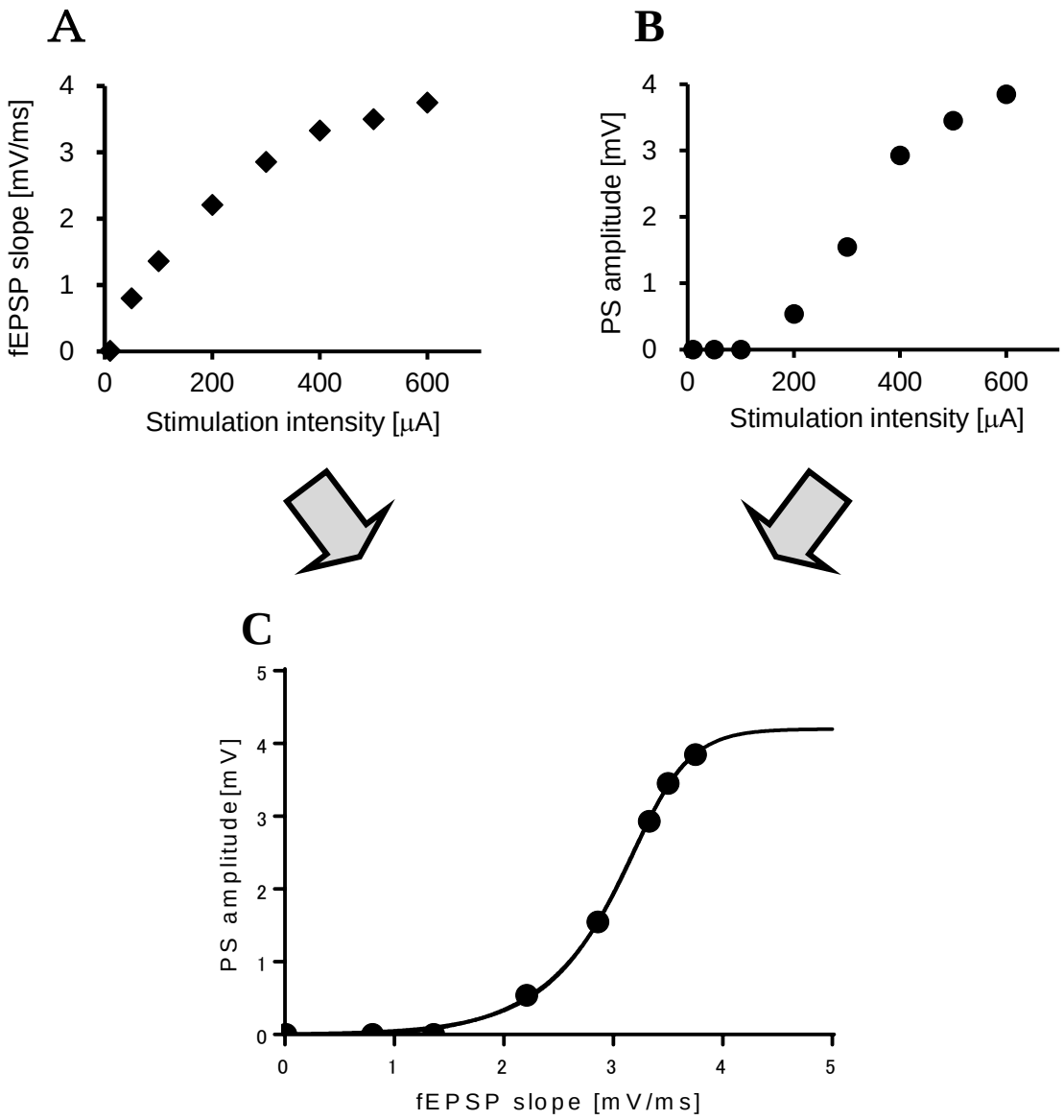

図 4　fEPSP-spike (E-S) coupling と　その非線形回帰モデル

A: 電気刺激の大きさに対する集合興奮性シナプス後電位の傾き(fEPSP slope)

B: 電気刺激の大きさに対する集合スパイク電位の振幅(PS amplitude)

C: fEPSP-spike (E-S) coupling のグラフ。

集合興奮性シナプス後電位の傾き(fEPSP slope)に対する集合スパイク電位の振幅(PS amplitude)の変化を示しており、スライス 1 枚ごとの神経細胞群の入出力特性を一つのグラフで表現できる。回帰曲線は 5 パラメータロジステイック回帰曲線である。データは 700 ppm 群の 1 例である。

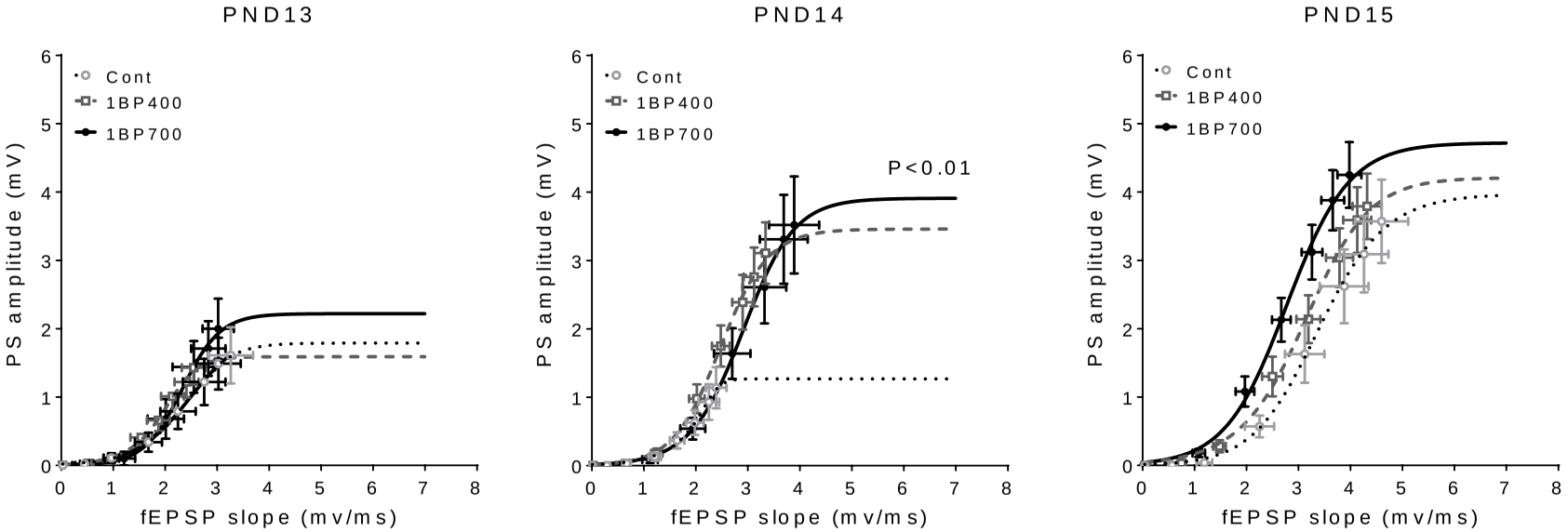

図 5　1BP 胎生期曝露による海馬刺激応答性の ES coupling とロジステイック曲線

PS 最大値（PSmax)、非線形回帰における 50%-PSmax 値の時の fEPSP slope 値、およびその座標における曲線の傾き（Hill 係数）において、 PND14 では対照群と 1BP 曝露群（400 および 700 ppm）との間に統計学的な有意差を認めた。

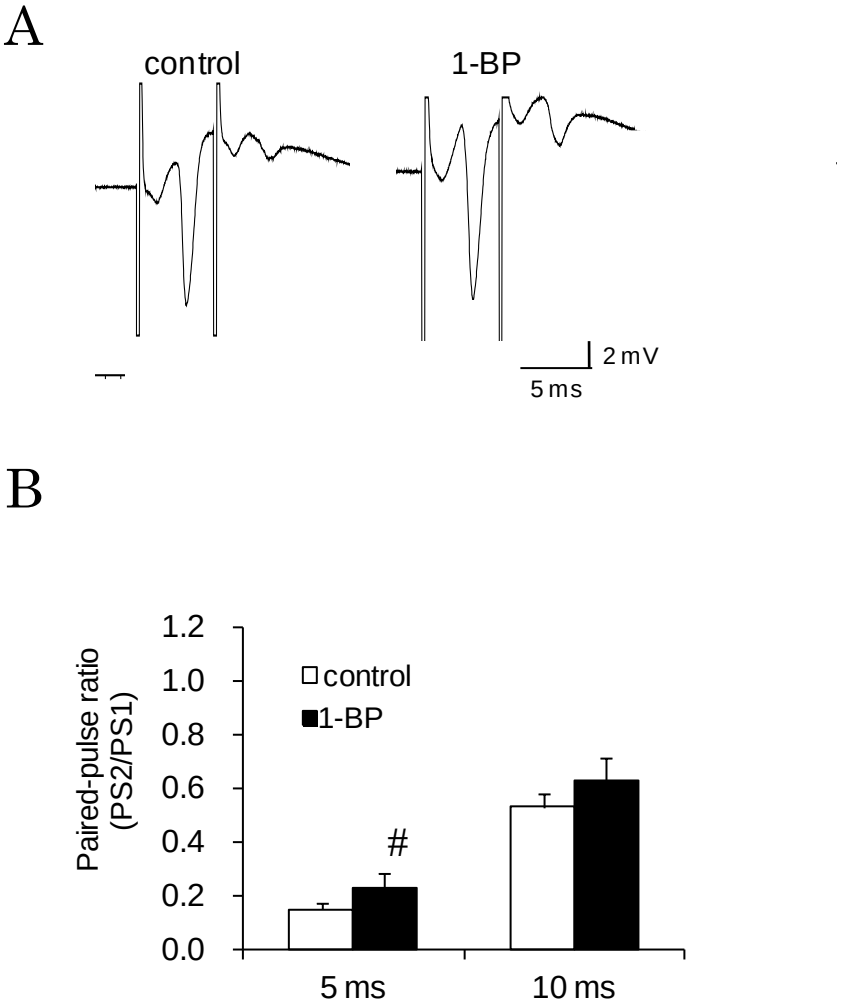

図 6　1BP 胎生期曝露ラット（8 週齢）の海馬におけるフィードバック抑制の減弱

刺激間隔 5 ms と 10 ms で誘発される PS1 と PS2 の振幅の比から、フィードバック抑制を評価した。A: 刺激間隔 5 ms において、対照群、1BP ともに、2 回目の刺激で誘発される PS 振幅は小さくなった。両群ともにフィードバック抑制が機能していることを示す。B: しかし、1BP 群では対照群と比較して、PS2/PS1 が有意に増加していることから（＃$p<0.05$ by Mann-Whitney U test）、フィードバック抑制が減弱していることが判明した。

A

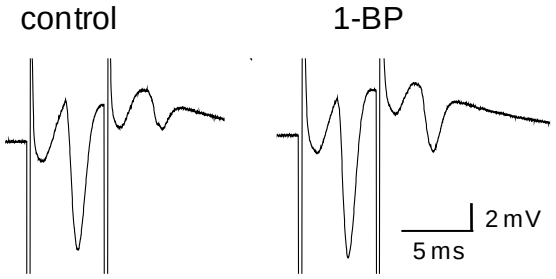

B

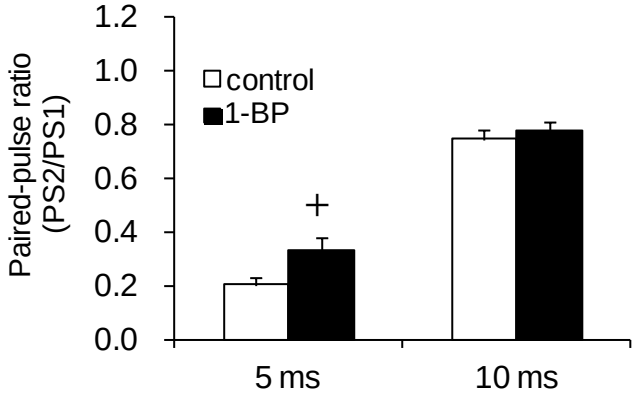

図 7　1-BP 胎生期曝露ラット（13 週齢）の海馬におけるフィードバック抑制の減弱

A: 8 週齢と同様に、刺激間隔 5 ms において、対照群、1BP ともに、2 回目の刺激で誘発される PS 振幅が小さくなったことから、両群ともにフィードバック抑制が機能していることを示す。B: しかし、対照群と比較して、1BP 群では PS2/PS1 が有意に増加していることから（＃$p<0.05$ by Welch's *t*-test）、8 週齢同様にフィードバック抑制の減弱が継続していることが示唆された。

厚生労働科学研究費補助金（化学物質リスク研究事業）
分担研究報告書

既存の毒性データおよびヒトデータとの検証

研究分担者　　国立研究開発法人国立成育医療研究センター研究所
周産期病態研究部　部長
秦　健一郎

要旨
近年、妊娠中の母親への摂取栄養の程度や栄養成分の偏りによって、胎児のエピゲノムに影響し、生後の発育や疾患の発症に寄与するという DoHaD（ Developmental Origins of Health and Disease）のコンセプトが提唱されており、そのメカニズムについて明らかになりつつある。本研究では動物実験を中心に DoHaD のメカニズムについて文献調査を行った。また、ヒトのエピゲノムデータに関しても調査を開始した。

A. 研究目的

本研究では動物実験を中心に DoHaD のメカニズムについて文献調査を行った。また、ヒトのエピゲノムデータに関しても調査を開始した。

B. 研究方法

DoHaD コンセプトをもとに動物実験によりメカニズムの解析を行っている文献を調査した。また、ヒトのエピゲノムデータを解析している文献についても調査研究を行った。

C. 研究結果

調査研究の結果を、以下に記載する。

（1）胎仔期・新生仔期の外因性内分泌かく乱物質への暴露が精子のインプリント領域 DNA メチル化異常を誘引し、その精子で受精した胚は最終的に流産あるいは不妊・不育症の原因となる（Guerrero-Bosagna et al. Curr Opin Genet Dev. 2014）。広く環境中に存在する合成エストロゲンのビスフェノール A（BPA）の新生仔期への暴露により、H19 インプリント領域の有意な低メチル化と遺伝子発現異常が認められ、かつこのラットの精子で受精した胚は着床後胚損失が生じた（Doshi et al. Mol Biol Rep. 2013）。農業用の防カビ剤の成分であるビンクロゾリンの胎仔の生殖腺の性分化が行われる時期の妊娠中雌ラットへの暴露は、胎仔の精子エピジェネティック異常と精子形成細胞のアポトーシスが 3 世代後まで遺残する（Anway et al. Science. 2005）。世代を超えたエピジェネティクス異常がいくつかのインプリント領域で生じる一方、世代を超えるごとに徐々に正常化する（Stouder et al. Reproduction. 2010）。ビンクロゾリン暴露による精子エピジェネティックへの影響は、胎生期の中でも始原生殖細胞ゲノムの DNA メチル化が一度すべて消去される時期での暴露が顕著（Skinner et al. PLoS ONE. 2013）。

（2）ヒト血中レベルの BPA の妊娠期間中マウスへの暴露は、出生直前（E18.5）の雌胎仔マウスの脳内の DNA メチル化酵素 Dnmt1 と Dnmt3a 量減少とグルタミン酸トランスポーター Slc1a1 発現を上昇させた

（Wolstenholme et al. PLoS One. 2011）。子宮内の BPA 暴露によって生後 28 日目の雌仔マウスの海馬 Bdnf の発現が上昇し、一方で雄仔マウスが減少。この影響は雌雄ともに生後 60 日目まで確認され、雄マウスの発現低下は Bdnf プロモータの高メチル化と連動していた。さらに、ヒトにおいても妊娠中の血中の BPA 濃度が高かった母親から生まれた男児の臍帯血 DNA で BDNF のメチル化が高くなった（Kundakovic et al. Proc Natl Acad Sci U S A. 2014）。最近の報告では、人体に影響はないといわれている濃度以下での動物実験において、妊娠中の BPA 暴露が新生仔の脳内の遺伝子発現を変化させている。影響に性差が認められる結果は一致しており、新生雌ラットでは、視床下部におけるエストロゲンレセプターα、βの発現と、海馬と視床下部のオキシトシンの発現が上昇していた。一方新生雄ラットでは海馬のオキシトシンの発現が減少していた（Arambula et al. Endocrinology. 2016）。妊娠中の BPA 暴露の影響は、孫世代の仔の行動異常にも認められた（Wolstenholme et al. Horm Behav. 2013）。

（3）妊娠中の喫煙はヒト臍帯血の解毒や免疫機能に関わる遺伝子（AHRR、MYO1G、CYP1A1、CNTNAP2 など）のメチル化を変化させ、この変化は 17 歳時点の血液中でも継続した（Richmond et al. Hum Mol Genet. 2015）。

（4）妊娠中のアルコール摂取が DNA メチル化をはじめエピジェネティック制御に及ぼす影響についても、動物モデルからヒト培養細胞を用いた解析、胎児性アルコール・スペクトラム障害（FASD）検体の解析までと、広く報告されている。アルコールは DNA メチル化酵素 DNMT1 の活性を低下させ、全体のメチル化レベルを抑制することが明らかにされており（Garro et al. Alcohol. Clin. Exp. Res. 1991）、この結果は、マウスの妊娠中のアルコール曝露実験でも、神経幹細胞のメチル化獲得の遅延として確認されている（Chen et al. PLoS One. 2013）。FASD である 3-6 歳の幼児の頬粘膜上皮細胞の DNA メチル化解析の結果、protocadherin 遺伝子上でクラスターを形成して 21 か所のメチル化サイトが高メチル化していること、メチル化変化が認められた遺伝子群は、hippo signaling, glutamatergic synapse, calcium signaling と神経細胞の機能を示唆するパスウェイ上の遺伝子で有意に濃縮されていることが認められている（図 1）(Laufer et al. Epigenomics 2015)。

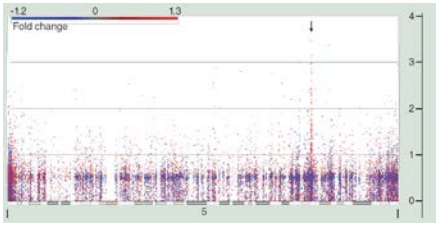

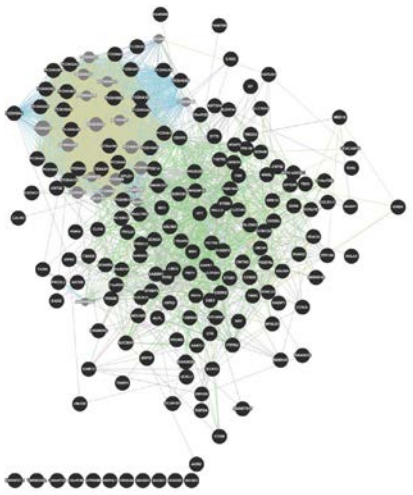

図 1 胎児性アルコール・スペクトラム障害患児に共通してメチル化変化が認められた遺伝子。*PCDHG* 遺伝子クラスターに集中して変化が認められた。（Laufer et al.より）

さらに多検体の FASD の児童を解析した報告でも、FASD の頬粘膜上皮細胞で有意に高メチル化していた遺伝子群に protocadherin 遺伝子が認められ、neurodevelopmental processes や anxiety, epilepsy, autism spectrum disorders に関連した遺伝子が有意に濃縮されていたことを明らかにした（Portales-Casamar et al. Epigenetics Chromatin 2016）。

（5）妊娠中の体重変化が至適でないと（妊娠中の体重増加が 7 kg 未満あるいは 12kg 以上だと）、出生児の胎盤の DNA メチル化状態に外れ値が多く観察された (図 2)（Kawai et al. SciRep.2015）。体重変化が至適でない妊婦では、何らかの栄養状態の偏りがあったと

推測されるが、その環境ストレスは胎児に影響を与えた結果、DNA メチル化値の外れ値の多寡（≒エピゲノムの「乱れ」）を引き起こしたと考えられる。妊娠中の体重増加が不適切な検体のなかの 3 例で、胎盤の GABA receptor subunit 遺伝子にメチル化外れ値が検出されたことより(図 3)、神経発生においても子宮内環境が同遺伝子のエピジェネティック制御に影響し、異常な発達に関与するかもしれない可能性が示唆された。

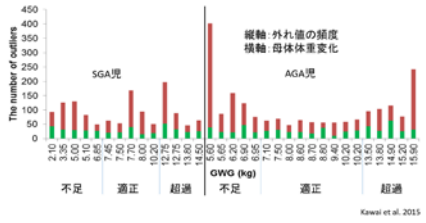

図 2 妊娠中の体重変化が至適でないと、出生児の体重は正常であっても、胎盤の DNA メチル化状態に外れ値が多く観察された。

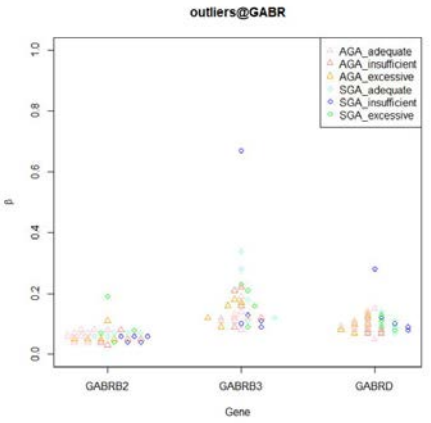

図 3 妊娠中の体重増加が不適切な検体のなかの 3 例で、胎盤の GABA receptor subunit 遺伝子にメチル化外れ値が検出された

D. 考察

上記の調査研究により、以下のことが示唆された。

・胎仔期・新生仔期の環境要因の影響が出生後も持続して認められる。

・発生段階の脳では、一過性の発現変化も結果的に不可逆的な脳機能変化を引き起こし、これは初期エピジェネティックな調節異常が遺残するためである。

・始原生殖細胞における親由来 DNA メチル化情報の消去が正常に行われることが生殖能力に重要。

・発生段階の脳において、外因性内分泌かく乱物質暴露によるエピジェネティック異常に伴う機能異常が生じる。

・発生初期の子宮内における環境要因の影響が、脳の発達においてエピジェネティックな制御を介し生後遺残する可能性。

・ヒトでもこれらのエピゲノム変化が起こる可能性。

・ヒトの子宮内環境の影響は、神経細胞以外の細胞でも、神経細胞の機能に関連する遺伝子の DNA メチル化変化として発達後も確認される。

E. 結論

調査研究により、胎児期あるいは新生児期に受けたことにより、ゲノムのメチル化が生じ生後長期に渡って継続し、疾患リスクとなる可能性が示唆された。

F. 研究発表

1. 論文発表

[1] Urushiyama D., Suda W., Ohnishi E., Araki R., Kiyoshima C., Kurakazu M., Sanui A., Yotsumoto F., Murata M., Nabeshima K., Yasunaga S., Saito S., Nomiyama M., Hattori M., Miyamoto S., Hata K. “Microbiome profile of the amniotic fluid as a predictive biomarker of perinatal outcome.” Sci Rep. (2017) 7:12171

[2] Kawai T., Hata K. “Reproductive/Developmental Abnormalities Induced by Epigenetic Aberrations and Possible Environmental Causes.” Nihon Eiseigaku Zasshi. (2016) 71:195-199

[3] Ito Y., Maehara K., Kaneki E., Matsuoka K., Sugahara N., Miyata T., Kamura H., Yamaguchi Y., Kono A., Nakabayashi K.,

Migita O., Higashimoto K., Soejima H., Okamoto A., Nakamura H., Kimura T., Wake N., Taniguchi T., Hata K. “Novel Nonsense Mutation in the NLRP7 Gene Associated with Recurrent Hydatidiform Mole.” Gynecol Obstet Invest. (2016) 81:353-358

[4] Nohara K., Okamura K., Suzuki T., Murai H., Ito T., Shinjo K., Takumi S., Michikawa T., Kondo Y., Hata K. “Augmenting effects of gestational arsenite exposure of C3H mice on the hepatic tumors of the F2 male offspring via the F1 male offspring.” J Appl Toxicol. (2016) 36:105-112

[5] Kawai T., Yamada T., Abe K., Okamura K., Kamura H., Akaishi R., Minakami H., Nakabayashi K., Hata K. “Increased epigenetic alterations at the promoters of transcriptional regulators following inadequate maternal gestational weight gain.” Sci Rep. (2015) 5:14224

2. 学会発表

[1] 秦健一郎：DOHaD theory in human cases: Inheritable epigenetic changes caused by environmental factors, 第60回日本神経化学会、2017 仙台

[2] 秦健一郎:『ART と DOHaD の相互理解と将来への展望』-生命誕生とエピジェネティクス、第 35 回日本受精着床学会総会・学術講演会、2017 米子

[3] 秦健一郎:DOHaD をひろげるために、DOHaD 研究会学術集会長講演、2016 東京

[4] 秦健一郎：Inadequate maternal gestational weight gain increased epigenetic alterations at the promoters of transcriptional regulators in placenta, Joint Japan-New Zealand DOHaD Researchers Seminar, 2016, Auckland

G. 知的財産権の出願・登録状況

該当なし

研究成果の刊行に関する一覧表

雑誌

発表者氏名	論文タイトル名	発表誌名	巻号	ページ	出版年
Yamada S., Kubo Y., Yamazaki D., Sekino Y., Nomura Y., Yoshida S., Kanda Y.	Tributyltin Inhibits Neural Induction of Human Induced Pluripotent Stem Cells.	論文投稿中			
Yamada S., Yamazaki D., Kanda Y.	5-Fluorouracil inhibits neural induction via Mfn1/2 reduction in human induced pluripotent stem cells.	論文投稿中			
Yamada S., Kubo Y., Yamazaki D., Sekino Y., Kanda Y.	Chlorpyrifos inhibits neural induction via Mfn1-mediated mitochondrial dysfunction in human induced pluripotent stem cells.	Sci Rep.	7	40925	2017
Yamazaki D., Kanda Y., Sekino Y.	Field potential recording method using multi-electrode array system-Cellular responses in human iPSC-derived cardiomyocytes and rodent brain-derived neurons-.	BUNSEKI	7	290-295	2017
Mabuchi H., Ong HY., Watanabe K., Yoshida S., Hozumi N.	Visualization of Spatially Distributed Bioactive Molecules Using Enzyme-Linked Photo Assay.	IEEJ Trans FM.	136	99-104	2016
Takanashi K., Washiya M., Ota K., Yoshida S., Hozumi N., Kobayashi K.	Quantitative evaluation method for differentiation of C2C12 myoblasts by ultrasonic microscopy.	Jpn J Appl Phys.	56	07JF11	2017
Tiong TKS., Chean TW., Yamada H., Takahashi K., Hozumi N., Kobayashi K., Yoshida S.	Effects of anticancer drugs on glia–glioma brain tumor model characterized by acoustic impedance microscopy.	Jpn J Appl Phys.	56	07JF15	2017
Fueta Y., Sekino Y., Yoshida S., Kanda Y., Ueno S.	Prenatal exposure to valproic acid alters the development of excitability in the postnatal rat hippocampus.	Neurotoxicology	65	1-8	2018
Zhang W., Qian L., Lambertini L., Finik J., Huang Y., Tsuchiya KJ., Pehme P., Buthmann J., Yoshida S., Chen J., Nomura Y.	Timing of Prenatal Exposure to Trauma and Altered Placental Expressions of HPA-Axis Genes and Genes Driving Neurodevelopment.	J Neuroendocrinol.		in press	2018
Fueta Y., Ishidao T., Ueno S., Yoshida Y., Kanda Y., Hori H.	Prenatal exposure to 1-bromopropane causes delayed adverse effects on hippocampal neuronal excitability in the CA1 subfield of rat offspring.	J Occup Health.	60	74-79	2018

Urushiyama D., Suda W., Ohnishi E., Araki R., Kiyoshima C., Kurakazu M., Sanui A., Yotsumoto F., Murata M., Nabeshima K., Yasunaga S., Saito S., Nomiyama M., Hattori M., Miyamoto S., Hata K.	Microbiome profile of the amniotic fluid as a predictive biomarker of perinatal outcome.	Sci Rep.	7	12171	2017
Kawai T., Hata K.	Reproductive/Developmental Abnormalities Induced by Epigenetic Aberrations and Possible Environmental Causes.	Nihon Eiseigaku Zasshi.	71	195-199	2016
Ito Y., Maehara K., Kaneki E., Matsuoka K., Sugahara N., Miyata T., Kamura H., Yamaguchi Y., Kono A., Nakabayashi K., Migita O., Higashimoto K., Soejima H., Okamoto A., Nakamura H., Kimura T., Wake N., Taniguchi T., Hata K.	Novel Nonsense Mutation in the NLRP7 Gene Associated with Recurrent Hydatidiform Mole.	Gynecol Obstet Invest.	81	353-358	2016
Nohara K., Okamura K., Suzuki T., Murai H., Ito T., Shinjo K., Takumi S., Michikawa T., Kondo Y., Hata K.	Augmenting effects of gestational arsenite exposure of C3H mice on the hepatic tumors of the F2 male offspring via the F1 male offspring.	J Appl Toxicol.	36	105-112	2016
Kawai T., Yamada T., Abe K., Okamura K., Kamura H., Akaishi R., Minakami H., Nakabayashi K., Hata K.	Increased epigenetic alterations at the promoters of transcriptional regulators following inadequate maternal gestational weight gain.	Sci Rep.	5	14224	2015

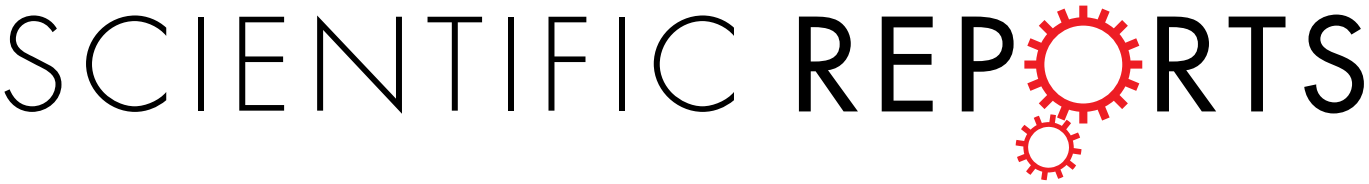

OPEN

Received: 21 October 2016
Accepted: 13 December 2016
Published: 23 January 2017

Chlorpyrifos inhibits neural induction via Mfn1-mediated mitochondrial dysfunction in human induced pluripotent stem cells

Shigeru Yamada[1,2], Yusuke Kubo[1], Daiju Yamazaki[1], Yuko Sekino[1] & Yasunari Kanda[1]

Organophosphates, such as chlorpyrifos (CPF), are widely used as insecticides in agriculture. CPF is known to induce cytotoxicity, including neurodevelopmental toxicity. However, the molecular mechanisms of CPF toxicity at early fetal stage have not been fully elucidated. In this study, we examined the mechanisms of CPF-induced cytotoxicity using human induced pluripotent stem cells (iPSCs). We found that exposure to CPF at micromolar levels decreased intracellular ATP levels. As CPF suppressed energy production that is a critical function of the mitochondria, we focused on the effects of CPF on mitochondrial dynamics. CPF induced mitochondrial fragmentation via reduction of mitochondrial fusion protein mitofusin 1 (Mfn1) in iPSCs. In addition, CPF reduced the expression of several neural differentiation marker genes in iPSCs. Moreover, knockdown of *Mfn1* gene in iPSCs downregulated the expression of *PAX6*, a key transcription factor that regulates neurogenesis, suggesting that Mfn1 mediates neural induction in iPSCs. Taken together, these results suggest that CPF induces neurotoxicity via Mfn1-mediated mitochondrial fragmentation in iPSCs. Thus, mitochondrial dysfunction in iPSCs could be used as a possible marker for cytotoxic effects by chemicals.

Growing evidence suggests the involvement of environmental chemicals in neurodevelopmental toxicity, leading to neurobehavioral outcomes such as learning disabilities, attention deficit hyperactivity disorder, cognitive impairment, and autism[1,2]. As the fetal brain is inherently more susceptible to chemical-induced toxicity compared to the adult brain, exposure to neurotoxic chemicals during early prenatal period can cause delayed neural disorders at lower doses than in adults[3,4].

Organophosphates, such as chlorpyrifos (CPF), are well known to affect brain structure and neurodevelopmental outcome, resulting in delayed neural disorders[5,6]. In regard to this, previous studies using magnetic resonance imaging have shown that prenatal exposure to CPF caused abnormalities in the structure, size, and thickness of cerebral cortex, where was responsible for several higher-order brain functions such as attention, cognition, and emotion[7]. Several reports indicate that CPF causes neurotoxicity in the developing brain of animals. In the developing brain of neonatal rats, CPF exposure impairs neurite outgrowth by inhibiting choline acetyltransferase activity[8]. Maternal exposure to CPF suppresses neurogenesis in the hippocampal dentate gyrus of rat offspring[9]. In addition to *in vivo* effects, there has been reported the cytotoxic effects of micromolar CPF levels *in vitro*. For example, CPF inhibited mitochondrial oxidative phosphorylation[10] and induced apoptosis in human neuroblastoma SH-SY5Y cells[11] or human neural precursor cells[12]. As micromolar CPF levels were detected in the blood of human newborns living in an agricultural community[13], the observations made using micromolar levels of CPF *in vitro* could potentially reflect the biological reactions in a living body. However, the effect of CPF on neurodevelopment has not been precisely elucidated.

[1]Division of Pharmacology, National Institute of Health Sciences, Tokyo, Japan. [2]Pharmacological Evaluation Institute of Japan (PEIJ), Kanagawa, Japan. Correspondence and requests for materials should be addressed to Y.K. (email: kanda@nihs.go.jp)

Morphological changes of mitochondria are known to contribute to homeostasis[14,15]. Under normal circumstances, mitochondria fuses together and forms excessive tubular networks (mitochondrial fusion). These fusion is regulated by fusion factors mitofusin 1 and 2 (Mfn1, Mfn2) and optic atrophy 1 (Opa1)[16,17]. In contrast, under stress conditions, mitochondrial networks convert into large numbers of small fragments with spherical and punctate morphology (mitochondrial fission), and are regulated by fission factors, such as fission protein 1 (Fis1) and dynamin-related protein 1 (Drp1)[18,19]. This morphological dynamics contributes to the maintenance of mitochondrial functions, including energy generation[14]. Moreover, several studies have shown the relationship between mitochondrial fragmentation and cellular and neurodevelopmental defects. For example, Mfn1 or Mfn2 knockout mice die in midgestation embryo, accompanying with developmental delay. In addition, embryonic fibroblasts from these knockout mice display distinct types of fragmented mitochondria, a phenotype due to a severe reduction in mitochondrial fusion[20]. Thus, Mfn1 is considered to be functionally different from Mfn2. In support to this, Mfn1, not Mfn2, is reported to contribute to Opa1-mediated fusion of mitochondrial inner membrane[16].

In the present study, we investigated the effect of CPF on neural differentiation using human induced pluripotent stem cells (iPSCs) as a model of human organ development. We focused on the effects of micromolar levels of CPF on mitochondrial dynamics, examining the molecular mechanisms of the process. Our results show that micromolar CPF levels inhibited ATP production through Mfn1 reduction, followed by mitochondrial fragmentation. Moreover, Mfn1-mediated mitochondrial dysfunction suppressed early neural induction by decreasing levels of *PAX6*, a key transcription factor that regulates neurogenesis. These data suggest that CPF-induced neurodevelopmental toxicity is based on impairment of mitochondrial functions in human iPSCs.

Results

Effect of CPF on neural differentiation of iPSCs. To investigate whether CPF affects early neurodevelopment, we examined neural differentiation capability of iPSCs, which was induced by dual SMAD inhibition protocol[21] (Fig. 1A). First, we determined the critical CPF concentration, affecting neural differentiation. At day 4 after neural induction with different concentrations of CPF, the expression of *PAX6*, an early neuroectodermal marker that regulates neurogenesis[22], was analyzed using real-time PCR. We found that exposure to 30 μM CPF significantly decreased *PAX6* gene expression (Fig. 1B). Next, we performed time course experiments for expression of several neural differentiation markers at days 2, 4, 6, and 8 after exposure to 30 μM CPF. At day 9, almost all cells exposed by CPF (30 μM) were detached from the culture dish. Real-time PCR analysis revealed upregulated expression of *PAX6* by day 4, and *FOXG1*, a neuroectodermal marker that also regulates neurogenesis[23], thereafter (Fig. 1C and D). Representative neural maturation marker *NCAM1*[24] continuously increased, confirming that further neural differentiation occurred (Fig. 1E). In addition, CPF exposure reduced the expression of these neural induction markers by day 6 (Fig. 1C–E). These data suggest that CPF has an inhibitory effect on early neural differentiation of iPSCs.

Mitochondrial function of iPSCs exposed to CPF. As neural differentiation process requires ATP as a source of energy[25], we examined intracellular ATP content in iPSCs. Treatment with 30 μM CPF significantly reduced the ATP content of the cells (Fig. 2A). We have previously shown that 0.1 μM carbonyl cyanide m-chlorophenyl hydrazone (CCCP), which functions as a mitochondrial uncoupler[26], decreased ATP levels in iPSCs. Because CPF inhibited ATP production, we focused on several mitochondrial functions. Mitochondrial membrane potential (MMP) was decreased by exposure to 30 μM CPF for 24 h (Fig. 2B and C). As a positive control, exposure to 0.1 μM CCCP reduced MMP (Figure S1). In addition, CPF exposure increased the number of cells with fragmented mitochondria displaying punctate morphology (Fig. 2D) and decreased the number of cells exhibiting mitochondrial fusion (Fig. 2E). We have already confirmed that 0.1 μM CCCP also increased the occurrence of fragmented mitochondria. These results suggest that CPF induces mitochondrial dysfunction, including MMP depolarization and mitochondrial fragmentation, in iPSCs.

Expression of mitochondrial fission and fusion factors in iPSCs exposed to CPF. To examine the molecular mechanisms by which CPF induces mitochondrial fragmentation in iPSCs, we assessed the expression levels of mitochondrial fission (*Fis1* and *Drp1*) and fusion genes (*Mfn1*, *Mfn2*, and *OPA1*). Real-time PCR analysis showed that the gene expression of the factors was not altered after CPF exposure (Fig. 3A). Interestingly, western blot analysis revealed that CPF significantly decreased Mfn1 protein levels. In contrast, protein expression levels of other factors, including Mfn2, were not changed (Fig. 3B and C). These data suggest that CPF-induced mitochondrial fragmentation is caused by reduction of Mfn1 protein levels.

Effects of CPF in iPSC-derived neural progenitor cells. To investigate whether the effects of CPF selectively occur in the early stage of neural differentiation in iPSCs, we used iPSC-derived neural progenitor cells (NPCs), which were induced by dual SMAD inhibition protocol[21] (Figure S1A). Treatment with 30 μM CPF had little effect on ATP content (Figure S1B). Similarly, exposure to 30 μM CPF had little effect on mitochondrial morphology (Figure S1C and D), which was confirmed by the fact that CPF did not alter the protein levels of mitochondrial fission and fusion factors containing Mfn1 (Figure S1E). These data suggest that iPSCs, not NPCs, are sensitive to CPF exposure.

Effect of Mfn1 knockdown on neural induction of iPSCs. To further investigate the involvement of Mfn1 in the effects of CPF on neural induction, we performed knockdown (KD) of Mfn1, using lentivirus-delivered shRNAs. Real-time PCR analysis showed that KD was selective for *Mfn1*, not *Mfn2*, and that the efficiency was approximately 70% (Fig. 4A). The KD effects were also confirmed by protein levels (Fig. 4B and C). The Mfn1 KD cells were used to perform neural induction. Real-time PCR analysis revealed that Mfn1 KD

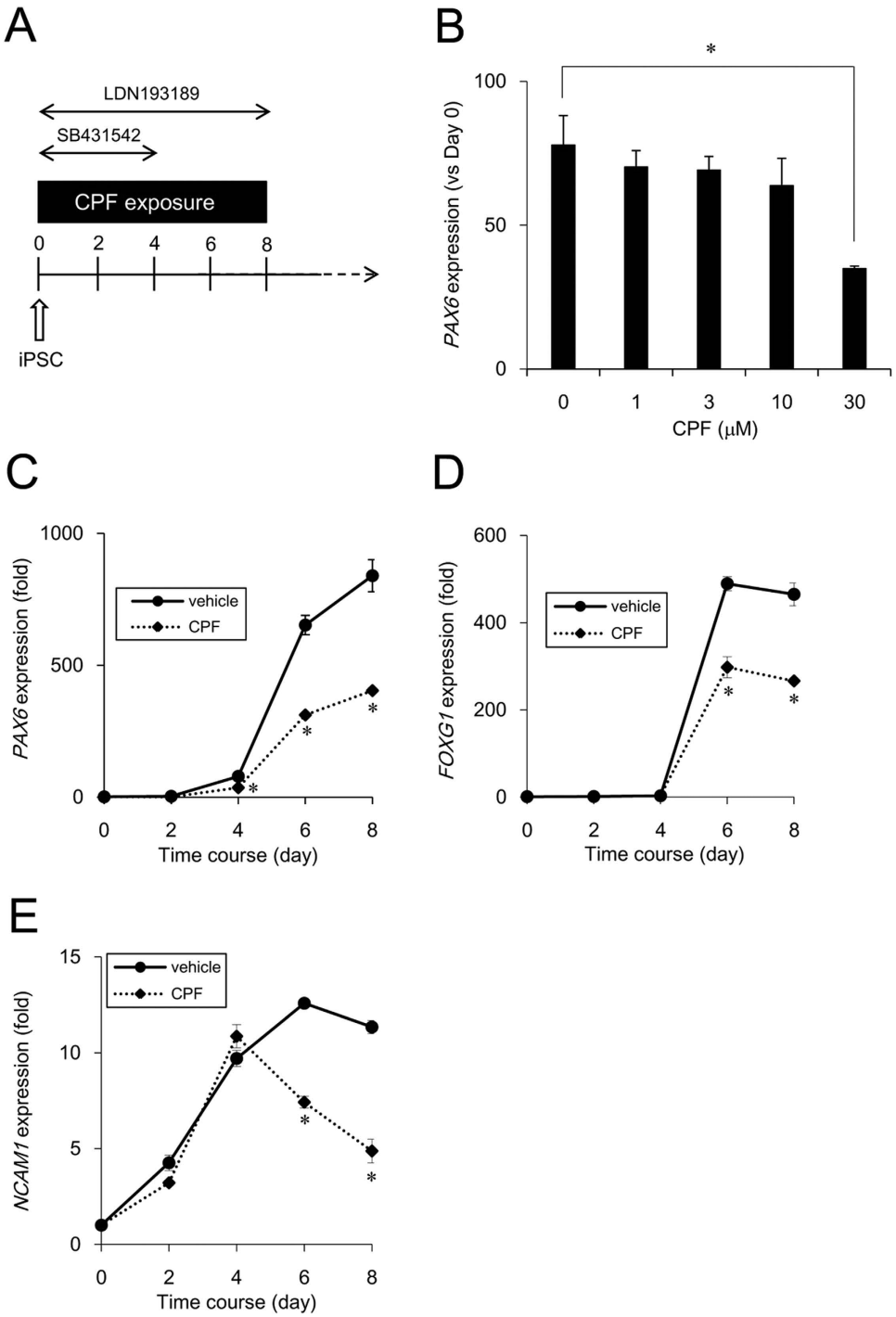

Figure 1. Time course studies of neural induction in iPSCs exposed to CPF. (**A**) Schematic time course of induction from iPSCs to NPCs by dual SMAD inhibition. Neural induction was initiated after exposure to CPF for 24 h. The cells were continuously exposed to CPF throughout neural differentiation. (**B**) At day 4 after neural induction with CPF (0–30 μM), expression of the neural differentiation marker *PAX6* was examined using real-time PCR analysis. (**C–E**) At days 2, 4, 6, and 8 after neural induction with CPF (30 μM), expression of neural differentiation markers, *PAX6*, *FOXG1*, and *NCAM1* was examined using real-time PCR analysis. Data are represented as means ± SD (n = 3). $^{*}P < 0.05$.

decreased the expression of *PAX6* (day 4), *FOXG1* (day 6) and *NCAM1* (day 6) (Fig. 4D). These data suggest that Mfn1 is involved in CPF-mediated negative effects on neural induction of iPSCs.

Negative regulation of neural induction by CPF exposure. A previous report indicates that ERK signaling inhibits neural induction via *PAX6* silencing in human embryonic stem cells[27]. ERK has been reported to be activated after depletion of Mfn1[28]. We focused on ERK signaling in the effect of CPF on neural induction.

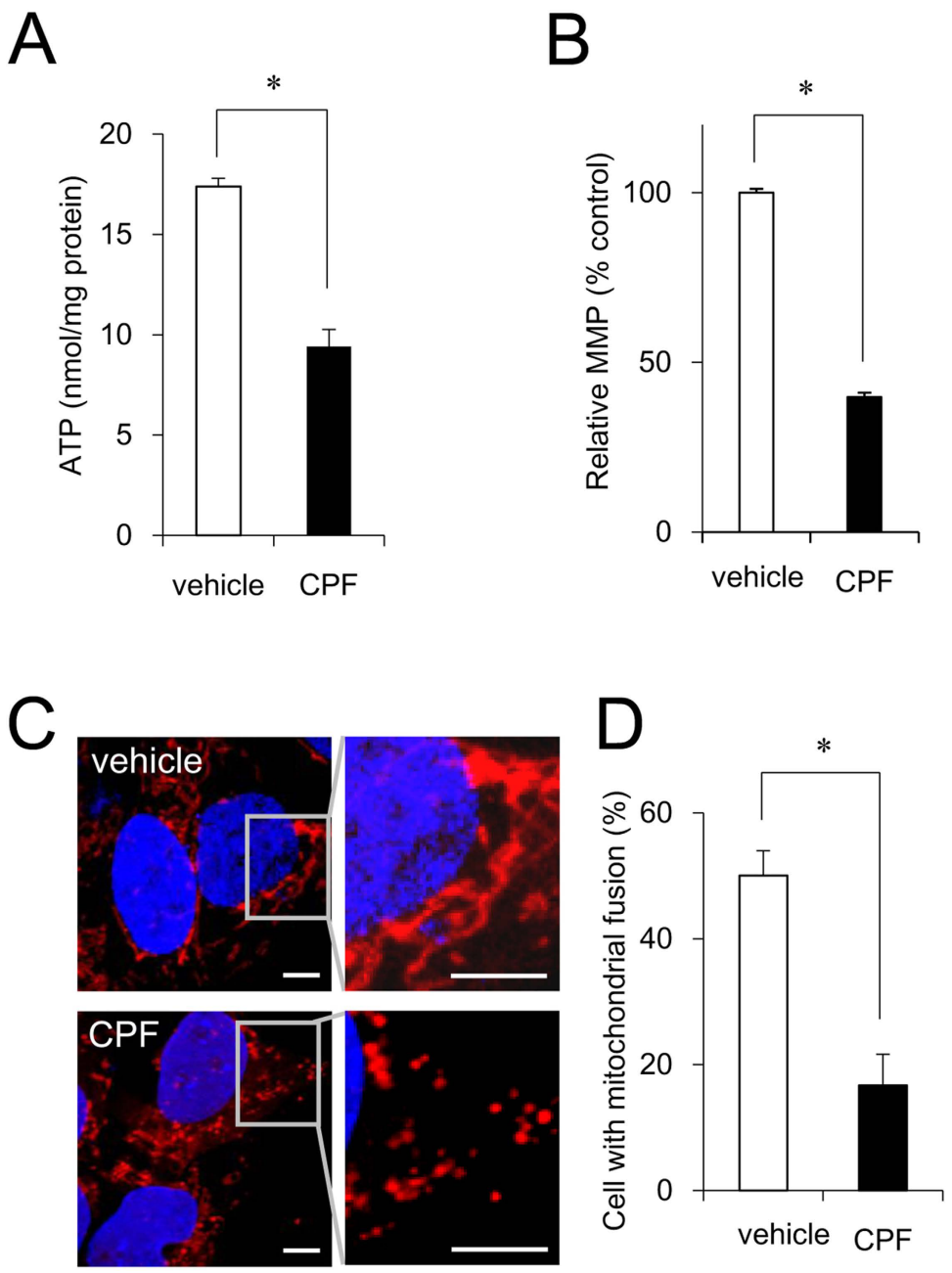

Figure 2. Mitochondrial function of iPSCs exposed to CPF. (**A**) Cells were exposed to CPF (30 μM) for 24 h. Intracellular ATP content was determined in the lysed cells (n = 3). (**B**) Cells were exposed to CPF for 24 h and stained with JC-10 for 20 min. MMP of JC-10 labeled cells was analyzed by flow cytometry. The histogram represents the ratio of JC-aggregate (F-590) to JC-monomer (F-535) fluorescence (n = 3). (**C**) Cells were exposed to CPF for 72 h and stained with MitoTracker Red CMXRos and Hoechst33342. Mitochondrial morphology was observed by confocal laser microscopy. Bar = 5 μm. (**D**) The number of cells with mitochondrial fusion (<10% punctiform) was determined in each image (n = 5). Data are represented as means ± SD. *$P < 0.05$.

We found that CPF exposure significantly increased basal ERK phosphorylation levels, which were abolished by treatment with the ERK inhibitor U0126 (Fig. 5A and B). To further study whether *PAX6* downregulation in CPF-exposed cells occurred through ERK signaling, we examined the effect of U0126 on *PAX6* expression. Incubation with U0126 recovered the expression levels of *PAX6* (Fig. 5C). These data suggest that CPF activates ERK and prevents neural induction via *PAX6* downregulation.

Effect of Mfn1 knockdown on neural induction. To confirm the involvement of Mfn1 in the inhibition of neural induction by CPF, we used Mfn1 KD cells. Mfn1 KD significantly increased basal ERK phosphorylation levels that were abolished by treatment with the ERK inhibitor U0126 (Fig. 6A and B). To further study

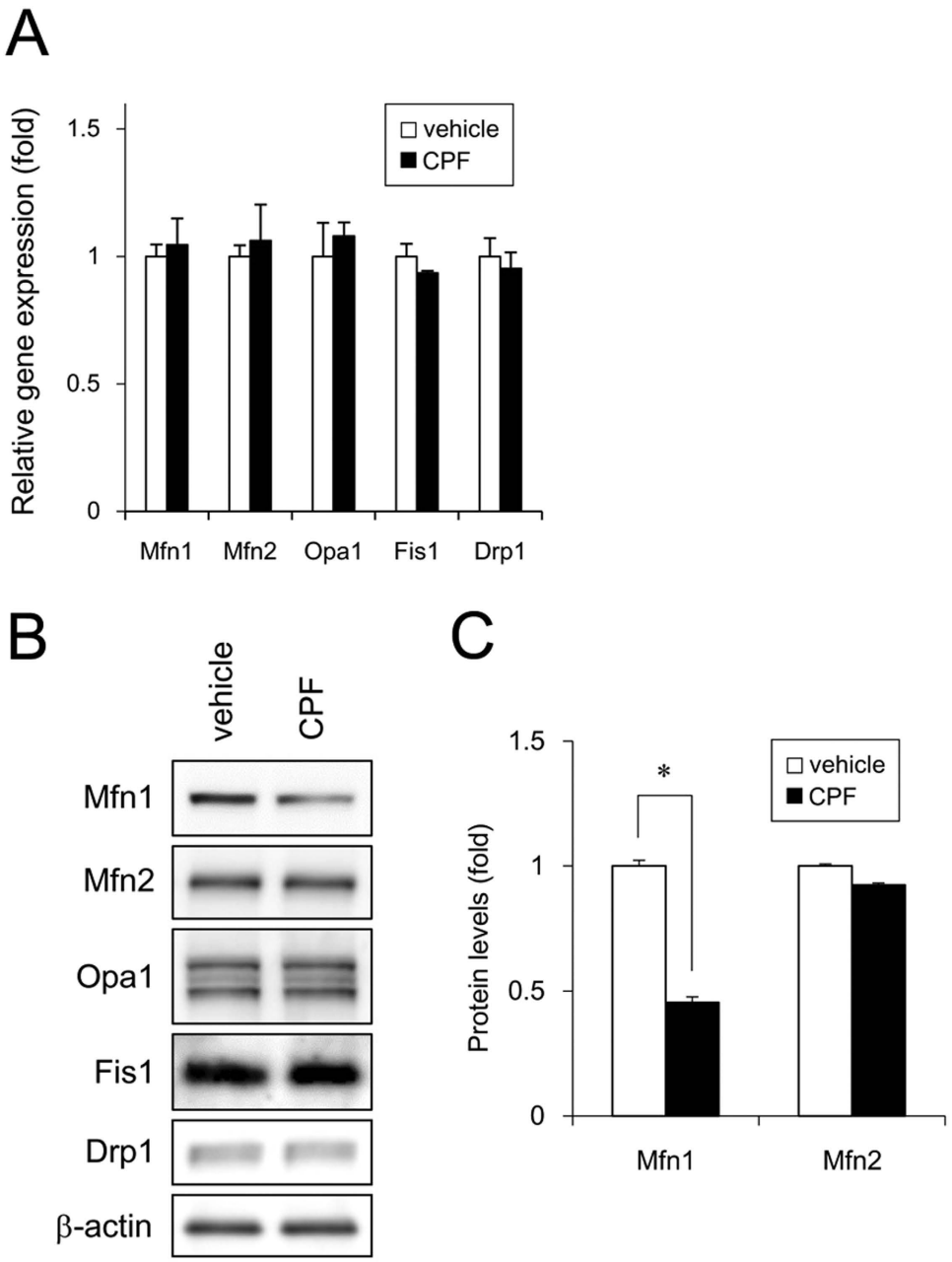

Figure 3. Expression of mitochondrial fission and fusion factors of iPSCs exposed to CPF. (**A**) After exposure to CPF (30 μM) for 24 h, expression of mitochondrial genes was analyzed by real-time PCR. (**B**) After exposure to CPF for 24 h, expression of mitochondrial proteins was analyzed by western blotting using anti-Drp1, anti-Fis1, anti-Mfn1, anti-Mfn2, anti-Opa1, or anti-β-actin antibodies. (**C**) Relative densities of bands were quantified with ImageJ software. Relative changes in expression were determined by normalization to β-actin. Data are represented as means ± SD (n = 3). $^{*}P < 0.05$.

whether *PAX6* downregulation in Mfn1 KD cells occurred through ERK signaling, we examined the effect of U0126 on *PAX6* expression. Mfn1 KD decreased *PAX6* by 64% by in the vehicle-treated cells. In contrast, Mfn1 KD decreased *PAX6* by 30% in the U0126-treated cells. Thus, incubation with U0126 partially recovered the *PAX6* expression in the Mfn1 KD cells (Fig. 6C). Taken together, these data suggest that Mfn1 reduction by CPF exposure activates ERK and prevents neural induction via *PAX6* downregulation.

Discussion

In the present study, we demonstrated that exposure to micromolar CPF targeted mitochondrial quality control in human iPSCs. We showed that CPF induced Mfn1 reduction, thereby promoting mitochondrial fragmentation. These negative effects of CPF on mitochondrial quality control could suppress ATP production and neural

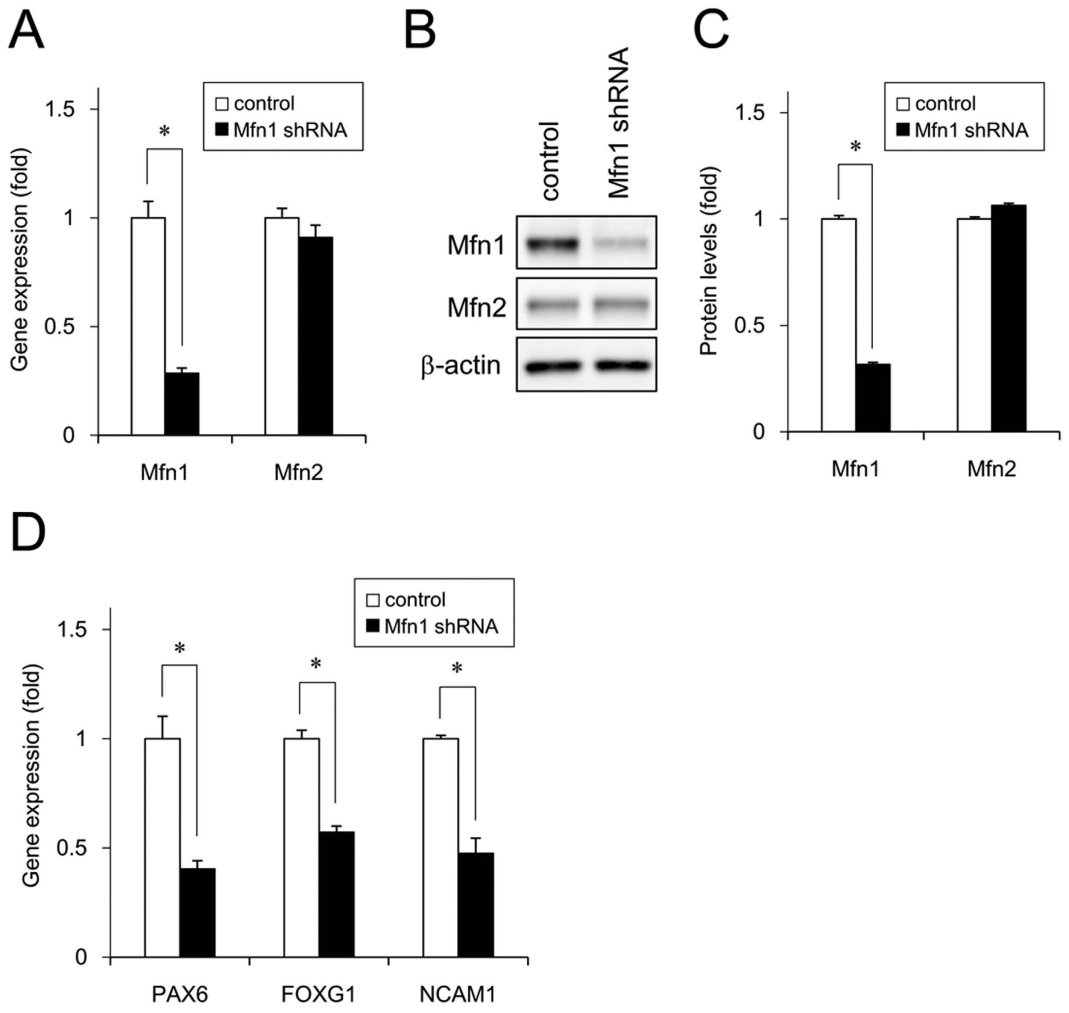

Figure 4. Effect of Mfn1 knockdown on neural induction of iPSCs. Cells were infected with lentiviruses containing a vector encoding a shRNA directed against *Mfn1* or a scrambled sequence shRNA (control) for 24 h. The infected cells were subjected to selection with puromycin (1 μg/ml) for 24 h and cultured for an additional 72 h prior to functional analyses. (**A**) The expression of *Mfn1* and *Mfn2* genes was analyzed by real-time PCR. (**B**) The expression of Mfn1 and Mfn2 proteins was analyzed by western blotting using anti-Mfn1, anti-Mfn2, or anti-β-actin antibodies. (**C**) Relative densities of bands were quantified with ImageJ software. Relative changes in expression were determined by normalization to β-actin. (**D**) Expression of neural differentiation markers *PAX6* (day 4), *FOXG1* (day 6), and *NCAM1* (day 6) was examined with real-time PCR. Data are represented as means ± SD (n = 3). $^*P < 0.05$.

differentiation. Based on the data observed in our study, Fig. 7 shows a proposed mechanism of CPF cytotoxicity via mitochondrial dysfunction.

Our studies showed that treatment with micromolar CPF levels caused mitochondrial dysfunction of human iPSCs (Fig. 2). We observed that iPSCs were sensitive to CPF exposure, unlike iPSC-derived NPCs (Figure S1). Previous reports support this difference in CPF sensitivity. The inhibitory effect of CPF on DNA synthesis in undifferentiated C6 glioma cells is found to be much higher than in differentiated cells[29]. *In vivo* studies indicate that immature organisms are more susceptible to CPF-induced toxicity compared to adults due to lower levels of CPF metabolizing enzymes[30]. Thus, the difference in CPF sensitivity between iPSCs and NPCs may be dependent on the maturation of CPF detoxification pathways. We are currently conducting experiments to determine the mechanism causing the differences in sensitivity to CPF.

We showed that CPF induced mitochondrial fragmentation via Mfn1 reduction (Figs 2 and 3). Consistent with this, our previous knockdown studies indicated that Mfn1 reduction was sufficient to promote mitochondrial dysfunction[31]. CPF-induced Mfn1 reduction might mediate mitochondrial fragmentation, decrease ATP levels, and inhibit iPSC growth. Although Mfn2 is also involved in mitochondrial fission and energy supply processes[32,33], our results indicated that CPF specifically targeted Mfn1, not Mfn2. Regarding this apparent CPF specificity, E3 ubiquitin ligase membrane-associated RING-CH 5 (MARCH5) has been reported to selectively bind to Mfn1 dependent on its acetylation, and degrade among all mitochondrial proteins, including Mfn2[34]. In addition, we have reported that organotin compounds induced Mfn1 degradation through MARCH5,

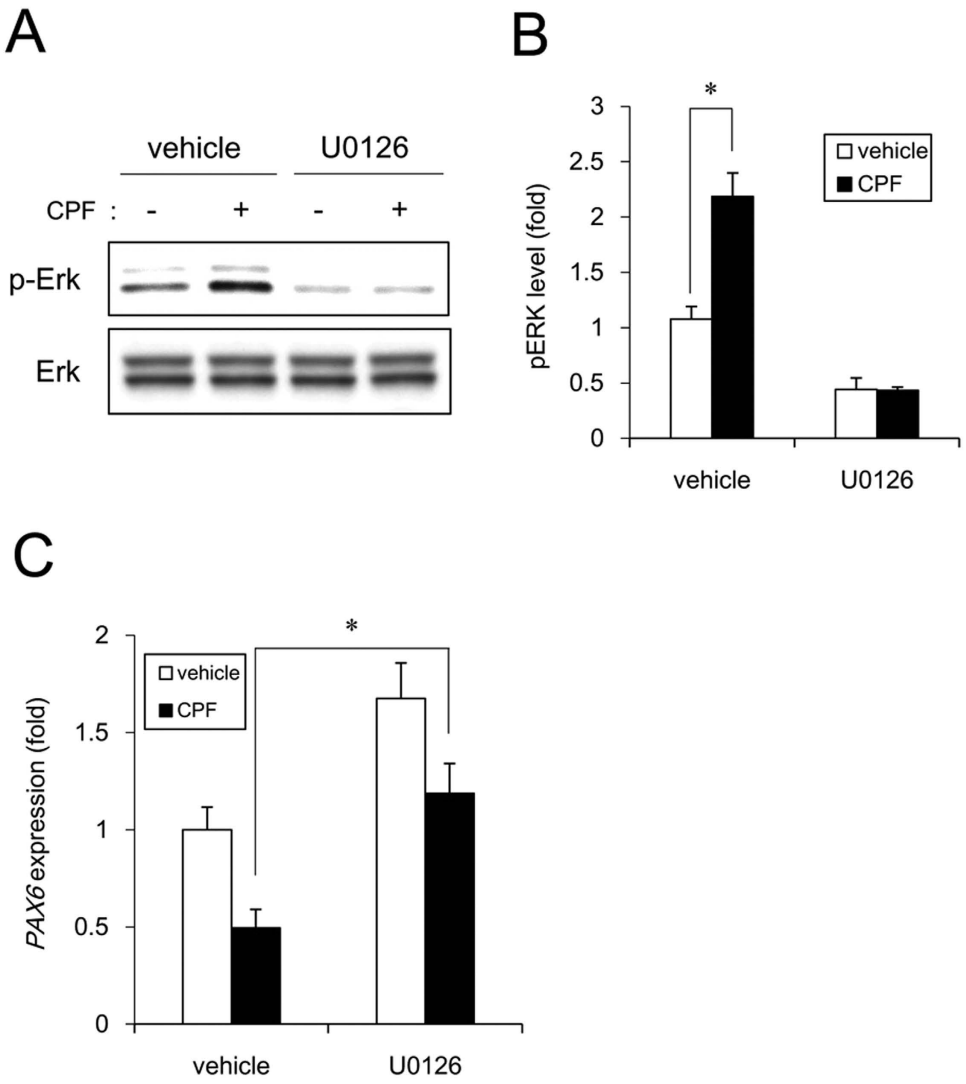

Figure 5. Negative regulation of neural induction by CPF exposure. (**A**) Cells were exposed to CPF (30 μM) or CPF + U0126 (5 μM) for 24 h. ERK phosphorylation was analyzed by western blotting using anti-phospho-ERK antibodies. (**B**) Relative densities of bands were quantified with ImageJ software. Relative changes in expression were determined by normalization to total ERK protein level. (**C**) At day 4 after neural induction with CPF or CPF + U0126, the expression of *PAX6* gene was analyzed by real-time PCR. Data are represented as means ± SD (n = 3). *$P < 0.05$.

thereby promoting mitochondrial fragmentation in iPSCs[31]. Thus, CPF may specifically target Mfn1 protein via MARCH5 in iPSCs without affecting mRNA levels. Furthermore, the difference in CPF sensitivity between iPSCs and NPCs may be dependent on Mfn1 and MARCH5 expression levels or MARCH5 activity. Further studies should determine whether CPF reduces Mfn1 via MARCH5-mediated degradation in iPSCs.

We demonstrated that ERK phosphorylation mediated the negative effects of CPF on early neural differentiation (Figs 1, 4 and 5). A previous report indicates that Mfn1 directly binds Ras and Raf, resulting in the inhibition of Ras-Raf-ERK signaling by the biochemical analysis[35,36]. Mfn1 reduction by CPF or shRNA may reverse this ERK signaling inhibition. Mobilization of Ca^{2+} from intracellular stores, including mitochondria was reported to result in phosphorylation of MAPKs, as the process was suppressed by chelation of intracellular Ca^{2+} in human T lymphoblastoid cells[37]. As mitochondria are known to uptake into the matrix of any Ca^{2+} that has accumulated in the cytosol, dependent on MMP[38], mitochondrial dysfunction by CPF exposure may cause an overload of Ca^{2+}, resulting in ERK activation. Moreover, ERK signaling was reported to inhibit neural induction by *PAX6* silencing via upregulation of stemness factors *NANOG/OCT4* and downregulation of homeobox transcription factor *OTX2*[27]. NANOG and OCT4 act as repressors of *PAX6* induction, whereas OTX2 is a positive inducer of *PAX6*[27]. Therefore, ERK signaling evoked by CPF could affect the expression of these transcriptional network, including *NANOG*, *OCT4* and *OTX2*, *by* regulating *PAX6*. In future studies, we should further investigate the mechanisms of CPF-induced negative regulation of neural induction via ERK.

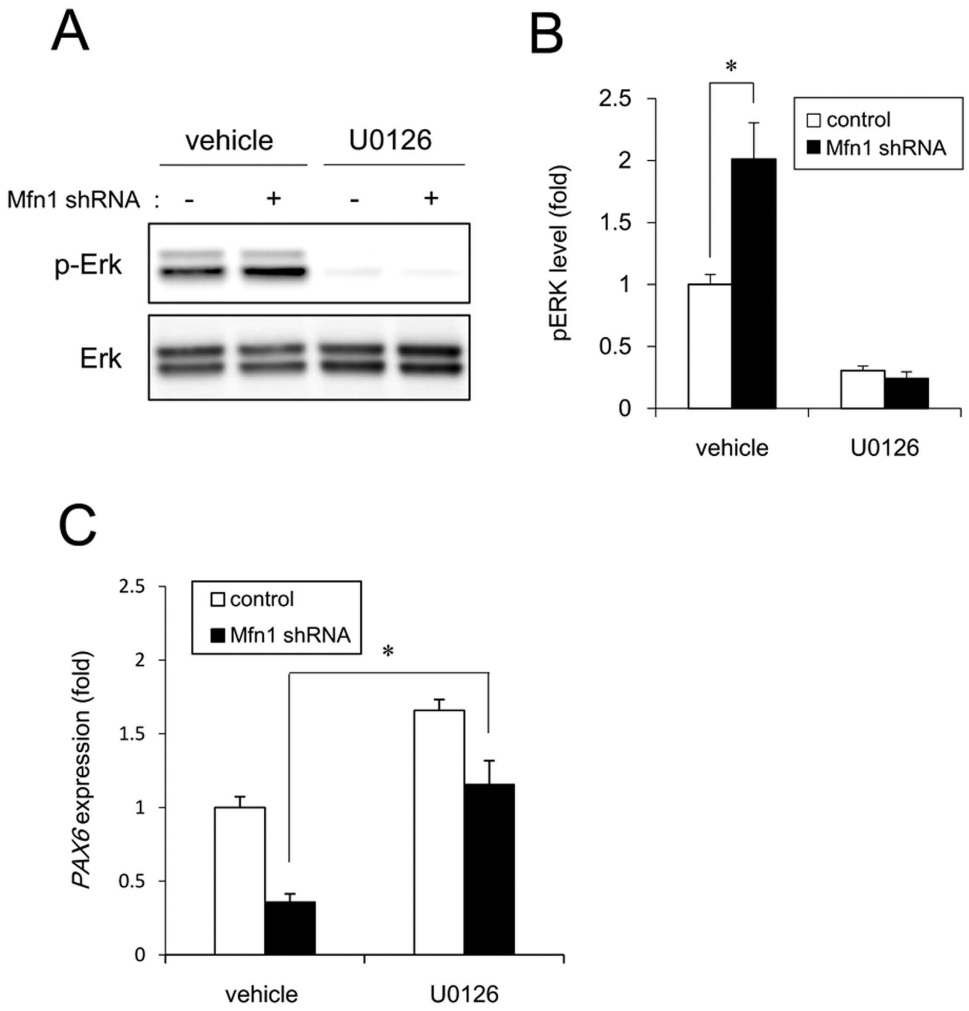

Figure 6. Negative regulation of neural induction by Mfn1 knockdown. The cells were infected with lentiviruses containing a vector encoding a shRNA directed against Mfn1 or a scrambled sequence shRNA (control) for 24 h. The infected cells were subjected to selection with 1 μg/ml puromycin for 24 h and cultured for an additional 72 h prior to functional analyses. (**A**) After incubation with U0126 for 24 h, ERK phosphorylation was analyzed by western blotting using anti-phospho-ERK antibodies. (**B**) Relative densities of bands were quantified with ImageJ software. Relative changes in expression were determined by normalization to total ERK protein level. (**C**) At day 4 after neural induction with U0126, the expression of *PAX6* gene was analyzed by real-time PCR. Data are represented as means ± SD (n = 3). $^{*}P < 0.05$.

We further demonstrated that Mfn1 reduction mediated cytotoxic effects of CPF on iPSCs via *PAX6* downregulation (Figs 5 and 6). *FOXG1* was downregulated, along with *PAX6*, during neural differentiation of iPSCs exposed to CPF. *PAX6* and *FOXG1* act as transcriptional regulators during forebrain development in vertebrates[39,40]. Targeted disruption of *PAX6* and *FOXG1* in rodents led to the loss of anterior neural tissues, suggesting the central role of these genes in forebrain development[41,42]. CPF causes various defects in the development of hippocampus and cortex of rodents[43]. Thus, CPF-induced defects of forebrain architecture may be caused by transcriptional silencing of anterior neural markers during early neurogenesis. As *NCAM1* was downregulated during neural differentiation of iPSCs exposed to CPF, further studies using NPCs are required to reveal how CPF affects neural maturation processes.

In summary, our results demonstrate a novel mechanism underlying cytotoxicity, including neurodevelopmental toxicity of CPF in iPSCs. Recently, significant progress has been made in the induction of differentiation of pluripotent stem cells into a variety of cell types[44]. Further studies are needed to evaluate the developmental effects of CPF on various types of iPSC-derived cells. Moreover, we show that CPF toxicity is caused by Mfn1-mediated mitochondrial dysfunction, which is involved in the cytotoxicity of organotin compounds[31]. Thus, mitochondrial functions influenced by Mfn1 might be a good starting point for investigating toxic mechanisms induced by exposure to other chemicals.

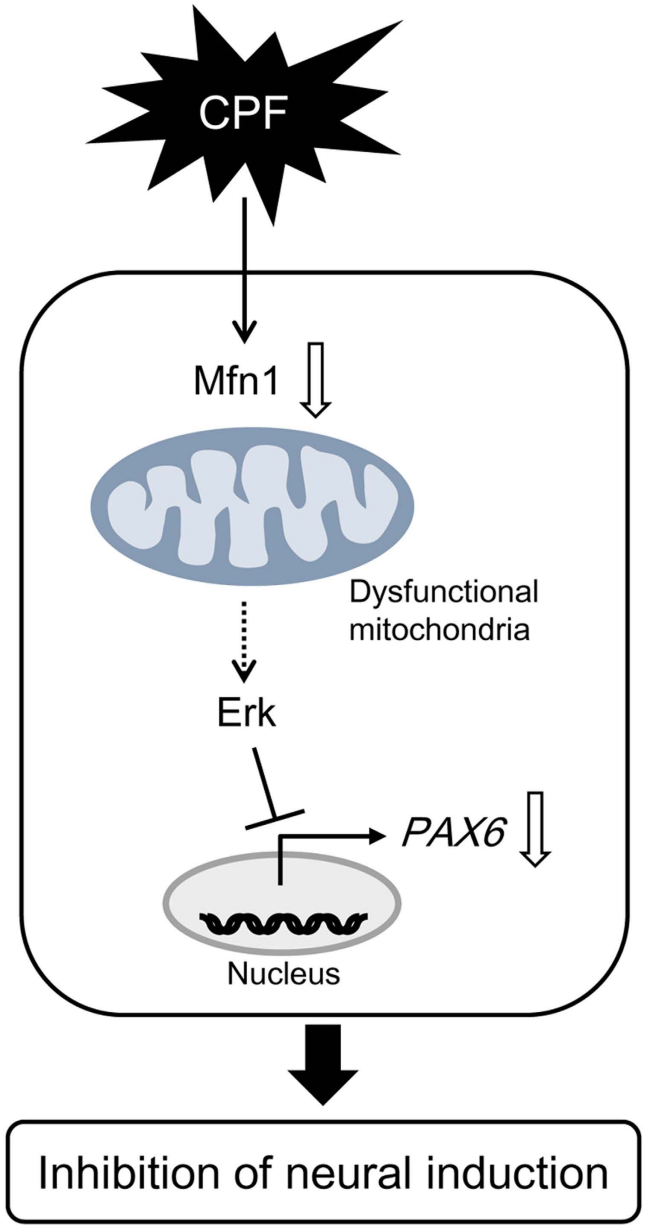

Figure 7. Proposed mechanism of CPF cytotoxicity in human iPSCs. CPF exposure causes Mfn1 reduction, which induces mitochondrial dysfunction, including mitochondrial fragmentation and decreased ATP levels. Mitochondrial dysfunction in turn evokes ERK phosphorylation, leading to the suppression of *PAX6*, which is an early marker of neurogenesis.

Methods

Chemicals. Chlorpyrifos (CPF), Y-27632, SB431542, and LDN193189 were obtained from Wako (Tokyo, Japan). Penicillin-streptomycin mixture (PS) was obtained from Thermo Fisher Scientific (Waltham, MA, USA). U0126 was obtained from Enzo Life Sciences (Farmingdale, NY, USA). Poly-L-ornithine, 2-mercaptoethanol (2-ME), and carbonylcyanide *m*-chlorophenylhydrazone (CCCP) were obtained from Sigma-Aldrich (St. Louis, MO, USA). All other reagents were of analytical grade and obtained from commercial sources.

Cell culture. Human iPSC line 253G1 (Riken BRC Cell Bank, Tsukuba, Ibaraki, Japan) was established through retroviral transduction of *OCT4*, *SOX2*, and *KLF4* into adult human dermal fibroblasts[45]. The cells were cultured under feeder-free conditions using human embryonic stem cell (ESC)-qualified Matrigel (BD Biosciences, San Jose, CA, USA) and TeSR-E8 medium (Stemcell Technologies, Vancouver, BC, Canada) at 37 °C in an atmosphere containing 5% CO_2. For passage, iPSC colonies were dissociated into single cells using Accumax (Innovative Cell Technologies, San Diego, CA, USA) and cultured in TeSR-E8 medium supplemented with Y-27632 (ROCK inhibitor, 10 μM). The NPCs derived from iPSCs were cultured on poly-L-ornithine and Laminin (Thermo Fisher Scientific) coated dishes at 37 °C in an atmosphere containing 5% CO_2. The culture

medium was Neural maintenance medium [NMM; a 1 : 1 mixture of DMEM/F12 (Thermo Fisher Scientific) and Neurobasal (Thermo Fisher Scientific) containing N2 (Thermo Fisher Scientific), B27 (Thermo Fisher Scientific), GlutaMAX (Thermo Fisher Scientific), non-essential amino acids (NEAA; Thermo Fisher Scientific), 2-ME, PS]. For passage, NPCs were dissociated into single cells using Accumax and cultured in NMM supplemented with EGF (20 ng/ml), FGF2 (20 ng/ml) and Y-27632.

Neural differentiation procedure. For the induction of neuronal lineages, dual SMAD inhibition protocol was used as previously described[21] with modifications. Briefly, iPSC colonies were dissociated into single cells with Accumax. The cells were seeded at a density of 7×10^4 cells/cm^2 in TeSR-E8 medium on Matrigel-coated plates in order to reach nearly confluent within two days after seeding. The initial differentiation medium was knockout serum replacement (KSR) medium [Knockout DMEM (Thermo Fisher Scientific) containing KSR (Thermo Fisher Scientific), L-glutamine, NEAA, 2-ME, PS] with SB431542 (TGFβ inhibitor, 10 μM) and LDN193189 (BMP inhibitor, 1 μg/ml). After 4 days, N2 medium [Neurobasal containing N2, B27, GlutaMAX, PS] was added to the KSR medium with LDN193189 every two days.

Measurement of intracellular ATP levels. Intracellular ATP content was measured using an ATP Determination Kit (Thermo Fisher Scientific), according to the manufacturer's protocol. Briefly, the cells were washed and lysed with 0.1% Triton X-100/PBS. The resulting cell lysates were added to a reaction mixture containing 0.5 mM D-luciferin, 1 mM DTT, and 1.25 μg/mL luciferase and incubated for 30 min at room temperature. Luminescence was measured using a Fluoroskan Ascent FL microplate reader (Thermo Fisher Scientific). The luminescence intensities were normalized to the total protein content.

Measurement of MMP. A Cell Meter JC-10 Mitochondrial Membrane Potential Assay Kit (AAT Bioquest, Sunnyvale, CA, USA) was used to detect MMP. Briefly, the cells were suspended in staining buffer containing JC-10 and incubated for 20 min at room temperature. After the cells were treated with CPF, a FACS Aria II cell sorter (BD Biosciences) was used to measure the fluorescence intensity ratio, JC-aggregate (F-590)/JC-monomer (F-535).

Assessment of mitochondrial fusion. After treatment with CPF (30 μM, 72 h), the cells were fixed with 4% paraformaldehyde and stained with 50 nM MitoTracker Red CMXRos (Cell Signaling Technology, Danvers, MA, USA) and 5 μg/mL Hoechst 33342 (Sigma-Aldrich). Changes in mitochondrial morphology were observed using a confocal laser microscope (Nikon A1). Images ($n = 5$) of random fields were taken, and the number of cells displaying mitochondrial fusion (<10% punctiform) was determined in each image, as previously reported[46].

Real-time polymerase chain reaction (PCR). Total RNA was isolated from iPSCs using TRIzol reagent (Thermo Fisher Scientific), and quantitative real-time reverse transcription (RT)-PCR was performed using a QuantiTect SYBR Green RT-PCR Kit (Qiagen, Valencia, CA, USA) on an ABI PRISM 7900HT sequence detection system (Applied Biosystems, Foster City, CA, USA) as previously reported[47]. Relative changes in transcript levels were normalized to the mRNA levels of glyceraldehyde-3-phosphate dehydrogenase (*GAPDH*). The following primer sequences were used for real-time PCR analysis: *Fis1*, forward, 5′-TACGTCCGCGGGTTGCT-3′ and reverse, 5′-CCAGTTCCTTGGCCTGGTT-3′; *Drp1*, forward, 5′-TGGGCGCCGACATCA-3′ and reverse, 5′-GCTCTGCGTTCCCACTACGA-3′; *Mfn1*, forward, 5′-GGCATCTGTGGCCGAGTT-3′ and reverse, 5′-ATTATGCTAAGTCTCCGCTCCAA-3′; *Mfn2*, forward, 5′-GCTCGGAGGCACATGAAAGT-3′ and reverse, 5′-ATCACGGTGCTCTTCCCATT-3′; *Opa1*, forward, 5′-GTGCTGCCCGCCTAGAAA-3′ and reverse, 5′-TGACAGGCACCCGTACTCAGT-3′; *PAX6*, forward, 5′-ATGTGTGAGTAAAATTCTGGGCA-3′ and reverse, 5′-GCTTACAACTTCTGGAGTCGCTA-3′; *FOXG1*, forward, 5′-GCCACAATCTGTCCCTCAACA-3′ and reverse, 5′-GACGGGTCCAGCATCCAGTA-3′; *NCAM1*, forward, 5′-GGCATTTACAAGTGTGTGGTTAC-3′ and reverse, 5′-TTGGCGCATTCTTGAACATGA-3′; *GAPDH*, forward, 5′-GTCTCCTCTGACTTCAACAGCG-3′ and reverse, 5′-ACCACCCTGTTGCTGTAGCCAA-3′.

Western blot analysis. Western blot analysis was performed as previously reported[48]. Briefly, the cells were lysed with Cell Lysis Buffer (Cell Signaling Technology). The proteins were then separated by sodium dodecyl sulfate-polyacrylamide gel electrophoresis (SDS-PAGE) and electrophoretically transferred to Immobilon-P membranes (Millipore, Billerica, MA, USA). The membranes were probed with anti-Drp1 monoclonal antibodies (1:1000; Cell Signaling Technology), anti-Fis1 polyclonal antibodies (1:200; Santa Cruz Biotechnology, Santa Cruz, CA, USA), anti-Mfn1 polyclonal antibodies (1:1000; Cell Signaling Technology), anti-Mfn2 monoclonal antibodies (1:1000; Cell Signaling Technology), anti-Opa1 monoclonal antibodies (1:1000; BD Biosciences), anti-ERK1/2 polyclonal antibodies (1:1000; Cell Signaling Technology), anti-phospho ERK1/2 (Thr202/Tyr204) monoclonal antibodies (1:2000; BD Biosciences), and anti-β-actin monoclonal antibodies (1:5000; Sigma-Aldrich). The membranes were then incubated with secondary antibodies against rabbit or mouse IgG conjugated to horseradish peroxidase (Cell Signaling Technology). The bands were visualized using an ECL Western Blotting Analysis System (GE Healthcare, Buckinghamshire, UK). Images were acquired using an LAS-3000 Imager (FUJIFILM, Tokyo, Japan).

Gene knockdown by shRNA. Knockdown experiments were performed using *Mfn1* shRNA lentiviruses from Sigma-Aldrich (MISSION shRNA), as previously reported[49]. A scrambled hairpin sequence was used as a negative control. Briefly, the cells were infected with the viruses at a multiplicity of infection of 1 in the presence

of 8 μg/mL hexadimethrine bromide (Sigma-Aldrich) for 24 h. After medium exchange, the cells were subjected to selection with 1 μg/mL puromycin for 24 h and cultured for an additional 72 h prior to functional analyses.

Statistical analysis. All data are presented as means ± standard deviation (SD). Analysis of variance (ANOVA) followed by post-hoc Bonferroni test was used to analyze data in Figs 1, 3C, 4, 5, and 6. Student's t test was used to analyze data in Figs 2, 3A, S1, and S2. *P*-values < 0.05 were considered statistically significant.

References

1. Landrigan, P. J., Lambertini, L. & Birnbaum, L. S. A research strategy to discover the environmental causes of autism and neurodevelopmental disabilities. *Environ. Health Perspect.* **120,** a258–a260 (2012).
2. Ross, E. J., Graham, D. L., Money, K. M. & Stanwood, G. D. Developmental consequences of fetal exposure to drugs: what we know and what we still must learn. *Neuropsychopharmacology* **40,** 61–87 (2015).
3. Rodier, P. M. Developing brain as a target of toxicity. *Environ. Health Perspect.* **103,** 73–76 (1995).
4. Rice, D. & Barone, S. Jr. Critical periods of vulnerability for the developing nervous system: evidence from humans and animal models. *Environ. Health* Perspect.**108,** 511–533 (2000).
5. Brown, M. A. & Brix, K. A. Review of health consequences from high-, intermediate- and low-level exposure to organophosphorus nerve agents. *J. Appl. Toxicol.* **18,** 393–408 (1998).
6. Ray, D. E. & Richards, P. G. The potential for toxic effects of chronic, low-dose exposure to organophosphates. *Toxicol. Lett.* **120,** 343–351 (2001).
7. Rauh, V. A. *et al.* Brain anomalies in children exposed prenatally to a common organophosphate pesticide. *Proc. Natl. Acad. Sci. USA* **109,** 7871–7876 (2012).
8. Slotkin, T. A., Levin, E. D. & Seidler, F. J. Comparative developmental neurotoxicity of organophosphate insecticides: effects on brain development are separable from systemic toxicity. *Environ. Health Perspect.* **114,** 746–751 (2006).
9. Ohishi, T. *et al.* Reversible effect of maternal exposure to chlorpyrifos on the intermediate granule cell progenitors in the hippocampal dentate gyrus of rat offspring. *Reprod. Toxicol.* **35,** 125–136 (2013).
10. Salama, M., El-Morsy, D., El-Gamal, M., Shabka, O. & Mohamed, W. M. Mitochondrial complex I inhibition as a possible mechanism of chlorpyrifos induced neurotoxicity. *Ann. Neurosci.* **21,** 85–89 (2014).
11. Lee, J. E., Park, J. H., Jang, S. J. & Koh, H. C. Rosiglitazone inhibits chlorpyrifos-induced apoptosis via modulation of the oxidative stress and inflammatory response in SH-SY5Y cells. *Toxicol. Appl. Pharmacol.* **278,** 159–171 (2014).
12. Lee, J. E., Lim, M. S., Park, J. H., Park, C. H. & Koh, H. C. Nuclear NF-κB contributes to chlorpyrifos-induced apoptosis through p53 signaling in human neural precursor cells. *Neurotoxicology* **42,** 58–70 (2014).
13. Huen, K. *et al.* Organophosphate pesticide levels in blood and urine of women and newborns living in an agricultural community. *Environ. Res.* **117,** 8–16 (2012).
14. Youle, R. J. & van der Bliek, A. M. Mitochondrial fission, fusion, and stress. *Science* **337,** 1062–1065 (2012).
15. van der Bliek, A. M., Shen, Q. & Kawajiri, S. Mechanisms of mitochondrial fission and fusion. *Cold Spring Harb. Perspect. Biol.* **5,** pii: a011072 (2013).
16. Cipolat, S., De Brito, O. M., B. Dal Zilio, B. & Scorrano, L. OPA1 requires mitofusin 1 to promote mitochondrial fusion. *Proc. Natl. Acad. Sci. USA* **101,** 15927–15932 (2004).
17. Koshiba, T. *et al.* Structural basis of mitochondrial tethering by mitofusin complexes. *Science* **305,** 858–862 (2004).
18. Smirnova, E., Griparic, L., Shurland, D.-L. & van der Bliek, A. M. Dynamin-related protein Drp1 is required for mitochondrial division in mammalian cells. *Mol. Biol. Cell* **12,** 2245–2256 (2001).
19. Yoon, Y., Krueger, E. W., Oswald, B. J. & McNiven, M. A. The mitochondrial protein hFis1 regulates mitochondrial fission in mammalian cells through an interaction with the dynamin-like protein DLP1. *Mol. Biol. Cell* **23,** 5409–5420 (2003).
20. Chen, H. *et al.* Mitofusins Mfn1 and Mfn2 coordinately regulate mitochondrial fusion and are essential for embryonic development. *J. Cell Biol.* **160,** 189–200 (2003).
21. Chambers, S. M. *et al.* Highly efficient neural conversion of human ES and iPS cells by dual inhibition of SMAD signaling. *Nat. Biotechnol.* **27,** 275–280 (2009).
22. Manuel, M. N., Mi, D., Mason, J. O. & Price, D. J. Regulation of cerebral cortical neurogenesis by the Pax6 transcription factor. *Front. Cell Neurosci.* **9,** 70 (2015).
23. Shen, L., Nam, H. S., Song, P., Moore, H. & Anderson, S. A. FoxG1 haploinsufficiency results in impaired neurogenesis in the postnatal hippocampus and contextual memory deficits. *Hippocampus* **16,** 875–890 (2006).
24. Polo-Parada, L., Bose, C. M., Plattner, F. & Landmesser, L. T. Distinct roles of different neural cell adhesion molecule (NCAM) isoforms in synaptic maturation revealed by analysis of NCAM 180 kDa isoform-deficient mice. *J. Neurosci.* **24,** 1852–1864 (2004).
25. Cheng, A., Hou, Y. & Mattson, M. P. Mitochondria and neuroplasticity. *ASN. Neuro.* **2,** e00045 (2010).
26. Tanaka, A. *et al.* Proteasome and p97 mediate mitophagy and degradation of mitofusins induced by Parkin. *J. Cell Biol.* **191,** 1367–1380 (2010).
27. Greber, B. *et al.* FGF signalling inhibits neural induction in human embryonic stem cells. *EMBO J.* **30,** 4874–4884 (2011).
28. Son, M. J. *et al.* Mitofusins deficiency elicits mitochondrial metabolic reprogramming to pluripotency. *Cell Death Differ.* **22,** 1957–1969 (2015).
29. Garcia, S. J., Seidler, F. J., Crumpton, T. L. & Slotkin, T. A. Does the developmental neurotoxicity of chlorpyrifos involve glial targets? Macromolecule synthesis, adenylyl cyclase signaling, nuclear transcription factors, and formation of reactive oxygen in C6 glioma cells. *Brain Res.* **891,** 54–68 (2001).
30. Basha, M. & Poojary, A. Cold stress offered modulation on chlorpyrifos toxicity in aging rat central nervous system. *Toxicol. Int.* **19,** 173–181 (2012).
31. Yamada, S. *et al.* Tributyltin induces mitochondrial fission through Mfn1 degradation in human induced pluripotent stem cells. *Toxicol. In Vitro.* **34,** 257–263 (2016).
32. Leboucher, G. P. *et al.* Stress-induced phosphorylation and proteasomal degradation of mitofusin 2 facilitates mitochondrial fragmentation and apoptosis. *Mol. Cell* **47,** 547–557 (2012).
33. Yue, W. *et al.* A small natural molecule promotes mitochondrial fusion through inhibition of the deubiquitinase USP30. *Cell Res.* **24,** 482–496 (2014).
34. Park, Y. Y., Nguyen, O. T., Kang, H. & Cho, H. MARCH5-mediated quality control on acetylated Mfn1 facilitates mitochondrial homeostasis and cell survival. *Cell Death Dis.* **5,** e1172 (2014).
35. Chen, K. H. *et al.* Dysregulation of HSG triggers vascular proliferative disorders. *Nat. Cell Biol.* **6,** 872–883 (2004).
36. Chen, K. H. *et al.* Role of mitofusin 2 (Mfn2) in controlling cellular proliferation. *FASEB J.* **28,** 382–394 (2014).
37. Yu, Z. P., Matsuoka, M., Wispriyono, B., Iryo, Y. & Igisu, H. Activation of mitogen-activated protein kinases by tributyltin in CCRF-CEM cells: role of intracellular Ca(2+). *Toxicol. Appl. Pharmacol.* **168,** 200–207 (2000).
38. Pizzo, P., Drago, I., Filadi, R. & Pozzan, T. Mitochondrial Ca^{2+} homeostasis: mechanism, role, and tissue specificities. *Pflugers Arch.* **464,** 3–17 (2012).

39. Danesin, C. & Houart, C. A. Fox stops the Wnt: implications for forebrain development and diseases. *Curr. Opin. Genet. Dev*. **22,** 323–330 (2012).
40. Georgala, P. A., Carr, C. B. & Price, D. J. The role of Pax6 in forebrain development. *Dev. Neurobiol.* **71,** 690–709 (2011).
41. Tuoc, T. C. *et al.* Selective cortical layering abnormalities and behavioral deficits in cortex-specific Pax6 knock-out mice. *J. Neurosci.* **29,** 8335–8349 (2009).
42. Tian, C. *et al.* Foxg1 has an essential role in postnatal development of the dentate gyrus. *J. Neurosci.* **32,** 2931–2949 (2012).
43. Chen, X. P., Chen, W. Z., Wang, F. S. & Liu, J. X. Selective cognitive impairments are related to selective hippocampus and prefrontal cortex deficits after prenatal chlorpyrifos exposure. *Brain Res.* **1474,** 19–28 (2012).
44. Li, K. *et al.* Differentiation of pluripotent stem cells for regenerative medicine. *Biochem. Biophys. Res. Commun.* **471,** 1–4 (2016).
45. Nakagawa, M. *et al.* Generation of induced pluripotent stem cells without Myc from mouse and human fibroblasts. *Nat. Biotechnol.* **26,** 101–106 (2008).
46. Fan, X., Hussien, R. & Brooks, G. A. H_2O_2-induced mitochondrial fragmentation in C2C12 myocytes. *Free Radic. Biol. Med.* **49,** 1646–1654 (2010).
47. Hirata, N. *et al.* Sphingosine-1-phosphate promotes expansion of cancer stem cells via S1PR3 by a ligand-independent Notch activation. *Nat. Commun.* **5,** 4806 (2014).
48. Kanda, Y. *et al.* Reactive oxygen species mediate adipocyte differentiation in mesenchymal stem cells. *Life Sci.* **89,** 250–258 (2011).
49. Yamada, S. *et al.* NAD-dependent isocitrate dehydrogenase as a novel target of tributyltin in human embryonic carcinoma cells. *Sci. Rep*. **4,** 5952 (2014).

Acknowledgements

This work was supported by a Health and Labour Sciences Research Grant from the Ministry of Health, Labour, and Welfare, Japan (#H25-Kagaku-Ippan-002 and #H28-Kagaku-Ippan-003 to Y.Ka.), a Grant-in-Aid for Scientific Research from the Ministry of Education, Culture, Sports, Science, and Technology, Japan (#26293056 and #26670041 to Y.Ka.), the Japan Agency for Medical Research and Development, AMED (#15mk0104053h0101 and #16mk0104027j0002 to Y.S.), and a grant from the Smoking Research Foundation (Y.Ka.).

Author Contributions

Y.S. and Y.Ka. planned the project. S.Y. performed most of the experiments. S.Y. and Y.Ka. wrote the manuscript. Y.Ku. and D.Y. provided technical advices. All authors reviewed the manuscript.

Additional Information

Supplementary information accompanies this paper at http://www.nature.com/srep

Competing financial interests: The authors declare no competing financial interests.

How to cite this article: Yamada, S. *et al.* Chlorpyrifos inhibits neural induction via Mfn1-mediated mitochondrial dysfunction in human induced pluripotent stem cells. *Sci. Rep.* **7**, 40925; doi: 10.1038/srep40925 (2017).

Publisher's note: Springer Nature remains neutral with regard to jurisdictional claims in published maps and institutional affiliations.

展　望

多点電極システムを用いた細胞外電位記録法

――ヒト iPS 心筋細胞および齧歯類神経細胞における医薬品・化学物質の作用解析――

多点電極システムは心筋細胞や神経細胞の電気的活動を簡便に細胞外電位記録するために開発され，これまで様々な研究分野において応用されてきている。近年，本システムを使って医薬品の心臓安全性評価法や化学物質リスク評価法の開発が進められ，これら評価法の標準化について国際的な議論が開始されている。本稿では，多点電極システムの概要，実験への応用例や今後の展開などについて概説する。

山崎　大樹，諫田　泰成，関野　祐子

1　多点電極システムとは

心筋細胞や神経細胞の詳細な電気生理学的特性を調べるには，Neher と Sakmann がノーベル生理学・医学賞を受賞したことでも有名なパッチクランプ法[1]によりイオン電流を測定する方法が最適である。この方法で各種のイオン電流を詳細に記録するためには，外部環境（蛍光灯や各種電源等）からの電気的ノイズの影響を取り除くことを目的として金網のシールドによって顕微鏡・サンプルを囲み，外部からの振動を除去するための除振台を必要とするなど非常に大掛かりなセットが必要である。さらに，先端の径が 1 μm ほどのガラス電極を精密マニピュレーターによって単一細胞へ接触させ僅かな陰圧を保つことによりギガオームシール（細胞膜とパッチ電極間で，ピペット内外の抵抗が 1 ギガオーム以上となる強固な抵抗）を形成させて，漏洩電流を最小限に抑える必要がある。このようにパッチクランプ法によって電気生理学的特性を調べるには，大掛かりなセットに加えて相当に熟練された正確なテクニックが必要である。ところが，医薬品の安全性評価や化学物質のリスク評価では数多くの化合物が対象となるためハイスループット性が強く要求される。したがって，パッチクランプ法での詳細な解析を行うことは，副作用などのメカニズム解明には必要であっても，これらリスク評価で利用することは非現実的である。

近年，多点電極（micro-electrode array：MEA）システムを使って医薬品の心臓安全性評価法や化学物質リスク評価法が開発され，これら評価法の標準化について国際的な議論が開始されている。1997 年に世界で初めて商業製品化された MEA システムが原型であるが，大量のデータ処理が可能になったことから近年になって急速に利用が進んでいる。MEA システムに用いられるプローブには平面に複数の微小電極がパターニングされており，その上に試料を載せて，細胞外電位（field potential：FP）を計測する。特徴を列挙すると次のようになる。①平面微小電極のインピーダンスは非常に小さく，外来ノイズの影響を受けにくいため，シールドや除振台等の特別な実験設備を必要としない。②低ノイズ故に高い SN 比が得られ，急性組織片や未成熟な幹細胞由来分化細胞の微弱応答も簡単・確実に計測できる。さらに，③平面微小電極上に試料を載せた状態で培養でき，細胞に電極を刺入しないことから，安定した状態を保ったまま数週間から数ヶ月にわたって計測が可能である。

現在，MEA システムとして MED64（アルファメッドサイエンティフィック社，日本），Maestro（Axion BioSystems 社，米国），MEA2100－Systems・Mul-

表 1　代表的な MEA システムメーカーとデバイス名や測定プローブ・プレートの詳細

メーカー	本社所在地	デバイス名	ウェル数	電極数
アルファメッドサイエンティフィック社	日本	MED64	1	64
			4	16
			8	8
Axion BioSystems 社	アメリカ	Muse	1	64
		Maestro	12	64
			48	16
			96	8
Multi Channel Systems 社	ドイツ	MEA2100-Systems	1	60
			6	9
		Multiwell-MEA-Systems	24	12
			72	4
			96	3

Field Potential Recording Method Using Micro-Electrode Array System: Cellular Responses in Human iPSC-Derived Cardiomyocytes and Rodent Brain-Derived Neurons.

本稿にある「医薬品」および「化学物質」は，それぞれ日本薬局方および化審法（化学物質の審査および製造等の規制に関する法律）記載の定義に従うものとする。

tiwell-MEA-Systems（Multi Channel Systems 社，ドイツ）などが日米欧から販売されており，様々なアプリケーションで使用されるようになってきた。表1にメーカー・デバイス名・プレートあるいはプローブのウェル数・1ウェルあたりの電極数をまとめたので参照いただきたい。

現在，MEA を用いたアプリケーションとして最も開発が進んでいるのが，ヒト iPS 細胞由来心筋細胞（ヒト iPS 心筋細胞）を用いた医薬品の心臓安全性評価系，ならびにげっ歯類の胎児培養神経細胞を用いた化学物質のリスク評価系である。筆者らは，これらの方法の標準化を目指して様々な化合物を用いて試験法の再現性の検証に取り組んでおり，これら二つについての最新情報と方法論・課題等を以下にご紹介したい。

2　MEA システムによるヒト iPS 心筋細胞を用いた医薬品の安全性評価法

新薬の承認申請にはヒトへの医薬品の安全性を評価する安全性薬理試験の実施が求められている。その試験では現在，致死性の多形性心室頻拍（torsade de pointes：dP）の主な原因である hERG チャネル（心臓において心電図の QT 間隔を主に規定している細胞膜上のタンパク質）の阻害作用を調べる *in vitro* 非臨床試験とヒトの心電図の QT 延長作用を調べる臨床試験が行われている。しかし hERG チャネル阻害や QT 延長は必ずしも TdP 誘発にはつながらないことや，他のタイプの催不整脈性を予測できないことなどの課題があり，非臨床試験の段階でヒトへの安全性をこれまでよりも正確に評価する方法が求められている。ヒト iPS 細胞技術の登場によりヒト心筋細胞を使った試験が可能となり，ヒト iPS 心筋細胞を用いた試験系の開発と安全性薬理試験への利用に大きな期待が寄せられている。

筆者ら，国立医薬品食品衛生研究所薬理部では，ヒト iPS 心筋細胞を利用した医薬品の心臓安全性評価系の構築に世界に先駆けて取り掛かった[2]。新規試験法においては，ハイスループット性に優れ簡便で高い再現性が期待できる MEA システムを採用した（図 1A, B）。細胞外電位の 1 st ピークから次の 1st ピークまでの間隔は inter-spike interval（ISI）と呼ばれ，拍動間隔を表す（図 1C）。心筋細胞は電気刺激により心筋細胞に発現している Na^+ チャネル，Ca^{2+} チャネル，K^+ チャネルを適切なタイミングで活性化あるいは不活性化させて活動電位（action potential: AP）を生じる。心室筋細胞における活動電位の持続時間（AP duration: APD）は細胞外電位波形の 1st ピークと 2nd ピークの間隔を示す FP の持続時間（FP duration: FPD，図 1C）とある程度相関しており[3]，さらにこれらは心電図における QT 間隔に相当する（図 2A）。TdP の発生に主に関与している hERG チャネル阻害は，FPD の延長により評価でき，

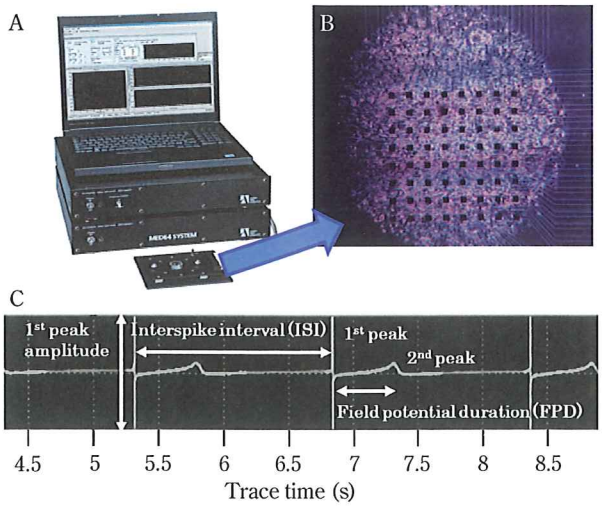

アルファメッドサイエンティフィック社製の多点電極システムである MED64（A）にヒト iPS 心筋細胞のシート（B）をプローブ上に播種し，細胞外電位波形（C）を取得した。1st ピークから次の 1st ピークまでを Inter spike interval（ISI），1st ピークから 2nd ピークまでを Field potential duration（FPD）という。文献 3 および 8 の一部を改変。

図 1　ヒト iPS 心筋細胞における多点電極システムの活用

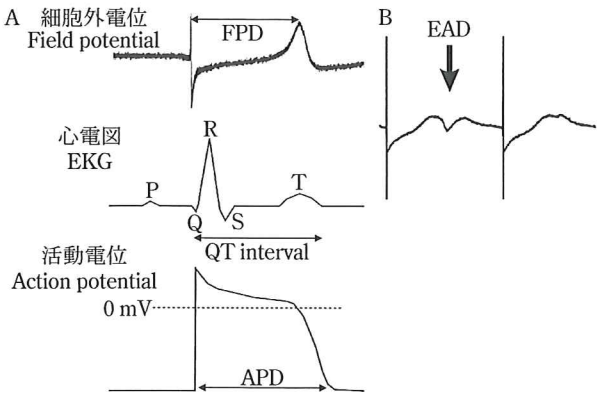

(A) 細胞外電位波形（上段）の FPD に対して心電図波形（中段）の QT 間隔および活動電位波形（下段）の APD80（活動電位がピークから 80%減衰したときの間隔）が時間的に相当する。(B) 細胞外電位波形における異常波形の一つである EAD を示した。

図 2　細胞外電位波形，心電図波形，活動電位波形の比較と細胞外電位波形における異常波形

また TdP の前触れとして考えられている Early after-depolarization（EAD）も観測できる（図 2B）。この試験法の予測性の高さは，hERG チャネルおよび Ca チャネルを同時に阻害するベラパミルの評価で見ることができる。現行の試験法においてベラパミルは，hERG チャネル阻害のみが評価され TdP リスクを有する物質に分類されるが，Ca チャネル阻害作用がこれを相殺するため，実際には TdP を誘発しない。一方，ヒト iPS 心筋細胞と MEA システムを用いた評価系では，Ca チャネル阻害作用も同時に確認できるため，TdP リスクを含めたベラパミルの安全性を正確に評価することができる

ことがわかった。

ヒトiPS心筋細胞には，心臓を構成する複数の細胞が含まれている。実際，ヒトiPS心筋細胞を培養して，単一細胞での活動電位波形を記録すると，心房筋タイプ，心室筋タイプや洞房結節タイプなど複数の活動電位波形が得られる[4]。二次元で細胞を高密度に培養すると，細胞同士は融合し心筋細胞シートが形成され自発的な活動電位および自律拍動がシート全体で同期し，心電図と類似した波形を記録することができる。筆者らは高密度培養を使った方法を標準化して，多施設で再現性を確認することとした。エーザイ（産），東邦大学（学），国立衛研（官）の3者において同一機器（MED64，アルファメッドサイエンティフィック社）・同一細胞（iCell cardiomyocytes, Cellular Dynamics International社）・同一化合物（選択的hERGチャネル阻害薬，E-4031）を用いて実験方法の再現性を検証するバリデーション試験を行った（プレバリデーション試験）。1プローブあたり13000～26000細胞を播種（はしゅ）し，E-4031によるFPD延長率やEADが検出された濃度を比較したところ，3施設間の差は3倍以内に収まっていた[5]。MEAシステムにおいて，FPDは医薬品の薬理反応を評価する上で重要なパラメーターの一つである。筆者らは，計測時の高周波域通過フィルターの違いによって，FPDの値が異なることを明らかにした[6]。さらに播種する細胞密度を厳密に規定することで，標本ごとのばらつきや施設間の差を最小限にできると考えられたことから，播種細胞数の検討を行った。その結果，細胞数依存的に拍動数が減少する一方で，設定したクライテリア（1stピーク振幅≥±200 μV，2ndピーク振幅≥15 μV，inter-spike interval＜1715 msec，FPDcF≥340 msec）を満たす電極数は増加した。1stピーク振幅や2ndピーク振幅の大きさも十分なことから，iCell cardiomyocytesについては1プローブあたり25000細胞以上で播種することが望ましいと結論づけた[6]。

筆者らは最近，厳密な実験条件のもと4施設での大規模検証試験を行い，二つの論文を報告した。一つは，ヒトiPS心筋細胞から得られた拍動数に相当するISIとQT間隔に相当するFPDの関係性が，5000人規模の心拍数とQT間隔との関係を調べた大規模住民研究（フラミンガム心臓研究[7]）の成績に類似していること，およびTdPを誘発する薬剤が，徐脈になるほどFPDを延長することを明らかにしたものである[8]。また，TdPリスクの異なる60化合物を選択し，ヒトiPS心筋細胞における薬剤応答性を様々な薬剤濃度で評価した。得られた結果を実際の臨床データであるCredibleMedsと比較したところ，薬剤誘発性の致死性不整脈の発生リスクの予測度が83％と非常に高かった[9]。

以上のデータは，1種類のヒトiPS心筋細胞と1種類の機器により得られた結果である。筆者らが，ヒトiPS心筋細胞とMEAシステムを組み合わせた医薬品の心臓安全性評価系の構築を始めた頃は，性質が安定しており恒常的に供給可能なヒトiPS心筋細胞は1種類のみであった。近年ではMEAシステムの開発が進むにつれてヒトiPS心筋細胞にもバリエーションが増え，今では日本企業を含む複数のベンダーからヒトiPS心筋細胞が販売され，また筆者らの研究班の成果としてアカデミアからのヒトiPS心筋細胞も検証実験に用いることが可能かどうかの検討を行っている段階である。今後，性質の異なる複数のヒトiPS心筋細胞をMEAシステムで評価することで，ヒトiPS心筋細胞を用いた医薬品のTdPリスク予測に対してなんらかのクライテリアが見いだせるものと期待している。

3　MEAシステムを用いた化学物質リスク評価法

これまで医薬品安全性評価へのMEAシステムの応用を述べてきたが，ここでは神経細胞を用いたMEAシステムの応用を述べたい。当初MEAシステムは，海馬スライス標本での長期増強を記録するために開発されたデバイスである[10]。開発以降，海馬だけでなく大脳皮質[11]や脊髄[12]，網膜[13]などの急性スライス標本や初代培養神経細胞[14]，幹細胞由来神経細胞[15]へも応用されてきており，神経細胞の活動電位の細胞外記録に優れている。近年，化学物質の発達神経毒性評価系にもMEAシステムを応用しようとする動きが世界中で広がってきている。米国環境保護庁（Environmental Protection Agency：EPA）ではMEAシステムによる初代培養ラット大脳皮質神経細胞を用いた化学物質リスク評価法の検討を行った[16)~18)]。この報告では，評価すべき陽性・陰性対照物質（陽性対照物質：発達神経毒性を発現することが知られている化学物質，陰性対照物質：発達神経毒性を発現しないことが知られている化学物質）がいくつか挙げられている（表2）。筆者らも，厚生労働省科学研究費補助金（化学物質リスク研究事業）の支援を受けて，平成28年度よりMEAシステムによる凍結ラット胎児海馬神経細胞を用いた神経ネットワーク評価系の構築を開始した（図3A）。現在筆者らは，群馬大学・白尾研究室から提供された細胞を用いて再現性の高いデータの取得を目指してプロトコル整備を行い，EPAと情報交換しながら評価系の構築を行っている。また，その他にも国際的な動向として発達神経毒性以外にもMEAシステムを化学物質リスク評価に応用しようとする動きがある。その動きの中心になっているのは米国の保健環境科学研究所（HESI）である。HESIは，産官学等の戦略的パートナーから科学者の参画を通じて地球の健康と環境に関する課題を解決するために支援を行っている非営利機関である。HESIでの課題の一つとしてNeuTox（イメージングや形態および神経病理学的な指標等

表2　評価すべき陽性・陰性対照物質一覧

陽性対照物質	分　類	CAS#
ビククリン	$GABA_A$ アンタゴニスト	40709-69-1
ビフェントリン	電位依存性ナトリウムチャネル・殺虫剤	82657-04-3
カルバリル	アセチルコリンエステラーゼ阻害剤	63-25-2
クロルピリホス	アセチルコリンエステラーゼ阻害剤	5598-15-2
シフルトリン	電位依存性ナトリウムチャネル・殺虫剤	68359-37-5
デルタメトリン	電位依存性ナトリウムチャネル・殺虫剤	52918-63-5
ジアゼパム	$GABA_A$ アンタゴニスト	439-14-5
ドウモイ酸	グルタミン酸受容体アンタゴニスト	14277-97-5
フィプロニル	$GABA_A$ アンタゴニスト	120068-37-3
フルオキセチン	セロトニン選択的再取り込み阻害剤	114247-09-5
イミダクロピリド	ニコチン性アセチルコリン受容体・殺虫剤	138261-41-3
ケタミン	NMDA 受容体アンタゴニスト	33795-24-3
鉛	重金属	6080-56-4
L-グルタミン酸	グルタミン酸受容体アゴニスト	19285-83-7
リンデン	$GABA_A$ アンタゴニスト	58-89-9
メチル水銀	重金属	115-09-3
ムッシモール	$GABA_A$ アゴニスト	18174-72-6
ニコチン	ニコチン性アセチルコリン受容体アゴニスト	54-11-5
ペルメトリン	電位依存性ナトリウムチャネル・殺虫剤	52645-53-1
RDX	$GABA_A$ アンタゴニスト	121-82-4
トリメチルスズ	重金属	56-24-6
バルプロ酸	抗けいれん薬	1069-66-5
ベラパミル	電位依存性ナトリウムチャネル阻害剤	152-11-4
陰性対照物質	**分　類**	**CAS#**
アセトアミノフェン	Cox-2 阻害剤	103-90-2
アモキシシリン	抗生物質	26787-78-0
グリホサート	除草剤	1071-83-6
パラコート	除草剤	1910-42-5
サッカリン	甘味料	82385-42-0
サリチル酸	植物ホルモン	69-72-7
D-ソルビトール	甘味料	50-70-4

（文献 16 の一部を改変）

の連携により，既知の神経毒性・発達神経物質の曝露（ばくろ）によって生じる毒性の予測が可能なバイオマーカーの同定を目的とした活動）がある。神経細胞ネットワークの活動を指標として既知の神経毒性の曝露による毒性予測が可能かを検証する MEA サブチームでは，MEA プラットフォームにおけるラット神経細胞や脳スライス，ヒト iPS 神経細胞の違いを比較するとともに，てんかんを引き起こすことが知られている医薬品を用いたプレバリデーションの実施内容について現在議論されている。

MEA システムを用いて神経ネットワークの形成を評価する場合の指標について，現状では有効的かつ効果的な指標は決まっていない。そのため，10 を超えるパラメーターについて解析し，評価するのに最適なパラメーターを検討する必要がある。すでに解析パラメーターに関する論文が報告されている[19]ので，それを例にとって説明する。

未成熟な胎児神経細胞は，頻度は低いが神経細胞の活性化を示すスパイクと呼ばれる電位変化を生じる。この電位変化は非常に短い（数 msec）間に起こるが，これを MEA システムによって検出する。MEA システムではスパイクの検出閾値をノイズレベルの 6〜8 倍に設定することでノイズの検出を防いでおり，検出閾値を超えたスパイクはラスタープロットとして表される（図 3B）。神経細胞の成熟とともにスパイクの発生頻度は増加し，やがて神経細胞の突起同士がシナプスを形成することで神経ネットワークを構築する。神経ネットワークの構築により各神経細胞で独立に発生しているスパイクが同期し，最終的にはバーストやネットワークスパイクと呼ばれる連続的でウェル中の複数の電極で同期した電位変化が起こるようになる（図 3C）。スパイクやバーストの発生を電極ごとの発生頻度として算出するためには，それらの現象が起こっている電極の数についても算出する必要がある。1 ウェルで 1 分間に発生したスパイクを活性化電極数（Active electrodes，1 分間に 5 回以上のスパイクを生じた電極数）で除算した値を MFR（Mean firing rate）という（図 4）。さらにそれぞれの現象が発生するまでの間隔，同期して生じるスパイクやバーストの発生頻度，持続時間，発生までの間隔等の合計 12 のパラメーターについて算出し（表 3），主成分分析などによって評価指標としてより相関性の高いパラメーターを提案することになる。今後は，現在構築中の評価系において上述の陽性対照物質や陰性対照物質を急性投与や慢性投与によりリスク評価を行う予定である。

神経ネットワーク形成の機能評価について，現在はげっ歯類の神経細胞を用いて評価が行われている。動物実験代替の観点からヒト iPS 神経細胞を利用できることが理想であるが，ヒト iPS 神経細胞はそれのみの培養では成熟しにくいことが知られている。ヒト iPS 神経細胞においてスパイクが検出されるためには長期間（数か月程度）の培養期間を設けるか，グリア細胞との共培養系あるいはグリア細胞の条件培地を用いる系にするかである。しかし培養の長期化は評価の複雑化につながり，グリア細胞との共培養や条件培地の使用は再現性

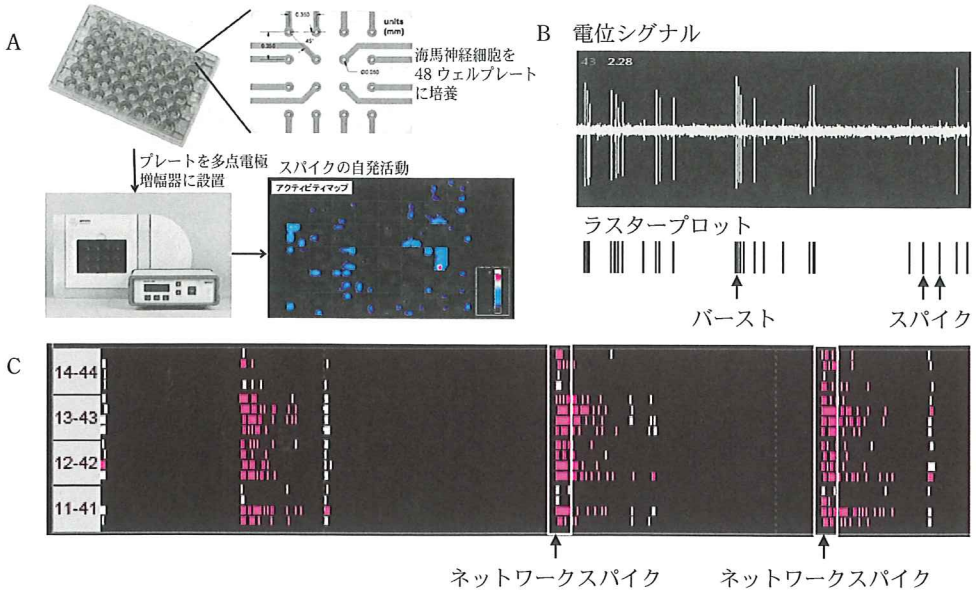

A. 各ウェルに 16 個の電極が埋め込まれている 48 ウェルプレートにラット海馬神経細胞を 1 ウェルあたり 50000 細胞を播種・培養し，Axion 社製多点電極システムに設置し，神経活動を記録する。神経活動（スパイク）がアクティビティマップとして疑似カラー表示される。B. 1 電極ごとに電位シグナルが検出され，検出閾値よりも大きなシグナルはラスタープロットとして表示される。ラスタープロット 1 本 1 本はスパイクを表しており，スパイクがまとまって発生した場合にはバーストと呼ばれる。C. 1 ウェル（16 電極）のラスタープロット。同期したスパイクをネットワークスパイクと呼ぶ。白のラスタープロットは単一のスパイク，赤のラスタープロットはバーストを表している。

図 3　神経細胞を用いた多点電極システム

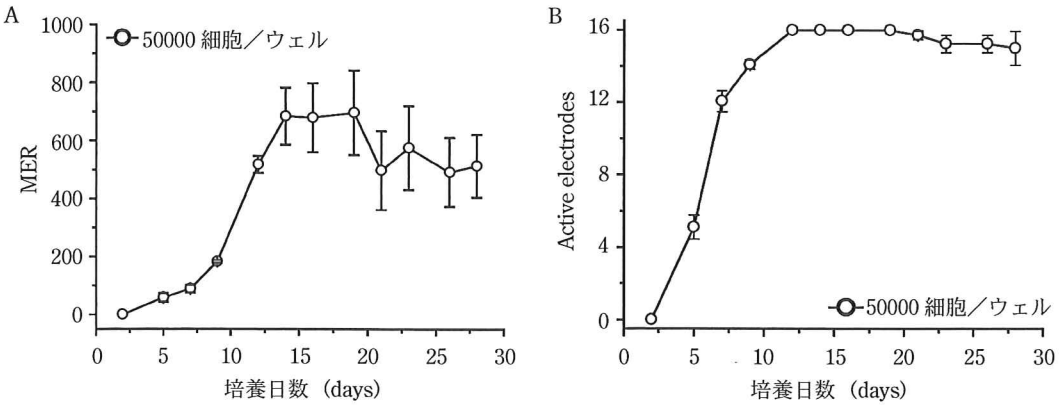

(A) 28 日目までの神経活動を経時的に表した。4 ウェル分の平均値を示す。縦軸は 1 分間に観察された 1 電極あたりのスパイク数を示した。培養 14 日目から 19 日目では 1 電極あたりのスパイク数が維持された。(B) A と同じウェルでの 1 分間に 5 回以上スパイクが記録された電極数（Active electrodes）の経時変化を示した。培養日数 7 日目にはすでに半数以上の電極が活性化状態となり，12 日目以降はほぼすべての電極が活性化していた。その状態は培養 28 日目まで持続した。

図 4　経時的な神経活動計測

を担保するのが難しいと考えられることから，ヒト iPS 神経細胞を用いた MEA システムでの評価系を構築するには更なる検討が求められている。

4　おわりに

本稿では，心筋細胞や神経細胞の電気的活動を簡便に測定可能な MEA システムの開発の背景と，現在応用されている二つのアプリケーション例について紹介した。ヒト iPS 心筋細胞を用いた医薬品の心臓安全性評価では，日本国内のみならず世界規模でその評価に係（かかわ）るガイドライン改訂の動きがあり，ヒト iPS 心筋細胞と MEA システムを組合せた評価系の導入が検討されている。

また，神経毒性における化学物質リスク評価における MEA システムの利用は今まさに開発段階であり，*in vivo* 試験を主とする医薬品の薬理試験や化学物質の発達神経毒性評価系への導入の提案に向けて世界規模で動いている。今後，ますます MEA システムの応用は増えて

表3　多点電極システムにおける神経ネットワーク形成の解析パラメーター

解析パラメーター	説　明
スパイク頻度	1電極あたり1分間のスパイク数
バースト頻度	1電極あたり1分間のバースト数
バースト間隔	1電極におけるバーストの間隔
起バースト電極	バーストが観察された電極数
バースト内のスパイク頻度	バースト中に生じたスパイクの頻度
バースト内のスパイクの割合	バースト中に生じたスパークの割合
バースト間隔の変動係数	バーストの間隔の標準偏差
バースト内のスパイク間隔の変動係数	バースト中に観察されたスパイクの間隔の標準偏差
ネットワークスパイク頻度	1分間に生じた同期したスパイク数
ネットワークスパイク間隔	1分間に生じた同期したスパイクの間隔
ネットワークスパイクピーク	1分間に生じた同期したスパイクが観察された電極数
平均相関係数	1対の電極ごとの組合せを係数を用いて算出

（文献19の一部を改変）

いくものと思われる。

謝辞　本研究は，厚生労働省科学研究費補助金（H24-Iyaku-Shitei-030 to YS）ならびに国立研究開発法人日本医療研究開発機構（AMED）の医薬品等規制調和・評価研究事業委託研究「ヒトiPS分化細胞技術を活用した医薬品の次世代毒性・安全性評価試験系の開発と国際標準化に関する研究」（#15mk0104053h0101 for 2015, #16mk0104027j0002 for 2016 to YS），厚労省化学研究費補助金（化学物質リスク研究事業）「発達期における統合的な遅発性神経毒性試験法の開発」（H28-化学-一般-003 to YK）のサポートにより実施されました。

文　献

1) E. Neher, B. Sakmann : *Nature*, **260**, 799 (1976).
2) Y. Kanda, D. Yamazaki, J. Kurokawa, T. Inutsuka, Y. Sekino : *J. Pharmacol. Toxicol. Methods.*, **81**, 196 (2016).
3) Y. Ide, D. Yamazaki, Y Kanda, Y. Sekino : *Kokuritsu Iyakuhin Shokuhin Eisei Kenkyusho Hokoku*, in press.
4) J. Zhang, G. F. Wilson, A. G. Soerens, C. H. Koonce, J. Yu, S. P. Palecek, J. A. Thomson, T. J. Kamp : *Circ. Res.*, **104**, e30 (2009).
5) Y. Nakamura, J. Matsuo, N. Miyamoto, A. Ojima, K. Ando, Y. Kanda, K. Sawada, A. Sugiyama, Y. Sekino : *J. Phamacol. Sci.*, **124**, 494 (2014).
6) K. Asakura, S. Hayashi, A. Ojima, T. Taniguchi, N. Miyamoto, C. Nakamori, C. Nagasawa, T. Kitamura, T. Osada, Y. Honda, C. Kasai, H. Ando, Y. Kanda, Y. Sekino, K. Sawada : *J. Pharmacol. Toxicol. Methods.*, **75**, 17 (2015).
7) A. Sagie, M. G. Larson, R. J. Goldberg, J. R. Bengtson, D. Levy : *Am. J. Cardiol.*, **70**, 797 (1992).
8) W. Yamamoto, K. Asakura, H. Ando, T. Taniguchi, A. Ojima, T. Uda, T. Osada, S. Hayashi, C. Kasai, N. Miyamoto, H. Tashibu, T. Yoshinaga, D. Yamazaki, A. Sugiyama, Y. Kanda, K. Sawada, Y. Sekino : *PLoS One*, **11**, e0167348 (2016).
9) H. Ando, T. Yoshinaga, W. Yamamoto, K. Asakura, T. Uda, T. Taniguchi, A. Ojima, R. Shinkyo, K. Kikuchi, T. Osada, S. Hayashi, C. Kasai, N. Miyamoto, H. Tashibu, D. Yamazaki, A. Sugiyama, Y. Kanda, K. Sawada, Y. Sekino : *J. Pharmacol. Toxicol. Methods.*, in press.
10) H. Oka, K. Shimono, R. Ogawa, H. Sugihara, M. Taketani : *J. Neurosci. Methods.*, **93**, 61 (1999).
11) M. Kobayashi, K. Imamura, T. Sugai, N. Onoda, M. Yamamoto, S. Komai, Y. Watanabe : *Eur. J. Neurosci.*, **12**, 264 (2000).
12) H. Zhang, N. Robinson, C. Wu, W. Wang, M. A. Harrington : *PLoS One*, **5**, e11696 (2010).
13) L. Li, Y. Hayashida, T. Yagi : *Vision Res.*, **45**, 263 (2005).
14) S. Honma, T. Shirakawa, Y. Katsuno, M. Namihira, K. Honma : *Neurosci. Lett.*, **250**, 157 (1998).
15) Y. Fujimoto, M. Abematsu, A. Falk, K. Tsujimura, T. Sanosaka, B. Juliandi, K. Semi, M. Namihira, S. Komiya, A. Smith, K. Nakashima : *Stem Cells.* **30**, 1163 (2012).
16) E. R. McConnell, M. A. McClain, J. Ross, W. R. Lefew, T. J. Shafer : *Neurotoxicology.* **33**, 1048 (2012).
17) P. Valdivia, M. Martin, W. R. LeFew, J. Ross, K. A. Houck, T. J. Shafer : *Neurotoxicology.* **44**, 204 (2014).
18) J. P. Brown, D. Hall, C. L. Frank, K. Wallace, W. R. Mundy, T. J. Shafer : *Toxicol. Sci.*, **154**, 126 (2016).
19) E. Cotterill, D. Hall, K. Wallace, W. R. Mundy, S. J. Eglen, T. J. Shafer : *J. Biomol.. Screen.* **21**, 510 (2016).

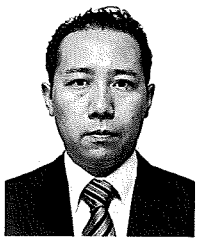

山崎大樹（Daiju YAMAZAKI）
国立医薬品食品衛生研究所薬理部（〒158-8501 東京都世田谷区上用賀1-18-1）。名古屋市立大学大学院薬学研究科博士後期課程修了。薬学博士。≪現在の研究テーマ≫医薬品・化学物質のMEAシステムによる評価系の構築と国際標準化。≪趣味≫テニス，スポーツ観戦，ドライブ。
E-mail: daiju-y@nihs.go.jp

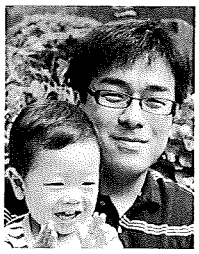

諫田泰成（Yasunari KANDA）
国立医薬品食品衛生研究所薬理部（〒158-8501 東京都世田谷区上用賀1-18-1）。東京大学大学院薬学系研究科修士課程修了。博士（薬学）。≪現在の研究テーマ≫幹細胞を用いた医薬品および化学物質の安全性評価と国際標準化。≪趣味≫旅行，食べ歩き，子育て。
E-mail: kanda@nihs.go.jp

関野祐子（Yuko SEKINO）
国立医薬品食品衛生研究所薬理部（〒158-8501 東京都世田谷区上用賀1-18-1。東京大学薬学部卒。医学博士。≪現在の研究テーマ≫ヒトiPS分化細胞技術を活用した医薬品の次世代安全性評価試験系の開発と国際標準化。
E-mail: yukos@mol.f.u-tokyo.ac.jp

電気学会論文誌 A（基礎・材料・共通部門誌）
IEEJ Transactions on Fundamentals and Materials
Vol.136 No.2 pp.99-104 DOI: 10.1541/ieejfms.136.99

Paper

Visualization of Spatially Distributed Bioactive Molecules using Enzyme-Linked Photo Assay

Hikaru Mabuchi* Student Member, HongYao Ong* Associate
Kazunori Watanabe* Non-member, Sachiko Yoshida* Non-member
Naohiro Hozumi*a) Senior Member

(Manuscript received March 18, 2015, revised Oct. 4, 2015)

In this paper, we propose a new simple device for visualizing bioactive molecules with a fine spatial resolution by using a membrane in which a specific enzyme is immobilized. The layer produces fluorescence after association with a specific substance. The layer, on which a biological tissue is to be mounted, is deposited on a quartz substrate that is used as a light guide to introduce UV light to the layer. Substance release is observed by a CCD camera from the opposite side of the substrate. In order to shorten the experiment time, we had automated the optical device. The paper also describes the reduction of background fluorescence by means of image processing technique. Images were acquired by employing two UV-LEDs with slightly different angle. Image processing was performed to separate background and target fluorescence by means of independent component analysis. Finally the release of GABA(γ-aminobutyric acid) and glutamate from specific layers in rat cerebellum was successfully observed. It is expected that, using this method, both real-time transmitter release and its response to medicine can be observed.

Keywords : bioactive molecules, enzyme-linked photo assay, independent component analysis

1. Introduction

Light guide is composed of a dielectric material that can enclose the light propagation. In addition to being applied to communication, it is useful for sensing as well. In chemical sensing the surface of the light guide has to be coated with some specific chemical that may change its optical property depending on chemical reactions. Such a function can be applied to chemical imaging, if the light guide has a flat surface. This study proposes an application of two-dimensional light guide, of which surface is chemically modified, to biochemical imaging.

Neurotransmitter molecules released from neurons are not only regulators of neuronal transduction but also indicators of neuronal conditions. Glutamate and γ-aminobutyric acid (GABA) are known as typical transmitters in brain cortex that play important roles as stimulator and suppresser, respectively. Lack of balance in the release of glutamate and GABA may lead to autism, epilepsy or Parkinson's disease[(1)(2)].

In order to observe the spatio-temporal release in cerebellar cortex, we have newly proposed the enzyme-linked photo assay system, which is realized even using normal CCD camera, and observed GABA release in developing cerebellar slice using either new or authorized methods[(3)].

In this paper, we propose a new simple device for this purpose by using a reactive layer in which a specific enzyme is immobilized, and produces fluorescence after association with a specific substance released from mounted slice. This layer is bound a quartz substrate that is used as a light guide for UV light excitation. Fluorescence derived from a substance is observed by a CCD camera from the opposite side of the substrate.

The paper describes the reduction of background fluorescence by means of image processing technique. Finally it will be shown that the release of transmitters from specific layers in rat cerebellum was successfully observed.

2. Specimen Preparation and Photo Excitation System

Imaging of neurotransmitter release was monitored the reaction of oxidoreductases generating reduced nicotinamide adenine dinucleotide (NAD^+) or diphosphonucleotide ($NADP^+$). For glutamate and GABA, we used glutamate dehydrogenase and GABA disassembly enzyme (GABase), respectively.

Enzymes were covalently immobilized on the quartz glass substrate using a silane coupling agent and a crosslink agent. The substrate was as thick as 1 mm. Stoichiometrically generated NADH or NADPH emits 480 nm fluorescence after excitation at 340-365 nm.

Existence of glutamate and GABA lead to fluorescence when co-existing with specific enzyme and co-enzyme. A glass substrate on which specific enzyme is coated is in contact with the biological specimen. A chamber space is created around the specimen. The space is filled with buffer liquid and co-enzyme. On the glass substrate therefore, the specimen is in contact with both enzyme and co-enzyme.

Consequently glutamate or GABA, that is released from the tissue spontaneously by stimulation, makes an oxidation-reduction reaction on the substrate. Although both glutamate and GABA do not produce fluorescence by themselves, NAD(P)H that is created as the result of the above chemical reaction makes fluorescence. As the ratio of glutamate or GABA and NAD(P)H is 1:1, the

a) Correspondence to: Naohiro Hozumi. E-mail: hozumi@icceed.tut.ac.jp
* Toyohashi University of Technology
1-1, Hibarigaoka, Tenpaku, Toyohashi 441-8580, Japan

fluorescence can be correlated to the amount of released glutamate or GABA.

In the experiment, rat cerebellum was sliced sagittally at 400 μm thick and incubated in oxygen-aerated HEPES-Na^+ buffer for 40 min. The slice was placed on the quartz glass substrate with both $NADP^+$ and α-ketoglutarate. Figure 1 shows the schematic diagram of the observation system including the device. The enzyme was immobilized covalently on the glass as shown in Fig. 2. Figure 3 shows chemical reactions taking place on the substrate. $NADP^+$ (nicotinamide adenine dinucleotide phosphate) changes into NADPH (reduced nicotinamide adenine dinucleotide phosphate) just as glutamate and GABA degeneration. Synthesized NADPH was illuminated by 360 nm surface UV-LED, and emitted the 480 nm fluorescent light observed by cooled CCD (ORCA ER, Hamamatsu Photonics). The quartz substrate can be recognized as a light guide to illuminate the surface of the substrate.

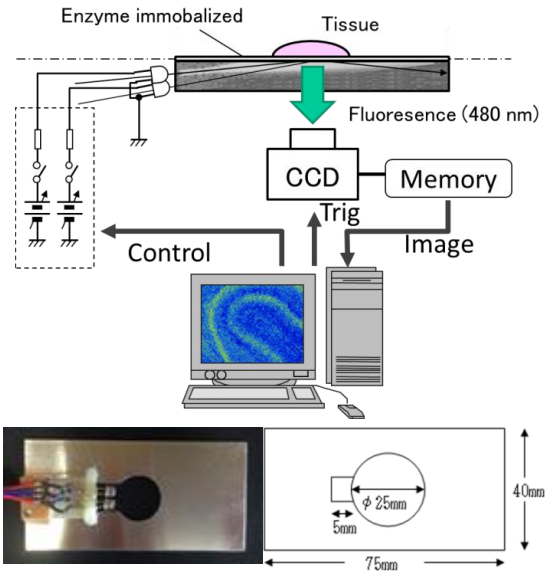

Fig. 1. Schematic diagram of the observation system including the device and its outlook

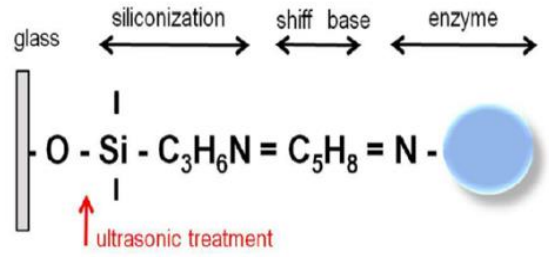

Fig. 2. Immobilized enzyme

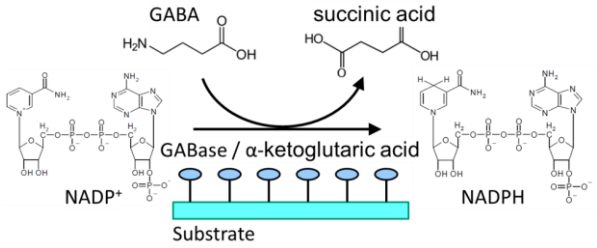

Fig. 3. Chemical reaction on the substrate

3. Image Processing

The fluorescent light detected by the CCD camera is divided into target light and background light. As significant intensity of background light is detected, it is assumed that fluorescence is excited by the light that is refracted on the interface between the substrate and tissue system including the layer. The light, being generated by LEDs and propagates though the substrate, can be decomposed into plane waves with different angles of propagation. Each plane wave transfers across the enzyme layer and comes into the tissue. We assume that both target and background light were predominantly excited by normal light. As the background light significantly damage the quality of the image, it should be reduced as much as possible. Making use of the evanescent light may be a solution, however, it may make the system complicated, and the target light may be not as significant as this case. Therefore we tried to reduce the background by means of a simple image processing.

Assuming that the light is a plane wave and scatter can be neglected, wave propagation and detected fluorescence can be illustrated as Fig. 4. In the figure, fluorescence, attributed to the layer where the enzyme is fixed, is represented as I_0. This is

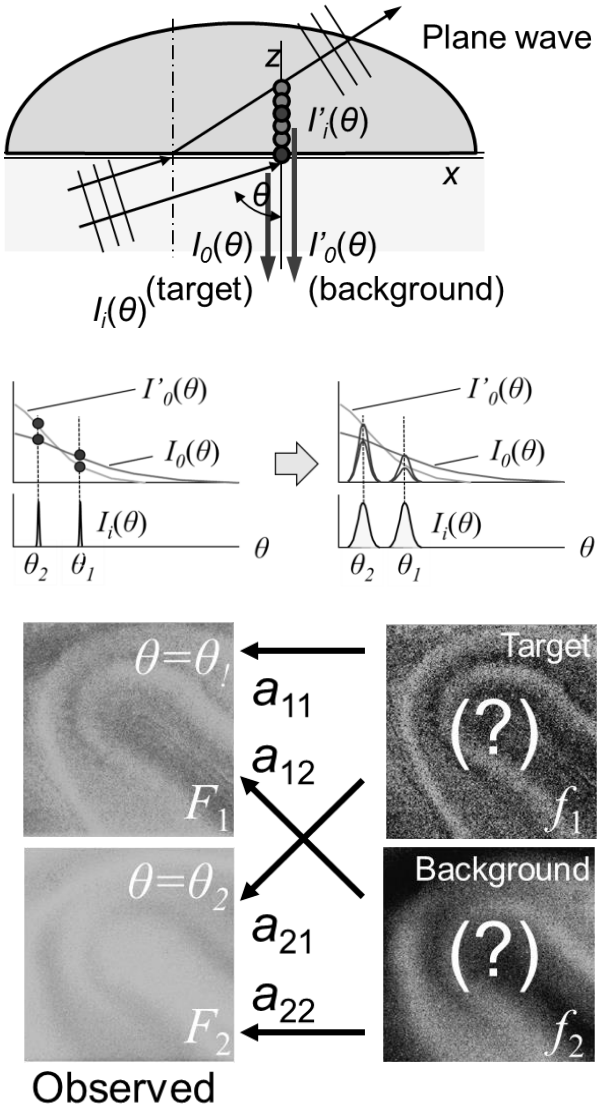

Fig. 4. Fluorescence detected by CCD camera

defined as to be the target. The fluorescence attributed to the tissue is represented as I'_0 . This is defined as to be the background. Both I_0 and I'_0 depends on the incident angle θ. The thickness of the quartz plate, which is used as a light guide, is as thick as 1 mm. As it is much thicker than the diameter of normal optical fiber it is relatively easy to introduce two kinds of lights of which angles of center axes are significantly different. In addition, in practice, they depend differently on the incident angle. As the result, the proportion (I_0/I'_0) is not the same along θ. This is true even if the incident angle has distributed.

As the result, the captured fluorescence with different angle of optical axis is composed of target and background fluorescence with different mixture ratios. This can be represented as:

$$\begin{pmatrix} F_1 \\ F_2 \end{pmatrix} = \begin{pmatrix} a_{11} & a_{12} \\ a_{21} & a_{22} \end{pmatrix} \begin{pmatrix} f_1 \\ f_2 \end{pmatrix} \quad \cdots\cdots (1)$$

where $F_1(x,y)$ and $F_2(x,y)$ are captured fluorescence image, $f_1(x,y)$ and $f_2(x,y)$ are spatial distributions of fluorescence as the target and background, a_{11}, a_{12}, a_{21}, a_{22} are constants. Although the image acquisition is sequential, ICA is performed by assuming that two images, $F_1(x,y)$ and $F_2(x,y)$ are acquired with a negligible time lag. Reproduced images $f'_1(x,y)$ and $f'_2(x,y)$ are calculated from F_1 and F_2. As the result of periodical acquisitions of F_1 and F_2, time dependent images of f'_1 and f'_2 are calculated. Eq. (1) can also be described using a matrix expression as:

$$\mathbf{F} = \mathbf{A} \cdot \mathbf{f} \quad \cdots\cdots (2)$$

The target and background fluorescence distribution can be calculated by applying $\mathbf{A}^{-1}$ to $\mathbf{F}$. In practice, only contrast of the image would be enough to recognize the distribution. In such a case $\mathbf{A}^{-1}$ can be represented as:

$$\begin{pmatrix} 1 & \alpha \\ \beta & 1 \end{pmatrix} \quad \cdots\cdots (3)$$

After capturing two images $\mathbf{F}_1$ and $\mathbf{F}_2$ by changing the angle of optical axis, the target and background images can be separated by finding appropriate numbers for α and β. α and β can be tuned manually by monitoring the quality of reproduced image, however, the theory of independent component analysis (ICA) may be powerful for solving such a problem[4].

Stochastic distribution of pixel intensity in images f'_1 and f'_2 are represented as $p(y_{1i})$ and $p(y_{2j})$, where y_{1i} and y_{2j} represent the intensity.

$$\left.\begin{aligned} p(y_1) &\equiv \{p(y_{11}), \cdots, p(y_{1i}), \cdots p(y_{1n})\} \\ p(y_2) &\equiv \{p(y_{21}), \cdots, p(y_{2j}), \cdots p(y_{2n})\} \end{aligned}\right\} \quad \cdots\cdots (4)$$

$p(y_{1i}, y_{2j})$ represents the probability that the intensity of a pixel in image f'_1 is y_{1i} and that of the corresponding point in image f'_2 is y_{2j}. In other words $p(y_1)$ and $p(y_2)$ are probabilities that cases y_1 and y_2 take place, respectively, and $p(y_1, y_2)$ is the probability that cases y_1 and y_2 takes place simultaneously. Variables y_1 and y_2 are considered to be independent when

$$p(y_1, y_2) = p(y_1)p(y_2) \quad \cdots\cdots (5)$$

is established. Kullback-Leibler (K-L) parameter is often employed to indicate the independency of variables:

$$KL \equiv \sum_{i,j} p(y_{1i}, y_{2j}) \log \frac{p(y_{1i}, y_{2j})}{p(y_{1i})p(y_{2j})} \quad \cdots\cdots (6)$$

The K-L parameter is zero when two sets of variables y_1 and y_2 are completely independent together. In practice, α and β in Eq. (3), which determine the probabilities $p(y_1)$, $p(y_2)$ and $p(y_1, y_2)$, can be tuned so that the K-L parameter indicates the minimum.

The process of ICA is illustrated in Fig. 5. The equation described in the form of matrix indicates that two images, F_1 and F_2, derive from linear combination of unknown original images f_1 and f_2. If an appropriate inverse matrix can be found then the original images can be reproduced. However as the matrix to describe the linear combination is unknown as well, ICA algorithm is applied to find the most appropriate matrix (as the inverse matrix). In the

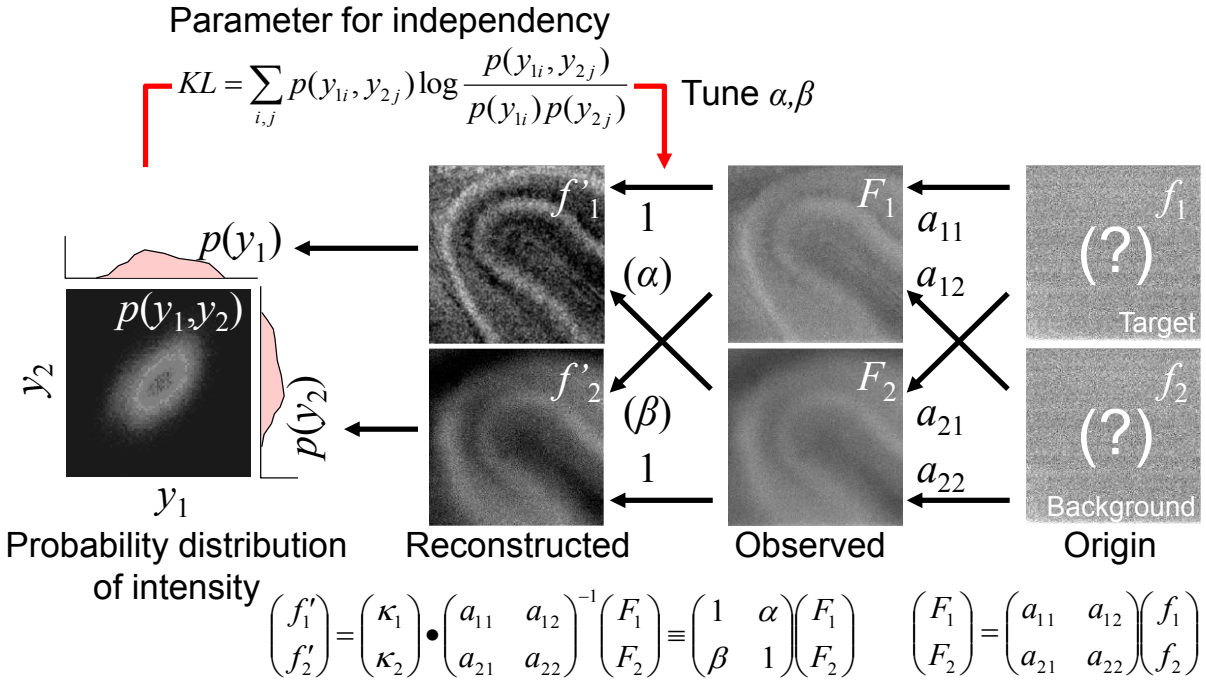

Fig. 5. Illustration for image processing based on independent component analysis

ICA process K-L parameter is calculated in order to evaluate the probabilistic independency of images f'_1 and f'_2. It can be considered that in the reproduction algorithm the core process is the calculation of the K-L parameter. In this preliminary study K-L parameter is successively calculated by manually changing the inverse matrix, and images are assumed to be reproduced when the K-L parameter indicates the minimum.

4. Results and Discussion

4.1 Image Processing using the ICA Figure 6 (a) shows visible light image of the cerebellum with postnatal 21 days. In developing cerebellum, granule cells, small input neurons, proliferate and migrate down from the external granular layer (EGL) to the internal granular layer (IGL). As the development proceeds, EGL turns into molecular layer (ML) whereas IGL remains. Purkinje cells, big output neurons, develop their dendrites and associate neuronal connections between granule cells and other interneurons. Neuronal circuit layer forms the ML. As the cerebellum shown in Fig. 6 (a) is mature, ML, PL, IGL are clearly visible. Note that ML is on the outer side of the cerebellum, and a wrinkle surrounded by the ML is seen in Fig. 6 (a).

As for fluorescence observation, three different images were acquired. Two were with different inclination of the excitation light source, and one was with no excitation light. Each of the two images with excitation light was subtracted with the image with no excitation light, in order to reduce the background light from the outside. These two images after the subtraction were defined as images A and B.

Figure 6 (b) shows these images for a rat cerebellum. Both images are very unclear, because of the background fluorescence. Figure 6 (c) shows the result of image processing. It is clearly shown in the image entitled as "target" that the fluorescence intensity is high in two layers, whereas that entitled as "background" is not clear. By morphological inspection these layers are recognized as ML and IGL. These layers are known that GABAergic neurons distribute in mature cerebellum. Studies using HPLC and electrophysiological method have shown that GABA is released from the postnatal cerebellar cortex even before synaptogenesis, and that GABA receptors act on the developing cerebellar Purkinje cells[4][5]. However, dynamic GABA release could not be observed unless the enzyme-linked photo assay is used. In addition, because cytoplasmic autofluorescence becomes noisy background light, it is useful that the image processing system extracted the image of GABA release from the autofluorescence-contained image. Using this method, both real-time transmitter release and its response to medicine can be observed.

4.2 Transition after Chemical Stimulation In relatively developed cerebellum, cells distributed in the ML and IGL are only the neurons of glutamate release, so that both layers showed fluorescent activities. Figure 7 indicates release distribution of glutamate in comparison with normal optical image illuminated with visible light. The fluorescent image, indicating glutamate release, is after the ICA processing. Figure 7 (c) indicates the regions of interest for analysis. Regions highlighted as ML and IGL have relatively strong intensity in fluorescence. They have a contrast to the region highlighted as PL. Release from white matter (WM), which is mostly composed of fatty materials, is much less significant.

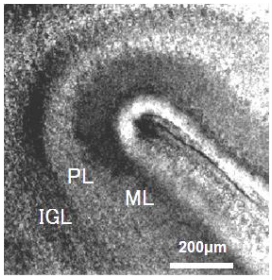

(a) Visible light image

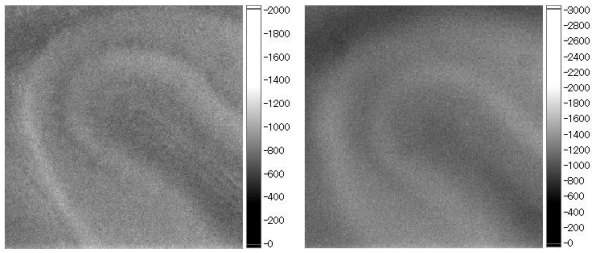

Small angle (image A). Large angle (image B).

(b) Fluorecence images before image processing

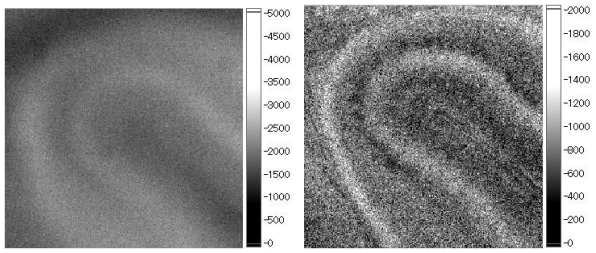

Background Target

(c) Fluorecence images after image processing

Fig. 6. Cross sectional mages of cerebellar cortex: (a) Visible light image, (b) original fluorescent images with different angle of optical axes, and (c) fluorescent images after the image processing. Scales are indicated in arbitrary unit. Specimen: rat cerebellum (postnatal 21 days), target: GABA

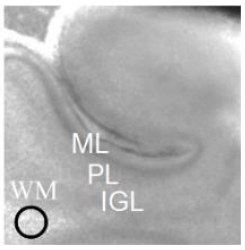

(a) Visible light image

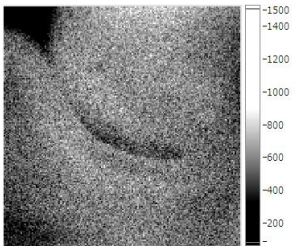

(b) Fluorescent image

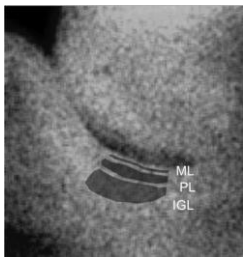

(c) Regions of interest for analysis

Fig. 7. Cerebellum with postnatal 7 days observed with visible light and fluorescent light indicating glutamate release. 0.9 mm × 0.9 mm. Gray scale is arbitrary. ML: molecular layer, PL: Purkinje layer, IGL: internal granular layer, WM: white matter. Specimen: rat cerebellum (postnatal 7 days)

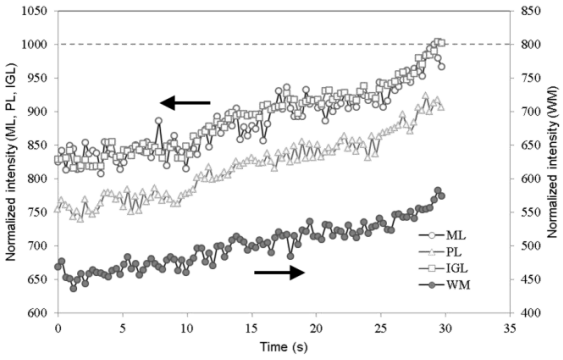

Fig. 8. Transition in fluorescence intensity in each layer (normalized by the intensity of ML 30 s after stimulation that is indicated as 1000). Specimen: rat cerebellum (postnatal 7 days), target: glutaminate

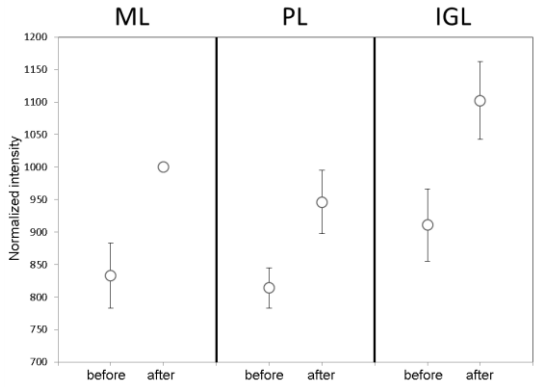

Fig. 9. Change in fluorescence intensity before and after AMPA stimulation (normalized by the intensity of ML 30 s after stimulation that is indicated as 1000). Specimen: rat cerebellum (postnatal 7 days), target: glutaminate

Our system can visualize both spontaneous and responsive transmitter release with about 0.2 s time resolution. Figure 8 shows the transition of glutamate release in response to 100 μmol/ℓ (S)-alpha-Amino-3-hydroxy- 5 methylisoxazole-4-propionic acid (AMPA) application in cerebellar slices. All values are normalized by the intensity of ML 30 s after stimulation that is indicated as 1000. Fluorescence, as indication glutamate release, was intense in both the IGL and ML, whereas the PL was indicated with lower intensity. As shown in Fig. 8, a clear increase in fluorescence was observed after stimulation. Transition in fluorescence was similar for ML and IGL, suggesting that these layers are activated. However PL, which was not expected to release glutamate, showed fluorescence as well although it was less intense than ML and IGL. As this specimen was taken from relatively young rat (postnatal 7 days), the cerebellar development was not totally completed, and the layers were not separated enough. It is hence considered that diffusion from ML and IGL to PL would take place, leading to an increase in fluorescence in this layer. The increase in fluorescence in WM suggests that glutamate might have been diffused into WM as well, although the absolute value was much lower than ML and IGL.

Figure 9 compares the fluorescence in each layer before and after stimulation. Four different specimens were used for the observation, in order to confirm reproducibility. It is clear that the AMPA stimulation brought a significant glutamate release from ML and IGL, although the increase is also seen with PL.

5. Conclusions

A new method for visualization of spatially distributed bioactive molecules using enzyme-linked photo assay has been proposed. It is based on fluorescent reaction assisted by an enzyme immobilized on the substrate, however, background fluorescence disturbs the observation. In order to reduce the background fluorescence, two images were acquired by changing the optical axis of UV illumination. Image processing based on independent component analysis made the target image clear. Observation of rat cerebellum was successfully performed and GABA and glutamate release from two specific layers was clearly indicated.

Acknowledgement

The study was partially supported by grants from Scientific Research (C) 23500516, 26350498 and Health Labor Sciences Research.

References

(1) N. C. Danbolt : "Glutamate Uptake", *Neurobiology*, Vol.65, pp.1-105 (2001)
(2) N. Kasai, Y. Jimbo, O. Niwa, T. Matsue, and K. Torimitsu : "Rea-time Multisite Observation of Glutamate Release in Rat Hippocampal Slices", *Neurosdence Lett.*, Vol.304, pp.112-116 (2001)
(3) T. Morishima, M. Uematsu, T. Furukawa, Y. Yanagawa, A. Fukuda, and S. Yoshida : "GABA Imaging in Brain Slices Using Enzyme-linked Photo Analysis", *Neurosci. Res.*, Vol.67, pp.347-353 (2001)
(4) V. Calhoun, G. Pearlson, and T. Adali : "Independent Component Analysis to fMRI Data, A Generative Model for Validating Results", VLSI Signal Processing, Vol.37, pp.281-291 (2004)
(5) F. F. Trigo, M. Chat, and A. Marty : "Enhancement of GABA Release through Endogenous Activation of Axonal GABA(A) Receptors in Juvenile Cerebellum", *J. Neurosci*., Vol.27, No.46, pp.12452-63 (2007)
(6) K. Obata : "Excitatory and Trophic Action of GABA and Related Substances in Newborn Mice and Organotypic Cerebellar Culture", *Dev Neurosci*, Vol.19, No.1, pp.117-119 (1997)

Hikaru Mabuchi

(Student Member) was born in Hokkaido, Japan on July 25, 1992. He is 1st-year student in Graduate School of Toyohashi University of Technology. His major is electric and electronic information. He has been engaged in research on bio-sensing by means of optical measurement. He is a student member of IEEJ.

HongYao Ong

(Associate) was born in Malaysia on June 30, 1990. He received his B.S degree in 2014 from Toyohashi University of Technology, Japan. His major is electric and electronic information. He is currently engaged in GS Reality Sdn. Bhd., Malaysia. His major is electric and electronic information. He is an associate member of IEEJ.

Kazunori Watanabe

(Non-member) was born in Asahikawa, Japan on February 3, 1992. He is 2nd-year student in Graduate School of Toyohashi University of Technology. His research focuses both the optimization of surface modification for biosensor, and detection of neurotransmitters. He is a member of Japan neuroscience Society.

Sachiko Yoshida

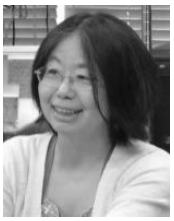

(Non-member) was born in Toyama, Japan on January 24, 1961. She received her B.S., M.S. and Ph.D. degrees in 1983, 1986 and 1990 from University of Tokyo. She was engaged in JSPS Postdoctoral Researcher from 1990 to 1992, JST PRESTO Researcher from 1992 to 1994, and Research Associate at Toyohashi University of Technology from 1995 to 1996. Since 1996, she has been a lecturer of Toyohashi University of Technology. Her research interests focus the physiological interaction and morphological transformation through brain differentiation, and these detections. She is a member of a member of IEEE, International Brain Research Organization, Society for neuroscience, Japan neuroscience Society, and the Physiological Society of Japan.

Naohiro Hozumi

(Senior Member) was born in Kyoto, Japan on April 2, 1957. He received his B.S., M.S. and Ph.D. degrees in 1981, 1983 and 1990 from Waseda University. He was engaged in Central Research Institute of Electric Power Industry (CRIEPI) from 1983 to 1999. He was an associate professor of Toyohashi University of Technology from 1999 to 2006, and a professor of Aichi Institute of Technology from 2006 to 2011. Since 2011, he has been a professor of Toyohashi University of Technology. He has been engaged in the research in insulating materials and diagnosis for high voltage equipment, acoustic measurement for biological and medical applications, etc. He was awarded in 1990 and 1999 from IEE of Japan for his outstanding research papers. He is a member of IEEE, IEE of Japan and the Acoustic Society of Japan.

Quantitative evaluation method for differentiation of C2C12 myoblasts by ultrasonic microscopy

2017 Jpn. J. Appl. Phys. 56 07JF11

(http://iopscience.iop.org/1347-4065/56/7S1/07JF11)

Japanese Journal of Applied Physics **56**, 07JF11 (2017)
https://doi.org/10.7567/JJAP.56.07JF11

REGULAR PAPER

Quantitative evaluation method for differentiation of C2C12 myoblasts by ultrasonic microscopy

Kyoichi Takanashi[1]*, Mamoru Washiya[1], Kazuki Ota[1], Sachiko Yoshida[1], Naohiro Hozumi[1]*, and Kazuto Kobayashi[2]

[1]*Department of Electrical and Electronic Information Engineering, Toyohashi University of Technology, Toyohashi, Aichi 441-8580, Japan*
[2]*Honda Electronics Co., Ltd., Toyohashi, Aichi 441-3139, Japan*

*E-mail: k143239@edu.tut.ac.jp; hozumi@iceed.tut.ac.jp

Received November 25, 2016; accepted February 6, 2017; published online June 14, 2017

Cell differentiation was evaluated by ultrasonic microscopy. However, there were some regions that showed a lower acoustic impedance than the culture liquid. It was considered that, in such regions, the cells were not perfectly in contact with the film substrate. Hence, a waveform analysis was performed, and compensated acoustic impedances in such regions were in a reasonable range of values. By the same analysis, the displacements of partially floated cells were also successfully calculated. The elapsed day transitions of the compensated acoustic impedances and displacements were successfully evaluated. In the process of differentiation, actin fibers comprising the cytoskeleton are supposed to loosen in order to induce cellular fusion. In addition, the progress in cell differentiation accompanied by a change into a three-dimensional structure can partially be assessed by the displacement between a cell and a cultured film. Hence, we believe that cell differentiation can be evaluated using an ultrasonic microscope.

1. Introduction

An optical microscope is often used for the measurement of biological tissues and an antibody staining technique is often employed to observe the biological structure. However, such a measurement process may take a long time because the staining process takes several hours or days. In addition, the biological function of matter may be lost completely after staining.

On the other hand, an ultrasonic microscope makes it possible to indicate an acoustic characteristic (e.g., elastic parameter or sound speed) of cells as a two-dimensional profile.[1–13] An acoustic characteristic is an important parameter for the quantitative characterization of living tissues. As chemical staining is not necessary, the measurement can be performed without losing the biological functions of cells.[14–17] This reduces cost and time for staining as well. In addition, ultrasound can be directly digitized as a waveform three-dimensional structure that may be estimated by various waveform analyses. In this study, we will propose the nondestructive measurement of living cells using an ultrasonic microscope that we developed. C2C12 myoblast cells will be targeted.

As a requirement for cell measurement, regenerative medicine using stem cells is being developed markedly.[18,19] When cells are being transplanted, nondifferentiated cells or tissues should be never included, which may produce teratomas in vivo.[20,21] For such reasons, monitoring cell differentiation is highly advantageous. This series of studies is conducted to determine whether a quantitative ultrasonic microscope can be used to monitor cell differentiation. The transition of the acoustic impedance of the cells during differentiation was monitored. In addition, displacement from the culture film substrate after cell differentiation was evaluated in order to assess cell growth.

2. Experimental methods

2.1 C2C12 myoblasts

The C2C12 myoblasts used in this study are clones of mouse myoblasts. These cells remain undifferentiated at the initial expression of heart and skeletal muscles. The C2C12 myoblasts (DS Pharma Biomedical) were cultured in Minimum Essential Medium Eagle with Hanks' salt (HMEM; Sigma-Aldrich M4780 Hank's MEM) supplemented with l-glutamine, 10% fetal bovine serum (FBS), some vitamins, amino acids, and 0.1 g/L kanamycin (proliferation medium, PM), and the medium was replaced every other day. To induce the differentiation of myoblasts into myotubes, C2C12 cells at an 80–90% confluency were transferred to HMEM without FBS (differentiated medium, DM). All cells were cultured and observed in OptiCell™ (Thermo Scientific Nunc), which is composed of two polystyrene films of 50 cm^2 in culture area and 75 μm in film thickness. C2C12 myoblasts were injected and cultured in the space between the two films.[22]

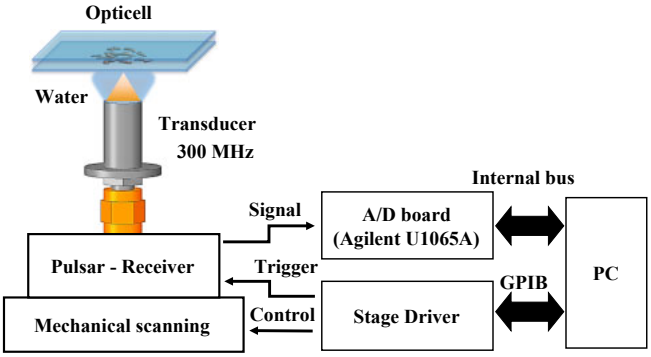

Fig. 1. (Color online) Schematic diagram of the measurement system.

2.2 Measurement system

The details of the measurement system that we developed can be found in Refs. 23–25. As shown in Fig. 1, the scanning ultrasonic microscope is composed of an ultrasonic transducer, a mechanical scanning unit, a pulsar/receiver, an A/D converter (Agilent U1065A Acqiris DC222 8 GS/s), and a stage controller.

The pulsed ultrasound was focused at the interface between a cell and the film substrate. The reflection was received and interpreted into a characteristic acoustic impedance. The two-dimensional acoustic impedance profile was obtained by mechanical scanning.

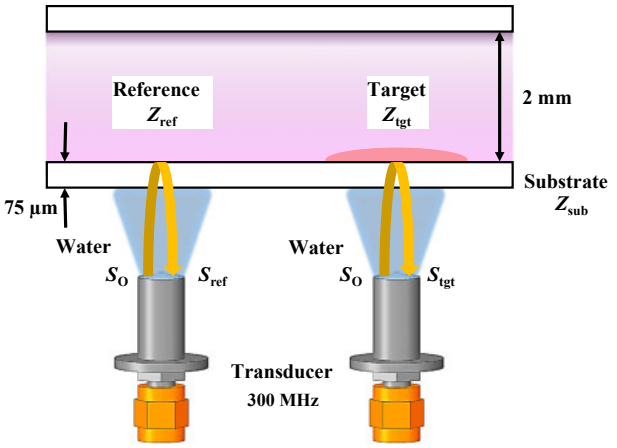

Fig. 2. (Color online) Illustration for calibration of the acoustic impedance.

An acoustic wave was transmitted and received by the same transducer. The ultrasonic transducer was composed of a ZnO thin film attached to a sapphire lens (aperture half-angle: 60°), and its frequency after being driven by an electric pulse ranged briefly from 100 to 500 MHz. The central frequency was 300 MHz. The transducer had a focal length of about 0.288 mm. The measurement was performed with eight times of averaging (sampling frequency was 4 GSamplings/s) in order to reduce random noise before being introduced into the computer. Distilled water was used as the coupling medium between the film substrate and the transducer. Two-dimensional profiles of the acoustic impedance can be obtained by mechanically scanning the transducer.

Figure 2 illustrates the basic concept of determining the acoustic impedance. The reference waveform is the reflection from the interface between the film substrate and the culture liquid, which appears in the field of view, the acoustic impedance of which is known to be 1.52 MN·s/m^3. The target waveform is the reflection from the interface between a cell and the culture liquid.

The acoustic impedance of the target substance, Z_{target}, is determined by comparing these two reflections as

$$Z_{target} = \frac{1 - \frac{S_{target}}{S_{ref}} \cdot \frac{Z_{sub} - Z_{ref}}{Z_{sub} + Z_{ref}}}{1 + \frac{S_{target}}{S_{ref}} \cdot \frac{Z_{sub} - Z_{ref}}{Z_{sub} + Z_{ref}}} Z_{sub}, \quad (1)$$

where S_{ref} and S_{target} are the reference and target signals, and Z_{sub} and Z_{ref} are the acoustic impedances of the film substrate (2.46 MN·s/m^3) and cultured liquid (1.52 MN·s/m^3), respectively. By considering the oblique incident component of the ultrasonic wave, the longitudinal wave acoustic impedance is obtained by using the result of sound field analysis in order to obtain a more accurate value.

2.3 Investigation of low-acoustic-impedance area of the measurement result

Figure 3 shows the acoustic impedance profiles of undifferentiated and differentiated C2C12 myoblasts and their corresponding histograms. In the profiles, the regions measured at around 1.52 MN·s/m^3 correspond to the culture liquid. Cells are normally higher in acoustic impedance than the culture liquid.[7,25–30] However, some regions after differentiation induction are measured at a significantly low acoustic impedance. Hence, some comparisons of waveforms from different points of the measurement result were performed as shown in Fig. 4(a). Firstly, the waveform of the culture liquid, which is defined as the reference waveform, was extracted from point 1. Then, target waveforms from a cell (point 2) and a significantly low acoustic impedance area (point 3) were extracted. Consequently, subtractions between both target waveforms with the reference waveform were performed as shown in Figs. 4(b) and 4(c). From Fig. 4(c), it is clear that the residual waveform obtained from the subtraction of the target waveform from the cell and the reference waveform was relatively larger than that in Fig. 4(b). Here, we can conclude that some interference must have happened in the target waveforms of an area with a significantly low acoustic impedance. Hence,

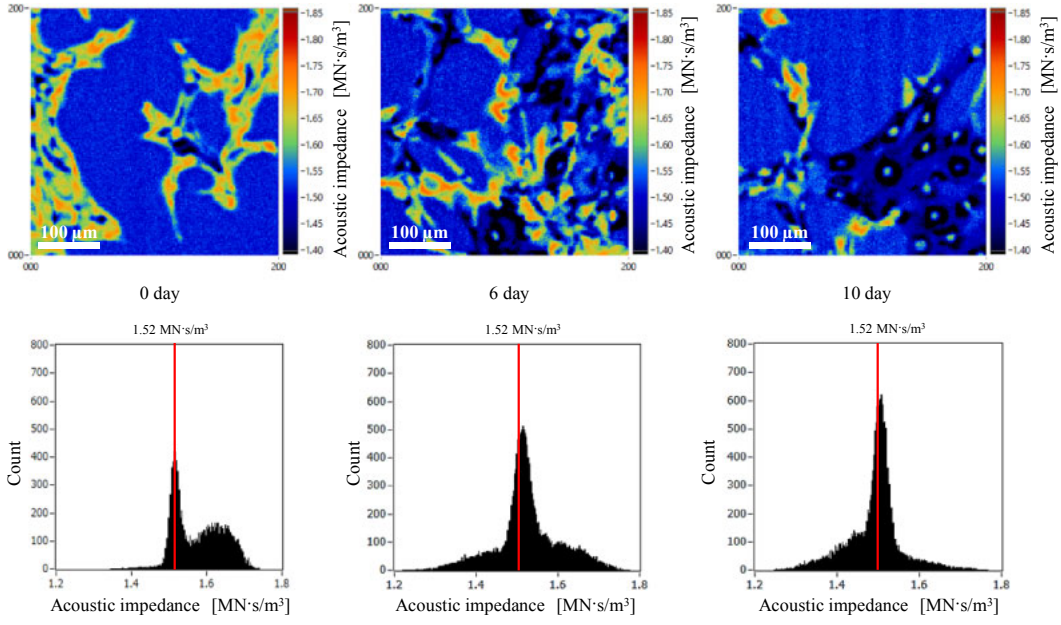

Fig. 3. (Color online) Acoustic impedance profiles of undifferentiated and differentiated C2C12 myoblasts, and their corresponding histograms.

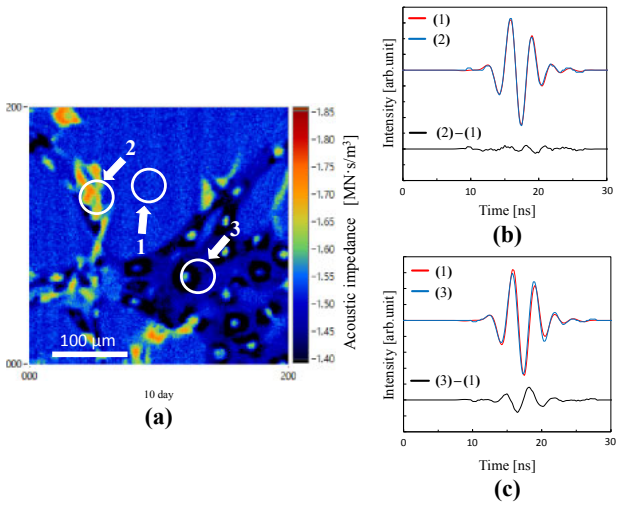

Fig. 4. (Color online) Some comparisons of waveforms from different points. (a) Acoustic impedance profile measured at the 10th day after differentiation induction. (b) Comparison of target waveforms from point 1 and high-acoustic-impedance area (point 2). (c) Comparison of target waveforms from point 1 and significantly low acoustic impedance area (point 3).

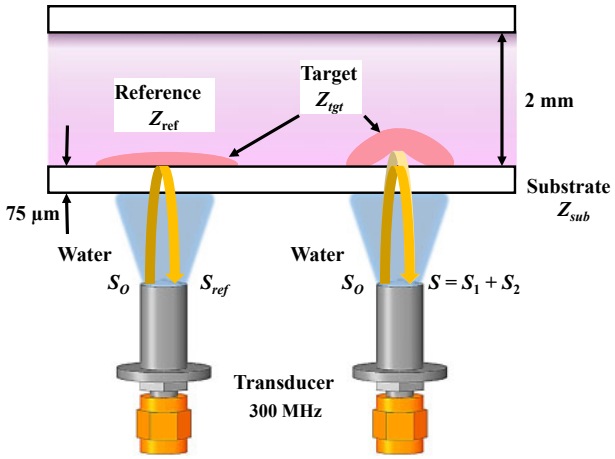

Fig. 5. (Color online) Illustration for compensation of the acoustic impedance.

in order to eliminate interference, the waveform was subjected to the waveform analysis described in the next chapter.

3. Compensation of acoustic impedance

3.1 Interference due to nonperfect contact of cells to the film

C2C12 myoblasts have such a characteristic that F-actin coagulates through differentiation and grows into a tissue with a contractile ability through the expression of various proteins.[26–31] Cell contraction will create a gap between the cell and the film substrate during differentiation. Figure 3 illustrates that, at such a stage, the cells are not perfectly in contact with the film substrate. For this reason, the interference of reflected waves may occur, leading to an error in acoustic impedance estimation. At such a point, it can be assumed that the reflection wave S is composed of two different reflection components (S_1 and S_2).

Figure 5 illustrates the compensation of the acoustic impedance. S_1 is very similar in both shape and intensity to the reference wave S_{ref}, which is the reflection from the interface between the film substrate and the culture liquid. S_2, which can be considered the reflection from the interface between the culture liquid and the cell, is relatively small in intensity, as there is only a small difference in acoustic impedance at the boundary between materials. In addition, these two wave components are opposite in polarity, because the acoustic impedance is high in the culture film, low in the culture liquid, and relatively high again in the cell.

The acquired waves can be separated into these two components by an appropriate waveform analysis. The acoustic impedance of the cell would be evaluated using the separated reflection intensities.

It is assumed that the acquired waveform can be described as a linear combination of the components as

$$S_{(t)} = S_1 + S_2, \tag{2}$$

$$S_{1(t)} = P_1 \exp\left[A_1(t-t_1) - \beta_1(t-t_1)^2\right] \times \cos[2\pi f_0(t-t_1)], \tag{3}$$

$$S_{2(t)} = P_2 \exp\left[A_1(t-t_1) - \beta(t-t_1)^2\right] \times \cos[2\pi f_0(t-t_2)], \tag{4}$$

where P_1 and P_2 are the intensities, A_1 and A_2 are the attenuation constants, f_0 is the central frequency of the pulse ($f_0 = 300\,\mathrm{MHz}$), β_1 and β_2 ($\mathrm{cm}^2/\mathrm{kg}$) are the coefficients of compressibility for the media, and t_1 and t_2 are the delay times. These parameters (P_1, P_2, A_1, A_2, β_1, β_2, t_1, and t_2) can be determined by the gradient descent method. β_1 and β_2 are set as constants with a value of $0.1\,\mathrm{cm}^2/\mathrm{kg}$ to improve the analysis speed. In performing the gradient descent method, a partial derivative is applied to a function, and it searches the local minimum (or maximum) of the function. The reproduced waveform $S_{(t)}$ is modified as

$$\begin{aligned} S_{(t)}^{(k+1)} &= S_{(t)}^{(k)} - \alpha \cdot \mathrm{grad}[f(S_{(t)}^{(k)})] \\ &= S_{(t)}^{(k)} - \alpha \left[\frac{\partial f(S_{(t)}^{(k)})}{\partial P_1^{(k)}} \frac{\partial f(S_{(t)}^{(k)})}{\partial P_2^{(k)}} \frac{\partial f(S_{(t)}^{(k)})}{\partial A_1^{(k)}} \frac{\partial f(S_{(t)}^{(k)})}{\partial A_2^{(k)}} \frac{\partial f(S_{(t)}^{(k)})}{\partial t_1^{(k)}} \frac{\partial f(S_{(t)}^{(k)})}{\partial t_2^{(k)}} \right]^{\mathrm{t}}, \end{aligned} \tag{5}$$

where k is the repetitive number and α is the learning rate. The parameters are determined so that the difference between the waveform reproduced by Eq. (2) and the practically acquired waveform is minimized.

3.2 Compensation of acoustic impedance

The compensation of acoustic impedance was performed by solving

$$S_1 = \frac{Z_{\mathrm{ref}} - Z_{\mathrm{sub}}}{Z_{\mathrm{ref}} + Z_{\mathrm{sub}}} S_0, \tag{6}$$

$$S_2 = \frac{Z_{\mathrm{target}} - Z_{\mathrm{ref}}}{Z_{\mathrm{target}} + Z_{\mathrm{ref}}} TS_0, \tag{7}$$

where S_0 is the transmitted signal, and Z_{sub} and Z_{ref} are the acoustic impedances of the film substrate ($2.46\,\mathrm{MN{\cdot}s/m^3}$)

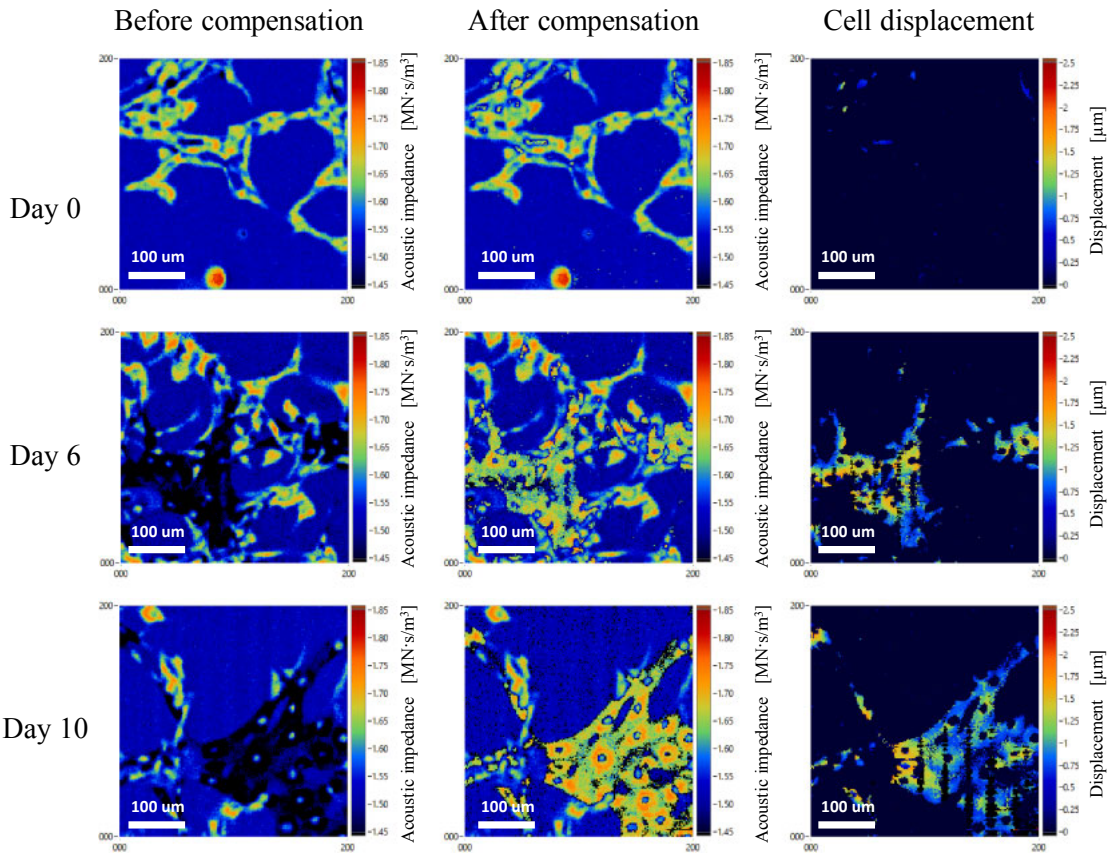

Fig. 6. (Color online) Profiles measured before and after compensation of acoustic impedance and the displacement distance.

and cultured liquid (1.52 MN·s/m^3), respectively. T is the echo transmittance represented as

$$T = \frac{4Z_{\mathrm{sub}}Z_{\mathrm{ref}}}{(Z_{\mathrm{sub}} + Z_{\mathrm{ref}})^2}. \tag{8}$$

By simultaneously solving Eqs. (6)–(8) and considering that S_1 and S_2 are in opposite phases, the cell acoustic impedance Z_{target} at the gap is shown as

$$Z_{\mathrm{target}} = \frac{1 + \frac{S_2}{S_1} \cdot \frac{Z_{\mathrm{sub}}^2 - Z_{\mathrm{ref}}^2}{4Z_{\mathrm{sub}}Z_{\mathrm{ref}}}}{1 - \frac{S_2}{S_1} \cdot \frac{Z_{\mathrm{sub}}^2 - Z_{\mathrm{ref}}^2}{4Z_{\mathrm{sub}}Z_{\mathrm{ref}}}} Z_{\mathrm{ref}}. \tag{9}$$

3.3 Displacement of cells from the culture film

As illustrated in Fig. 5, it is considered that, in the low-acoustic-impedance region in Fig. 3, cells are not perfectly in contact with the film substrate. Therefore, the time lag Δt of the two reflection components was calculated by using t_1 and t_2. The displacement distance d (μm) is shown as

$$d = \frac{1}{2} \cdot c \cdot \Delta t, \tag{10}$$

where c is the sound speed ($c = 1500$ m/s) through the culture liquid and Δt is the time lag of the two reflection components ($\Delta t = t_2 - t_1$).

4. Results and discussion

Figure 6 shows the profiles measured before and after compensation in the low-acoustic-impedance region, and the distance of displacement calculated by using the above-mentioned method. After compensation, the region where the acoustic impedance was originally low showed an acoustic impedance of around 1.65–1.75 MN·s/m^3. This would be a reasonable acoustic impedance of cells.[7,25–30] A significantly high acoustic impedance area appeared around the nucleus. This high-acoustic-impedance area was assumed to be due to F-actin, which protects and supports the nucleus. In addition, the distance of displacement was around 0.8–2.0 μm. Although the spatial resolution in the lateral direction determined by the diffraction limit is expected to be as high as 5 μm at 300 MHz, note that the gap distance of 0.8–2 μm between the cell and the film substrate was successfully assessed, as the spatial resolution in the depth direction is generally much higher than that in the lateral direction at a sufficient sampling speed.

Changes in acoustic impedance accompanied by differentiation were evaluated by the compensated profiling method. Intracellular changes with differentiation in a single cell have been reported; however, the change in differentiating cell population is unknown. Our evaluation first provides the tools to clarify this. Figure 7 shows the transition of the acoustic impedance of cells for 10 days after shifting to DM. This graph represents the ratio of the relatively high acoustic impedance area to the total cellular area in the measurement area. The threshold was changed from 1.55 to 1.70 MN·s/m^3 at an interval of 0.01. When the acoustic impedance was set at 1.68 MN·s/m^3, the transition rate of the area was measured and is as shown in Fig. 7; hence, this value was determined by the threshold value. As shown in this graph, the ratio of the high-acoustic-impedance

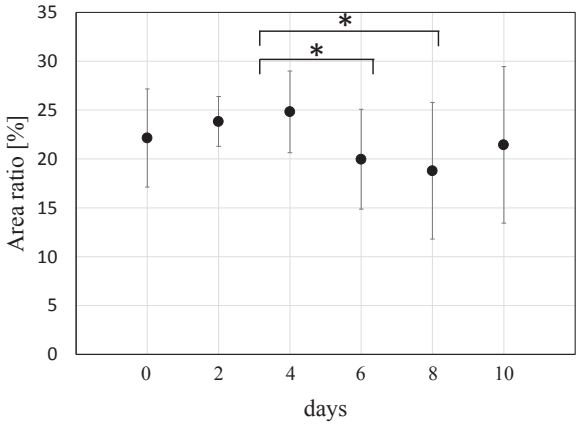

Fig. 7. Area ratio of the high-acoustic-impedance ($\geqq$1.68 MN·s/m^3) area to the total cellular area. Each point shows the average area ratio and standard deviation of eight samples ($^*P = 0.07$).

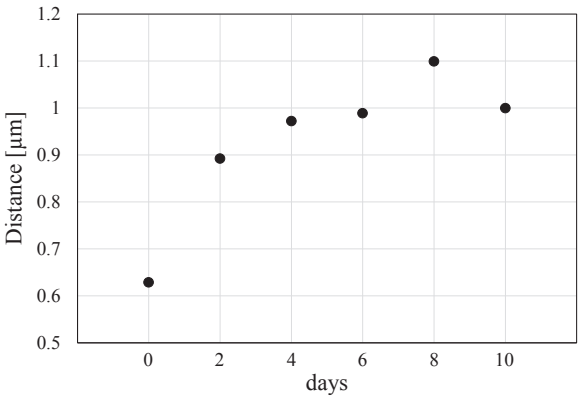

Fig. 8. Elapsed day transition of the average displacement. Each point shows the average displacement of eight samples.

area tended to decrease. The asterisk in the graph shows a tendency to decrease as determined by Student's *t*-test ($P = 0.07$).

This change would be consistent with the change in the intracellular condition of F-actin, which is one of the important factors in cell development. In undifferentiated cells, F-actin exists abundantly in the periphery of the nucleus. During differentiation, myoblast cells simultaneously fuse together to form a myotube. F-actin would defuse within the cytoplasm temporarily. The areal ratio would be reduced after the loosening of F-actin. After cell fusion, F-actin would reassemble in the vicinity of the nucleus and the parenchyma in order to support the cell membranes. Therefore, the ratio of high acoustic impedance would increase as the cells differentiate after the 10th day.

Moreover, Fig. 8 shows the transition of displacement between the cells and the basal film for 10 days after shifting to DM. It tended to increase with a constant rate during differentiation, suggesting the formation of a three-dimensional structure.

However, these measurements were disturbed by the existence of non-negligible noise. For this reason, it is necessary to suppress vibration and reduce noise in order to increase the calculation accuracy of the displacement distance.

5. Conclusions

The differentiation of C2C12 cells was assessed by means of an acoustic microscope. An ultrasonic beam was transmitted across a plastic film substrate on which cells were cultured, and the reflection was interpreted as the acoustic impedance and displacement of cells from the culture film. This quantitative measurement was considered perfectly non-invasive to cells, as well as it made it possible to continuously monitor the change in acoustic response through the differentiation process.

The acoustic impedance was often determined to be extremely low when the reflection intensities from the cell and reference material were simply compared. A waveform analysis made it possible to assess the displacement between a cell and the film substrate, which is also a factor for monitoring the degree of differentiation. In such a case, the acquired waveform was composed of two different reflections. During cell differentiation, the change in the section of impedance was measured, suggesting the loosening of F-actin in the cells. The waveform analysis made it possible to assess the displacement between a cell and the film substrate. The displacement was successfully assessed to be 0.8–2 μm, as the spatial resolution in the depth direction is generally much higher than that in the lateral direction at a sufficient sampling speed. This method would be a good tool for monitoring the degree of differentiation.

The results suggest that monitoring the transition of the acoustic impedance is useful for evaluating the differentiation of muscle fibers. Furthermore, the displacement was found to be reflected by the three-dimensional conformation of the organ.

1) S. Saito, Y. Kameyama, and K. Nakamura, Jpn. J. Appl. Phys. **40**, 3664 (2001).
2) N. Hozumi, R. Yamashita, C.-K. Lee, M. Ngao, K. Kobayashi, Y. Saijo, M. Tanaka, and S. Ohtsuki, Ultrasonics **42**, 717 (2004).
3) Y. Saijo, N. Hozumi, C. Lee, M. Nagao, K. Kobayashi, N. Oakada, N. Tanaka, E. S. Filho, H. Sasaki, M. Tanaka, and T. Yambe, Ultrasonics **44**, e51 (2006).
4) N. Hozumi, A. I. Gunawan, S. Kajima, S. Yoshida, Y. Saijo, K. Kobayashi, and S. Yamamoto, 2013 Joint UFFC/EFTF/PFM Symp., 2013, p. 1212.
5) K. Kobayashi, S. Yoshida, Y. Saijo, and N. Hozumi, Ultrasonics **54**, 1922 (2014).
6) N. Hozumi, R. Yamashita, C.-K. Lee, M. Nagao, K. Kobayashi, Y. Saijo, M. Tanaka, N. Tanaka, and S. Ohtsuki, Acoust. Sci. Technol. **24**, 386 (2003).
7) Y. Saijo, T. Miyakawa, H. Sasaki, M. Tanaka, and S. Nitta, Ultrasonics **42**, 695 (2004).
8) T. Higuchi, S. Hirata, T. Yamaguchi, and H. Hachiya, Jpn. J. Appl. Phys. **52**, 07HF19 (2013).
9) T. Higuchi, S. Hirata, T. Yamaguchi, and H. Hachiya, Jpn. J. Appl. Phys. **53**, 07KF27 (2014).
10) K. Tachi, H. Hasegawa, and H. Kanai, Jpn. J. Appl. Phys. **53**, 07KF17 (2014).
11) H. Isono, S. Hirata, and H. Hachiya, Jpn. J. Appl. Phys. **54**, 07HF15 (2015).
12) Z. Qu and Y. Ono, Jpn. J. Appl. Phys. **54**, 07HF01 (2015).
13) M. Omura, K. Yoshida, M. Kohta, T. Kudo, T. Ishiguro, K. Kobayashi, N. Hozumi, and T. Yamaguchi, Jpn. J. Appl. Phys. **55**, 07KF14 (2016).
14) Y. Saijo, E. S. Filho, H. Sasaki, T. Yambe, M. Tanaka, and N. Hozumi, IEEE Trans. Ultrason. Ferroelectr. Freq. Control **54**, 1571 (2007).
15) Y. Saijo, A. Kimura, S. Terauchi, M. Nagao, S. Yoshida, K. Kobayashi, and N. Hozumi, IEEE Ultrasonics Symp., 2006, p. 1421.
16) Y. Hagiwara, Y. Saijo, A. Ando, E. Chimoto, H. Suda, Y. Onoda, and E. Itoi, Ultrasonics **49**, 386 (2009).
17) Y. Tanaka, Y. Saijo, Y. Fujihara, H. Yamaoka, S. Nishizawa, S. Nagata, T.

Ogasawara, Y. Asawa, T. Takato, and K. Hoshi, J. Biosci. Bioeng. **113**, 252 (2012).
18) O. Ishii, M. Shin, T. Sueda, and J. P. Vacanti, J. Thorac. Cardiovasc. Surg. **130**, 1358 (2005).
19) Y. Kuroyanagi, K. Kubo, H. Matsui, H. J. Kim, S. Numari, Y. Mabuchi, and S. Kagawa, Artif. Organs **28**, 13 (2004).
20) M. Abad, L. Mosteiro, C. Pantoja, M. Cañamero, T. Rayon, I. Ors, O. Graña, D. Megias, O. Domindues, D. Martinez, M. Manzanares, S. Ortega, and M. Serrano, Nature **502**, 340 (2013).
21) W. Y. Wendy, P. E. de Almeida, and J. C. Wu, *Teratoma Formation: A Tool for Monitoring Pluripote ncy in Stem Cell Research* (Stembook, Boston, MA, 2012) p. 1.
22) S. T. Cooper, A. L. Maxwell, E. Kizana, M. Ghoddusi, E. C. Hardeman, I. E. Alexander, D. G. Allen, and K. N. North, Cell Motility Cytoskeleton **58**, 200 (2004).
23) N. Hozumi, A. Kimura, S. Terauchi, M. Nagao, S. Yoshida, K. Kobayashi, and Y. Saijo, IEEE Ultrasonics Symp., 2005, p. 170.
24) A. I. Gunawan, N. Hozumi, S. Yoshida, Y. Saijo, K. Kobayashi, and S. Yamamoto, Ultrasonics **61**, 79 (2015).
25) A. I. Gunawan, N. Hozumi, K. Takahashi, S. Yoshida, Y. Saijo, K. Kobayashi, and S. Yamamoto, Ultrasonics **63**, 102 (2015).
26) J. A. Hildebrand, D. Rugar, R. N. Johnston, and C. F. Quate, Proc. Natl. Acad. Sci. U.S.A. **78**, 1656 (1981).
27) S. Y. Chou, C. M. Cheng, and P. R. LeDuc, Biomaterials **30**, 3136 (2009).
28) H. Haga, S. Sasaki, K. Kawabata, E. Ito, T. Ushiki, and T. Sambongi, Ultramicroscopy **82**, 253 (2000).
29) S. Kidoaki, T. Matsuda, and K. Yoshikawa, Biomech. Model. Mechanobiol. **5**, 263 (2006).
30) S. Kidoaki and T. Matsuda, J. Biomed. Mater. Res., Part A **81A**, 803 (2007).
31) S. Burattini, P. Ferri, M. Battistelli, R. Curci, F. Luchetti, and E. Falcieri, Eur. J. Histochem. **48**, 223 (2004).

Effects of anticancer drugs on glia–glioma brain tumor model characterized by acoustic impedance microscopy

2017 Jpn. J. Appl. Phys. 56 07JF15

(http://iopscience.iop.org/1347-4065/56/7S1/07JF15)

Japanese Journal of Applied Physics **56**, 07JF15 (2017)
https://doi.org/10.7567/JJAP.56.07JF15

REGULAR PAPER

Effects of anticancer drugs on glia–glioma brain tumor model characterized by acoustic impedance microscopy

Thomas Tiong Kwong Soon[1], Tan Wei Chean[2], Hikari Yamada[1], Kenta Takahashi[2], Naohiro Hozumi[2], Kazuto Kobayashi[3], and Sachiko Yoshida[1*]

[1]*Department of Environmental and Life Sciences, Toyohashi University of Technology, Toyohashi, Aichi 441-8580, Japan*
[2]*Department of Electrical and Electronic Information Engineering, Toyohashi University of Technology, Toyohashi, Aichi 441-8580, Japan*
[3]*Honda Electronics Co., Ltd., Toyohashi, Aichi 441-3147, Japan*

*E-mail: syoshida@ens.tut.ac.jp

Received November 25, 2016; accepted February 6, 2017; published online June 15, 2017

An ultrasonic microscope is a useful tool for observing living tissue without chemical fixation or histochemical processing. Two-dimensional (2D) acoustic impedance microscopy developed in our previous study for living cell observation was employed to visualize intracellular changes. We proposed a brain tumor model by cocultivating rat glial cells and C6 gliomas to quantitatively analyze the effects of two types of anticancer drugs, cytochalasin B (CyB) and temozolomide (TMZ), when they were applied. We reported that CyB treatment (25 μg/ml, $T = 90$ min) significantly reduced the acoustic impedance of gliomas and has little effect on glial cells. Meanwhile, TMZ treatment (2 mg/ml, $T = 90$ min) impacted both cells equally, in which both cells' acoustic impedances were decreased. As CyB targets the actin filament polymerization of the cells, we have concluded that the decrease in acoustic impedance was in fact due to actin filament depolymerization and the data can be quantitatively assessed for future studies in novel drug development.

1. Introduction

Gliomas are the most common and serious type of brain cancer and arise from glial cells, which are the supportive cells for neurons, and their incidence is increasing over time.[1)] It is an umbrella term for various glial tumors: astrocytoma, oligodendroglioma, ependymoma, and glioblastoma.[2)] They are characterized by highly proliferative growth and malignancy, which make up approximately 30% of all brain and central nervous system tumors and 80% of all malignant brain tumors.[3)] Therefore, combined therapy is vital, for instance, treating patients with a combination of surgery, chemotherapy, radiotherapy, and immunotherapy, as this may prolong patients' survival while reducing morbidity. Despite intensive research, the prognosis for glioma patients remains poor.[1,4,5)] Although many novel anticancer drugs are constantly sought, most of them have proven to be toxic to even normal cells or organs. Thus, it is essential to determine the effect of each drug on cell viability.

Two common anticancer drugs, cytochalasin B (CyB) and temozolomide (TMZ), were used in this study to quantitatively investigate their effects on the constructed brain tumor model. CyB is a type of cell-permeable alkaloid mycotoxin, which can be extracted from the fungus *Helminthosporium dematioideum*.[6)] It targets actin filaments, a major component of the cytoskeleton that controls cell mobility and morphology, by inhibiting network formation in actin polymerization. This causes the cytoskeleton to depolymerize, and hence reduce the cell membrane integrity.[7,8)] Meanwhile, TMZ is an imidazotetrazine derivative that is also a novel oral alkylation agent commonly used in brain cancer treatment for glioblastoma multiforme and astrocytoma.[9)] It damages the DNA of cancer cells by alkylating guanine bases of cancer cell DNA because cancer cells proliferate faster than normal cells, which make them more sensitive to DNA damage. It is a modestly effective anticancer drug that also displays significant toxicity.[10,11)] Moreover, zinc (Zn) was used in this study to help us distinguish between normal cells and cancer cells. It is critical for cell growth, development, and differentiation.[12)] Moreover, it is required for DNA synthesis, RNA transcription, cell division, and tissue repair and growth.[13)] Many reports have suggested that Zn is involved in cancer development, and it has been widely recognized that the leucine zipper is upregulated in most cancers.[14)] Increased concentration of Zn in most tumors indicates that Zn accumulation occurs in cancer cells.[15–17)] Hence, we employed Zn as a cancer-cell-accumulating metal in this study to identify cancer cells.

Nonclinical studies that investigate the effects of anticancer drugs using cultured cells play an important role in new drug development. Optical microscopy is often used to determine the effects of drugs in these types of experiment by evaluating morphological changes of the cells. For that reason, it can only distinguish between living cells and dead or damaged cells. Therefore, we propose an ultrasonic microscope for cell observation that targets cell morphology based on their elasticity, as it is reported that the elasticity is different between healthy cells and cancer cells.[18)] It is a powerful tool for the live observation of intracellular conditions.[19)] We have observed nuclear and cytoskeletal distributions of rat cerebellar tissue, glia cells, glioma cells, and C2C12 cells, and their dynamical changes in cultured living cells. It has been employed in the observation of living tissue, which works quickly and nondestructively without chemical staining.[20–30)] In this study, two-dimensional (2D) acoustic impedance microscopy that was developed in our previous study was employed to aid us in the quantitative observation of the brain tumor model, before and after the anticancer drug injection. The acoustic impedance images obtained through this observation visualize the intracellular conditions of the brain tumor model under treatment with anticancer drugs. Therefore, the observation can be made quickly without damaging cells as it does not require staining. These features enable the development of a novel evaluation system for drug screening.

2. Experimental methods

2.1 Cell culture

Glial cells were extracted from a model animal VGAT-Venus rat cerebellum P0–P2 (P = postnatal), whereas C6 glioma

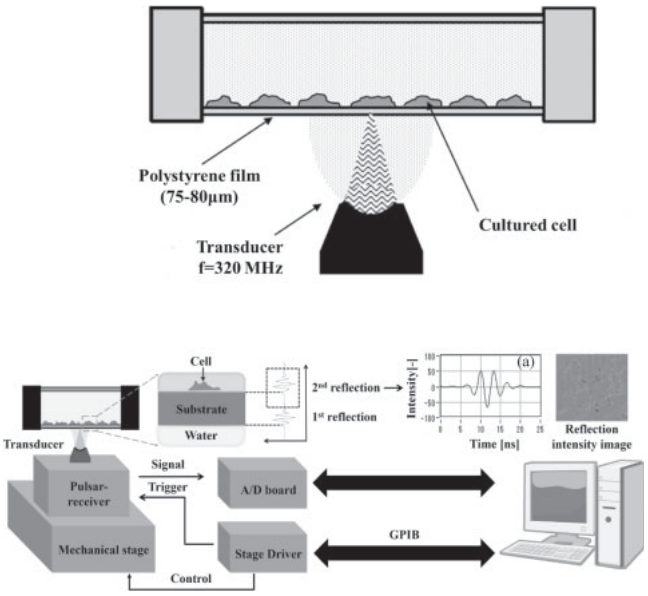

Fig. 1. Schematic diagram of measurement system. Typical acoustic waveform reflected from target (a).

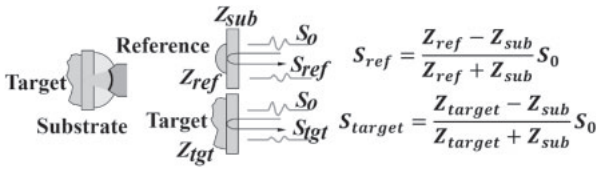

Fig. 2. Basic concept for calibration of acoustic impedance assuming perpendicular incidence.

cells[31] were obtained commercially (DS Pharma Biomedical). The extracted glial cells were genetically labeled with the endogenous fluorescent protein Venus[32] to visualize their position in a culture vessel. Cell cultivation was carried out in a commercial culture vessel, OptiCell™ (Thermo Scientific Nunc). It was composed of two polystyrene films in which each film has a thickness of 75 μm and the gap between the two films was 2 mm. All cells were proliferated in Minimum Essential Medium Eagle with Hanks' salt (HMEM) supplemented with 4 g/L D-glucose, 10% calf serum, and 0.1 g/L kanamycin, and the medium was replaced every other day.

2.2 Brain tumor model

A glia–glioma brain tumor model was constructed by cocultivating both glial cells and gliomas in the same culture vessel to quantitatively analyze the effects of anticancer drugs when they were applied to the brain tumor model.[33]

2.3 Anticancer drugs

Two types of anticancer drugs commonly used in cancer treatment, CyB (25 μg/ml) and TMZ (2 mg/ml), were used in this research to investigate their effects on the constructed glia–glioma brain tumor model. Additionally, zinc sulphate ($ZnSO_4$, 400 μM) was applied as a cancer-cell-accumulating metal that helps us to distinguish between normal cells and cancer cells.

2.4 Acoustic impedance microscopy

Figure 1 illustrates the schematic diagram of the observation system employed in this research, which was established in our previous study. The transducer consists of a flat ZnO as piezoelectric material attached with a sapphire lens of (assumed uniform) half curvature of 60°. Its aperture diameter and focal length (from the bottom of the lens) were 0.43 and 0.29 mm, respectively.[20–24] The central frequency of the transducer was designed as 320 MHz. Acoustic pulse wave spreading (200–400 MHz) was focused on the interface between the cell and the substrate, and sent through the substrate. The acoustic wave transmitted and received by the same transducer was focused on the interface between the substrate and the specimen. OptiCell™ containing cultured cells was placed above the transducer, which mechanically scanned the specimen by attaching it to a stage driver while maintaining the focal point on the rear surface of the film. The reflection from the surface was subsequently interpreted into a 2D profile of reflection intensity. All the measurements were performed at room temperature. Figure 2 shows the basic concept of calibration, in which the signal reflected from the target is compared with that reflected from the reference material. If the incident angle was approximated to be perpendicular to the substrate, the target signal compared with the reference signal can be interpreted into acoustic impedance as

$$T_{\mathrm{tgt}} = \frac{1 + \frac{S_{\mathrm{tgt}}}{S_0}}{1 - \frac{S_{\mathrm{tgt}}}{S_0}} \cdot Z_{\mathrm{sub}} = \frac{1 - \frac{S_{\mathrm{tgt}}}{S_{\mathrm{ref}}} \cdot \frac{Z_{\mathrm{sub}} - Z_{\mathrm{ref}}}{Z_{\mathrm{sub}} + Z_{\mathrm{ref}}}}{1 + \frac{S_{\mathrm{tgt}}}{S_{\mathrm{ref}}} \cdot \frac{Z_{\mathrm{sub}} - Z_{\mathrm{ref}}}{Z_{\mathrm{sub}} + Z_{\mathrm{ref}}}} \cdot Z_{\mathrm{sub}}, \qquad (1)$$

where S_0 is the transmitted signal, S_{tgt} and S_{ref} are reflections from the target and reference, and Z_{tgt}, Z_{ref}, and Z_{sub} are the acoustic impedances of the target, reference, and substrate, respectively. As for the substrate, polystyrene film ($Z_{\mathrm{sub}} = 2.46\,\mathrm{N\,s\,m^{-3}}$) was chosen, and for the reference material, culture medium ($Z_{\mathrm{ref}} = 1.52\,\mathrm{N\,s\,m^{-3}}$) was employed. This equation was practically corrected by considering the focused sound field.[20]

In this research, we measured a coculture system with glial cells and C6 glioma cells. $ZnSO_4$ and the anticancer drugs CyB and TMZ were injected into the OptiCell™ after the setup for experiment. The treatment time for glial cells and gliomas was 120 min each and 90 min for cocultured cells.

2.5 Statistical analysis

Each experiment was repeated 3 times for each drug. More than 10 pieces of both glial cells and glioma cells in each OptiCell™ treated with each drug were subjected to observation and analysis using the acoustic impedance profile. Data are reported as means ± standard deviation. All experimental procedures were approved by the committees for the use of animals in Toyohashi University of Technology and the Prime Minister's Office in Japan.

3. Results and discussion

Acoustic observation using high-frequency ultrasound is almost noninvasive because it does not change the cellular impedance even in continuous irradiation for 90 min. The mean values for the acoustic impedance of both cells were approximately $1.61\,\mathrm{N\,s\,m^{-3}}$. Treatment with 25 μg/ml CyB decreased the intracellular acoustic impedance of both glial cells and glioma cells for 120 min (Fig. 3). This suggests that long-lasting CyB treatment would cause damage to both types of cells. In contrast, 90 min of CyB treatment to glia–glioma coculture showed that the impedance of glioma cells was more decreased than that of glial cells (Fig. 4). Moreover, the impedance change of both cells was

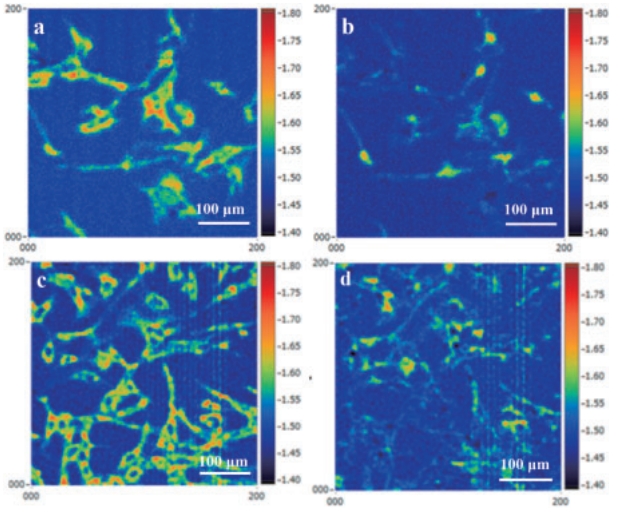

Fig. 3. (Color) Acoustic impedance changes with CyB treatment (25 mg/ml). (a) and (b), glial cells, and (c) and (d), glioma cells. (a) and (c) show untreated cells, and (b) and (d) show cells treated with CyB for 120 min.

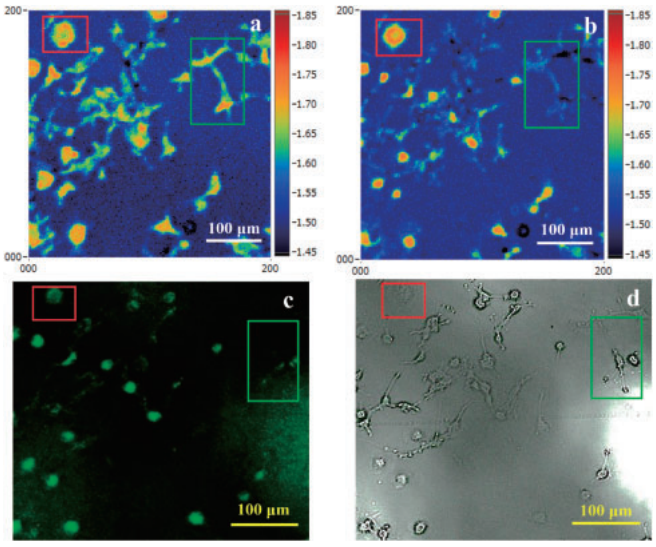

Fig. 4. (Color) Acoustic impedance changes with CyB treatment in glia–glioma coculture. The red square shows a typical glial cell, and the green square shows glioma cells. (a) Untreated coculture, and (b) coculture treated with CyB for 90 min. (c) Venus fluorescent image, and (d) phase contrast light microscopy image.

normalized and shown in Fig. 5. The impedance of glioma cells was decreased by about 1.5%, while normal glial cells showed little change. We also used confocal microscopy to confirm the position of glial cells inside the culture vessel as they were labeled by endogenous fluorescence. Green fluorescence proteins were observed when the specimen is excited by laser light. In addition, the glioma cells with decreased impedance did not disappear or die. Almost all the cells were present even after 90 min of CyB treatment. However, the cytoskeletal structures of the glioma cells were damaged. On the other hand, 2 mg/ml TMZ treatment for 90 min slightly decreased the acoustic impedance of both cells (Fig. 6). The impedance of glioma was decreased by about 1.0%, whereas that of normal glia was decreased by about 0.5%. TMZ is reported as the most sufficient antitumor drug and administrated clinically, while it is not harmless to

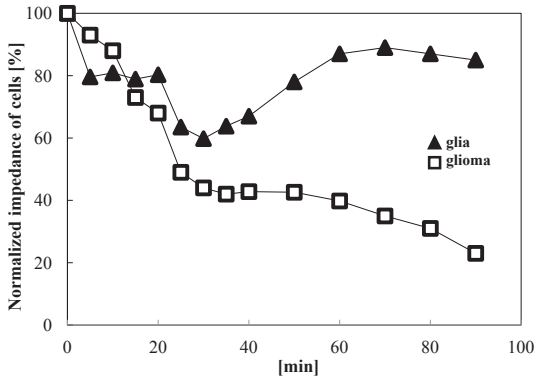

Fig. 5. Normalized impedance changes with CyB treatment in glia–glioma coculture.

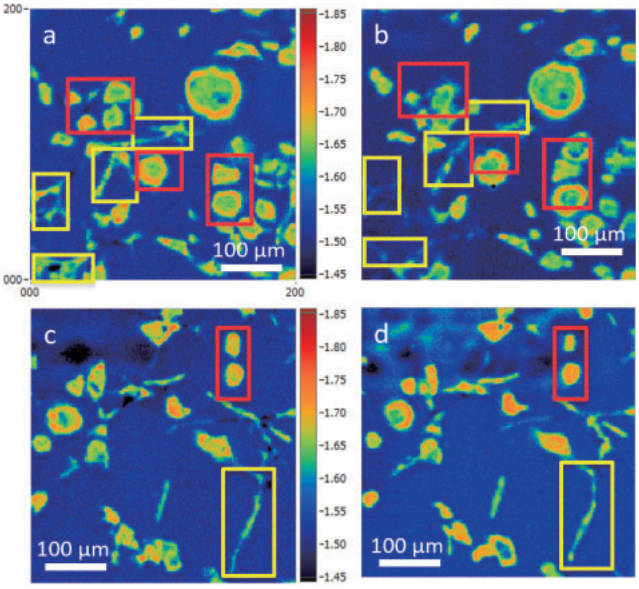

Fig. 6. (Color) Acoustic impedance changes with Zn treatment and TMZ treatment (2 mg/ml) in glia–glioma coculture. The red square shows a typical glial cell, and the yellow square shows glioma cells. (a) and (c), untreated coculture, and (b) and (d), coculture treated with TMZ for 90 min.

normal cells. Summarized data of the impedance changes following anticancer treatments are shown in Fig. 7.

Acoustic impedance microscopy (AIM) developed from our previous studies was employed in this study by interpreting the reflection intensity into 2D acoustic impedance. This system is suitable for the observation of biological soft tissue (rat cerebellar tissue) and cells (rat-derived glial cells, glioma cells, C2C12 cells) as the internal structure of cells, mainly the cytoskeleton, can be clearly observed and indicated considerably by high acoustic impedance. This enables us to elucidate the drug mechanism within the cells, which provides us with new insights for drug screening.[19–30] Thus, the effects of Zn and the anticancer drugs CyB and TMZ on the aforementioned brain tumor model were quantitatively analyzed to help us develop a new observation system for drug screening.

Long-lasting CyB treatment ($T = 120$ min) causes cytotoxicity to even normal cells. Glioma cells proliferate faster than glial cells, and hence are more affected by CyB treatment that promotes actin filament depolymerization by binding to F-actin. Recent studies showed that the cytoskeleton partic-

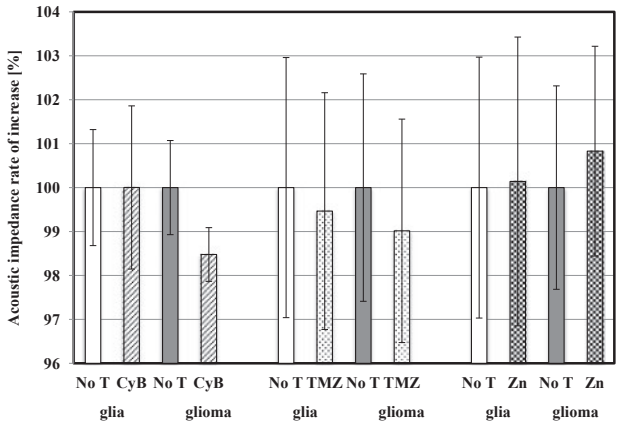

Fig. 7. Acoustic impedance changes with Zn treatment and anticancer drug treatment. No T, no treatment; Zn, Zn treatment; CyB, 90 min CyB treatment; TMZ, 90 min TMZ treatment. All data were normalized with the impedance of untreated samples.

ipates in various vital cellular activities, such as gene expression, cell movement, division and proliferation, and the transition to cancer. Therefore, rapidly dividing glioma cells undergo rapid F-actin polymerization. Once CyB binds to F-actin, it inhibits the superposition of G-actin, and hence depolymerization occurs, which decreases the integrity of the cytoskeleton.[7,34–40] However, when we treated glial cells with CyB long enough, the cytotoxicity of CyB towards glial cells was observed as the impedance of the glial cells decreased. This is because when normal cells treated with CyB proliferate, they are also affected by its inhibitory effect. The damaged cells can be observed in the 2D acoustic impedance image with lower impedance. When we shortened the treatment time to 90 min in the glia–glioma coculture, CyB showed little to no effect toward normal glial cells as the impedance did not change much after treatment. This suggests that AIM can be used as a monitoring system that can observe intracellular changes in living cells in real time.

In the glia–glioma coculture, both CyB and TMZ showed inhibitory effects on glioma cells because they decreased intracellular impedance. However, TMZ also affected normal glial cells, as it interferes with DNA replication by alkylation. It mainly targets cells with a high proliferation rate, such as cancer cells and normal cells that proliferate frequently, such as bone marrow and gastrointestinal tract cells.[9–11,41–43] In this case, glial cells were extracted from a model animal on P0–P2, which have a high proliferation rate, and hence were sensitive to TMZ treatment. We chose TMZ because we wanted to observe changes around nuclei, which house chromosomes, by AIM. Nevertheless, the acoustic impedance image only showed shrunken cells, suggesting that both cells were damaged. No significant changes around the nucleus were observed, as we anticipated.

On the other hand, Zn treatment showed a prominent result. Zn is an essential trace element, which is critical for nucleic acid replication and cell proliferation and is involved in cancer development.[12–14,44] Many research studies have shown that the concentration of Zn in tumors increased, indicating Zn accumulation in cancer cells.[15–17] We confirmed the accumulation of Zn in both cells as the impedance increased, especially around the cell nucleus. This suggests that the accumulation of Zn enhanced the reflection signal, which increased the acoustic impedance. Moreover, this suggests that AIM can be used for intracellular dynamics observation by carefully choosing the right indicator, such as Zn in this case instead of TMZ.

4. Conclusions

This study shows that acoustic impedance microscopy helps us to reveal the intracellular changes in living cells upon drug application without invasion. This is unprecedented in any other observation tools that are commonly used in potential anticancer drug development and cancer treatment, which require biopsy, cell staining, immunochemistry, and many other procedures. We are very optimistic that this study will provide us a simpler approach in potential anticancer drug screening before clinical trial. Potential anticancer drug candidates are usually tested on a huge number of animals before they are used in clinical trials. However, our result suggests that acoustic impedance microscopy would be more useful to decrease the necessity of conducting animal experiments. Furthermore, the visualization of the intracellular changes may aid us in elucidating both the mechanism of anticancer drugs and the physiological behavior of cancer cells. Consequently, acoustic impedance microscopy would help us to improve the current anticancer drug development.

Acknowledgment

This work was supported by JSPS KAKENHI Grant Numbers JP15H04017 and JP24360160.

1) S. M. Chang, I. F. Parney, W. Huang, F. A. Anderson, A. L. Asher, M. Bernstein, K. O. Lillehei, H. Brem, M. S. Berger, E. R. Laws, and Glioma Outcomes Project Investigators, JAMA **293**, 557 (2005).
2) D. N. Louis, A. Perry, G. Reifenberger, A. von Deimling, D. Figarella-Branger, W. K. Cavenee, H. Ohgaki, O. D. Wiestler, P. Kleihues, and D. W. Ellison, Acta Neuropathol. **131**, 803 (2016).
3) M. L. Goodenberger and R. B. Jenkins, Cancer Gen. **205**, 613 (2012).
4) E. R. Laws, I. F. Parney, W. Huang, F. Anderson, A. M. Morris, A. Asher, K. O. Lillehei, M. Bernstein, H. Brem, A. Sloan, and M. S. Berger, J. Neurosurg. **99**, 467 (2003).
5) K. R. Lamborn, S. M. Chang, and D. P. Michael, Neuro-Oncology **6**, 227 (2004).
6) D. C. Aldridge, J. J. Armstrong, R. N. Speake, and W. B. Turner, J. Chem. Soc. C, 1667 (1967).
7) S. F. Pedersen, E. K. Hoffmann, and J. W. Mills, Comput. Biochem. Physiol. A **130**, 385 (2001).
8) D. Cimini, D. Fioravanti, C. Tanzarella, and F. Degrassi, Chromosoma **107**, 479 (1998).
9) A. I. Omar and W. P. Mason, Core Evidence **4**, 93 (2009).
10) A. Carmo, H. Carvalheiro, I. Crespo, I. Nunes, and M. C. Lopes, Oncol. Lett. **2**, 1165 (2011).
11) W. J. Kil, D. Cerna, W. E. Burgan, K. Beam, D. Carter, P. S. Steeg, P. J. Tofilon, and K. Camphausen, Clin. Cancer Res. **14**, 931 (2008).
12) A. S. Prasad, Nutrition **11** [Suppl], 93 (1994).
13) A. S. Prasad, J. Trace Elem. Exp. Med. **11**, 63 (1998).
14) E. John, T. C. Laskow, W. J. Buchser, B. R. Pitt, P. H. Basse, L. H. Butterfield, P. Kalinski, and M. T. Lotze, J. Transl. Med. **8**, 118 (2010).
15) I. L. Mulay, R. Roy, B. E. Knox, N. H. Suhr, and W. E. Delaney, J. Natl. Cancer Inst. **47**, 1 (1971).
16) M. K. Schwartz, Cancer Res. **35**, 3481 (1975).
17) M. Murakami and H. Toshio, Cancer Sci. **99**, 1515 (2008).
18) X. Tang, T. B. Kuhlenschmidt, J. Zhou, P. Bell, F. Wang, M. S. Kuhlenschmidt, and T. A. Saif, Biophys. J. **99**, 2460 (2010).
19) K. Kobayashi, S. Yoshida, Y. Saijo, and N. Hozumi, Ultrasonics **54**, 1922 (2014).
20) A. I. Gunawan, N. Hozumi, S. Yoshida, Y. Saijo, K. Kobayashi, and S. Yamamoto, Ultrasonics **61**, 79 (2015).
21) A. I. Gunawan, N. Hozumi, K. Takahashi, S. Yoshida, Y. Saijo, K. Kobayashi, and S. Yamamoto, Ultrasonics **63**, 102 (2015).

22) N. Hozumi, K. Takanashi, M. Washiya, S. Yoshida, K. Kobayashi, and Y. Saijo, J. Acoust. Soc. Am. **140**, 3245 (2016).
23) S. Yoshida, R. H. Rahayu, K. Takanashi, K. Kishikawa, H. Kurita, K. Takashima, N. Hozumi, K. Kobayashi, and S. Yamamoto, J. Acoust. Soc. Am. **140**, 3139 (2016).
24) K. Takahashi, A. I. Gunawan, S. Yoshida, N. Hozumi, and K. Kobayashi, Proc. 4th Int. Symp. Engineering, Energy and Environments, 2015, p. 89.
25) S. Irie, K. Inoue, K. Yoshida, J. Mamou, K. Kobayashi, H. Maruyama, and T. Yamaguchi, J. Acoust. Soc. Am. **139**, 512 (2016).
26) D. Rohrbach, Q. V. Hoang, Q. Wen, S. A. McFadden, R. H. Silverman, and J. Mamou, IEEE Int. Ultrasonics Symp., 2015, p. 1.
27) Y. Saijo, E. Santos Filho, H. Sasaki, T. Yambe, M. Tanaka, N. Hozumi, K. Kobayashi, and N. Okada, IEEE Trans. Ultrason. Ferroelectr. Freq. Control **54**, 1571 (2007).
28) H. Kumagai, K. Yokoyama, K. Katsuyama, S. Hara, H. Yamamoto, T. Yamagata, N. Taniguchi, N. Hirota, and K. Itoh, Ultrasound Med. Biol. **40**, 2499 (2014).
29) S. Rajagopal, N. Sadhoo, and B. Zeqiri, Ultrasound Med. Biol. **41**, 317 (2015).
30) K. Miura, Y. Egawa, T. Moriki, H. Mineta, H. Harada, S. Baba, and S. Yamamoto, Pathol. Int. **65**, 355 (2015).
31) B. Grobben, P. De Deyn, and H. Slegers, Cell Tissue Res. **310**, 257 (2002).
32) M. Uematsu, Y. Hirai, F. Karube, S. Ebihara, M. Kato, K. Abe, K. Obata, S. Yoshida, M. Hirabayashi, Y. Yanagawa, and Y. Kawaguchi, Cereb. Cortex **18**, 315 (2008).
33) E. I. Fomchenko and E. C. Holland, Clin. Cancer Res. **12**, 5288 (2006).
34) X. L. Zeng, M. D. Jiao, X. G. Wang, and S. Hao, Acta Bot. Sin. **39**, 691 (1997).
35) J. A. Cooper, J. Cell Biol. **105**, 1473 (1987).
36) C. Stournaras, E. Stiakaki, S. B. Koukouritaki, P. A. Theodoropoulos, M. Kalmanti, Y. Fostinis, and A. Gravanis, Biochem. Pharmacol. **52**, 1339 (1996).
37) T. D. Pollard and J. A. Cooper, Science **326**, 1208 (2009).
38) K. M. K. Rao and H. J. Cohen, Mutat. Res./DNAging **256**, 139 (1991).
39) B. Buendia, M. H. Bré, G. Griffiths, and E. Karsenti, J. Cell Biol. **110**, 1123 (1990).
40) Y. Hirose, M. Katayama, O. K. Mirzoeva, M. S. Berger, and R. O. Pieper, Cancer Res. **65**, 4861 (2005).
41) M. C. Chamberlain, Expert Rev. Neurother. **10**, 1537 (2010).
42) T. Kanzawa, I. M. Germano, T. Komata, H. Ito, Y. Kondo, and S. Kondo, Cell Death Differ. **11**, 448 (2004).
43) B. Bergman, U. Friberg, S. Lohmander, and T. Öberg, Eur. J. Oral Sci. **80**, 486 (1972).
44) A. H. Shankar and A. S. Prasad, Am. J. Clin. Nutr. **68**, 447S (1998).

NeuroToxicology 65 (2018) 1–8

Contents lists available at ScienceDirect

NeuroToxicology

Full Length Article

Prenatal exposure to valproic acid alters the development of excitability in the postnatal rat hippocampus

Yukiko Fueta[a], Yuko Sekino[b,c], Sachiko Yoshida[d], Yasunari Kanda[b], Susumu Ueno[e,*]

[a] Department of Environmental Management and Control, School of Health Sciences, University of Occupational and Environmental Health, 1-1 Iseigaoka, Yahatanishi-ku, Kitakyushu, Fukuoka 807-8555, Japan
[b] Division of Pharmacology, National Institute of Health Sciences, 3-25-26 Tonomachi, Kawasaki-ku, Kawasaki, Kanagawa 210-9501, Japan
[c] Laboratory of Chemical Pharmacology, Graduate School of Pharmaceutical Sciences, The University of Tokyo, 7-3-1 Hongo, Bunkyo-ku, Tokyo 113-0033, Japan
[d] Department of Environment and Life Sciences, Toyohashi University of Technology, 1-1 Hibarigaoka, Tempaku-cho, Toyohashi, Aichi 441-8580, Japan
[e] Department of Occupational Toxicology, Institute of Industrial Ecological Sciences, University of Occupational and Environmental Health, 1-1 Iseigaoka, Yahatanishi-ku, Kitakyushu, Fukuoka 807-8555, Japan

ARTICLE INFO

Article history:
Received 5 December 2016
Received in revised form 3 December 2017
Accepted 4 January 2018
Available online 5 January 2018

Keywords:
Developmental neurotoxicity
Valproic acid
Prenatal exposure
Hippocampus
Slice preparation
Electrophysiology

ABSTRACT

Prenatal valproic acid (VPA) exposure is a well-known animal model of autism spectrum disorder (ASD) that produces alterations in embryonic and adult neurogenesis as well as adolescent/adulthood neurobehavioral phenotypes. However, the effects of prenatal VPA exposure on neural network excitability, especially during the synaptogenic period around eye opening, are not fully understood. In this study, we orally administered VPA (300 mg/kg) to pregnant Wistar rats on gestation day 15 and subsequently performed field potential recording in the CA1 area of hippocampal slices obtained from control (saline-exposed) and VPA-exposed rat pups between postnatal day (PND) 13 and PND18. In control slices, we observed an abrupt enhancement of stimulation-dependent responses including population spike (PS) amplitudes and field excitatory postsynaptic potential (fEPSP) slopes at PND16, which coincided with the average day of eye opening. In contrast, VPA-exposed pups exhibited delayed eye opening (PND17) and gradual rather than abrupt increases in PS amplitudes and fEPSP slopes over the duration of the synaptogenic period. We next investigated the involvement of ambient GABA (γ-aminobutyric acid) in PS generation using bicuculline methiodide (BMI), a GABA type A ($GABA_A$) receptor antagonist. In control slices, BMI enhanced PS amplitudes during PND14–15 (before eye opening) and had little effect thereafter during PND16–17; a subsequent regression model analysis of BMI ratios (the ratio of PS amplitudes in the presence and absence of BMI) indicated a possible developmental change between these periods. In contrast, almost identical regression models were obtained for BMI ratios during PND14–15 and PND16–17 in the VPA-exposed group, indicating the absence of a developmental change. Our results suggest that prenatal VPA exposure accelerates the development of hippocampal excitability before eye opening. Moreover, our experimental model can be used as a novel approach for the evaluation of developmental neurotoxicity.

1. Introduction

The impact of exogenous chemical substances on childhood neural development, also known as developmental neurotoxicity, is an important social issue (Andersen et al., 2000; Grandjean and Landrigan, 2006). Valproic acid (VPA) is an antiepileptic drug and mood stabilizer that has been reported to increase the risk of autism spectrum disorders (ASD) in children when women take VPA during early pregnancy (Chomiak et al., 2013). Similarly, rodent models of ASD have been established using prenatal exposure to VPA; in VPA exposure-based models, offspring exhibit autism-like behaviors including impaired social interactions and repetitive behaviors (Markram et al., 2008; Rodier et al., 1997; Roullet et al., 2013; Schneider and Przewlocki, 2005). In addition to neurobehavioral phenotypes, ASD model animals exhibit alterations in embryonic and adult neurogenesis (Juliandi et al., 2015). It has been reported that prenatal exposure to VPA suppresses early neurogenesis in fetal rat brain due to a prolongation of neural

* Corresponding author.
E-mail addresses: yukiko@med.uoeh-u.ac.jp (Y. Fueta), yukos@tkg.att.ne.jp (Y. Sekino), syoshida@ens.tut.ac.jp (S. Yoshida), kanda@nihs.go.jp (Y. Kanda), susumu@med.uoeh-u.ac.jp (S. Ueno).

https://doi.org/10.1016/j.neuro.2018.01.001
0161-813X/

progenitor cell proliferation (Go et al., 2012), and that early postnatal one-week (7–14 postnatal days) exposure to VPA also perturbs neuroblast production and postnatal neurogenesis (Foti et al., 2013). However, it is not well known whether prenatal exposure to VPA also affects neural network formation especially during the synaptogenic period.

Neural activity is a critical regulator of neural network development. It was recently demonstrated that spine density is remarkably increased in the hippocampal CA1 area of mice between postnatal day (PND) 11 and PND21, i.e. during the synaptogenic period (Johnson-Venkatesh et al., 2015). Interestingly, when intrinsic neural activity was suppressed by overexpression of Kir2.1, an inwardly rectifying K^+ channel, increases in spine density during the synaptogenic period were abolished. Thus, neural network activity in the hippocampal CA1 area is necessary for healthy neural development during the synaptogenic period including around eye opening.

Chloride conductance due to ambient concentrations of GABA (γ-aminobutyric acid) also plays a role in regulating neural network excitability during postnatal neural development (Cellot and Cherubini, 2013; Kilb et al., 2013). Ambient GABA originates from the spillover of neurotransmitter escaping the synaptic cleft and from astrocytes via a non-vesicular Ca^{2+}-independent process and mediates tonic inhibition via extrasynaptic GABA type A ($GABA_A$) receptors. However, there is little evidence demonstrating effects of prenatal exposure to toxicants including VPA on ambient GABA-mediated inhibition of neural network excitability.

In the present study, we used a model of prenatal VPA exposure and evaluated effects on neural network activity in the hippocampal CA1 area during the synaptogenic period using hippocampal slices from PND13–18 rat pups. We not only observed the ability of prenatal VPA exposure to abolish development-associated enhancements in stimulation-dependent neural responses, but also confirmed the ability of prenatal exposure to influence ambient GABA-mediated inhibition even prior to eye opening.

2. Material and methods

2.1. Animals

Adult Wistar/ST rats were purchased from Japan SLC *Inc.* (Japan). Rats were housed in plastic cages on paper chip bedding (ALPHA-dri, Shepherd Specialty Papers, USA) and maintained on a 12 h light/dark cycle (light period: 07:00–19:00) in a room with controlled temperature (23 ± 1 °C) and relative humidity (50 ± 15%). Animals were given free access to food (CE2, CLEA Japan Inc., Japan) and filtered water (TCW-PPS filter, Advantech Co., LTD., Japan) dispensed in glass water supply bottles.

The proestrus stage was verified with an impedance checker (MK-10B, Muromachi Kikai Co., Ltd., Japan). When the observed impedance was >3 kΩ female rats were provided with a male rat for mating. The presence of a vaginal plug or sperm in the vaginal smear the following morning confirmed coition, and it was regarded as gestation day (GD) "zero" (Fig. 1). Pregnant rats were randomly divided into two groups: a control group and a VPA exposure group.

VPA was purchased from Wako Pure Chemical Industries, Ltd. (Japan), dissolved in physiological saline (Otsuka Pharmaceutical Co., Ltd, Japan), and orally administered to dams (300 mg/kg) on GD15 under 5% isoflurane gas anesthesia (Pfizer Japan Inc., Japan).

All dams gave birth on GD21, and the date of birth was defined as PND0. If there were more than 10 pups in a litter, the litter size was adjusted to 10 pups on PND1. Litters of less than 10 pups were not adjusted. All pups were housed with their dams during the lactation period. Rat pup body weights were measured on PND1, PND7, PND14, and PND21. The day of eye opening was determined by checking the eyes of pups at 14:00 on each day from PND15–18.

For the electrophysiological study, the control group included pups from 16 control dams and the VPA-exposed group included pups from 17 VPA-exposed dams. All studies were approved by the Ethics Committee on Animal Care and Experimentation and performed in accordance with the guidelines of the University of Occupational and Environmental Health, Japan.

2.2. Slice preparation and recordings

Hippocampal slices (600 μm thickness) were prepared from male pups on each postnatal day between PND13–18 as previously described (Fueta et al., 2004; Fueta et al., 2002). Slices were perfused with artificial cerebrospinal fluid (ACSF) containing 124 mM NaCl, 2 mM KCl, 2 mM $MgSO_4$, 2 mM $CaCl_2$, 1.25 mM KH_2PO_4, 26 mM $NaHCO_3$, and 10 mM glucose; saturated with an O_2 95%/CO_2 5% gas mixture; and stored in a thermostatic bath (27.6 °C). The perfusion rate of ACSF was 1 ml/min for all experiments.

Population spikes (PSs) and field excitatory synaptic potentials (fEPSPs) were simultaneously recorded from the CA1 area of hippocampal slices using glass microelectrodes (Fig. 2A). For slices obtained during the period from PND13–15, PSs were recorded from the area between the pyramidal cell layer and the alveus. The recording positions for PSs and fEPSPs were similar between the control and VPA-exposed groups. Bipolar stimulation electrodes

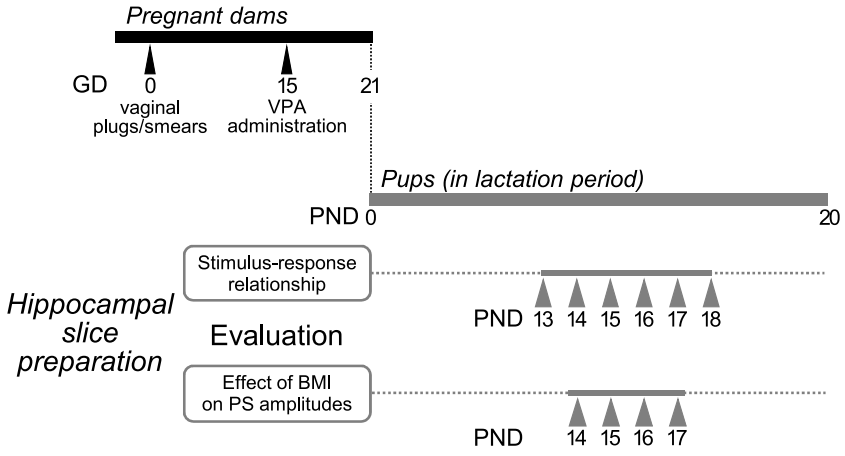

Fig. 1. Scheme of the experimental design.

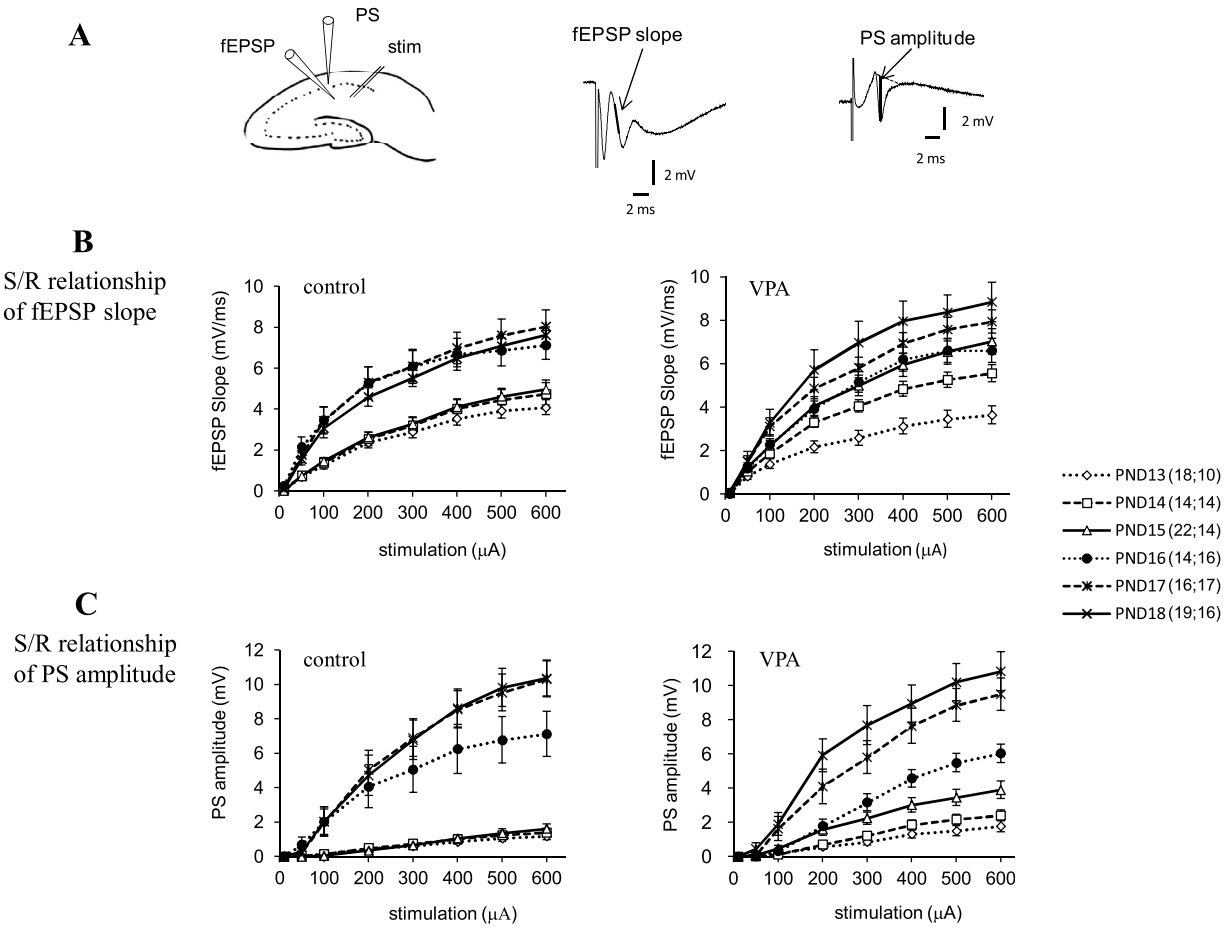

Fig. 2. Stimulation/response (S/R) relationships for population spike (PS) amplitudes and field excitatory postsynaptic potential (fEPSP) slopes recorded from the hippocampal CA1 area of rats that were prenatally exposed to valproic acid (VPA). (A) Illustration depicting the procedure of fEPSP and PS recordings from CA1. Responses were evoked with a stimulating electrode placed in the stratum radiatum. Thick lines on the left traces indicate how measurements of fEPSP slopes and PS amplitudes were taken. (B, C) In control rats (left graphs), the S/R relationships for both fEPSP slopes and PS amplitudes were enhanced between PND15–16. Data were collected from 14 to 22 slices obtained from pups of 4–5 different litters. In VPA-exposed rats (right graphs), these relationships were gradually enhanced between PND13–18. Data were gathered from 10 to 17 slices obtained from pups of 5–6 different litters. The x-axis is stimulation intensity and the y-axis is size of the fEPSP slope or PS amplitude. Data represent the mean ± standard error of the mean. The numbers in parentheses shown with data plot legends are the ones of slices tested for the control and VPA-exposed groups, respectively.

made of stainless wires (50 μm in diameter) were placed on Shaffer collateral/commissural fibers at a distance of about 250 μm from the fEPSP recording electrodes. Stimulation-response relationships were observed with stimulation intensities from 10 to 600 μA. The stimulation interval was 2 min in order to avoid the measurement of overlapping stimulation effects. Between PND14–17, experiments evaluated the effects of bicuculline methiodide (BMI, Tocris Bioscience, U.K.), a $GABA_A$ receptor antagonist, on the generation of PSs. Average PS amplitudes in response to 600 μA stimulation were recorded in triplicate (with 2 min intervals) in the absence and presence of BMI; after PS measurements in the absence of BMI, slices were perfused with ACSF containing BMI (1 μM) for 10 min and subsequently tested. Pups were obtained from at least two different dams, and a total of 3–4 slices per rat pup were tested. Accordingly, we examined 14–22 slices obtained from pups of 4–5 different litters for the control group, and 10–17 slices obtained from pups of 5–6 different litters for the VPA-exposed groups.

2.3. Distribution analysis

Histogram distribution and nonlinear regression analyses of BMI ratios (PS amplitude in the presence of BMI divided by that in the absence of BMI) were conducted using GraphPad Prism software (GraphPad Software, Inc., USA).

2.4. Statistical analysis

Litter sizes and sex ratios as well as pup body weights and the day of eye opening are expressed as the mean ± standard deviation (SD). Electrophysiological results are expressed as the mean ± standard error of mean (SEM), where n refers to the number of hippocampal slices tested. Statistical differences between the control and VPA-exposed groups were determined using two-sided Student's *t*-tests or Mann-Whitney *U* tests at a significance level of $P < 0.05$.

3. Results

For the purpose of our study, the time of eye opening in our rat models was needed to confirm. In consequence, the average day of eye opening was significantly delayed in the VPA-exposed group compared to the control group ($P < 0.01$, Table 1). We also examined general toxicity induced by one-time prenatal VPA exposure at GD15, and found that there were no significant differences between the control and VPA-exposed groups in terms of litter size, litter sex ratio, or changes in pup body weight. Moreover, the number of pups that died before experimentation or weaning was not significantly different between groups (control group, 2 of 206 pups; VPA-exposed group, 4 of 195 pups).

Table 1
Litter sizes and sex ratios as well as pup weight gain and the day of eye opening for the control and VPA-exposed groups.

	Control		VPA-exposed	
Litter size of dams	12.0 ± 2.0	(21)	13.0 ± 3.0	(20)
Sex ratio of pups (percent of males)	48.5 ± 0.1	(21)	49.5 ± 0.1	(20)
Male pup weight (g)				
PND1	6.0 ± 0.6	(55)	5.7 ± 0.4	(53)
PND7	14.9 ± 1.6	(54)	14.1 ± 1.3	(47)
PND14	30.1 ± 1.9	(47)	28.6 ± 2.2	(45)
PND21	50.2 ± 4.3	(20)	46.9 ± 3.7	(23)
Day of eye opening	16.5 ± 0.6	(67)	17.3 ± 0.7**	(77)

Data represent the mean ± standard deviation. Numbers in parentheses are total numbers of dams/pups examined.
** $P < 0.01$, compared to the control. Abbreviations: PND, postnatal day; VPA, valproic acid.

Next, to investigate neural network excitability during the synaptogenic period, we studied stimulation-response (S/R) relationships for fEPSP slopes and PS amplitudes using hippocampal slice preparations, in which the cytoarchitecture and synaptic circuits of the hippocampus are largely retained. S/R relationships exhibited two different stages; similar degrees of stimulation-dependent responses were observed in control pups between PND13–15. However, responses (fEPSP slopes and PS amplitudes) were suddenly augmented on PND16, which seemed to correspond with eye opening. Responses were maintained at an enhanced level for fEPSP slopes and slightly enhanced for PS amplitudes between PND17–18 (Fig. 2B, C).

In contrast, a gradual enhancement of S/R relationships was observed between PND13–18 in the VPA-exposed group, and did appear to correspond with eye opening. Therefore, we reanalyzed fEPSP slopes and PS amplitudes in response to a stimulation intensity of 600 μA, which evoked the maximal responses. PS amplitudes obtained from the control group showed an abrupt increase between PND15–16, whereas those from the VPA-exposed group again demonstrated a gradual increase over the period examined, with significant differences at PND14 and PND15 compared to the control group. A similar but smaller developmental change was observed in the fEPSP slope, with a significant difference between the control and VPA-exposed groups on PND15 (Fig. 3).

Next we investigated the effect of BMI on PS generation in order to elucidate the role of ambient GABA in postnatal PS generation. Fig. 4 shows the effect of BMI on PS amplitudes in the control group before eye opening (PND14–15) and after eye opening (PND16–17). PS amplitudes were enhanced in the presence of BMI during PND14–15 (Fig. 4A, left), but this enhancement was attenuated during PND16–17 (Fig. 4B, left). The mean BMI ratios (ratio of the PS amplitude in the presence of BMI to that in the absence of BMI) were 1.80 ± 0.17 (n = 13) for PND14–15 and 1.14 ± 0.04 (n = 10) for PND16–17. Histograms of BMI ratios (Fig. 4A and B, right) and nonlinear regression analyses revealed a clear developmental change in the probability distribution of BMI ratios for PS amplitudes (Fig. 6, left).

In contrast, for the VPA-exposed group, PS amplitudes generated in the presence of BMI showed small or little increases during both the PND14–15 and PND16–17 periods (Fig. 5A and B, left). The mean BMI ratios were 1.34 ± 0.14 (n = 17) for PND14–15 and 1.14 ± 0.05 (n = 17) for PND16–17. Moreover, histograms of BMI ratios and nonlinear regression analyses (Fig. 5A and B, right) were almost identical between the PND14–15 and PND16–17 periods, suggesting attenuation of the developmental change observed in the control group (Fig. 6, right). We also investigated the responses to BMI for fEPSP slopes, but minimal (non-significant) BMI responses and alterations in developmental change were observed.

4. Discussion

In this study, we investigated the effect of prenatal VPA exposure on the development of neural network activity in the hippocampal CA1 area during the synaptogenic period, including during the period of eye opening. A single dose of VPA (300 mg/kg) was orally administered to dams on GD15 and was not noted to affect dam maternal behavior or fetal/neonatal mortality. In animal models of ASD, VPA is often administered repeatedly or earlier than GD11.5 prior to closure of the neural tube (Rodier et al., 1997). Therefore, the most effective period for observing the effects of prenatal VPA exposure as it relates to ASD may be earlier than GD15.

Brain slice preparation is a well-known laboratory technique for electrophysiology and pharmacology research. Since local neuronal circuits remain intact in brain slices, this neurophysiological preparation is useful for studying neurotoxicity (Fountain et al., 1992) as well as the specific effects of neurotoxic agents on synaptic transmission and plasticity (Varela et al., 2012; Wiegand and Altmann, 1994). The electrophysiological strategy used in the present work has been previously implemented to study the effects of prenatal/perinatal ethanol exposure (Puglia and Valenzuela, 2010), lead (Carpenter et al., 2002; Sui et al., 2000), polychlorinated biphenyl exposure (Altmann et al., 1998; Carpenter et al., 2002; Kim and Pessah, 2011), and toluene exposure (Chen et al., 2011). Thus, we deemed the present model to be useful for

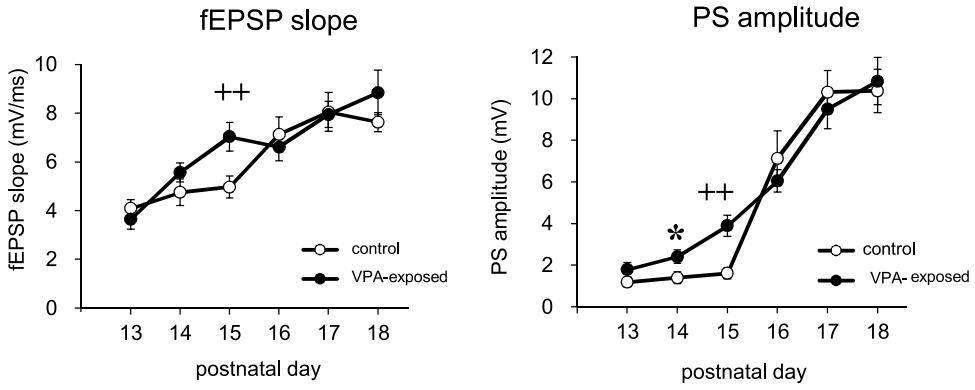

Fig. 3. Developmental changes in field excitatory postsynaptic potentials (fEPSPs) slopes and population spike (PS) amplitudes in the control and valproic acid (VPA)-exposed groups. One-time prenatal exposure to VPA (300 mg/kg) led to postnatal increases in fEPSP slope and PS amplitude at PND15 and during PND14–15, respectively. There were no between-group differences in excitability between PND16–18. The stimulation intensity was 600 μA. * indicates $P < 0.05$ using a Student's *t*-test. ++ indicates $P < 0.01$ using a Mann-Whitney *U* test.

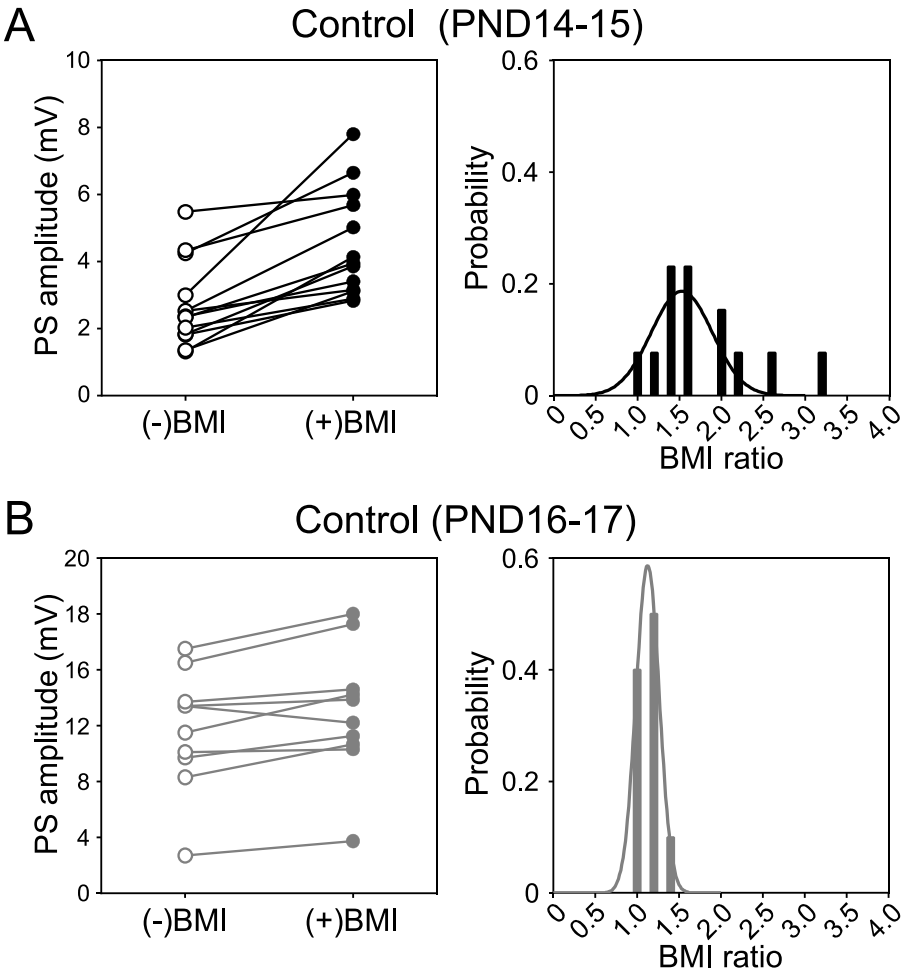

Fig. 4. Development-associated changes in population spike (PS) amplitude responses to BMI in the control group. (A) At PND14–15, application of the $GABA_A$ receptor antagonist BMI to hippocampal slices during recording remarkably increased PS amplitudes; the mean BMI ratio was 1.80 (n = 13, 95% confidence interval = 1.44–2.16). (B) Increased PS amplitudes in response to BMI application were not observed at PND16–17; the mean ratio was 1.14 (n = 13, 95% confidence interval = 1.04–1.24).

evaluating excitatory/inhibitory function and developmental neurotoxicity after VPA exposure.

Our first main finding was that stimulation-dependent responses for fEPSPs and PSs in the hippocampal CA1 area showed two different periods of development in normal pups; one from PND13–15 before eye opening on PND16, and another after eye opening from PND16–18. S/R relationships for neural excitability in the CA1 area exhibited drastic enhancements after eye opening. Alternatively, we did not observe clear discrimination between stimulation-dependent responses before and after eye opening in the VPA-exposed group; enhancements in stimulation-dependent CA1 excitability were observed on PND14 and/or PND15 in the VPA-exposed group compared to the control group, and gradual changes were observed in the subsequent postnatal days. In other words, prenatal VPA exposure appeared to accelerate developmental changes in neural excitability that otherwise appeared in association with eye opening in healthy pups.

Ambient GABA is a critical factor that regulates neural network excitability. Therefore, we also investigated the involvement of ambient GABA in PS generation using BMI, a $GABA_A$ receptor antagonist. On PND14 and PND15 before eye opening, PS amplitudes evoked in the presence of BMI were greater than those in the control condition, suggesting a possible role for PS inhibition by ambient GABA. On PND16 and PND17 on or after eye opening, BMI had little effect on PS amplitudes. These results indicated that ambient GABA was involved in suppressing neural excitability in the CA1 area during neural development prior to eye opening. The centering of this developmental change around the event of eye opening is consistent with a previous report that demonstrated notable increases in spine density on PND15 (Johnson-Venkatesh et al., 2015).

In contrast, BMI had little effect on PS generation before or after eye opening in the VPA-exposed group. Indeed, nonlinear regression models of distribution histograms obtained during PND14–15 and PND16–17 were virtually identical. These results suggest that prenatal exposure to VPA may eliminate ambient GABA suppression of neural excitability prior to eye opening, and are consistent with the observation of enhanced stimulation-dependent responses at PND14 and PND15 in the VPA-exposed group. Accordingly, prenatal exposure to VPA may accelerate neural development in CA1 area during the synaptogenic period.

Ambient GABA-mediated tonic inhibition in hippocampal neurons is synergistically modulated by two GABA transporters (GATs): GAT-1 located on presynaptic membranes and GAT-3 on astrocytes (Egawa and Fukuda, 2013; Kersante et al., 2013). GAT-1 is predominantly responsible for GABA reuptake under resting conditions; alternatively, GAT-3 plays an important role in controlling hippocampal cell excitability during neural activation (Kersante et al., 2013). Therefore, our findings raise the question of whether developmental changes in evoked PS responses to BMI were related to alterations in the expression and/or function of GATs in the CA1 area during development. Further investigations are in progress to address this issue.

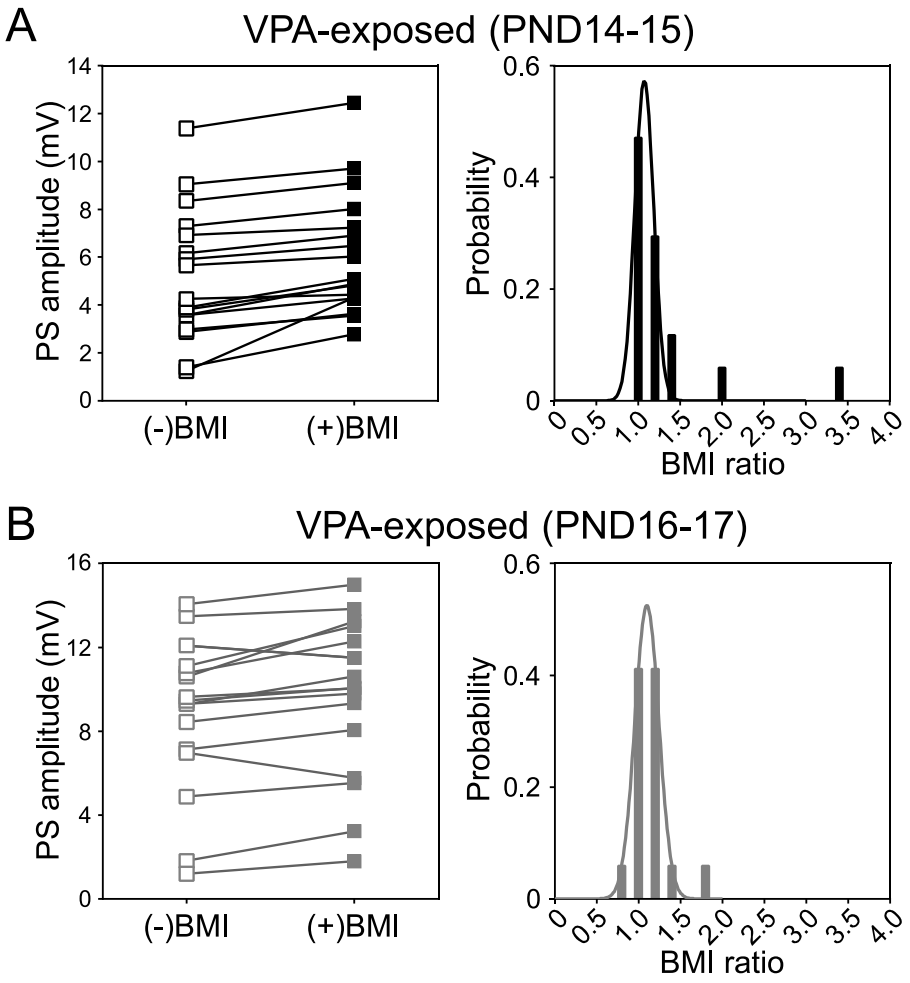

Fig. 5. Development-associated changes in population spike (PS) amplitude responses to BMI in the valproic acid (VPA)-exposed group. Hippocampal slices from the VPA-exposed group were virtually insensitive to BMI during both the PND14–15 (A) and PND16–17 (B) periods; the mean BMI ratios were 1.34 (n = 17, 95% confidence interval = 1.04–1.64) and 1.14 (n = 17, 95% confidence interval = 1.04–1.25), respectively.

Among several hypothetical mechanisms underlying ASD, the disruption of excitation/inhibition (E/I) balance in neuronal circuits has been proposed as a unifying explanation for the complexity and diversity of ASD presentations arising from genetic (Gkogkas et al., 2013; Gogolla et al., 2009; Rubenstein, 2010; Rubenstein and Merzenich, 2003) and environmental factors (Rubenstein and Merzenich, 2003). Although the precise mechanisms of altered E/I balance after prenatal exposure to VPA have not been fully elucidated, this effect has been replicated in several rodent studies. Rinaldi et al. showed that prenatal injection of VPA (500 mg/kg, intraperitoneally) increased N-methyl-D-aspartate (NMDA) receptor subunit protein expression in the whole brains

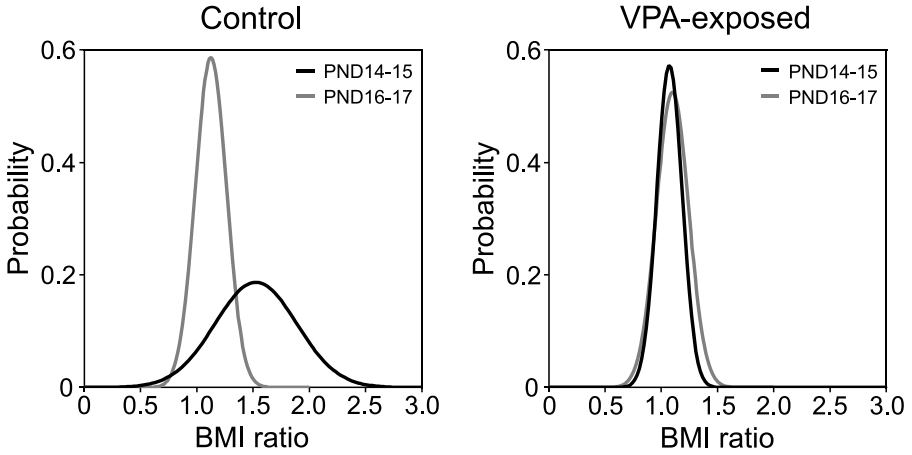

Fig. 6. Developmental alterations in nonlinear regression models of BMI ratios for population spike (PS) responses. Data from right figure panels of 4 and 5 were re-plotted and summarized for the control (left panel) and VPA-exposed groups (right panel).

of pups and enhanced NMDA receptor-mediated synaptic currents in neocortical slices obtained from pups during PND12–16 (Rinaldi et al., 2007). These authors further reported that prenatal VPA exposure induced local circuits hyperconnectivity and enhancements in both excitatory and inhibitory systems in the sensory cortex (Rinaldi et al., 2008). Banerjee et al. reported that a single intraperitoneal injection of VPA (600 mg/kg) at GD11.5 impaired postnatal GABAergic synaptic transmission using slice preparations of the auditory cortex from PND23–45 offspring (Banerjee et al., 2013).

To the best of our knowledge, this is the first report to describe a possible role for GABA-mediated inhibition in the development of evoked PSs during the synaptogenic period around eye opening. Moreover, our data suggest that prenatal exposure to VPA and potentially other developmental neurotoxicants at specific points of the gestation period can accelerate this developmental change. Changes in PS amplitudes evoked from hippocampal slices during prenatal development, especially in the presence of BMI, may be useful as an index for the normal development of neural circuits; to this end, our assay may have utility for testing other candidate drugs/chemicals affecting neural network formation during synaptogenic period. Studies with other known toxicants including organometallic compounds and pesticides are in progress to determine whether similar developmental alterations can be observed using the current experimental approach.

5. Conclusions

In summary, we report that one-time prenatal exposure to VPA at GD15 produced enhancements in stimulation-dependent responses for fEPSP slopes and PS amplitudes in the CA1 area of offspring, and moreover altered offspring PS amplitude responses to BMI. Taken together, prenatal VPA exposure may transiently alter E/I balance, resulting in the acceleration of neural development before eye opening. This effect corresponds with the hypothetical mechanisms underlying ASD; that is, the disruption of E/I balance in developing brain circuits. Although further investigations are required, our results provide an approach for studying effects of chemicals on neural network formation, which is one of important endpoints for the evaluation of developmental neurotoxicity.

Funding

This study was supported by Health and Labor Sciences Research Grants of the Ministry of Health, Labour and Welfare in Japan.

Conflict of interest

The authors declare that there are no conflict of interest.

Acknowledgements

The authors would like to thank Kaoru Sato, Seiichi Ishida, and Daiju Yamazaki for helpful discussion.

References

Altmann, L., Lilienthal, H., Hany, J., Wiegand, H., 1998. Inhibition of long-term potentiation in developing rat visual cortex but not hippocampus by in utero exposure to polychlorinated biphenyls. Brain Res. Dev. Brain Res. 110, 257–260.
Andersen, H.R., Nielsen, J.B., Grandjean, P., 2000. Toxicologic evidence of developmental neurotoxicity of environmental chemicals. Toxicology 144, 121–127.
Banerjee, A., Garcia-Oscos, F., Roychowdhury, S., Galindo, L.C., Hall, S., Kilgard, M.P., Atzori, M., 2013. Impairment of cortical GABAergic synaptic transmission in an environmental rat model of autism. Int. J. Neuropsychopharmacol. 16, 1309–1318.
Carpenter, D.O., Hussain, R.J., Berger, D.F., Lombardo, J.P., Park, H.Y., 2002. Electrophysiologic and behavioral effects of perinatal and acute exposure of rats to lead and polychlorinated biphenyls. Environ. Health Perspect. 110 (Suppl. 3), 377–386.
Cellot, G., Cherubini, E., 2013. Functional role of ambient GABA in refining neuronal circuits early in postnatal development. Front. Neural Circuits 7, 136.
Chen, H.H., Lin, Y.R., Chan, M.H., 2011. Toluene exposure during brain growth spurt and adolescence produces differential effects on N-methyl-D-aspartate receptor-mediated currents in rat hippocampus. Toxicol. Lett. 205, 336–340.
Chomiak, T., Turner, N., Hu, B., 2013. What we have learned about autism spectrum disorder from valproic acid. Pathol. Res. Int. 2013, 712758.
Egawa, K., Fukuda, A., 2013. Pathophysiological power of improper tonic $GABA_A$ conductances in mature and immature models. Front. Neural Circuits 7, 170.
Foti, S.B., Chou, A., Moll, A.D., Roskams, A.J., 2013. HDAC inhibitors dysregulate neural stem cell activity in the postnatal mouse brain. Int. J. Dev. Neurosci. 31, 434–447.
Fountain, S.B., Ting, Y.L., Teyler, T.J., 1992. The in vitro hippocampal slice preparation as a screen for neurotoxicity. Toxicol. In Vitro 6, 77–87.
Fueta, Y., Ishidao, T., Arashidani, K., Endo, Y., Hori, H., 2002. Hyperexcitability of the hippocampal CA1 and the dentate gyrus in rats subchronically exposed to a substitute for chlorofluorocarbons, 1-bromopropane vapor. J. Occup. Health 44, 156–165.
Fueta, Y., Fukuda, T., Ishidao, T., Hori, H., 2004. Electrophysiology and immunohistochemistry in the hippocampal ca1 and the dentate gyrus of rats chronically exposed to 1-bromopropane, a substitute for specific chlorofluorocarbons. Neuroscience 124, 593–603.
Gkogkas, C.G., Khoutorsky, A., Ran, I., Rampakakis, E., Nevarko, T., Weatherill, D.B., Vasuta, C., Yee, S., Truitt, M., Dallaire, P., Major, F., Lasko, P., Ruggero, D., Nader, K., Lacaille, J.C., Sonenberg, N., 2013. Autism-related deficits via dysregulated eIF4E-dependent translational control. Nature 493, 371–377.
Go, H.S., Kim, K.C., Choi, C.S., Jeon, S.J., Kwon, K.J., Han, S.H., Lee, J., Cheong, J.H., Ryu, J. H., Kim, C.H., Ko, K.H., Shin, C.Y., 2012. Prenatal exposure to valproic acid increases the neural progenitor cell pool and induces macrocephaly in rat brain via a mechanism involving the GSK-3β/β-catenin pathway. Neuropharmacology 63, 1028–1041.
Gogolla, N., Leblanc, J.J., Quast, K.B., Sudhof, T.C., Fagiolini, M., Hensch, T.K., 2009. Common circuit defect of excitatory-inhibitory balance in mouse models of autism. J. Neurodev. Disord. 1, 172–181.
Grandjean, P., Landrigan, P.J., 2006. Developmental neurotoxicity of industrial chemicals. Lancet 368, 2167–2178.
Johnson-Venkatesh, E.M., Khan, M.N., Murphy, G.G., Sutton, M.A., Umemori, H., 2015. Excitability governs neural development in a hippocampal region-specific manner. Development 142, 3879–3891.
Juliandi, B., Tanemura, K., Igarashi, K., Tominaga, T., Furukawa, Y., Otsuka, M., Moriyama, N., Ikegami, D., Abematsu, M., Sanosaka, T., Tsujimura, K., Narita, M., Kanno, J., Nakashima, K., 2015. Reduced adult hippocampal neurogenesis and cognitive impairments following prenatal treatment of the antiepileptic drug valproic acid. Stem Cell Rep. 5, 996–1009.
Kersante, F., Rowley, S.C., Pavlov, I., Gutierrez-Mecinas, M., Semyanov, A., Reul, J.M., Walker, M.C., Linthorst, A.C., 2013. A functional role for both γ-aminobutyric acid (GABA) transporter-1 and GABA transporter-3 in the modulation of extracellular GABA and GABAergic tonic conductances in the rat hippocampus. J. Physiol. 591, 2429–2441.
Kilb, W., Kirischuk, S., Luhmann, H.J., 2013. Role of tonic GABAergic currents during pre- and early postnatal rodent development. Front. Neural Circuits 7, 139.
Kim, K.H., Pessah, I.N., 2011. Perinatal exposure to environmental polychlorinated biphenyls sensitizes hippocampus to excitotoxicity ex vivo. Neurotoxicology 32, 981–985.
Markram, K., Rinaldi, T., La Mendola, D., Sandi, C., Markram, H., 2008. Abnormal fear conditioning and amygdala processing in an animal model of autism. Neuropsychopharmacology 33, 901–912.
Puglia, M.P., Valenzuela, C.F., 2010. Repeated third trimester-equivalent ethanol exposure inhibits long-term potentiation in the hippocampal CA1 region of neonatal rats. Alcohol 44, 283–290.
Rinaldi, T., Kulangara, K., Antoniello, K., Markram, H., 2007. Elevated NMDA receptor levels and enhanced postsynaptic long-term potentiation induced by prenatal exposure to valproic acid. Proc. Natl. Acad. Sci. U. S. A. 104, 13501–13506.
Rinaldi, T., Perrodin, C., Markram, H., 2008. Hyper-connectivity and hyper-plasticity in the medial prefrontal cortex in the valproic acid animal model of autism. Front. Neural Circuits 2, 4.
Rodier, P.M., Ingram, J.L., Tisdale, B., Croog, V.J., 1997. Linking etiologies in humans and animal models: studies of autism. Reprod. Toxicol. 11, 417–422.
Roullet, F.I., Lai, J.K., Foster, J.A., 2013. In utero exposure to valproic acid and autism–a current review of clinical and animal studies. Neurotoxicol. Teratol. 36, 47–56.
Rubenstein, J.L., Merzenich, M.M., 2003. Model of autism: increased ratio of excitation/inhibition in key neural systems. Genes Brain. Behav. 2, 255–267.
Rubenstein, J.L., 2010. Three hypotheses for developmental defects that may underlie some forms of autism spectrum disorder. Curr. Opin. Neurol. 23, 118–123.
Schneider, T., Przewlocki, R., 2005. Behavioral alterations in rats prenatally exposed to valproic acid: animal model of autism. Neuropsychopharmacology 30, 80–89.
Sui, L., Ge, S.Y., Ruan, D.Y., Chen, J.T., Xu, Y.Z., Wang, M., 2000. Age-related impairment of long-term depression in area CA1 and dentate gyrus of rat

hippocampus following developmental lead exposure in vitro. Neurotoxicol. Teratol. 22, 381–387.
Varela, C., Llano, D.A., Theyel, B.B., 2012. An introduction to in vitro slice approaches for the study of neuronal circuitry. In: Fellin, T., Halassa, M. (Eds.), Neuronal Network Analysis: Concepts and Experimental Approaches. Humana Press, Totowa, pp. 103–125.
Wiegand, H., Altmann, L., 1994. Neurophysiological aspects of hippocampal neurotoxicity. Neurotoxicology 15, 451–458.

DR WEI ZHANG (Orcid ID : 0000-0002-9192-9549)

Article type : Original Article

Timing of Prenatal Exposure to Trauma and Altered Placental Expressions of HPA-Axis Genes and Genes Driving Neurodevelopment

Wei Zhang[1], Qian Li[2], Maya Deyssenroth[2], Luca Lambertini[2], Jackie Finik[1,3,4], Jacob Ham[5], Yongling Huang[3], Kenji J Tsuchiya[6], Patricia Pehme[1,3], Jessica Buthmann[1,3], Sachiko Yoshida[7], Jia Chen[2], & Yoko Nomura[1,2,3,5]

[1] Queens College, CUNY, Psychology, New York, NY, United States
[2] Icahn School of Medicine at Mount Sinai, Department of Environmental Medicine and Public Health, New York, NY, USA
[3] The Graduate Center, CUNY, Psychology, New York, NY, United States
[4] Graduate School of Public Health and Health Policy, CUNY, New York, NY, United State
[5] Icahn School of Medicine at Mount Sinai, Psychiatry, New York, NY, United States
[6] Hamamatsu University School of Medicine, Research Center for Child Mental Development, Shizuoka, Japan
[7] Department of Environmental & Life Sciences, Toyohashi University of Technology, Toyohashi, Japan

Corresponding authors:

Yoko Nomura
Queens College, CUNY
Department of Psychology
65-39 Kissena Blvd, Flushing, NY 11467
718-797-3164
Yoko.nomura@qc.cuny.edu

Jia Chen
Icahn School of Medicine at Mount Sinai
Environmental Medicine and Public Health
One Gustav L. Levy Place, NY 10029
212-241-7492
jia.chen@mssm.edu

Abstract

Prenatal maternal stress increases the risk for negative developmental outcomes in offspring, however the underlying biological mechanisms remain largely unexplored. In this study, alterations in placental gene expression associated with maternal stress were examined to elucidate potential underlying epi/genetic mechanisms. Expression levels of 40 selected genes involved in regulating fetal HPA-axis and neurodevelopment were profiled in placental tissues collected from a birth cohort established around the time of Superstorm Sandy. Objective prenatal traumatic stress was defined as whether mothers were exposed to Superstorm Sandy during pregnancy. Among the 275 mother-infant dyads, 181 dyads were delivered before Superstorm Sandy (i.e., Control), 66 dyads were exposed to Superstorm Sandy during the first trimester (i.e., Early Exposure) and 28 were exposed to Superstorm Sandy during the second or third trimester (i.e., Mid-Late Exposure). Across all trimesters, expression of *HSD11B2*, *MAOA*, *ZNF507,* and *DYRK1A* was downregulated among those exposed to Superstorm Sandy during pregnancy. Furthermore, trimester specific differences were also observed: exposure during early gestation was associated with downregulation of *HSD11B1* and *MAOB,* and upregulation of *CRHBP*; exposure during mid-late gestation was associated with upregulation of *SRD5A3*. Our findings suggest that placental gene expression may be altered in response to traumatic stress exposure during pregnancy, and the susceptibility of these genes is dependent on the time of the exposure during pregnancy. Further studies can elucidate the biological mechanisms that underlie trimester-specific exposure by evaluating the differential impact on offspring neurodevelopment later in childhood.

Key words: pregnancy; prenatal stress; mRNA; placenta

Introduction

During critical periods in pregnancy, the fetus has a heightened susceptibility to prenatal maternal stress (PNMS) [1,2]. Animal research shows that PNMS is associated with altered development of fetal neurobiological systems, particularly the central nervous system (CNS) and the hypothalamic-pituitary-adrenal (HPA) axis, which subsequently leads to impairment of health, cognition, affect, and behavior [3]. Human population studies also have demonstrated associations between PNMS, fetal CNS, HPA-axis development [4,5] and offspring's long-term neurobehavioral and neurodevelopmental aberrations [6]. However, these human studies are not yet able to causally link PNMS and CNS/HPA development due to possible confounds in recalling stress during pregnancy. While random assignment to reduce the impact of confounds is possible in animal research, a controlled experiment with random assignment of stress is not ethically feasible using a human population. Alternatively, a stressor with substantial negative valence, such as war or natural disaster, where individuals in the same region are independently and randomly exposed regardless of their demographic, genetic and psychosocial characteristics can be leveraged to study its effects on subsequent changes and health consequences. Indeed, studies have already shown that PNMS as a result of acute trauma, natural and man-made disasters increased risks for emotional, cognitive, behavioral, and physical problems in offspring [7–9].

In an attempt to understand the underlying biological mechanisms that influence sub/optimal development of the fetus due to PNMS, changes in placental gene expression have attracted interest in the research community in recent years [10–13]. The human placenta is the major interface between the mother and fetus, and is the critical organ that regulates fetal homeostasis, growth, and development. The disruption of the maternal milieu by stress can program vital aspects of placental functioning in response, including the expression of placental genes. In addition, since the placenta is derived from the extraembryonic layer of the blastocyst, the placenta shares genetic and epigenetic characteristics of the developing embryo/fetus [14]. PNMS has been linked to fetal growth and development, which may be partially explained by changes in placental functioning and its underlying genomics. These

programming processes have been studied in greater detail for the genes encoding 11-beta hydroxysteroid dehydrogenase enzymes (*HSD11B2*) [11,12,15], glucocorticoid and mineralocorticoid receptors (*NR3C1* and *NR3C2*) [11–13,16], and monoamine oxidase A (*MAOA*)[10]. However, the types of PNMS investigated also vary, from prenatal depression and prenatal anxiety, to prenatal perceived stress. For example, prenatal depression was associated with upregulation of *NR3C1* and/or *NR3C2* [13,16]. Prenatal depression was also associated with downregulation of *MAOA* [10]. In addition, decreased *HSD11B2* expression was found to be associated with prenatal anxiety but not with prenatal depression [15]; while increased *HSD11B2* expression was associated with perceived prenatal stress and negative health related stress [11]. The types and degree of PNMS may affect distinct molecular pathways/placental processes, and the role of placental gene expression in relaying the effects of PNMS from disaster or trauma exposure remains elusive.

Furthermore, examinations aimed at elucidating the role of PNMS exposure timing on placental functioning are underexplored. Animal studies (e.g., mice, rats, guinea pigs) suggest that the programming effects of PNMS on offspring outcomes are subject to the time of exposure [17–20]. For example, one study has found that only rats exposed to PNMS during the first trimester suffered behavioral and physiological deficits [20]. Male mice exposed to stress in early or mid-gestation showed increased stress reactivity (e.g., elevated levels of corticotrophin releasing factors, reduced hippocampal glucocorticoid receptor expression), cognitive deficits in learning and memory and anxiety-related behaviors [18]. Stress early in pregnancy was also associated with upregulation of placental peroxisome proliferator-activated receptor alpha (*PPARa*), insulin-like growth factor binding protein 1 (*IGFBP-1*), hypoxia-inducible factor 3a *(HIF3a*), and glucose transporter 4 (*GLUT4*) gene expression in male mice [18]. These studies broadly suggest that early pregnancy is a sensitive period for development. Stress exposure, especially during the first trimester, may disrupt developmental programming and potentially increase the risk of long-term neurodevelopmental disorders in offspring. Similarly, human studies provide evidence suggesting that PNMS exposure during early pregnancy may bring about the most

devastating consequences [17]. One study reported that women exposed to an earthquake in their first trimester experienced the highest level of stress and had infants with lower gestational ages at birth than women exposed during later trimesters [21]. King and Laplante (2005) found that exposure to a natural disaster in early and mid-pregnancy was associated with lower mental development scores [8]. In addition, many prior studies show that increased risk for schizophrenia is associated with extreme stress in early pregnancy [22–25]. For example, Khashan et al. (2008) found that pregnant women who experienced a familial death during the first trimester of pregnancy had children who were at a higher risk for schizophrenia and related disorders later in life [22]. Another study also linked higher risk for schizophrenia to first trimester exposure to the Dutch famine of 1944-1945 [24]. However, there is also evidence that the risks for other outcomes, such as autism, are associated with stress experienced in mid- or late- pregnancy. For instance, Beversdorf et al. (2005) reported the PNMS during the second and third trimesters, but not the first trimester, was associated with greater risk for autism [26]. Similarly, a study that investigated the effect of PNMS from a tropical storm or hurricane found that storm exposure during mid (5-6 months) and late (9-10 months) pregnancy predicted an increased risk for autism [27]. Taken together, it is of importance to examine whether early trimester has specific noxious influences on developing organisms and if so through what molecular mechanisms.

Studies specifically investigating stress exposure on placental changes also observe differences based on the timing of exposure. For example, Reynolds et al. (2015) found that higher prenatal depression throughout pregnancy was associated with upregulated placental *NR3C1* and *NR3C2* expression, and these effects were particularly significant for symptoms experienced in the third trimester for *NR3C1* and in the second trimester for *NR3C2* [16]. However, this study focused on a small subset of genes.

To date, differences in the timing of the exposure to PNMS on gene expression in the placenta have not yet been systematically investigated. Uncovering the biological mechanisms that are associated with earlier or later stress exposure and its subsequent

influence on developmental and mental health outcomes could further explain the somewhat inconsistent findings and move our understanding forward.

In this study, we aimed to evaluate acute PNMS experienced earlier and later in pregnancy by virtue of a devastating natural disaster, Superstorm Sandy. Superstorm Sandy was one of the worst natural disasters on record in the United States and was the second costliest cyclone to hit the U.S. since 1900. The New York metropolitan area was severely affected by the storm in October 2012 [28]. Superstorm Sandy drove extensive storm surge, waves, rainfall and flooding into the New York coastlines, where residences, businesses, cars and other property was heavily damaged. In New York, over 300,000 homes were severely destroyed primarily due to the storm. Significant damage also occurred to public transportation, particularly the subway system, resulting in suspensions of services, which ranged from a few hours to as long as several weeks. Other significant effects included widespread and prolonged power outages and a gasoline shortage. There were 117 deaths total (53 deaths in New York) attributed to Superstorm Sandy [29]. Because of its magnitude in size and impact, Superstorm Sandy brought to the population residing in the affected area both economical and psychological damages as a result of the destruction, providing us with a unique opportunity to conduct a quasi-experimental study. The quasi-experiment allows us to understand whether PNMS as a result of a natural disaster and its gestational timing may lead to dysregulation of the placental genome, particularly for 40 candidate genes known to be associated with HPA-axis functioning and neurodevelopment (Supplementary Table 1).

Materials and Methods

Study Population

The Stress in Pregnancy (SIP) Study is an on-going longitudinal study that enrolls and follows mothers throughout pregnancy and their offspring after their birth. All women were recruited as part of the SIP Study from the prenatal obstetrics and gynecological clinics at Mount Sinai Medical Center and New York Presbyterian Queens in New York City. The unexposed participants are comprised mainly of women who reside in Manhattan and

received obstetric care at Mount Sinai Hospital, while the Sandy exposed participants are comprised of women who reside in regions of Queens and Long Island devastated by the storm. Participants were excluded if positive for HIV infection, maternal psychosis, maternal age < 15 years, life-threatening medical complications related to the mother, and congenital or chromosomal abnormalities in the fetus. A detailed description of the study population can be found elsewhere [14,30]. Demographic information, such as mother's race, marital status, education, age, smoking behavior during pregnancy and prenatal normative psychosocial stress measures were collected during the second trimester. Data on mode of delivery, gestational age (in weeks) at birth, infant sex, and birth weight (grams) were recorded at birth.

A total of 328 placental tissues collected from mothers who were pregnant before or during Superstorm Sandy were included in the current study. Preterm infants born before 34 weeks (n = 10) were not included due to higher risks of developing severe health and developmental problems [31,32]. An additional 43 cases were excluded due to missing normative psychosocial stress measures, resulting in a final sample of 275 in this current study. Table 1 shows the demographic characteristics of the sample used in the current study. Included (N = 275) and excluded participants (N = 43) did not differ on major demographic characteristics, such as infant sex, gestational age at birth, birthweight, maternal age, race, or education. Missing education (n = 1), marital status (n = 1) and mode of delivery data (n = 7) have been imputed.

All participants gave written informed consent before any assessment or data collection. All procedures involving human subjects in this study were approved by the Institutional Review Boards at the City University of New York, New York Presbyterian/Queens, and the Icahn School of Medicine at Mount Sinai.

Timing of Trauma Exposure during Pregnancy

Among the 275 mother-infant dyads, 181 mothers included in this study gave birth before Superstorm Sandy (Control) and 94 mothers were pregnant during Superstorm Sandy. Among these 94, 66 were exposed to Superstorm Sandy during the first trimester

(Early Exposure), and 28 were exposed to Superstorm Sandy during the second or the third trimester (Mid-Late Exposure).

Selected genes known to modulate HPA-axis and neurodevelopment

The 40 candidate genes were identified *a priori* for their involvement in HPA-axis functioning and neurodevelopment, as based on extensive literature search and the Ingenuity ® Knowledge Data. Among the 20 HPA-axis functioning genes, 14 genes were expressed in the placenta and 6 genes were not sufficiently expressed. Among the remaining 20 genes associated with neurodevelopment, 13 genes were sufficiently expressed in the placenta and 7 genes were not sufficiently expressed. Details regarding candidate genes can be found in Supplementary Table 1.

Placenta Collection and Gene Expression Profiling

Biopsies, free of maternal decidua, were collected from each placenta quadrant midway between the cord insertion and the placenta rim, within one hour of delivery to prevent RNA degradation. The collected tissues were first snap-frozen in liquid nitrogen and then stored at -80°C. RNA was extracted with the Maxwell 16 automated DNA/RNA extraction equipment (Promega – Madison, WI, USA) using the proprietary extraction kits following the manufacturer's protocol. RNA was quantified with Nanodrop spectrophotometer (Thermo Electron North America – Madison, WI, USA).

Placental RNA expression was profiled using the nCounter platform (nanoString Technologies, Seattle, WA) as previously described [33]. The nanoString Norm package [34] was used to normalize data. Differences in sample content were accounted for by normalizing the data against the geometric mean of the housekeeping genes Glyceraldehyde-3-Phosphate Dehydrogenase (*GAPDH*), Ribosomal Protein L19 (*RPL19*), and Ribosomal Protein Lateral Stalk Subunit P0 (*RPLP0*). Genes where more than 50% of the samples fell below the limit of detection were considered unexpressed. After filtering out unexpressed genes, a total of 27 genes remained in the final analysis.

Covariates

Demographic variables. Various maternal and child demographic and health characteristics were included as covariates. Maternal characteristics included: maternal age, race (white, non-white), education, marital status (married/common law, single, divorced/separated/widowed), and smoking behavior during pregnancy (smoking, non-smoking). Infant characteristics included infant sex (male, female), gestational age, and mode of delivery (C-section, vaginal).

Normative psychosocial stress measures. Normative psychosocial stress during pregnancy was defined as a composite of prenatal depression, pregnancy related anxiety, perceived stress, state and trait anxiety, and negative stressful events. The co-experience of multiple types of normative psychosocial stress during pregnancy is relatively commonplace, capturing various domains of stress that mothers experience during pregnancy and using an aggregate measure of stress would increase the validity and reliability of the normative prenatal stress measure, as opposed to relying on only a single stressor [35–37]. These variables were measured using maternal self-report scales completed during the second trimester of the pregnancy and were used as a covariate when investigating the relationship between effects of prenatal trauma exposure and gene expression in the placenta. *Prenatal depression* was measured by the Edinburgh Postnatal Depression Scale (EPDS) [38]. Mothers were asked to report how they felt during the past seven days on a 4-point Likert scale based on severity. This inventory is well-validated in several languages and has acceptable reliability ranging from 0.79 to 0.86 [39–42]. *Pregnancy related anxiety* was measured by the Pregnancy Related Anxieties Questionnaire-revised (PRAQ-R) [43], which measures pregnancy related fears and worries. *Perceived stress during pregnancy* was measured by the Perceived Stress Scale (PSS-14) [44], which assessed the degree to which the rater appraises situations as stressful. The PSS-14 has good reliability and validity [44]. *State and trait anxiety during pregnancy* was measured by the State-Trait Anxiety Inventory (STAI) [45], which assessed temporary “state anxiety” and long-standing, characterological “trait anxiety.” Each of the two subscales consists of 20 items rated on a 4-point Likert scale. A meta-analysis of 45 articles reporting Cronbach’s alpha for internal consistency for this

inventory determined the mean to be 0.92 [46]. *Negative stressful events during pregnancy* was measured by the Psychiatric Epidemiology Research Interview Life Events Scale (LES) [47], assessed the occurrence of stressful events in five major areas of life: relationships, health, legal matters, work and financials, and friendships. This measure is widely used, has been shown to have good validity with narrative reports of life events, and has low intra-category variability [48].

The measures of normative psychosocial stress above were categorized to create a composite latent measure created by latent profile analysis (LPA). Model fits were assessed by Bayesian Information Criteria (BIC) [49], adjusted BIC (ABIC) [50], Lo-Mendell-Rubin (L-M-R) test [51] *p* values, and the entropy values for the two to four class models. LPA was performed using the full maximum likelihood estimation using Mplus version 6 [52]. Methodological details on the extraction of the latent confounding variable are provided in the Supplementary Methods. Overall, all stress variables were significantly correlated (Supplementary Table 2). LPA indicated that the three-class solution provided the best solution (Supplementary Table 3). The composite latent measure was categorized into three values from (0) low normative stress, (1) medium normative stress, to (2) high normative stress. 104 individuals were labeled as “low normative stress”, 127 individuals as “medium normative stress”, and 44 as “high normative stress” (Supplementary Table 4).

Main Statistical Analysis

Analyses of variance (ANOVAs) for continuous variables and Chi-square/Fisher’s exact tests for categorical variables were conducted to examine the differences among groups (Control, Early Exposure, and Mid-Late Exposure) across demographic and psychosocial factors. Generalized linear model (GLM) was used to evaluate the effects of acute PNMS on gene expression by comparing group differences on the placental expression of each gene, adjusting for covariates determined *a priori*. Significance of main effects (significance $p < 0.05$) was further examined using the sequential Bonferroni (Holm)

multiple comparison tests. All main statistics were conducted using SPSS version 19; while LPA was done using Mplus version 6.

Results

Characteristics of Study Population

The distribution of the demographic characteristics of the 275 dyads included in the present study is shown in Table 1. The population consisted of infants (mean age at gestation = 39.31 weeks), with roughly equivalent numbers of males and females (females = 45.5%). The SIP study consists of an urban, ethnically diverse cohort, with over half of the population reported to be of Hispanic/Latino descent (52.7%). Enrolled mothers were largely single (57.8%) and of mixed educational background ranging from no high school degree (19.3%) to post/college degree (18.5%).

Except for significant differences in maternal education ($p = 0.003$) and marital status ($p < 0.001$), with relatively more educated and married women in the exposed groups as opposed to the control; no significant group differences were observed for other demographic or psychosocial factors (Table 1).

Timing of Superstorm Sandy Exposure and Gene Expression in Placental HPA-axis Genes

Table 2 and Figure 1 show results for the overall group differences and follow-up pairwise comparisons with Holm correction for multiple testing. There are significant overall group differences in *CRHBP*, *DYRK1A*, *HSD11B1*, and *HSD11B2.* When adjusted for multiple comparisons, *CRHBP* gene expression level was upregulated in those exposed in early gestation as compared to the unexposed controls ($p = 0.030$). *DYRK1A* gene expression level was downregulated in those exposed in mid-late gestation as compared to the unexposed controls ($p = 0.005$). *HSD11B1* gene expression level was downregulated in those exposed in early gestation when compared with the unexposed controls ($p = 0.038$) and those exposed in mid-late gestation ($p = 0.038$). *HSD11B2* gene expression level was

downregulated in those exposed in early gestation (p = 0.043) and mid-late gestation (p < 0.001) as compared to the unexposed controls.

Timing of Superstorm Sandy Exposure and Gene Expression in Placental Neurodevelopment Genes

The bottom half of Table 2 shows significant group differences in neurodevelopment genes, including *MAOA*, *MAOB*, *MECP2*, *SRD5A3*, and *ZNF507*. As indicated in Figure 1, when adjusted for multiple comparisons, *MAOA* gene expression level was downregulated in those exposed in early (p = 0.039) and mid-late gestation (p = 0.011) compared to the unexposed controls. *MAOB* gene expression level was downregulated in those exposed in early gestation compared to the unexposed controls (p < 0.001). *SRD5A3* gene expression level was upregulated in those exposed in mid-late gestation when compared with the unexposed controls (p = 0.019) and those exposed in early gestation (p = 0.019). *ZNF507* gene expression level was downregulated in those exposed in early (p = 0.005) and mid-late gestations (p = 0.001) when compared to the unexposed controls.

Discussion

Accumulating evidence from animal and human research suggests that PNMS exposure exerts long-term impacts on fetal programming by altering placental function, which may be reflected in the gene expression profile in placenta. Given the predominant fetal origin of the placenta, our findings offer interesting insights into the impacts of acute PNMS on offspring.

Our results showed that PNMS, as a result of exposure to a natural disaster, at different stages of pregnancy was associated with downregulation of *HSD11B2*, *MAOA* and *ZNF507* genes. The trend of downregulation of *DYRK1A* across pregnancy was also observed, while the effect was significant for mid-late gestation, it was marginally significant for early gestation (p = 0.084). Overall, many of these downregulated genes across trimesters are vital for placental function and fetal development.

The placental 11*β*-hydroxysteroid dehydrogenase type 2 (11*β*-HSD2) enzyme (encoded by the *HSD11B2* gene), which converts active cortisol into inactive cortisone, acts as a barrier regulating the transfer of the maternal cortisol to the fetus [53]. Cortisol is essential to fetal growth but, may be harmful to the fetus when in high concentrations [54]. Under normal circumstances, 11*β*-HSD2 largely converts cortisol into cortisone, thereby protecting the fetus from excessive glucocorticoid exposure [53]. This is supported by the finding that fetal blood has 13-fold lower cortisol concentrations than maternal blood [55]. Studies demonstrate that stressed mothers commonly secrete greater amounts of glucocorticoids [56,57], despite contradictory evidence [58,59]. As a consequence, elevated levels of glucocorticoids may enter the fetal circulation and influence fetal HPA-axis development. Our results suggest that when exposed to acute PNMS, the protective effect of placental *HSD11B2* can be overwhelmed. Indeed, lower placental *HSD11B2* has been associated with poor infant outcomes, including decreased infant movement quality and lower muscle tone [60,61]. Our findings are inconsistent with some of the previous literature regarding stress-related effects on *HSD11B2* gene expression. For example, prenatal anxiety, but not depression, has been associated with lower *HSD11B2* expression [15]. The distinction may be explained by a lack of evolutionary benefit for prenatal depression as compared to prenatal anxiety, such that a depressed mother may not perceive danger, and therefore it may not play a role in affecting fetal and child development in future dangerous and stressful situations [62]. Furthermore, prenatal perceived stress and health related stress were reported to be positively associated with *HSD11B2* [11]. It has also been suggested that mild to moderate levels of PNMS may not decrease, but in fact may enhance development. For example, mid-level PNMS, such as nonspecific stress and prenatal depressive symptoms, were found to be positively associated with mental and motor development in younger children [63]. Our study is the first to have associated acute PNMS due to a natural disaster and decreased *HSD11B2* expression and therefore requires further replication. Nevertheless, this finding advocates that different types of stressors may exert differential impacts on gene expression that in turn program distinct fetal and child outcomes [64].

In addition to maternal glucocorticoids, serotonin is an important stress related neurotransmitter [65] which is synthesized in the placental and fetal compartments and is vital for fetal brain development. *MAOA* metabolizes serotonin, dopamine and norepinephrine. Maternal blood serotonin can cross the placenta and enter the fetal circulation; overexposure to serotonin disrupts fetal brain development [66]. Recent research suggests that PNMS is associated with elevated levels of serotonin [67] and a reduction in *MAOA* gene expression [10,67]. Mutations in *MAOA* have been linked to disordered neurodevelopment and behaviors, including autism-like disorders and antisocial behaviors [68,69].

Little is known about how the expression levels of placental genes, such as *DYRK1A* and *ZNF507,* influence the development of brain function and behavior in typically developing children. *DYRK1A* is involved in cell proliferation and has been implicated in Down syndrome [70]. *ZNF507* modulates transcriptional regulation; reduced expression of *ZNF507* has been related to schizophrenia [71]. Stress induced downregulation of these genes may also have an impact on placental function, intrauterine homeostasis and fetal growth.

Furthermore, these downregulated genes are more markedly altered among women exposed during mid-late gestation, which suggests that the impact of PNMS may be exaggerated as women advance throughout pregnancy, yet this warrants further investigation. Our group comparison results reflect no significant statistical differences between early and mid-late gestation (*HSD11B2*, $p = 0.053$; *MAOA*, $p = 0.270$, *ZNF507*, $p = 0.168$ and *DYRK1A*, $p = 0.124$), which may be attributed to the relatively small sample of exposed participants during mid-late gestation.

Prior animal and human research suggests the timing of exposure appears to be crucial when considering the effect of PNMS on offspring outcomes [67]. PNMS is believed to be associated with adverse outcomes, particularly in cases of early gestation exposure. Our findings are partially consistent with this line of research. Specifically, our results show that upregulation of *CRHBP* and downregulation of *HSD11B1* and *MAOB* were observed among those exposed to Superstorm Sandy in early pregnancy. Due to a relatively small group of

mid-late gestation, we did not observe significant differences between early and mid-late gestation exposure for *CRHBP* (p = 0.697) and *MAOB* (p = 0.055) expression.

CRHBP encodes the corticotrophin-releasing hormone (CRH)-binding protein, which inactivates CRH that stimulates the production of adrenocorticotropic hormone (ACTH) and cortisol throughout pregnancy in the maternal and the fetal compartments [72,73]. Increased circulating maternal CRH concentrations have been associated with lower concentrations of CRHBP [73]. In a normal human pregnancy, maternal CRH, derived from the placenta, provides information on the length of gestation [74,75]. Circulating maternal CRH concentrations rise over the course of gestation, correlating with increased placental *CRH* mRNA expression [73]. While an elevation in circulating maternal CRH concentrations increases risks for fetal growth restriction during early gestation [76]; an increase in these concentrations during the last few weeks of pregnancy accompanied by a fall in the concentrations of CRH-binding proteins allows for the preparation of events leading to parturition [77]. It has been suggested that exposure to stress, especially during early gestation, is associated with an increase in placental CRH concentrations in plasma [78]. Our results suggest that for individuals exposed to Superstorm Sandy in early pregnancy, a rise in CRH may lead to upregulation of *CRHBP,* which can produce prolong excessive CRH-binding proteins that prevent inappropriate pituitary-adrenal stimulation but disrupts the developmental increase of maternal CRH concentrations. In adults, *CRHBP* dysfunctionality is associated with posttraumatic stress and depression symptoms [79,80].

Comparably, the expression and activity of *HSD11B1,* which is primarily involved in reactivation of cortisol from cortisone*,* increases during normal pregnancy. Decreased *HSD11B1* has been associated with reduced cortisol regeneration and increased risks for newborns with intrauterine growth restriction, i.e., small-for-gestational-age [81]. Offspring exposed to the traumatic event in early gestation may be more vulnerable to these disruptions as the consequences of deficient *HSD11B1* expression.

Similar to *MAOA*, *MAOB* plays a critical role in regulating dopamine metabolism and dietary amines including phenylethylamine [82]. The placental tissue contains a small amount

of *MAOB* [83,84]. *MAOB* activity increases with aging in humans and is associated with neurodegenerative diseases such as Parkinson's and Alzheimer's diseases [85,86]. The role of *MAOB* gene expression in the placenta has not been well described. Lower *MAOB* platelet activity has been linked to mood disorders, alcoholism, sensation seeking and impulsivity [87]. Downregulation of placental *MAOB* may increase risks for neuropsychiatric and behavior disorders in offspring exposed to PNMS in early gestation.

Finally, upregulation of *SRD5A3* was observed among those exposed to Superstorm Sandy in mid-late pregnancy. *SRD5A3* plays an important role in protein glycosylation [88], is widely expressed in the human brain tissues and body organs (e.g., retina, skin, kidney), and plays a crucial role in brain development [89]. Mutations in *SRD5A3* have been linked to a congenital defect in dolichol metabolism [89,90]. Animal research has found that placental *SRD5A3* is altered by Triclosan (an antimicrobial agent often used in personal care products) exposure [91]. The three human 5α-reductases are encoded by the *SRD5A1*, *SRD5A2*, and *SRD5A3* genes. During pregnancy, the 5α-reductases in the placenta provide precursors for the synthesis of allopregnanolone, a neurosteroid that may exert neuroprotective effects on fetal brain development [92,93]. Therefore, it is essential to further investigate the prenatal risk factors such as maternal stress that may influence the allopregnanolone synthesis pathway. One recent investigation found that maternal plasma allopregnanolone concentrations were not related to the genotypes of *SRD5A1* and *SRD5A2* and maternal depressive symptoms during pregnancy [94]. However, little is known about the role of *SRD5A3* gene in the human placenta and its relation to the prenatal stress influences.

Our findings suggest that trauma exposure may uniquely impact developmental processes through changes in expression of genes which foster distinct developmental processes. Furthermore, it is likely that some of the genes we identified are fully developed and begin functioning during early pregnancy, whereas others only begin functioning during mid-late pregnancy. Although we were able to identify changes in gene expression as a result of placental development, the underlying molecular mechanisms by which this occurs requires further exploration, thus replication is needed. Expression of placental genes likely

varies across gestation to accommodate the dynamically changing needs of the developing fetus, although the molecular basis of placental development has yet to be fully uncovered [95]. Our findings suggest that several genes may be more vulnerable to maternal trauma exposure depending on the timing of exposure during gestation.

We acknowledge several limitations of this study. Although we observed associations between PNMS and differences in gene expression, implications of these findings on neurodevelopmental outcomes in childhood and adulthood remain unknown. As we see significant observations between CRH binding proteins and maternal stress in the current study, follow up studies will include further characterizing the response of the corticotrophin signaling pathway, HPA-axis functioning, and maternal stress, by evaluating additional components of the pathway, including placental levels of *CRH*, *ACTH* and *CORT*. Furthermore, the RNA integrity and quality were not assessed in the present study, while they should have been evaluated for each extraction especially since placental tissues contain high levels of RNase. Our opportunistic sample was relatively small especially once divided it into groups by windows of exposure, requiring that our conclusions be corroborated by future studies with larger sample sizes. The small size of our groups also supported the combining of mid and late trimester groups into one. This grouping is justifiable given that results of prior animal studies show that the first trimester is when the fetus might be most vulnerable to PNMS; however, it may have been more informative to have kept each trimester as a separate group. Furthermore, while prior research has shown that sex is likely a significant moderator of the effect of PNMS, our small sample size did not provide us with sufficient power to evaluate potential sex-specific effects [96]. Readers should also be reminded that the control and exposed groups were different with regards to marital status and education. Prior research has associated socio-economic status (i.e., education level) and altered placental gene expression levels [97]. While these differences could have happened by chance alone, the control group was composed of mainly women residing in Manhattan who received obstetric care at Mount Sinai Hospital, while the exposed group was mainly composed of women residing in storm devastated regions, Queens and Long

Island due to the study design. As such, while our findings were independent of a range of covariates; statistical control may not have been fully adequate in addressing group differences. Additionally, investigating the associations between gene expression and the covariates was outside the scope of the current study, and exploring such relationships may be worth pursuing in future studies. Finally, stress is a subjective experience and we did not include measures of how subjectively stressful each mother's experience of Superstorm Sandy was.

Despite these shortcomings, this is the first study, to our knowledge, to present an analysis of a list of candidate genes in HPA-axis regulation and neurodevelopment in a functional organ (placenta) by exposure to a traumatic event during pregnancy. In comparison with previous research, we were able to study how the timing of trauma exposure impacts placental gene expression. Our observations suggest that PNMS from trauma across trimesters downregulates placental expression of *DYRK1A*, *HSD11B2, MAOA,* and *ZNF507.* However, traumatic stress exposure in early gestation is associated with upregulation of *CRHBP* and downregulation of *HSD11B1* and *MAOB*, while exposure in mid-late gestation is associated with upregulation of *SRD5A3*. Our findings also demonstrated the importance of corroborating and extending the results of animal research in human populations. Longitudinal follow-up studies are needed to investigate how the alterations in the expression of these genes affect the neurobehavioral and neurodevelopmental outcomes in the offspring.

Acknowledgements

We thank all the parents and children who consented to participate in this study. We also thank current and former research staff and assistants at Queens College, City University of New York for their contributions to this study.

This research work was supported by the grants K01-080062, K01-080062S and R01-102729 from the National Institutes of Mental Health (NIMH), and PSC-CUNY, Queens College Research Enhancement Grant (to Nomura).

References

1. DiPietro JA, Hodgson DM, Costigan KA, Hilton SC, Johnson TR. Fetal neurobehavioral development. *Child Dev*. 1996;67(5):2553-2567. http://www.ncbi.nlm.nih.gov/pubmed/9022256.
2. Wadhwa PD, Sandman CA, Garite TJ. Chapter 9 The neurobiology of stress in human pregnancy: Implications for prematurity and development of the fetal central nervous system. *Prog Brain Res*. 2001;133:131-142. doi:10.1016/S0079-6123(01)33010-8.
3. Charil A, Laplante DP, Vaillancourt C, King S. Prenatal stress and brain development. *Brain Res Rev*. 2010;65:56-79. doi:10.1016/j.brainresrev.2010.06.002.
4. Babenko O, Kovalchuk I, Metz GAS. Stress-induced perinatal and transgenerational epigenetic programming of brain development and mental health. *Neurosci Biobehav Rev*. 2015;48:70-91. doi:10.1016/j.neubiorev.2014.11.013.
5. Glover V, O 'Connor TG, O 'Donnell K. Prenatal stress and the programming of the HPA axis. *Neurosci Biobehav Rev*. 2009;35:17-22. doi:10.1016/j.neubiorev.2009.11.008.
6. Talge NM, Neal C, Glover V. Antenatal maternal stress and long-term effects on child neurodevelopment: How and why? *J Child Psychol Psychiatry Allied Discip*. 2007;48(3-4):245-261. doi:10.1111/j.1469-7610.2006.01714.x.
7. Brand SR, Engel SM, Canfield RL, Yehuda R. The effect of maternal PTSD following in utero trauma exposure on behavior and temperament in the 9-month-old infant. *Ann N Y Acad Sci*. 2006;1071(1):454-458. doi:10.1196/annals.1364.041.
8. King S, Laplante DP. The effects of prenatal maternal stress on children's cognitive development: Project Ice Storm. *Stress*. 2005;8(1):35-45. doi:10.1080/10253890500108391.
9. Yehuda R, Engel SM, Brand SR, Seckl J, Marcus SM, Berkowitz GS. Transgenerational effects of posttraumatic stress disorder in babies of mothers

exposed to the World Trade Center attacks during pregnancy. *J Clin Endocrinol Metab*. 2005;90(7):4115-4118. doi:10.1210/jc.2005-0550.

10. Blakeley PM, Capron LE, Jensen AB, O'Donnell KJ, Glover V. Maternal prenatal symptoms of depression and down regulation of placental monoamine oxidase A expression. *J Psychosom Res*. 2013;75(4):341-345. doi:10.1016/j.jpsychores.2013.07.002.
11. Chen J, Li Q, Rialdi A, et al. Influences of maternal stress during pregnancy on the epi/genome: Comparison of placenta and umbilical cord blood. *J Depress Anxiety*. 2014;3(2). doi:10.4172/2167-1044.1000152.
12. Ponder KL, Salisbury A, McGonnigal B, Laliberte A, Lester B, Padbury JF. Maternal depression and anxiety are associated with altered gene expression in the human placenta without modification by antidepressant use: Implications for fetal programming. *Dev Psychobiol*. 2011;53(7):711-723. doi:10.1002/dev.20549.
13. Räikkönen K, Pesonen A-K, O'Reilly JR, et al. Maternal depressive symptoms during pregnancy, placental expression of genes regulating glucocorticoid and serotonin function and infant regulatory behaviors. *Psychol Med*. 2015;45(15):3217-3226. doi:10.1017/S003329171500121X.
14. Lambertini L, Chen J, Nomura Y. Mitochondrial gene expression profiles are associated with maternal psychosocial stress in pregnancy and infant temperament. *PLoS One*. 2015;10(9):1-20. doi:10.1371/journal.pone.0138929.
15. O'Donnell KJ, Bugge Jensen A, Freeman L, Khalife N, O'Connor TG, Glover V. Maternal prenatal anxiety and downregulation of placental 11β-HSD2. *Psychoneuroendocrinology*. 2012;37(6):818-826. doi:10.1016/j.psyneuen.2011.09.014.
16. Reynolds RM, Pesonen A-K, O'Reilly JR, et al. Maternal depressive symptoms throughout pregnancy are associated with increased placental glucocorticoid sensitivity. *Psychol Med*. 2015;45(10):2023-2030. doi:10.1017/S003329171400316X.

17. Bale TL. Epigenetic and transgenerational reprogramming of brain development. *Nat Rev Neurosci*. 2015;16(6):332-344. doi:10.1038/nrn3818.

18. Mueller BR, Bale TL. Sex-Specific Programming of Offspring Emotionality after Stress Early in Pregnancy. *J Neurosci*. 2008;28(36):9055-9065. doi:10.1523/JNEUROSCI.1424-08.2008.

19. Mueller BR, Bale TL. Early prenatal stress impact on coping strategies and learning performance is sex dependent. *Physiol Behav*. 2007;91(1):55-65. doi:10.1016/j.physbeh.2007.01.017.

20. Suchecki D, Palermo Neto J. Prenatal stress and emotional response of adult offspring. *Physiol Behav*. 1991;49(3):423-426. doi:10.1016/0031-9384(91)90259-Q.

21. Glynn LM, Wadhwa PD, Dunkel-Schetter C, Chicz-DeMet A, Sandman CA. When stress happens matters: Effects of earthquake timing on stress responsivity in pregnancy. *Am J Obstet Gynecol*. 2001;184(4):637-642. doi:10.1067/mob.2001.111066.

22. Khashan AS, Abel KM, McNamee R, et al. Higher risk of offspring schizophrenia following antenatal maternal exposure to severe adverse life events. *Arch Gen Psychiatry*. 2008;65(2):146. doi:10.1001/archgenpsychiatry.2007.20.

23. Robinson M, Mattes E, Oddy WH, et al. Prenatal stress and risk of behavioral morbidity from age 2 to 14 years: The influence of the number, type, and timing of stressful life events. *Dev Psychopathol*. 2011;23(2):507-520. doi:10.1017/S0954579411000241.

24. Susser ES, Lin SP. Schizophrenia after prenatal exposure to the Dutch hunger winter of 1944-1945. *Arch Gen Psychiatry*. 1992;49(12):983. doi:10.1001/archpsyc.1992.01820120071010.

25. van Os J, Selten JP. Prenatal exposure to maternal stress and subsequent schizophrenia. The May 1940 invasion of The Netherlands. *Br J Psychiatry*. 1998;172(4). http://bjp.rcpsych.org/content/172/4/324.short. Accessed September 5, 2017.

26. Beversdorf DQ, Manning SE, Hillier A, et al. Timing of Prenatal Stressors and Autism. *J Autism Dev Disord*. 2005;35(4):471-478. doi:10.1007/s10803-005-5037-8.

27. Kinney DK, Miller AM, Crowley DJ, Huang E, Gerber E. Autism prevalence following prenatal exposure to hurricanes and tropical storms in Louisiana. *J Autism Dev Disord*. 2008;38(3):481-488. doi:10.1007/s10803-007-0414-0.

28. Blake ES, Kimberlain TB, Berg RJ, Cangialosi JP, Beven II JL. Tropical Cyclone Report Hurricane Sandy Rep. AL182012: National Hurricane Center. 2013.

29. MMWR. Deaths Associated with Hurricane Sandy — October – November 2012. *Centers Dis Control Prev*. 2013;62(20):2010-2013.

30. Finik J, Nomura Y. Cohort Profile: Stress in Pregnancy (SIP) Study. *Int J Epidemiol*. January 2017:dyw264. doi:10.1093/ije/dyw264.

31. Loftin RW, Habli M, Snyder CC, Cormier CM, Lewis DF, DeFranco EA. Late preterm birth. *Rev Obstet Gynecol*. 2010;3(1):10-19. doi:10.3909/riog0098.

32. Vohr B. Long-term outcomes of moderately preterm, late preterm, and early term infants. *Clin Perinatol*. 2013;40(4):739-751. doi:10.1016/j.clp.2013.07.006.

33. Kappil MA, Green BB, Armstrong DA, et al. Placental expression profile of imprinted genes impacts birth weight. *Epigenetics*. 2015;10(9):842-849. doi:10.1080/15592294.2015.1073881.

34. Waggott D, Chu K, Yin S, Wouters BG, Liu F-F, Boutros PC. NanoStringNorm: An extensible R package for the pre-processing of NanoString mRNA and miRNA data. *Bioinformatics*. 2012;28(11):1546-1548. doi:10.1093/bioinformatics/bts188.

35. Lobel M, Cannella DL, Graham JE, DeVincent C, Schneider J, Meyer BA. Pregnancy-specific stress, prenatal health behaviors, and birth outcomes. *Heal Psychol*. 2008;27(5):604-615. doi:10.1037/a0013242.

36. Rini CK, Dunkel-Schetter C, Wadhwa PD, Sandman CA. Psychological adaptation and birth outcomes: The role of personal resources, stress, and sociocultural context in pregnancy. *Heal Psychol*. 1999;18(4):333-345. doi:10.1037/0278-6133.18.4.333.

37. Roesch SC, Schetter CD, Woo G, Hobel CJ. Modeling the types and timing of stress in pregnancy. *Anxiety, Stress Coping*. 2004;17(1):87-102. doi:10.1080/1061580031000123667.

38. Murray L, Carothers AD. The validation of the Edinburgh Post-natal Depression Scale on a community sample. 1990;157(2):288-290. doi:10.1192/bjp.157.2.288.

39. Kheirabadi GR, Maracy MR, Akbaripour S, Masaeli N. Psychometric properties and diagnostic accuracy of the edinburgh postnatal depression scale in a sample of Iranian women. *Iran J Med Sci*. 2012;37(1):32-38. doi:10.1007/s00737-007-0204-x.

40. Mazhari S, Nakhaee N. Validation of the Edinburgh Postnatal Depression Scale in an Iranian sample. *Arch Womens Ment Health*. 2007;10(6):293-297. doi:10.1007/s00737-007-0204-x.

41. Montazeri A, Torkan B, Omidvari S. The Edinburgh Postnatal Depression Scale (EPDS): Translation and validation study of the Iranian version. *BMC Psychiatry*. 2007;7(1):11. doi:10.1186/1471-244X-7-11.

42. Small R, Lumley J, Yelland J, Brown S. The performance of the Edinburgh Postnatal Depression Scale in English speaking and non-English speaking populations in Australia. *Soc Psychiatry Psychiatr Epidemiol*. 2007;42(1):70-78. doi:10.1007/s00127-006-0134-3.

43. Huizink AC, Mulder EJ. H, Robles De Medina PG, Visser GH. A, Buitelaar JK. Is pregnancy anxiety a distinctive syndrome? *Early Hum Dev*. 2004;79(2):81-91. doi:10.1016/j.earlhumdev.2004.04.014.

44. Cohen S, Kamarck T, Mermelstein R. A Global Measure of Perceived Stress. *J Health Soc Behav*. 1983;24(4):385. doi:10.2307/2136404.

45. Spielberger CD. *State-Trait Anxiety Inventory: A Comprehensive Bibliography.* Consulting Psychologists Press; 1989.

46. Barnes L, Harp D, Jung W. Reliability Generalization of Scores on the Spielberger State-Trait Anxiety Inventory. *Educ Psychol Meas*. 2002;62(4):603-618. doi:10.1177/0013164402062004005.

47. Dohrenwend B, Krasnoff L, Askenasy A, Dohrenwend B. The psychiatric epidemiology research interview life events scale. In: *Handbook of Stress: Theoretical and Clinical Aspects*. New York: Free Press; 1982:320-331.

48. Dohrenwend BP. Inventorying Stressful Life Events as Risk Factors for Psychopathology: Toward Resolution of the Problem of Intracategory Variability. *Psychol Bull*. 2006;132(3):477-495. doi:10.1037/0033-2909.132.3.477.

49. Schwarz G. Estimating the Dimension of a Model. *Ann Stat*. 1978;6(2):461-464. doi:10.1214/aos/1176344136.

50. Sclove SL. Application of model-selection criteria to some problems in multivariate analysis. *Psychometrika*. 1987;52(3):333-343. doi:10.1007/BF02294360.

51. Lo Y, Mendell NR, Rubin DB. Testing the number of components in a normal mixture. *Biometrika*. 2001;88(3):767-778. doi:10.1093/biomet/88.3.767.

52. Muthen LK, Muthen BO. Mplus. 2006.

53. Benediktsson R, Calder a a, Edwards CR, Seckl JR. Placental 11 beta-hydroxysteroid dehydrogenase: A key regulator of fetal glucocorticoid exposure. *Clin Endocrinol (Oxf)*. 1997;46(2):161-166. doi:10.1046/j.1365-2265.1997.1230939.x.

54. Isaksson J, Lindblad F, Valladares E, Högberg U. High maternal cortisol levels during pregnancy are associated with more psychiatric symptoms in offspring at age of nine - A prospective study from Nicaragua. *J Psychiatr Res*. 2015;71:97-102. doi:10.1016/j.jpsychires.2015.09.016.

55. Gitau R. Fetal hypothalamic-pituitary-adrenal stress responses to invasive procedures are independent of maternal responses. *J Clin Endocrinol Metab*. 2001;86(1):104-109. doi:10.1210/jc.86.1.104.

56. Moisiadis VG, Matthews SG. Glucocorticoids and fetal programming part 2: mechanisms. *Nat Rev Endocrinol*. 2014;10(7):403-411. doi:10.1038/nrendo.2014.74.

57. Glover V, O'Connor TG, O'Donnell K. Prenatal stress and the programming of the HPA axis. *Neurosci Biobehav Rev*. 2010;35(1):17-22. doi:10.1016/j.neubiorev.2009.11.008.

58. Davis EP, Glynn LM, Schetter CD, Hobel C, Chicz-Demet A, Sandman CA. Prenatal exposure to maternal depression and cortisol influences infant temperament. *J Am Acad Child Adolesc Psychiatry*. 2007;46(6):737-746. doi:10.1097/chi.0b013e318047b775.

59. Baibazarova E, van de Beek C, Cohen-Kettenis PT, Buitelaar J, Shelton KH, van Goozen SHM. Influence of prenatal maternal stress, maternal plasma cortisol and cortisol in the amniotic fluid on birth outcomes and child temperament at 3 months. *Psychoneuroendocrinology*. 2013;38(6):907-915. doi:10.1016/J.PSYNEUEN.2012.09.015.

60. Conradt E, Lester BM, Appleton AA, Armstrong DA, Marsit CJ. The roles of DNA methylation of NR3C1 and 11β-HSD2 and exposure to maternal mood disorder in utero on newborn neurobehavior. *Epigenetics*. 2013;8(12):1321-1329. doi:10.4161/epi.26634.

61. Marsit CJ, Maccani MA, Padbury JF, Lester BM. Placental 11-Beta Hydroxysteroid Dehydrogenase methylation is associated with newborn growth and a measure of neurobehavioral outcome. Oudejans C, ed. *PLoS One*. 2012;7(3):e33794. doi:10.1371/journal.pone.0033794.

62. O'Connor TG, Heron J, Glover V. Antenatal anxiety predicts child behavioral/emotional problems independently of postnatal depression. *J Am Acad Child Adolesc Psychiatry*. 2002;41(12):1470-1477. doi:10.1097/00004583-200212000-00019.

63. DiPietro JA, Novak MFSX, Costigan KA, Atella LD, Reusing SP. Maternal psychological distress during pregnancy in relation to child development at age two. *Child Dev*. 2006;77(3):573-587. doi:10.1111/j.1467-8624.2006.00891.x.

64. Glover V. Annual research review: Prenatal stress and the origins of psychopathology: An evolutionary perspective. *J Child Psychol Psychiatry Allied Discip*. 2011;52(4):356-367. doi:10.1111/j.1469-7610.2011.02371.x.

65. Joëls M, Baram TZ. The neuro-symphony of stress. *Nat Rev Neurosci*. 2009;10(6):459. doi:10.1038/nrn2632.

66. Bonnin A, Levitt P. Fetal, maternal, and placental sources of serotonin and new implications for developmental programming of the brain. *Neuroscience*. 2011;197:1-7. doi:10.1016/j.neuroscience.2011.10.005.

67. Bronson SL, Bale TL. The placenta as a mediator of stress effects on neurodevelopmental reprogramming. *Neuropsychopharmacology*. 2015;41(1):1-12. doi:10.1038/npp.2015.231.

68. Brunner HG, Nelen M. Abnormal behavior associated with a point mutation in the structural gene for monoamine oxidase A. *Science (80-)*. 1993;262(5133):578. doi:10.1126/science.8211186.

69. Kisková J, Gabriková D. The role of MAOA gene in the etiology of autism spectrum disorder in males. *Int J Medical, Heal Biomed Bioeng Pharm Eng*. 2015;9(2):103-106. http://www.waset.org/publications/10000328. Accessed March 1, 2017.

70. Park J, Song WJ, Chung KC. Function and regulation of Dyrk1A: towards understanding Down syndrome. *Cell Mol Life Sci*. 2009;66(20):3235-3240. doi:10.1007/s00018-009-0123-2.

71. Vachev TI, Popov NT, Stoyanova VK. Down Regulation of MIR-320 Gene Family Members in the Peripheral Blood of Schizophrenia Patients. 2016;5(1):221-230. doi:http://dx.doi.org/10.20546/ijcmas.2016.501.020.

72. Kemp CF, Woods RJ, Lowry PJ. The corticotrophin-releasing factor-binding protein: An act of several parts. *Peptides*. 1998;19(6):1119-1128. doi:10.1016/S0196-9781(98)00057-6.

73. Challis JRG. Placental clock parturition. *Placenta*. 1998;19(2):361-374. http://www.placentajournal.org/article/S0143-4004(98)80054-4/pdf. Accessed July 16, 2017.

74. McLean M, Bisits A, Davies J, Woods R, Lowry P, Smith R. A placental clock controlling the length of human pregnancy. *Nat Med*. 1995;1(5):460-463. doi:10.1038/nm0595-460.

75. Gangestad SW, Caldwell Hooper AE, Eaton MA. On the function of placental corticotropin-releasing hormone: A role in maternal-fetal conflicts over blood glucose concentrations. *Biol Rev*. 2012;87(4):856-873. doi:10.1111/j.1469-185X.2012.00226.x.

76. Sandman CA, Wadhwa PD, Chicz-DeMet A, Porto M, Garite TJ. Maternal corticotropin-releasing hormone and habituation in the human fetus. *Dev Psychobiol*. 1999;34(3):163-173. doi:10.1002/(SICI)1098-2302(199904)34:3<163::AID-DEV1>3.0.CO;2-9.

77. Linton EA, Perkins A V, Woods RJ, et al. Corticotropin releasing hormone-binding protein (CRH-BP): plasma levels decrease during the third trimester of normal human pregnancy. *J Clin Endocrinol Metab*. 1993;76(1):260-262. doi:10.1210/jcem.76.1.8421097.

78. Sandman CA, Glynn L, Schetter CD, et al. Elevated maternal cortisol early in pregnancy predicts third trimester levels of placental corticotropin releasing hormone (CRH): Priming the placental clock. *Peptides*. 2006;27(6):1457-1463. doi:10.1016/j.peptides.2005.10.002.

79. Davydow DS, Kohen R, Hough CL, Tracy JH, Zatzick D, Katon WJ. A pilot investigation of the association of genetic polymorphisms regulating corticotrophin-releasing hormone with posttraumatic stress and depressive symptoms in medical-surgical intensive care unit survivors. *J Crit Care*. 2014;29(1):101-106. doi:10.1016/j.jcrc.2013.08.016.

80. Roy B, Shelton RC, Dwivedi Y. DNA methylation and expression of stress related genes in PBMC of MDD patients with and without serious suicidal ideation. *J Psychiatr Res*. 2017;89:115-124. doi:10.1016/j.jpsychires.2017.02.005.

81. Struwe E, Berzl GM, Schild RL, et al. Simultaneously reduced gene expression of cortisol-activating and cortisol-inactivating enzymes in placentas of small-for-gestational-age neonates. *Am J Obstet Gynecol*. 2007;197(1):43.e1-43.e6. doi:10.1016/j.ajog.2007.02.012.

82. Shih JC, Thompson RF. Monoamine oxidase in neuropsychiatry and behavior. *Am J Hum Genet*. 1999;65:593-598. doi:10.1086/302562.

83. Riley LA, Waguespack MA, Denney RM. Characterization and quantitation of monoamine oxidases A and B in mitochondria from human placenta. *Mol Pharmacol*. 1989;36(1). http://molpharm.aspetjournals.org/content/36/1/54.short. Accessed July 19, 2017.

84. Bach AW, Lan NC, Johnson DL, et al. cDNA cloning of human liver monoamine oxidase A and B: molecular basis of differences in enzymatic properties. *Proc Natl Acad Sci U S A*. 1988;85(13):4934-4938. http://www.pnas.org/content/85/13/4934.full.pdf. Accessed July 19, 2017.

85. Benedetti MS, Dostert P. Monoamine oxidase, brain ageing and degenerative diseases. *Biochem Pharmacol*. 1989;38(4):555-561. doi:10.1016/0006-2952(89)90198-6.

86. Jossan SS, Gillberg PG, Gottfries CG, Karlsson I, Oreland L. Monoamine oxidase B in brains from patients with Alzheimer's disease: A biochemical and autoradiographical study. *Neuroscience*. 1991;45(1):1-12. doi:10.1016/0306-4522(91)90098-9.

87. Shih JC, Chen K, Ridd MJ. Monoamine oxidase: From genes to behavior. *Annu Rev Neurosci*. 1999;22:197-217. doi:10.1146/annurev.neuro.22.1.197.

88. Stiles AR, Russell DW. SRD5A3: A surprising role in glycosylation. *Cell*. 2010;142(2):196-198. doi:10.1016/j.cell.2010.07.003.

89. Morava E, Wevers RA, Cantagrel V, et al. A novel cerebello-ocular syndrome with abnormal glycosylation due to abnormalities in dolichol metabolism. *Brain*. 2010;133(11):3210-3220. doi:10.1093/brain/awq261.

90. Cantagrel V, Lefeber DJ, Ng BG, et al. SRD5A3 is required for converting polyprenol to dolichol and is mutated in a congenital glycosylation disorder. *Cell*. 2010;142(2):203-217. doi:10.1016/j.cell.2010.06.001.

91. Feng Y, Zhang P, Zhang Z, Shi J, Jiao Z, Shao B. Endocrine disrupting effects of triclosan on the placenta in pregnant rats. Kanellopoulos-Langevin C, ed. *PLoS One*. 2016;11(5):e0154758. doi:10.1371/journal.pone.0154758.

92. Vu TT, Hirst JJ, Stark M, et al. Changes in human placental 5α-reductase isoenzyme expression with advancing gestation: Effects of fetal sex and glucocorticoid exposure. *Reprod Fertil Dev*. 2009;21(4):599-607. doi:10.1071/RD08224.

93. Hill M, Pařízek A, Kancheva R, Jirásek JE. Reduced progesterone metabolites in human late pregnancy biosynthesis of neuroactive steroids in human pregnancy. *Physiol Res*. 2011;60:225-241. www.biomed.cas.cz/physiolres. Accessed January 26, 2018.

94. Hellgren C, Comasco E, Skalkidou A, Sundström-Poromaa I. Allopregnanolone levels and depressive symptoms during pregnancy in relation to single nucleotide polymorphisms in the allopregnanolone synthesis pathway. *Horm Behav*. 2017;94:106-113. doi:10.1016/j.yhbeh.2017.06.008.

95. Gheorghe CP, Goyal R, Mittal A, Longo LD. Gene expression in the placenta: maternal stress and epigenetic responses. *Int J Dev Biol*. 2010;54(2-3):507-523. doi:10.1387/ijdb.082770cg.

96. Bale TL. Sex differences in prenatal epigenetic programming of stress pathways. *Stress*. 2011;14(4):348-356. doi:10.3109/10253890.2011.586447.

97. Räikkönen K, O'Reilly JR, Pesonen AK, et al. Associations between maternal level of education and occupational status with placental glucocorticoid regeneration and sensitivity. *Clin Endocrinol (Oxf)*. 2014;81(2):175-182. doi:10.1111/cen.12412.

Figure 1: Timing of trauma exposure and gene expression in placenta. Only significant overall differences in gene expression related to trauma exposure are reported. The bar represents the average expression level of each gene using housekeeping genes for normalization and the whisker the standard error. The pairwise comparisons were adjusted for multiple comparisons using sequential Bonferroni procedure. ns, nonsignificant; * $p < 0.05$; ** $p < 0.01$.

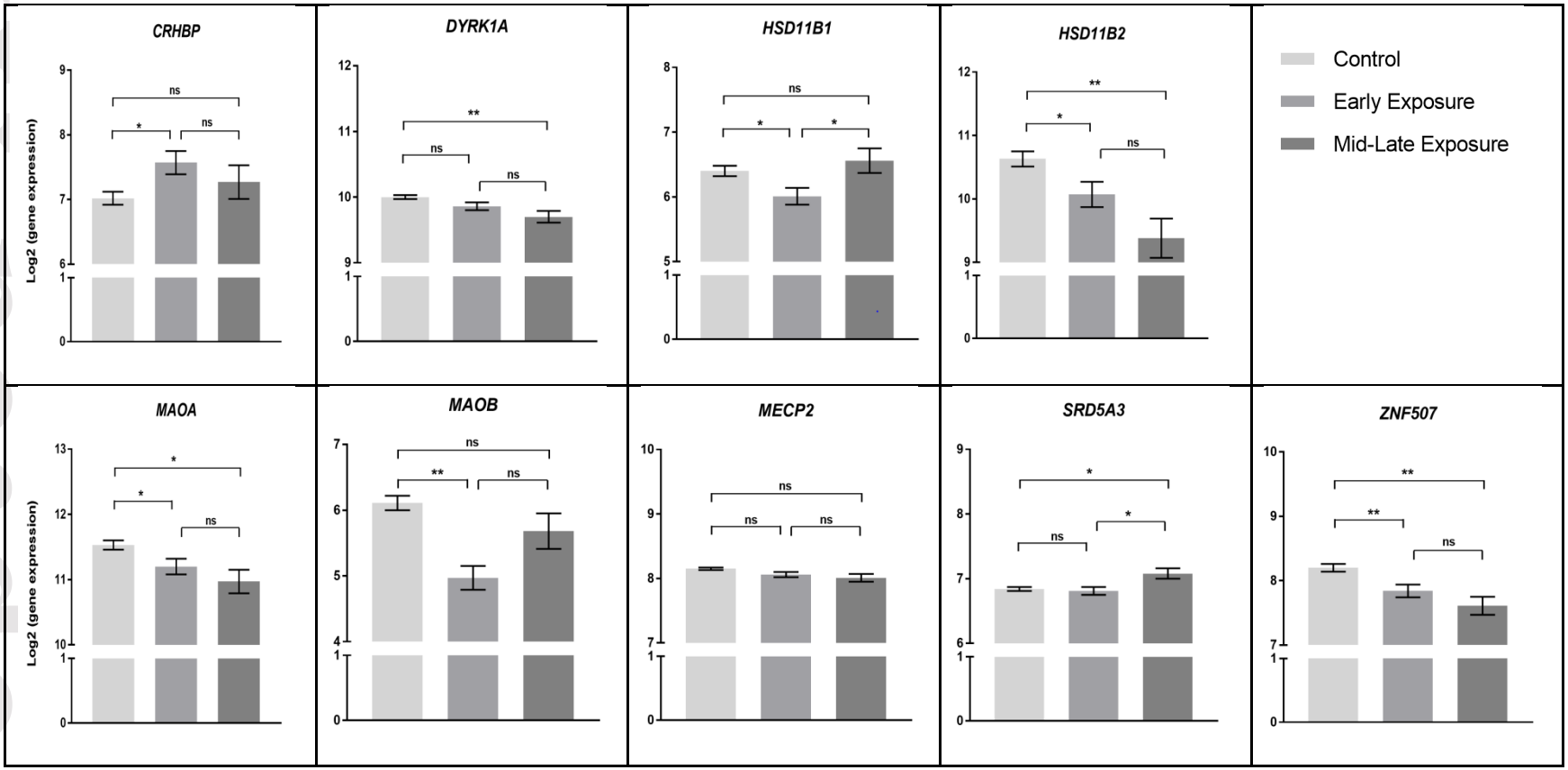

Table 1. Characteristics of the study population in total and by stress groups (Control, Early Exposure, and Mid-Late Exposure).

		Total (N = 275)	**Control (n = 181)**	**Early Exposure (n = 66)**	**Mid-Late Exposure (n = 28)**	***p* value** [a]
Infant sex						.282
Males	N (%)	150 (54.5)	98 (54.1)	40 (60.6)	12 (42.9)	
Females	N (%)	125 (45.5)	83 (45.9)	26 (39.4)	16 (57.1)	
Gestational age, weeks	Mean (SD)	39.31 (1.47)	39.30 (1.49)	39.31 (1.47)	39.33 (1.38)	.997
Birthweight						.196
< 2500 g	N (%)	15 (5.5)	13 (7.2)	1 (1.5)	1 (3.6)	
≥ 2500 g	N (%)	258 (93.8)	166 (91.7)	65 (98.5)	27 (96.4)	
Missing	N (%)	2 (.7)	2 (1.1)			
Mode of delivery						.389
C-section	N (%)	93 (33.8)	65 (36)	19 (28.7)	9 (32.1)	
Vaginal	N (%)	175 (63.6)	114 (63)	45 (68.2)	16 (57.1)	
Missing	N (%)	7 (2.5)	2 (1.1)	2 (3)	3 (10.7)	
Maternal age, years	Mean (SD)	27.76 (5.90)	27.65 (6.18)	27.70 (5.34)	28.68 (5.35)	.688
Mother's race						.219
White	N (%)	27 (9.8)	13 (7.2)	10 (15.2)	3 (10.7)	
Non-White	N (%)	248 (90.2)	168 (92.8)	56 (84.8)	25 (89.3)	
Black	N (%)	68 (24.7)	53 (29.3)	12 (18.2)	3 (10.7)	
Hispanic/Latino	N (%)	145 (52.7)	98 (54.1)	29 (43.9)	19 (67.9)	
Asian	N (%)	21 (7.76)	7 (3.9)	12 (18.2)	2 (7.1)	
Others	N (%)	14 (5.1)	10 (5.5)	3 (4.5)	1 (3.6)	
Maternal education						.003
Less than high school	N (%)	53 (19.3)	46 (25.4)	5 (7.6)	2 (7.1)	
High school graduate	N (%)	62 (22.5)	44 (24.3)	13 (19.7)	5 (17.9)	
Some college	N (%)	108 (39.2)	69 (38.1)	27 (40.9)	12 (42.9)	
College graduate	N (%)	30 (10.9)	13 (7.2)	11 (16.7)	6 (21.4)	
Graduate degree	N (%)	21 (7.6)	9 (5)	9 (13.6)	3 (10.7)	
Missing	N (%)	1 (.4)		1 (1.5)		

Mother's marital status						< .001
Married	N (%)	90 (32.7)	39 (21.5)	35 (53)	16 (60.7)	
Common law	N (%)	20 (7.3)	13 (7.2)	6 (9.1)	1 (3.6)	
Single	N (%)	159 (57.8)	126 (69.6)	22 (33.3)	11 (39.3)	
Divorced/separated/widowed	N (%)	5 (1.8)	3 (1.7)	2 (3.0)		
Missing	N (%)	1 (.4)		1 (1.5)		
Smoking during pregnancy						.246
No	N (%)	238 (86.5)	154 (85.1)	57 (86.4)	27 (96.4)	
Yes	N (%)	35 (12.7)	27 (14.9)	7 (10.6)	1 (3.6)	
Missing	N (%)	2 (.7)		2 (3)		
Prenatal depression	Mean (SD)	7.35 (5.4)	7.26 (5.36)	7.62 (5.37)	7.36 (5.88)	.902
Prenatal related anxiety	Mean (SD)	5.87 (2.3)	5.89 (2.28)	6.04 (2.34)	5.36 (2.32)	.423
Perceived stress during pregnancy	Mean (SD)	36.20 (7.43)	36.37 (7.47)	35.58 (7.58)	36.49 (6.96)	.748
State anxiety	Mean (SD)	38.00 (11.50)	37.87 (11.35)	38.58 (12.62)	37.57 (10.11)	.896
Trait anxiety	Mean (SD)	38.43 (10.75)	38.46 (10.83)	38.35 (10.31)	38.50 (11.61)	.997
Negative stressful events	Mean (SD)	1.57 (1.97)	1.55 (1.93)	1.62 (2.04)	1.57 (2.10)	.974
Normative psychosocial stress group						.744
Low	N (%)	104 (37.8)	69 (38.1)	24 (36.4)	11 (39.3)	
Moderate	N (%)	127 (46.18)	82 (45.3)	34 (51.5)	11 (39.3)	
High	N (%)	44 (16)	30 (16.6)	8 (12.1)	6 (21.4)	

NB. [a] *p* values for the test for the differences among the 3 groups: ANOVA for continuous variables and Chi-square/Fisher's exact tests for categorical variables.

Table 2. Gene expression differences among stress groups (Control, Early Exposure, and Mid-Late Exposure). There are significant overall group differences in HPA-axis genes (*CRHBP*, *DYRK1A*, *HSD11B1*, and *HSD11B2*) and genes driving neurodevelopment (*MAOA*, *MAOB*, *MECP2*, *SRD5A3*, and *ZNF507*). Mean value denotes the average expression level of each gene, using housekeeping genes for normalization. SE represents standard error.

Group	**Control (n = 181)**	**Early Exposure (n = 66)**	**Mid-Late Exposure (n = 28)**	
	Mean (*SE*)	**Mean (*SE*)**	**Mean (*SE*)**	**Overall *p* value**
HPA-Axis				
AVPR1B	3.80 (.06)	3.85 (.09)	4.00 (.14)	.453
CFL1	12.13 (.02)	12.06 (.03)	12.07 (.05)	.109
CREB1	9.23 (.03)	9.32 (.05)	9.25 (.07)	.282
CREBBP	4.33 (.05)	4.42 (.08)	4.38 (.12)	.599
CRHBP	7.02 (.10)	7.57 (.18)	7.27 (.26)	.035
DYRK1A	10.00 (.03)	9.86 (.06)	9.70 (.09)	.003
HSD11B1	6.40 (.08)	6.01 (.13)	6.56 (.19)	.016
HSD11B2	10.63 (.12)	10.07 (.20)	9.38 (.31)	<.001
NCOR1	10.39 (.03)	10.33 (.05)	10.25 (.07)	.121
NCOR2	9.35 (.04)	9.38 (.06)	9.45 (.10)	.664
NR3C1	10.85 (.03)	10.94 (.05)	10.76 (.08)	.107
NR3C2	7.22 (.05)	7.33 (.08)	7.00 (.12)	.078
NR4A1	7.53 (.07)	7.19 (.13)	7.60 (.19)	.053
POMC	3.62 (.06)	3.59 (.10)	3.68 (.14)	.869
Neurodevelopment				
ADRA2A	5.95 (.06)	5.82 (.10)	5.86 (.16)	.538
CDKL5	7.43 (.04)	7.43 (.06)	7.28 (.09)	.285

DBH	3.80 (.07)	3.96 (.11)	4.11 (.17)	.176
FOXP1	6.49 (.04)	6.42 (.07)	6.51 (.10)	.644
HTR1B	5.35 (.06)	5.30 (.10)	5.29 (.16)	.886
MAOA	11.53 (.07)	11.20 (.12)	10.97 (.18)	.004
MAOB	6.11 (.11)	4.97 (.18)	5.68 (.27)	<.001
MECP2	8.15 (.02)	8.06 (.04)	8.01 (.06)	.044
PON3	4.68 (.06)	4.89 (.09)	4.89 (.14)	.107
SNAP25	3.61 (.06)	3.66 (.10)	3.74 (.14)	.701
SRD5A3	6.84 (.03)	6.81 (.06)	7.08 (.08)	.017
ZNF507	8.20 (.06)	7.84 (.10)	7.61 (.14)	<.001
ZNHIT6	7.91 (.03)	7.89 (.05)	7.85 (.08)	.792

NB: *p* values are calculated based on generalized linear models controlling for maternal age, race, education, marital status, smoking behavior during pregnancy, infant sex, gestational age, mode of delivery, and normative psychosocial stress.

J Occup Health 2018; 60: 74-79

Journal of Occupational Health

Brief Report

Prenatal exposure to 1-bromopropane causes delayed adverse effects on hippocampal neuronal excitability in the CA1 subfield of rat offspring

Yukiko Fueta[1], Toru Ishidao[1], Susumu Ueno[2], Yasuhiro Yoshida[3], Yasunari Kanda[4] and Hajime Hori[1]

[1]Department of Environmental Management and Control, School of Health Sciences, University of Occupational and Environmental Health, Kitakyushu, Japan, [2]Department of Occupational Toxicology, University of Occupational and Environmental Health, Kitakyushu, Japan, [3]Department of Immunology and Parasitology, School of Medicine, University of Occupational and Environmental Health, Kitakyushu, Japan and [4]Division of Pharmacology, National Institute of Health Sciences, Tokyo, Japan

Abstract: Objectives: Neurotoxicity of 1-bromopropane (1-BP) has been reported in occupational exposure, but whether the chemical exerts developmental neurotoxicity is unknown. We studied the effects of prenatal 1-BP exposure on neuronal excitability in rat offspring. **Methods:** We exposed dams to 1-BP (700 ppm, 6 h a day for 20 days) and examined hippocampal slices obtained from the male offspring at 2, 5, 8, and 13 weeks of age. We measured the stimulation/response (S/R) relationship and paired-pulse ratios (PPRs) of the population spike (PS) at the interpulse intervals (IPIs) of 5 and 10 ms in the CA1 subfield. **Results:** Prenatal 1-BP exposure enhanced S/R relationships of PS at 2 weeks of age; however, the enhancement diminished at 5 weeks of age until it reached control levels. Prenatal 1-BP exposure decreased PPRs of PS at 2 weeks of age. After sexual maturation, however, the PPRs of PS increased at 5-ms IPI in rats aged 8 and 13 weeks. **Conclusions:** Our findings indicate that prenatal 1-BP exposure in dams can cause delayed adverse effects on excitability of pyramidal cells in the hippocampal CA1 subfield of offspring.
(J Occup Health 2018; 60: 74-79)
doi: 10.1539/joh.17-0009-BR

Key words: 1-Bromopropane, Delayed adverse effect, Electrophysiology, Excitability, Prenatal exposure, Rat hippocampal slices

Received January 10, 2017; Accepted September 29, 2017
Published online in J-STAGE November 1, 2017
Correspondence to: Y. Fueta, Department of Environmental Management, School of Health Sciences, University of Occupational and Environmental Health, Yahatanishi-ku, Kitakyushu, 807-8555, Japan (e-mail: yukiko@med.uoeh-u.ac.jp)

Introduction

Social concerns have been raised regarding the developmental neurotoxicity of prenatally absorbed environmental chemicals, which may exert delayed adverse effects on brain function after birth. It is now recognized that some industrial chemicals (e.g., lead, methylmercury, polychlorinated biphenyls, arsenic, and toluene) can exert developmental neurotoxicity, which results in clinical or subclinical brain dysfunction in humans and in laboratory animals[1)]. Many neurotoxic chemicals are present in industrial work settings, and it is not known whether prenatal exposure to industrial chemicals leads to developmental neurotoxicity.

1-Bromopropane (CH_3-CH_2-CH_2Br; 1-BP), one substitute for specific chlorofluorocarbons, is currently used as a solvent in a variety of industrial and commercial applications. Products containing 1-BP include degreasers and cleaners, spray adhesives, spot removers, coin cleaners, paintable mold release agents, automotive refrigerant flushes, and lubricants. Adverse effects on the central and peripheral nervous system have been found in industrial workers who used 1-BP[2-4)]. Adult rats exposed to 1-BP have also exhibited central neurotoxicity, alteration of mRNA levels of brain neurotransmitter receptors[5)], and hippocampal disinhibition caused by a decrease in γ-aminobutyric acid (GABA)-mediated function[6)]. In *in vitro* studies using rat hippocampal slices, 1-BP directly suppressed the synaptic plasticity, referred to as a long-term potentiation, in the granule cells of the dentate

gyrus[7].

Developmental toxicity is one reason for the threshold limit value set by the American Conference of Governmental Industrial Hygienists for 1-BP[8]. We recently reported that prenatal exposure to 1-BP suppressed the occurrence of kainate (KA)-induced "wet dog shake" behavior in 2-week-old rat pups[9]. However, whether or not prenatal 1-BP exposure changes neuronal function at the cellular level in the brain of the offspring remains unknown. Therefore, we studied the effects of prenatal 1-BP exposure on neuronal excitability after birth. In studying neuronal excitability, population spikes (PSs) were recorded in the CA1 subfield of hippocampal slices. We analyzed stimulation-dependent responses, stimulation/response (S/R) relationships, and the ratio of responses to double-pulse stimulations (paired-pulse ratios or PPRs). PPRs have been used as a simple method for assessing excitability in neuronal networks[6,10] In the present study, we evaluated rats at 2, 5, 8, and 13 weeks of age, to determine whether prenatal 1-BP exposure exerts delayed effects after birth.

Materials and Methods

Animals and exposure protocol

Preparation of rats and 1-BP inhalation were made according to our previous study[9]. Briefly, adult male and female Wistar rats were purchased from Kyudo Co., Ltd. (Tosu, Japan). The rats were housed in plastic cages with paper-made chips (ALPHA-dri, Shepherd Specialty Papers, Richland, MI, USA) on a 12-h light/dark cycle (light period: 7 AM-7 PM). The temperature was controlled at 22°C-23°C. The relative humidity was approximately 50%-70%. The animals were allowed to consume food and water ad libitum. Female rats at the proestrus stage were mated with male rats. On the morning of the following day, the existence of sperm in the vaginal plug or vaginal smear was verified as gestation day (GD) 0. 1-BP was purchased from Kanto Chemical Co., Ltd. (Tokyo, Japan). Dams were exposed to 1-BP vapor at a concentration of 700 ppm (6 h/day) for 20 days from GD 1 to GD 20 in an exposure chamber, whereas the other dams were provided fresh air in the same type of chamber. The exposure concentration was designed to be 700 ppm, which was higher than the LOAEL (400 ppm) for decrease in inhibition, so-called disinhibition[11]. Rats were not allowed access to food and water during the inhalation period. At postnatal day (PND) 2, the litter size was counted. Until the experimental days, male and female rat pups were housed separately after weaning. Some pups in the control and prenatally 1-BP-exposed groups were sourced from pups that were not injected with KA in our previous study[9]. The prenatally 1-BP-exposed groups are abbreviated as the 1-BP group. The number of dams in the control group and 1-BP group was 15 and 12, respectively. The total number of pups in the control group and 1-BP group was 29 and 20, respectively.

The experiments were conducted under the guidance of the Ethics Committee of Animal Care and Experimentation in accordance with the Guiding Principle for Animal Care Experimentation, University of Occupational and Environmental Health, Japan, which conforms to the National Institutes of Health Guide for the Care and Use of Laboratory Animals and the Japanese Law for Animal Welfare and Care.

Hippocampal slice preparation

Electrophysiological tests were conducted in male rats at 2 (PND 14), 5, 8, and 13 weeks of age. The total number of tested slices in the control group and 1-BP group was 119 and 86, respectively. The slices were prepared following previously reported methods[6]. Briefly, the rats were deeply anesthetized using a diethyl ether vapor. After decapitation, the brain was removed and dipped in an ice-cooled artificial cerebrospinal fluid (ACSF) (3°C-4°C) saturated with an O_2/CO_2 mixture (95%:5%). The ACSF was composed of 124 mM NaCl, 2 mM KCl, 1.25 mM KH_2PO_4, 2 mM $CaCl_2$, 2 mM $MgSO_4$, 26 mM $NaHCO_3$, and 10 mM glucose. The bilateral hippocampi were separated from the other brain regions. Further, transverse slices were obtained from the middle third region of the hippocampus using a McIlwain tissue chopper (Mickle Laboratory Engineering, Co., Ltd., Guildford, UK). The thickness of the slice was 600 μm for 2-week-old rats and 450 μm for 5-, 8-, and 13-week-old rats. The slices were transferred to an interface-type recording chamber, which was controlled at 32 ± 0.2°C, and perfused with ACSF saturated with a mixture of O_2/CO_2 (95%:5%) at a flow rate of 1 ml/min.

All the chemicals used in this study were of reagent grade and purchased from commercial sources.

Stimulation and recordings

After a stabilizing period of 1-2 h, bipolar stimulation electrodes made with stainless steel wires (50 μm in diameter) were placed on the stratum radiatum, where the Schaffer collateral and commissural fibers run up in the CA1 subfield (Fig. 1A). PS was recorded from the pyramidal cell layer in the CA1 subfield using glass microelectrodes (1-2 MΩ). Stimulations consisted of square-wave pulses (200 μs) from a stimulator (SEN7203, Nihon Koden Co., Tokyo, Japan) via an isolator (SS202J, Nihon Koden Co.). Stimulation intensities were 10 μA and 50 μA and increased by 100 μA every 2 min from 100 μA to a current of 600 μA in the slices from the 2-week-old rats. In the slices from the 5-, 8-, and 13-week-old rats, the stimulation was delivered every 30 sec with intensities of 20, 40, 60, 80, 100, 140, 200, and 300 μA. The S/R relationship in the extracellular recording configuration represents basic excitability of the local area responding to

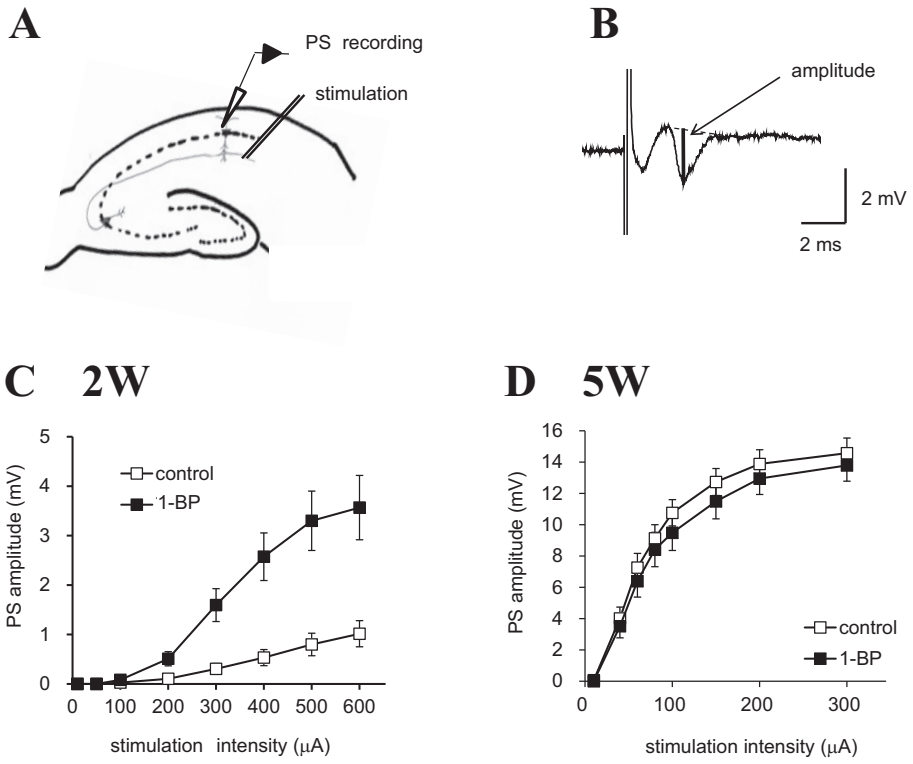

Fig. 1. Recording of population spikes (PSs) from the hippocampal CA1 field and PS stimulus/response (S/R) relationships
(A) Stimulation electrode and recording electrode set on the CA1 subfield of the hippocampal slice. The stimulation electrode was set in the stratum radiatum, supplying stimulation to Schaffer collateral and commissural fibers. The PS recording electrode was set in the pyramidal cell layer. (B) Typical PS recorded in the CA1 field of the hippocampal slice obtained from a 2-week-old control rat. The thick line represents the PS amplitude measurement; stimulation intensity was 600 μA. (C) At 2 weeks of age, S/R relationships of the PS amplitude obtained from the 1-BP-exposed rats were significantly enhanced compared to S/R relationships in control rats (p <0.001 by repeated-measure ANOVA). (D) At 5 weeks, the enhancement observed in the 1-BP-exposed rats disappeared, and the S/R relationship decreased to control levels (PS amplitude: p=0.5 by repeated-measure ANOVA). The horizontal axis represents stimulation intensity; the vertical axis represents PS amplitude. Data of 16-19 slices were averaged.

electrical stimulation, and the responses are prefigured to increase as the stimulation strengthens. For the paired-pulse configuration, after the S/R relationship experiment, the current amplitude was adjusted to result in an almost-maximum PS, 600 μA for slices from the 2-week-old rats, and 300 μA for slices from the 5-, 8-, and 13-week-old rats. Interpulse intervals (IPIs) of the paired-pulse stimulation were 5 and 10 ms and delivered every 2 min for slices from the 2-week-old rats and every 1 min for slices from older rats. Electrophysiological signals were amplified using a high-impedance amplifier (Axoclamp 2B, Molecular Devices, Sunnyvale, CA, USA). The signals were then digitized with an AD converter (Digidata 1200, Molecular Devices) and stored on a computer using pCLAMP software (Molecular Devices).

Electrophysiological analysis

PS amplitude was measured as described in our previous study[6] (Fig. 1B). PPRs were calculated as follows:

PPR of PS = second PS amplitude/first PS amplitude

In our previous inhalation studies using adult rats[6,11], PPRs of PS evoked with paired-pulse stimulation at IPIs of 5 and 10 ms in the CA1 subfield were <1 in the hippocampal CA1 of control adult rats, representing the presence of feedback inhibition. Compared to those of adult rats, PPRs of PS in immature rats can be 1 or higher[12]. Thus, in either case of inhibition or facilitation, paired-pulse configuration in extracellular recordings in the slices is useful to examine the excitability of the local area responding to double-pulse stimulations.

Statistical analysis

Statistical significance was evaluated by repeated-measure analysis of variance (ANOVA) for the S/R relationship. For PPRs, unpaired Welch's *t*-test was used to determine a difference between the 1-BP and control groups, when the data were normally distributed. Otherwise, the Mann-Whitney U test was applied, and p values <0.05 (two-tailed) were considered statistically significant. Electrophysiological data are expressed as means ± standard errors of the mean (SEMs). Litter size represents mean ± standard deviation. Statistical tests were performed in Ekuseru-Toukei 2010 for Windows (Social Survey Research Information Co., Ltd., Tokyo, Japan).

Results

There was no difference between the litter sizes of the control group and 1-BP group (control: 14 ± 2 pups, 15 dams; 1-BP: 14 ± 3 pups, 12 dams).

As shown in Fig. 1C, the PS amplitude was 4 times greater in the 1-BP group than in the control group at 600 μA of stimulation intensity in 2-week-old rats. In 5-week-old rats, the enhancement disappeared, and the levels decreased to the control level of the S/R relationship of the PS amplitude (Fig. 1D). No difference was observed between the 1-BP and control groups at 8 and 13 weeks of age (data not shown). Increased excitability of pyramidal neurons was a transient change.

The left column of Fig. 2 shows examples of paired-pulse responses recorded from the hippocampal CA1 subfield of the control and 1-BP groups. As shown in Fig. 2A, at 2 weeks of age, the averaged PPR was approximately 2 in the control group, suggesting a facilitatory effect. In contrast, inhibition rather than facilitation was observed at the 5-ms IPI in the 1-BP group. At the 10-ms IPI, PPRs showed a slight facilitation but were significantly decreased compared to PPRs in the control group. At 5 weeks of age, PPRs were lower than 0.2, displaying an apparent feedback inhibition in both groups (data not shown), and the effects of prenatal 1-BP exposure on PS PPRs disappeared. At 8 and 13 weeks of age, PPRs were still lower than 1 but increased significantly at 5 ms of IPI in the 1-BP group compared with that of the control group (Fig. 2B and 2C). There was no significant difference in the disinhibitory effects between 8- and 13-week-old rats.

Discussion

In general, the effects of prenatal chemicals on the brains of offspring with more littermates may be different from those with fewer littermates. In addition, litter size may be affected by inhalation of 1-BP by the dams. However, because there was no difference between the litter sizes of the control and 1-BP groups in this study, the delayed developmental toxicity observed was not likely to be associated with changes in litter size.

The present study revealed that prenatal exposure to 1-BP enhanced the excitability of CA1 pyramidal neurons and caused a decrease in PPRs of PS amplitude in hippocampal slices from 2-week-old rats. The lactation period after birth is considered to be the period of synaptogenesis in rat brains[13]; thus, neuronal development during the lactation period may be sensitive to prenatal chemical exposures. In a previous study[9], we reported that prenatal exposure to 1-BP suppressed KA-induced "wet dog shake" behaviors in 2-week-old rats. In this study, prenatal 1-BP exposure rendered the hippocampal CA1 subfield highly responsive to a single stimulation but suppressive to double stimulations. The decrease in PPRs in the 1-BP group shown in Fig. 2A may have been caused by the higher sensitivity of PS1. In the control group, PS1 may have been developmentally suppressed for some unknown reason (as shown in Fig. 1C), and the suppression may have been lifted following the second stimulation, as shown in PS2. Prenatal 1-BP exposure may weaken or lift the suppression in the PS1. The PS2 amplitude in the control group was similar to that seen in the 1-BP group. This indicates that prenatal 1-BP exposure may make CA1 neurons hyperexcitable at the developmental stage, which is quite different from normal brain development. Because 1-BP is metabolized in the womb of pregnant rats and biotransformed into metabolites, it is unclear whether those effects were caused by 1-BP itself.

Although a decrease in PPRs of PS amplitude was observed in the 1-BP group at 2 weeks of age, the difference diminished at 5 weeks of age, as did the S/R relationship. In contrast to that of the 2-week-old pups, the 8- and 13-week-old groups displayed an increase in PPRs of the PS, also known as disinhibition. In the 13-week-old rats, we observed that the disinhibitory effect induced by the prenatal 1-BP exposure was greater in female than in male rats (data not shown). It is unclear, however, whether sex-specific effects would be observed at other ages, and this should be investigated in the future. Thus, prenatal exposure to 1-BP can exert developmental effects linked to the excitatory function of neurons and network excitability. Disinhibition has been reported in relation to subclinical and clinical changes in brain excitability in epileptic patients and animals[14], as well as in anxiety disorders[15]. We did not observe any spontaneous abnormal behaviors in the 1-BP group during breeding. To date, developmental neurotoxic effects caused by 1-BP exposure have not been reported in children whose mothers were exposed occupationally during pregnancy. However, because disinhibition can be associated with the hyperexcitable brain and epilepsy, it should not be concluded that disinhibition is merely a phenomenon restricted to rats. Because disinhibition is interpreted as a disturbance of the excitation/inhibition balance in the hippocampal CA1 area, disin-

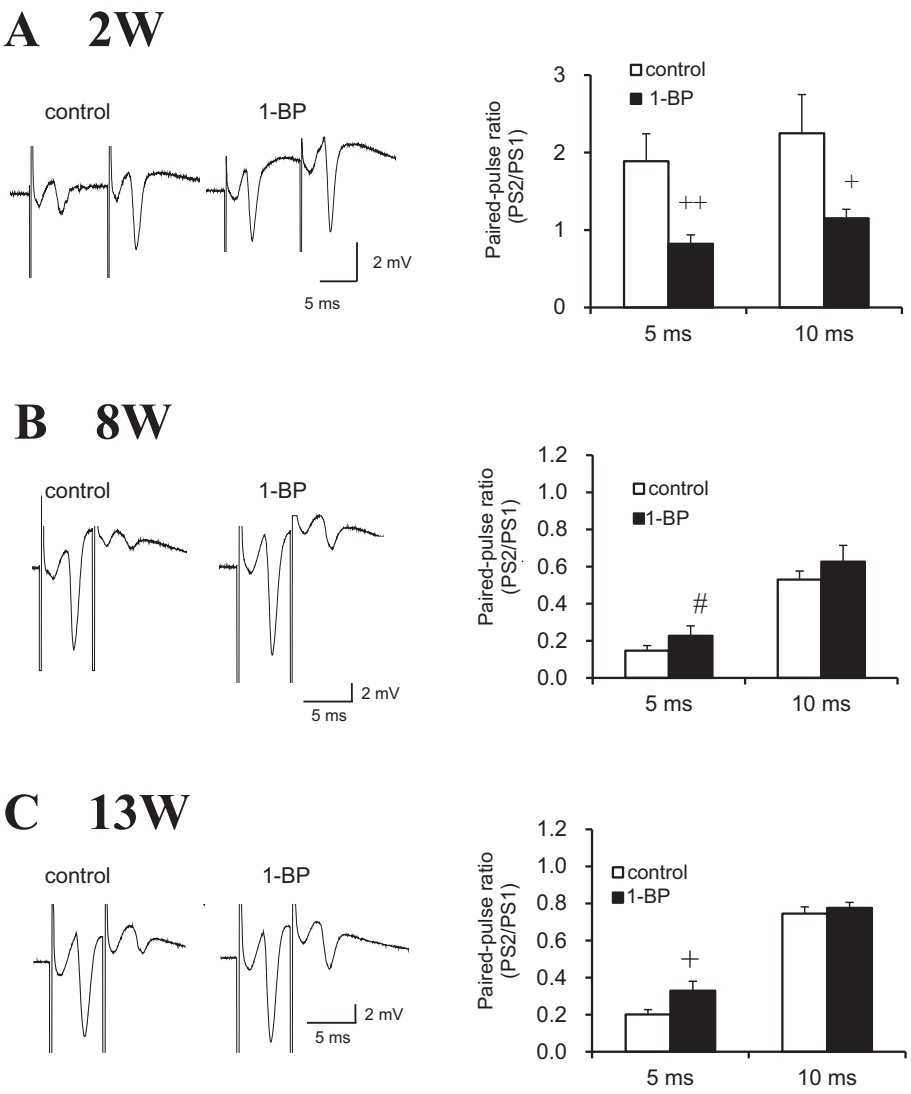

Fig. 2. Paired-pulse ratios (PPRs) of the population spikes (PSs) evoked with a double stimulation of 5 and 10 ms interpulse intervals (IPIs) in the CA1 subfield of hippocampal slices obtained from 2-, 8-, and 13-week-old male rats and 13-week-old female rats

Left column: Representative examples of paired-pulse responses recorded from the hippocampal CA1 subfield of the control and 1-BP groups. Right column: (A) At 2 weeks of age, PPRs decreased substantially in the 1-BP group (++p <0.01 vs. the control group at the 5-ms IPI, +p<0.05 vs. the control group at the 10-ms IPI by Welch's t-test). (B) At 8 weeks of age, PPRs were lower than 1 in both groups, indicating an apparent inhibition. At the 5-ms IPI, the PPR of the 1-BP group increased compared with that of the control group (#p <0.05 by Mann-Whitney U test). (C) Similar to the 5-ms IPI at 8 weeks of age, PPR of male rats in the 1-BP group increased compared with that of the control male rats at 13 weeks of age (+p <0.05 by Welch's t-test). The horizontal axis represents the IPIs; the vertical axis represents the PPRs of PS amplitude. Data of 16-25 slices were averaged.

hibitory effects can be classified as adverse effects.

The enhancement of excitability induced by prenatal 1-BP exposure was observed only in the 2-week-old group, and may therefore have been only a transient effect. Alternately, one could argue that the excess basal excitability during synaptogenesis is not coincidental with disinhibition after maturation. If so, the PS S/R relationship can be useful as a new index marker for developmental neurotoxicity of chemicals before the appearance of neurophysiological changes in the brain after maturation. To validate this method for assessing the developmental neurotoxicity of industrial chemicals, we should test chemi-

cals that are already known to exert developmental neurotoxicity. To this end, we are currently investigating valproic acid, an antiepileptic drug used in an established animal model of the developmental disorder, autism. Synaptic transmission generates action potentials; we are also studying field excitatory postsynaptic potentials.

In conclusion, we demonstrated that prenatal 1-BP exposure can cause delayed neurotoxicity, although the underlying mechanism is not known yet, and requires further investigation.

Acknowledgements: We gratefully acknowledge K. Egashira for animal care. This study was partly supported by the Grants-in-Aid Program of the Japan Society for the Promotion of Science (no. 23510084 to S.U. and no. 18510064 to Y.F.) and a Health and Labour Sciences Research Grant from the Ministry of Health, Labour and Welfare, Japan (to Y.K.).

Conflicts of interest: There are no conflicts of interest.

References

1) Grandjean P, Landrigan P. Developmental neurotoxicity of industrial chemicals. Lancet 2006; 368: 2167-2178.
2) Ichihara G, Kitoh J, Li W, Ding X, Ichihara S, Takeuchi Y. Neurotoxicity of 1-bromopropane: Evidence from animal experiments and human studies. J Adv Res 2012; 3: 91-98.
3) Samukawa M, Ichihara G, Oka N, Kusunoki S. A case of severe neurotoxicity associated with exposure to 1-bromopropane, an alternative to ozone-depleting or global-warming solvents. Arch Intern Med 2012; 172: 1257-1260.
4) Wang T, Wu M, Wu Y, et al. Neurotoxicity associated with exposure to 1-bromopropane in golf-club cleansing workers. Clin Toxicol 2015; 53: 823-826.
5) Ueno S, Yoshida Y, Fueta Y, et al. Changes in the function of the inhibitory neurotransmitter system in the rat brain following subchronic inhalation exposure to 1-bromopropane. Neurotoxicology 2007; 28: 415-420.
6) Fueta Y, Fukuda T, Ishidao T, Hori H. Electrophysiology and immunohistochemistry in the hippocampal CA1 and the dentate gyrus of rats chronically exposed to 1-bromopropane, a substitute for specific chlorofluorocarbons. Neuroscience 2004; 124: 593-603.
7) Kanemitsu M, Fueta Y, Ishidao T, Aou S, Hori H. Development of a direct exposure system for studying the mechanisms of central neurotoxicity caused by volatile organic compounds. Ind Health 2016; 54: 42-49.
8) ACGIH: 1-Bromopropane: TLV(R) Chemical Substances 7th Edition Documentation. [Online]. 2014; Available from: URL: https://www.acgih.org/forms/store/ProductFormPublic/1-bromopropane-tlv-r-chemical-substances-7th-edition-documentation
9) Fueta Y, Kanemitsu M, Egawa S, Ishidao T, Ueno S, Hori H. Prenatal exposure to 1-bromopropane suppresses kainate-induced wet dog shakes in immature rats. J UOEH 2015; 37: 255-261.
10) Waldbaum S, Dudek FE. Single and repetitive paired-pulse suppression: A parametric analysis and assessment of usefulness in epilepsy research. Epilepsia 2009; 50: 904-916.
11) Fueta Y, Ishidao T, Ueno S, Yoshida Y, Kunugita N, Hori H. New approach to risk assessment of central neurotoxicity induced by 1-bromopropane using animal models. Neurotoxicology 2007; 28: 270-273.
12) Papatheodoropoulos C, Kostopoulos G. Development of a transient increase in recurrent inhibition and paired- pulse facilitation in hippocampal CA1 region. Dev Brain Res 1998; 108: 273-285.
13) Ben-Ari Y. Developing networks play a similar melody. Trends Neurosci 2001; 24: 353-360.
14) Shumate MD, Lin DD, Gibbs JW III, Holloway KL, Coulter DA. GABA(A) receptor function in epileptic human dentate granule cells: Comparison to epileptic and control rat. Epilepsy Res 1998; 32: 114-128.
15) Bäckström T, Haage D, Löfgren M, et al. Paradoxical effects of GABA-A modulators may explain sex steroid induced negative mood symptoms in some persons. Neuroscience 2011; 191: 46-54.

SCIENTIFIC REPORTS

OPEN

Microbiome profile of the amniotic fluid as a predictive biomarker of perinatal outcome

Received: 11 May 2017
Accepted: 29 August 2017
Published online: 22 September 2017

Daichi Urushiyama[1,2], Wataru Suda[3,4], Eriko Ohnishi[1], Ryota Araki[2], Chihiro Kiyoshima[2], Masamitsu Kurakazu[2], Ayako Sanui[5], Fusanori Yotsumoto[2], Masaharu Murata[5], Kazuki Nabeshima[6], Shin'ichiro Yasunaga[7], Shigeru Saito[8], Makoto Nomiyama[9], Masahira Hattori[3,10], Shingo Miyamoto[2] & Kenichiro Hata[1]

Chorioamnionitis (CAM), an inflammation of the foetal membranes due to infection, is associated with preterm birth and poor perinatal prognosis. The present study aimed to determine whether CAM can be diagnosed prior to delivery based on the bacterial composition of the amniotic fluid (AF). AF samples from 79 patients were classified according to placental inflammation: Stage III (n = 32), CAM; Stage II (n = 27), chorionitis; Stage 0-I (n = 20), sub-chorionitis or no neutrophil infiltration; and normal AF in early pregnancy (n = 18). Absolute quantification and sequencing of 16S rDNA showed that in Stage III, the 16S rDNA copy number was significantly higher and the α-diversity index lower than those in the other groups. In principal coordinate analysis, Stage III formed a separate cluster from Stage 0-I, normal AF, and blank. Forty samples were classified as positive for microbiomic CAM (miCAM) defined by the presence of 11 bacterial species that were found to be significantly associated with CAM and some parameters of perinatal prognosis. The diagnostic accuracy for CAM according to miCAM was: sensitivity, approximately 94%, and specificity, 79–87%. Our findings indicate the possibility of predicting CAM prior to delivery based on the AF microbiome profile.

Preterm birth, which occurs in 5–18% of all pregnancies, is caused by multiple pathological conditions[1,2] and is the leading factor in perinatal mortality and morbidity, and childhood neurological problems[3–5]. Intrauterine infection is linked to spontaneous preterm labour, which accounts for about two-thirds of all preterm births[1,6,7], and a minimum of 25–40% of premature infants are born to mothers with intrauterine infection[7–9]. In 30% of intrauterine infections, bacteria are identified in the foetal circulation[1,10], and it is known that foetal infections induce a systemic inflammatory response[11], which is suggested to cause abnormalities in the central nervous system, especially the white matter, by epidemiologic studies and animal experiments[12–14].

Chorioamnionitis is an inflammation of the foetal membranes (amnion and chorion) histologically diagnosed by the presence of acute inflammatory cells, such as neutrophils. In addition to being a gold standard for corroborating intrauterine infection, chorioamnionitis is associated with preterm birth and poor infant prognosis and is recognized as a risk factor for cerebral palsy and chronic lung disease[15–19]. The proposed diagnostic criteria prior to delivery[19,20] have low prediction accuracy for chorioamnionitis and intrauterine infection, and do not help prevent prematurity and neonatal sepsis[19,21].

[1]Department of Maternal-Fetal Biology, National Research Institute for Child Health and Development, Tokyo, 157-8535, Japan. [2]Department of Obstetrics and Gynecology, Faculty of Medicine, Fukuoka University, Fukuoka, 814-0180, Japan. [3]Department of Computational Biology, Graduate School of Frontier Sciences, The University of Tokyo, Chiba, 277-8561, Japan. [4]Department of Microbiology and Immunology, Keio University School of Medicine, Tokyo, 160-0016, Japan. [5]Center for Maternal, Fetal and Neonatal Medicine, Fukuoka University Hospital, Fukuoka, 814-0180, Japan. [6]Department of Pathology, Fukuoka University School of Medicine and Hospital, Fukuoka, 814-0180, Japan. [7]Department of Biochemistry, Faculty of Medicine, Fukuoka University, Fukuoka, 814-0180, Japan. [8]Department of Obstetrics and Gynecology, University of Toyama, Toyama, 930-0194, Japan. [9]Department of Obstetrics and Gynecology, National Hospital Organization Saga Hospital, Saga, 849-8577, Japan. [10]Cooperative Major in Advanced Health Science, Graduate School of Advanced Science and Engineering, Waseda University, Tokyo, 169-8555, Japan. Correspondence and requests for materials should be addressed to K.H. (email: hata-k@ncchd.go.jp)

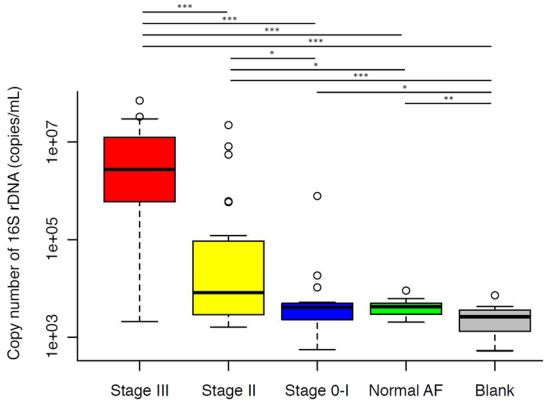

Figure 1. Microbial abundance in amniotic fluid samples. Microbial load was assessed based on 16S rDNA copy numbers per 1 mL AF using dPCR with universal primers 27Fmod and 338R and EvaGreen dye. The copy numbers in Stage III and Stage II were significantly higher than those in Stage 0-I/Normal AF/Blank; no differences were detected, only between Stage 0-I and Normal AF. Two-tailed probabilities were calculated by the Mann–Whitney test; $*P < 0.05$, $**P < 0.01$, $***P < 0.001$.

The amniotic fluid (AF) is considered to be sterile; however, this is frequently not the case in preterm birth, and a low gestational age at delivery is shown to be associated with bacterial infection in the AF[8]. Various bacterial species are detected in the AF in cases of preterm birth[22–26]. However, *Ureaplasma* spp. are also observed at 16–20 weeks in cases of normal delivery[27], and the detection rates of aerobic and anaerobic bacteria in the AF in full-term births are similar to those in preterm ones[28,29]; in addition, bacteria have been detected in umbilical cord blood and meconium[30,31]. These findings indicate that the AF is not necessarily sterile, even in normal pregnancies, and that the association between preterm deliveries and infection should be further clarified.

Molecular biology techniques have been proved effective for detecting *Ureaplasma* spp. and other bacteria difficult to identify using conventional culture methods[32]. However, to the best of our knowledge, metagenomic analysis with next-generation sequencing of the AF to verify the relationship between bacterial diversity and chorioamnionitis has not been conducted. Here, we performed absolute quantification of 16S ribosomal DNA (rDNA) copy numbers and sequencing of 16S rDNA amplified from the AF obtained by aseptic methods for comprehensive, quantitative analysis of AF microbiome. By examining the association between inflammation in the placenta and the bacterial composition of the AF, we demonstrated, for the first time, that microbial profiling of the AF can be used to diagnose chorioamnionitis with a high degree of accuracy prior to delivery, and to predict perinatal complications.

Results

Assessment of study subjects. Seventy-nine patients selected for the study were divided based on the stage of placental inflammation (Blanc's classification)[33]: Stage III (n = 32), chorioamnionitis; Stage II (n = 27), chorionitis; and Stage 0-I (n = 20), sub-chorionitis or no neutrophil infiltration. AF samples collected in the early second trimester (mean ± SD: 16.1 ± 0.6 weeks of pregnancy) during the same period were used as the AF control (Normal AF; n = 18), while laboratory-grade water was used as blank control (Blank; n = 24) for DNA extraction and library preparation (Table S1). Demographic and clinical characteristics for Stage III, Stage II, and Stage 0-I patients were extracted from medical records (Table S2).

Stage III was significantly different from Stage 0-I regarding multigravida, preterm premature rupture of membranes, antibiotic use before amniocentesis, number of caesarean sections, gestational age at amniocentesis, maternal inflammation (white blood cell [WBC] count, C-reactive protein [CRP] value), WBC count in the AF, funisitis of umbilical cord, extended days of hospital stay from admission to birth, neonatal inflammation (WBC count, CRP value, IgM level, funisitis of the umbilical cord), and antibiotic use for newborns (Table S2). Between Stage II and Stage 0-I, significant differences were observed only in caesarean sections, maternal CRP value, extended days of hospital stay, and neonatal IgM value (Table S2).

Quantification of microbial colonization. To assess bacterial load, we determined 16S rDNA copy numbers per 1 mL of AF using digital (d)PCR with a universal primer set[34,35] and EvaGreen dye. The median 16S rDNA copy number in Stage III was 328 and 656 times higher than that in Stage II and Stage 0-I, respectively (2.70×10^6 vs. 8.25×10^3 and 4.12×10^3, respectively; $P < 0.001$), and that in Stage II was 2.0 times higher than that in Stage 0-I ($P = 0.019$) (Figs 1, S1).

While Stage 0-I and Normal AF demonstrated significantly higher copy numbers than Blank ($P = 0.035$, 0.003, respectively), no difference was observed between Stage 0-I and Normal AF ($P = 0.696$), indicating that the AF in the early second trimester of a normal pregnancy is not necessarily as sterile as laboratory-grade water.

Comparison of bacterial diversity. Using the same universal primer set, we amplified and performed parallel sequencing of 16S rDNA in 97 AF samples and 24 blank controls. Only one sample (N11) did not yield sufficient reads for metagenomic analysis. Operational taxonomic units (OTUs) were created and within-community

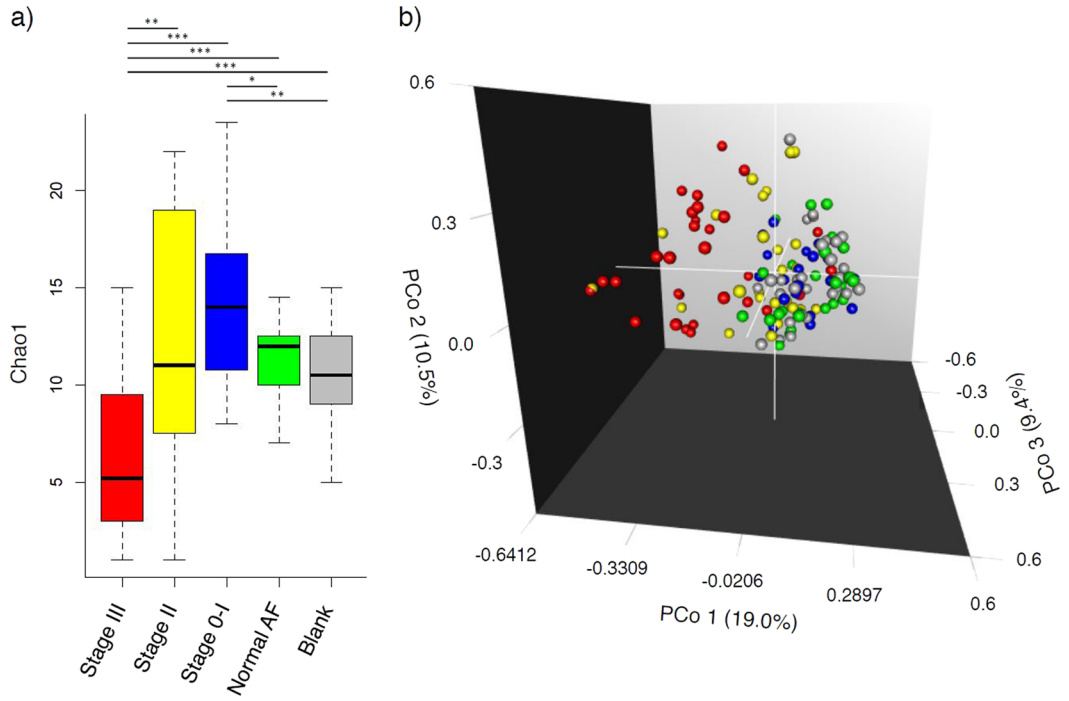

Figure 2. Numbers of OTUs (Chao1 index) and 3D-PCoA based on un-weighted UniFrac distances. Amplicons of 16S rDNA were sequenced using 27Fmod and 338R primers. (**a**) Sequences were clustered into OTUs with a 97% identity threshold and the α-diversity index (Chao1) was calculated for each sample. In Stage III, Chao1 was significantly lower than in the other groups. (**b**) Multidimensional composition of each group was determined based on matrix data for un-weighted UniFrac distance. Clustering of Stage III (red) samples differed from that of Stage 0-I (blue)/Normal AF (green)/Blank (grey); Stage II (yellow) was scattered between the two clusters. Three-D PCoA was performed with R; $*P<0.05$, $**P<0.01$, $***P<0.001$ by Mann–Whitney test.

(alpha) diversity was assessed by comparing the α-diversity index (Chao1) between the groups (Fig. 2a). Interestingly, Stage III demonstrated a significantly lower Chao1 than Stage II, Stage 0-I, Normal AF, and Blank ($P=0.001$, $P<0.001$, $P<0.001$, and $P<0.001$, respectively) and Stage 0-I demonstrated a significantly higher Chao1 than Normal AF and Blank ($P=0.038$, 0.008, respectively), while no other between-group differences were detected.

To compare phylogenetic relatedness of the microbial communities, we determined UniFrac distances between samples according to OTU data[34–36]. In principal coordinate analysis (PCoA) based on un-weighted UniFrac distances, Stage 0-I, Normal AF, and Blank clustered together, while Stage III formed a separate cluster, and Stage II was scattered between these two clusters (Fig. 2b). Analysis of un-weighted UniFrac distances with PERMANOVA revealed that Stage III and Stage II were significantly different from the other groups (Stage 0-I/Normal AF/Blank), and Stage 0-I was significantly different from Blank, but there were no differences among the other groups (Table S3). In analysis of weighted UniFrac distances with PCoA and PERMANOVA, similar to the results of un-weighted UniFrac distances, Stage III was significantly different from the other groups (Stage 0-I/Normal AF/Blank), and Stage II was scattered (Fig. S2, Table S3).

Analysis of bacterial composition in individual samples. Phylum-, genus-, and species-level OTUs were created with identity thresholds of 70%, 94%, and 97%, respectively, and taxonomic structure in each OTU was assessed by similarity searching against the standard database. Sample rearrangement by hierarchical cluster analysis using Ward's method based on un-weighted UniFrac distances (Figs 3a, S3a) mostly showed phylum-level distribution (Fig. 3). Consistent with the PCoA results, Stage III and Stage 0-I/Normal AF/Blank formed roughly separate clusters, while Stage II was scattered between the two clusters (Figs 3, S3). Consistent with the results shown in Fig. 1a, genus-level analysis indicated that multiple samples of Stage 0-I/Normal AF/Blank demonstrated a relatively high species richness, indicating complex compositions (Fig. S3). In contrast, the numbers of species in Stage III and in some samples of Stage II were extremely low (Fig. S3). Particularly noteworthy is the relative abundance of *Ureaplasma* spp. (minimum 35.5%) in fifteen samples (A2, 3, 6–8, 11, 13–15, 18, 20, 22, 24, 25, 31) of Stage III (64.3%) and six samples (B3, 4, 12, 16, 18, 19) of Stage II (22.2%) compared to all other samples (maximum 8.8%).

Selection of bacterial species as candidate diagnostic markers. To assess the association of particular bacterial species with chorioamnionitis, the data on relative abundance of the 28 most representative species were re-clustered according to the 79 samples in Stage III, Stage II, and Stage 0-I (Fig. 4).

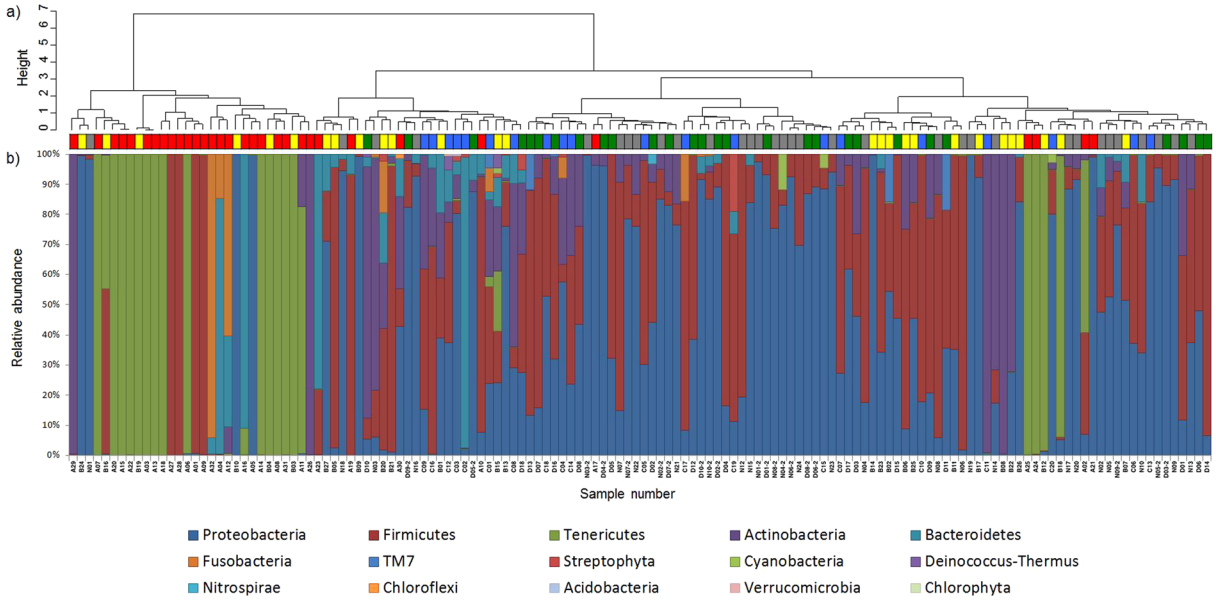

Figure 3. Relative abundances of different bacterial phyla in each sample. Sequences were clustered into OTUs with a 70% identity threshold and taxonomic assignments were performed by similarity searching against the standard database. The samples were rearranged by hierarchical cluster analysis using Ward's method based on un-weighted UniFrac distances. Stage III and Stage 0-I/Normal AF/Blank formed separate clusters, while Stage II was scattered between the two clusters.

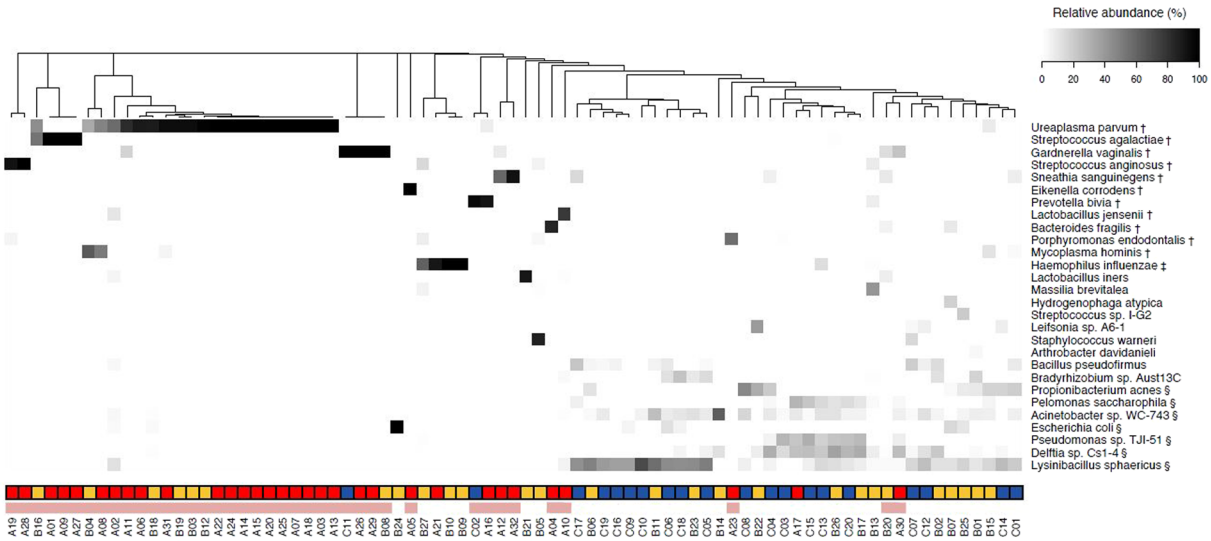

Figure 4. Relative abundances of the 28 most dominant species. Data on the relative abundances of the 28 most representative species were re-clustered according to the 79 samples in Stage III, Stage II and Stage 0-I. Stage III and Stage 0-I roughly formed separate clusters, while Stage II was scattered between the two clusters. The 11 most dominant species in Stage III (†) were almost non-existent in Stage0-I, while the seven most dominant species in Blank (§) were not dominant in Stage III and 40 miCAM samples (indicated by a pink bar). *H. influenza* (‡), which was dominant in one sample in Blank (N16), was dominant in some samples in Stage III and Stage II.

Stage III and Stage 0-I roughly formed separate clusters, while Stage II was scattered between the two clusters. In Stage III samples, the 12 most dominant species were *Ureaplasma parvum*, *Streptococcus agalactiae*, *Gardnerella vaginalis*, *Streptococcus anginosus*, *Sneathia sanguinegens*, *Eikenella corrodens*, *Prevotella bivia*, *Lactobacillus jensenii*, *Bacteroides fragilis*, *Porphyromonas endodontalis*, *Mycoplasma hominis*, and *Haemophilus influenzae*; however, except for *H. influenzae*, these species were nearly absent in Normal AF and Blank (maximum: 3.46%). In Blank samples, the most dominant species were *Lysinibacillus sphaericus*, *Delftia* sp. Cs1-4, *Pseudomonas* sp. TJI-51, *Escherichia coli*, *Acinetobacter* sp. WC-743, *Pelomonas saccharophila*, and *Propionibacterium acnes*, which can

be attributed to inevitable very low amounts of contamination during sample preparation. *H. influenzae*, which was dominant in some samples of Stage III and Stage II (A21; B9, 10, 27), was also dominant in one Blank sample (N16); indicating that contamination is nearly unavoidable.

The 11 species (*U. parvum, S. agalactiae, G. vaginalis, S. anginosus, S. sanguinegens, E. corrodens, P. bivia, L. jensenii, B. fragilis, P. endodontalis, and M. hominis*) that were remarkably dominant in Stage III but not in Blank were considered as candidate markers for prenatal diagnosis of chorioamnionitis; therefore, the samples in which any of these species demonstrated the highest abundance were considered positive for microbiomic chrioamnionitis (miCAM). According to this criterion, 30 out of 32 samples in Stage III (94%), 8 out of 27 samples in Stage II (30%), and 2 out of 20 samples in Stage 0-I (10%) were miCAM-positive (Table S4). The accuracy of chorioamnionitis diagnosis (Blanc's stage III) based on miCAM was as follows: sensitivity, 93.8%; specificity, 78.7%; positive predictive value, 75.0%; negative predictive value, 94.9%.

Comparison of clinical characteristics between miCAM and non-miCAM samples. We compared continuous variables related to maternal and infant perinatal outcomes between miCAM and non-miCAM samples (Fig. 5, Table S5). Although no significant difference was observed in gestational age and neonatal body weight at birth, Apgar score, or umbilical arterial pH; the miCAM subgroup demonstrated significantly shorter duration of maternal hospital stay from admission to birth, and higher WBC count, CRP value, and IgM levels in neonatal peripheral blood immediately after birth (Fig. 5). These results indicated a significant correlation between miCAM and adverse prognostic parameters in both mother and infant.

Diagnostic accuracy for miCAM and chorioamnionitis assessed by clinical and metagenomic sequence data. Next, we used clinical and laboratory data, DNA concentrations, and 16S rDNA copy numbers to calculate the area under the curve (AUC), the Youden index for the receiver operating characteristic (ROC) curve, cut-off value, and diagnostic sensitivity and specificity (Table S6, Fig. S4). Compared to body temperature, heart rate, WBC count, and CRP level in maternal peripheral blood, DNA amount and especially, 16S rDNA copy number demonstrated higher diagnostic accuracy for both miCAM and chorioamnionitis. Regarding miCAM, the diagnostic accuracy according to 16S rDNA copy number with an AUC of 0.909 (asymptotic 95% confidence interval [CI]: 0.838–0.980) and a cut-off value of 1.19×10^4 was: sensitivity, 94.9%, and specificity, 78.9%. For chorioamnionitis (Blanc's stage III), the diagnostic accuracy with an AUC of 0.926 (asymptotic 95% CI: 0.868–0.985) and a cut-off value of 1.73×10^4 was: sensitivity, 93.5%, and specificity, 87.0% (Table S6, Fig. S1).

Discussion

A close relationship between intrauterine infection and preterm labour have been confirmed[22,23,26,36], and recent studies have shown the association of placental microbiome composition with preterm birth and chorioamnionitis[37,38]. However, to the best of our knowledge, there was no report on metagenomic analysis of the AF to verify the relationship between bacterial community structure and placental inflammation. We conducted a metagenomic analysis of the AF obtained by aseptic methods from patients with or without chorioamnionitis and defined miCAM, which showed predictive utility in the identification of patients with poor prognosis regarding preterm delivery and neonatal status.

Of the 28 most dominant species identified (Fig. 4), the 12 most dominant species in Stage III (*U. parvum, S. agalactiae, G. vaginalis, S. anginosus, S. sanguinegens, E. corrodens, P. bivia, L. jensenii, B. fragilis, P. endodontalis, M. hominis, and H. influenzae*) primarily colonize the urogenital system (except *B. fragilis and P. endodontalis*, which are indigenous to the intestinal tract and oral environment, respectively); many of these may cause foetal infections such as meningitis and/or pulmonary disease, which can lead to brain dysfunction, epilepsy, hearing loss, and developmental disorders[19,39–45].

Eleven of the 12 bacterial species dominant in Stage III (except *P. endodontalis*) have been previously identified qualitatively in AF collected under sterile conditions[22–24,26,36]; among these, *Ureaplasma* spp. is frequently detected in spontaneous preterm birth[36,39]. Moreover, lipoprotein multiple-banded antigen from *U. parvum* has been shown to cause preterm birth in experimental animals[46], supporting the correlation between *Ureaplasma* presence and pregnancy outcome.

In the present study, we used samples from two distant hospitals, which were sequenced twice, to avoid regional and experimental bias. For the five most dominant species (*U. parvum*, *S. agalactiae*, *G. vaginalis*, *S. anginosus* and *S. sanguinegens*) in Stage III, the data for the two institutions corresponded well. In our previous study, we had confirmed a relationship between placental inflammation (Blanc's classification) and the 11 species defining miCAM[36]. In seven out of 10 cases (70%) with chorioamnionitis (Stage III), at least one of these species were dominantly detected; in two cases, different species, but from the same genera as those of the 11 dominant species, were detected; and in one case, no bacteria were detected[36]. These results were remarkably consistent with our current results. Moreover, in five major reports on the AF in cases of preterm birth[22–24,26,36], in at least 70% of all cases, at least one of the 10 most dominant genera in Stage III (*Ureaplasma*, *Streptococcus*, *Gardnerella*, *Sneathia*, *Eikenella*, *Prevotella*, *Lactobacillus*, *Bacteroides*, *Porphyromonas*, *Mycoplasma*) was qualitatively detected. Thus, our results can be regarded reliable.

The seven most dominant species in Blank (*L. sphaericus*, *Delftia* sp. Cs1–4, *Pseudomonas* sp. TJI-51, *E. coli*, *Acinetobacter* sp. WC-743, *P. saccharophila*, and *P. acnes*) were estimated to originate mainly from contamination during library preparation. Of the seven most dominant species in Blank, six genera (*Delftia*, *Pseudomonas*, *Escherichia*, *Acinetobacter*, *Pelomonas*, and *Propionibacterium*) have been previously reported as common contaminants[47]. *L. sphaericus* is primarily observed in mosquito larvae; it is a spore-forming bacterium resistant to heat and ultraviolet radiation, and common in aquatic environments[48–51]; therefore, trace amounts of DNA may have contaminated reagents, tubes, or instrumentation. The low abundance and high α-diversity (more complex

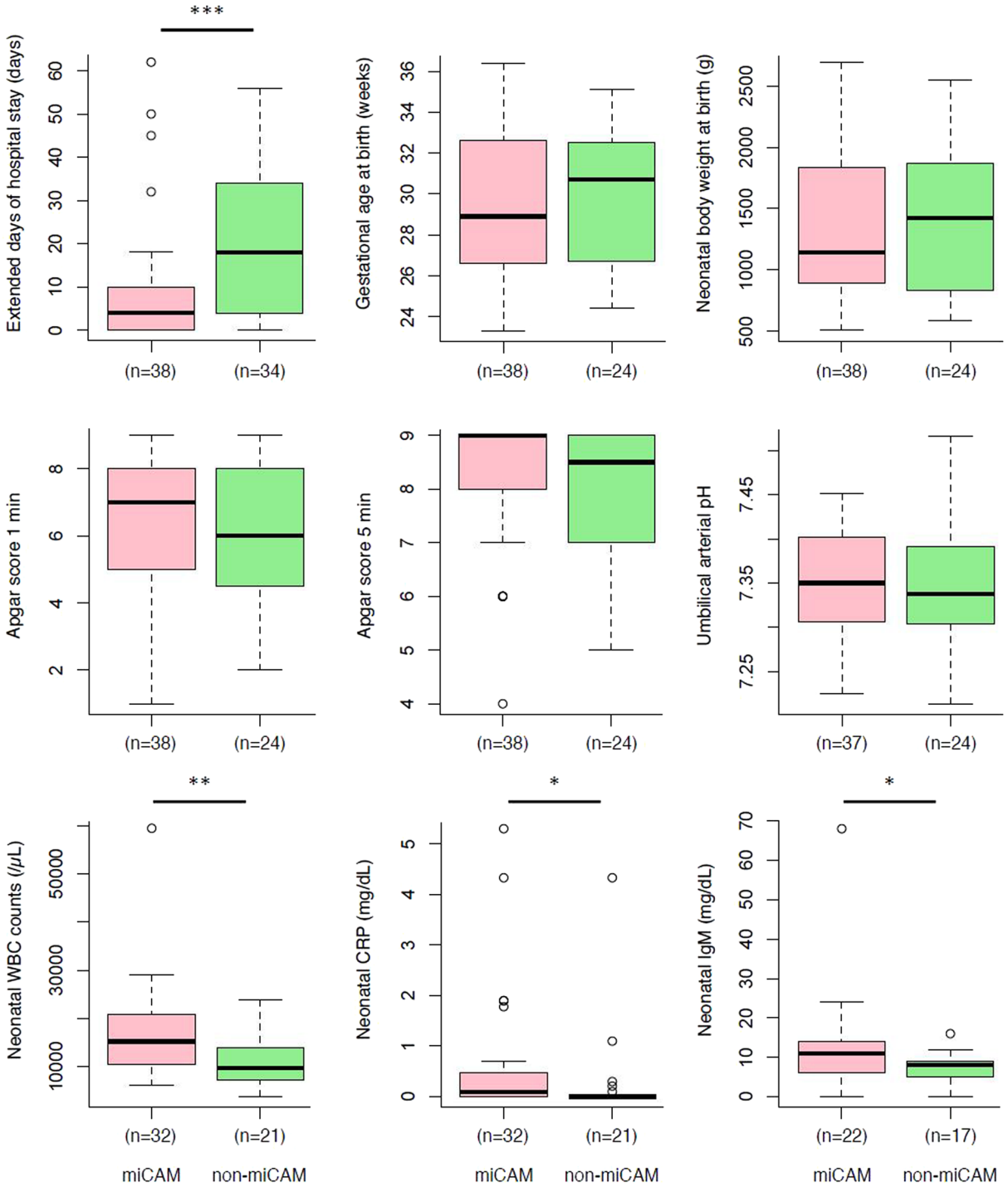

Figure 5. Comparison of perinatal outcomes between miCAM and non-miCAM subgroups. Comparison of continuous variables related to maternal and perinatal outcomes between miCAM and non-miCAM samples revealed that miCAM was significantly associated with many prognostic parameters of perinatal outcome. $*P < 0.05$, $**P < 0.01$, $***P < 0.001$ by Mann–Whitney test.

composition) of the seven species were consistently demonstrated in all samples dominated by these species, which is in agreement with previous reports.

For a long time, attempts have been made to diagnose chorioamnionitis and intrauterine infection prior to delivery[19,20,52–56]. Although high-accuracy diagnostic biomarkers have been reported[53], no diagnostic standards have been established[19,55] because of significantly overlapping confidence intervals and inconsistent associations between preterm birth and placental microbiome[1,37,38,55]. In the present study, we demonstrated that it is possible to diagnose chorioamnionitis with a high level of accuracy according to miCAM defined by metagenomic sequence profiles and 16S rDNA copy numbers in the AF. Therefore, miCAM can be used to assess the state of

intrauterine infection during pregnancy, which would help in the management of cases with high risk of preterm birth.

The quantification of 16S rDNA by dPCR has been recently reported useful for evaluating the prevalence of low-abundance bacteria[57,58]. We discovered, with high reproducibility, that when placental inflammation was mild (Stage $\leq$ I), microbial abundance in the AF was as low as in the early second trimester, even in preterm birth (Fig. 1).

Contamination of laboratory-grade water, PCR reagents, and DNA extraction kits can potentially significantly affect structural analysis of microbiome with low abundance[47,59]. Therefore, in this study, we made every effort to operate under strictly sterile conditions. However, complete prevention of contamination is considered impossible[47]. Therefore, we used a blank control (laboratory-grade water) in DNA extraction and library preparation, which, consistent with previous data[58], showed an extremely low presence of 16S rDNA (1–10 copies/μL). The blank samples were used to document bacterial sequences introduced during sample processing, which were excluded from the miCAM-defining species.

This study had some limitations. First, sample selection had a bias. The analysed AF specimens were obtained at caesarean section or were left-overs from clinical testing by amniocentesis[22], which is an invasive procedure resulting in miscarriage or preterm birth in approximately 0.1–2% of cases[60–63], and is not performed for all pregnancies. Therefore, the retrospective case-control study design made it difficult to achieve ideal control of patient characteristics, as evidenced by significant differences between groups in multigravida, preterm premature rupture of membranes, antibiotic administration before amniocentesis, caesarean section, and gestational age at amniocentesis. While there is a possibility that maternal use of antibiotics before amniocentesis influenced the results of metagenomic analysis, we considered it to be negligible; data of all of the 21 samples (A2, 10, 15, 18, 27; B6, 7, 14, 21–26; C6, 10, 12, 16–19) from patients that had not used antibiotics before amniocentesis, were in line with the findings based on the other samples. Second, 16S rDNA sequencing is inferior to whole-genome shotgun sequencing in terms of bacterial quantification potential, because 16S rDNA sequencing has a PCR bias. However, samples with low microbial abundance are contaminated with human DNA in typical DNA extraction methods, leading to enormous whole-genome shotgun sequencing costs; therefore, a method not susceptible to the effects of human DNA should be developed. Third, metagenomic analysis cannot distinguish between live and dead bacteria, and microbial profiles in antibiotic-treated patients may not be objective.

In the present study, we comprehensively and quantitatively analysed the microbiome of the AF and, by examining its association with the degree of placental inflammation, identified bacteria significantly associated with chorioamnionitis. Further studies should focus on achieving higher diagnostic sensitivity and specificity and on developing non-invasive testing methods, which would contribute to timely diagnosis and improve perinatal outcome.

Materials and Methods

Study design. In total, 8,172 births occurred at the Center for Maternal, Fetal, and Neonatal Medicine, Fukuoka University Hospital and at the National Hospital Organization Saga Hospital, between August 2009 and April 2017. Placental pathology examination was conducted in 4,373 cases; among them, amniocentesis was performed for 183 patients who provided informed consent for study participation, and left-over AF samples were cryopreserved. Moreover, 10 samples were added which were obtained at caesarean section within the same period under absolutely sterile condition. To minimize bias, we established the following exclusion criteria: multiple pregnancies and amniocentesis in the early second trimester. As a result, 79 patients who passed the exclusion criteria and for whom $\geq$ 3 mL AF was available by amniocentesis or caesarean section were included in the study.

Patients were divided into three groups based on Blanc's classification of placental inflammation severity[33]: Stage III (n = 32), Stage II (n = 27), and Stage 0-I (n = 20). We also established two control groups to ensure accuracy of data assessment considering the extremely low amounts of microbial DNA that can contaminate samples at any point from sample collection to sequencing. In the early second trimester (16.1 ± 0.6 weeks; mean ± S.D.), amniocentesis was performed for foetal genetic testing, and AF samples from normal pregnancies were considered as a control group (Normal AF; n = 18). Additionally, we used blank controls consisting of laboratory-grade water (Blank; n = 24) during DNA extraction and sequencing library preparation.

All methods were performed in accordance with the STARD guidelines and regulations for reporting diagnostic accuracy studies. The study was approved by the review boards of the Fukuoka University Hospital, National Hospital Organization Saga Hospital and the National Research Institute for Child Health and Development (protocol numbers 15-2-08, 23–4, and 699, respectively). Informed consent was obtained from all participants, who were explained the potential risks, including accidental leaks of personal information and project data, prior to the study. For patients who wished to withdraw content, we were able to dispose of the remaining samples, extracted DNA, and all project data at any time; however, we could not delete metagenomic sequence data which had been made publicly available through an open-access database.

Diagnostic criteria. Histological chorioamnionitis was defined as the presence of acute inflammatory lesions of the chorion or amnion according to Blanc's criteria[33]: stage I (sub-chorionitis): patchy or diffused accumulation of neutrophils within the sub-chorionic plate or decidua; stage II (chorionitis): more than a few scattered neutrophilic infiltrations in the chorionic plate or membranous chorionic connective tissue; and stage III (chorioamnionitis): neutrophilic infiltrates reaching sub-amniotic connective tissue and the amniotic epithelium. Funisitis was defined as neutrophilic infiltration in the umbilical vein wall or Wharton's jelly.

Sample collection and DNA extraction. AF samples were obtained by transabdominal ultrasound-guided amniocentesis performed percutaneously or at caesarean section under sterile conditions. The AF samples were collected in sterile tubes and preserved at 4 °C; leftover samples not needed for testing were

transported on ice within 24 h to a neighbouring laboratory. To minimize changes in bacterial composition, all laboratory procedures were performed rapidly on ice. Samples were centrifuged at low speed (1,450 × *g* at 4 °C for 10 min) as previously described[22,24]; the supernatant was rapidly frozen in liquid nitrogen and preserved at −80 °C until DNA extraction.

Samples were thawed and lysed using Pathogen Lysis Tubes L (Qiagen, Hilden, Germany), and DNA was extracted using the QIAamp UCP Pathogen Mini Kit (Qiagen) according to the manufacturer's protocol, at the National Research Institute for Child Health and Development and Fukuoka University.

Absolute quantification of 16S rDNA. dPCR was conducted with EvaGreen dye, using universal primers (27Fmod and 338R) for 16S rDNA sequencing, as previously described[34,35,58]. DNA (1 μL) was diluted in 19 μL of Bio-Rad QX200 reagents (Bio-Rad, Hercules, CA, USA), and each sample was then partitioned into approximately 20,000 droplets using the QX200 Droplet Generator (Bio-Rad). PCR was performed in a 96-well plate using the following cycling conditions according to the manufacturer's protocol: 5 min at 95 °C, 40 cycles of 30 s at 95 °C and 1 min at 60 °C, then 5 min at 4 °C and 5 min at 90 °C; the temperature was then decreased to 4 °C at a ramp rate of 2 °C/s. Fluorescence was detected using the QX200 Droplet Reader (Bio-Rad) and analysed using the Bio-Rad QuantaSoft software. Copy number of 16S rDNA per 1 mL of the sample was then calculated.

Sequencing of 16S rDNA amplicons. The same universal primers (27Fmod and 338R) were used for PCR amplification of the variable region (V1–2) of the 16S rRNA gene. A 16S Metagenomic Sequencing Library was prepared according to the Illumina protocol (16S Metagenomic Sequencing Library Preparation, Part # 15044223 Rev. A; Illumina, San Diego, CA, USA). PCR was performed using the KAPA HiFi HotStart Ready Mix (Kapa Biosystems, Boston, MA, USA) for 25 amplification cycles at 60 °C as an annealing temperature according to the manufacturer's recommendation. The amplified products were purified using the Agencourt AMPure XP Kit (Beckman Coulter, Tokyo, Japan) and tagged with indexes in eight cycles using the Nextera XT Index Kit (Illumina). Amplicons were quantified using the Agilent 2200 TapeStation (Agilent Technologies, Santa Clara, CA, USA) or the Agilent 2100 Bioanalyzer (Agilent Technologies) and thoroughly mixed to achieve homogeneity. Then, size selection for next-generation sequencing was performed using Pippin Prep (Sage Science, Beverly, MA, USA), with approximately 300–600 bp of the mixed library as a target. MiSeq sequencing (paired-end, 300 bp) was conducted using MiSeq Reagent Kit v3 (600-cycle format; Illumina) mixed with 20% of PhiX Control Kit v3 (Illumina) according to the manufacturer's protocol.

Analysis of sequencing data. Sequencing data was analysed as previously described[34–36]. Two paired-end reads were merged using the fastq-join program based on overlapping sequences. Low-quality sequence reads (quality value < 25) and suspected chimeric reads (BLAST match length of <90% with reference sequences in the databases [Ribosomal Database Project v. 10.27 and/or in-house 16S sequenced database in Tokyo University]) were filtered out (Table S7). Following adapter sequence trimming, 1,300 reads were randomly selected. Using a 97% pairwise-identity cut-off in the UCLUST program[64] version 5.2.32 (http://www.drive5.com/), the selected reads were clustered into OTUs.

Taxonomic assignment for each OTU was done by similarity searching against the above-mentioned databases using the GLSEARCH program (data provided in Supplementary Dataset 1). For the assignment at the phylum, genus, and species levels, sequence similarity thresholds of 70%, 94% and 97%, respectively, were applied.

UniFrac distance was used to assess dissimilarity (distance) between each sample pair[65], and a 3D PCoA model was plotted according to UniFrac distances using the R package.

Statistical analysis. Because of the relatively low sample number, we calculated exact significance probabilities (two-tailed) as *P*-values using the Mann–Whitney test for continuous variables and Fisher's exact test for categorical variables. To assess diagnostic accuracy, we constructed ROC curves and calculated the AUC. These analyses were performed using SPSS version 16.0J for Windows Base System SC (SPSS Japan, Tokyo, Japan). For comparison of bacterial composition between groups, we used vegan package in R to calculate R^2 and *P*-values in PERMANOVA. Differences at $P < 0.05$ were considered statistically significant.

Data and material availability. The 16S sequencing data generated in the present study have been deposited in DDBJ Sequence Read Archive (DRA) (accession number DRA005144).

References

1. Romero, R., Dey, S. K. & Fisher, S. J. Preterm labor: one syndrome, many causes. *Science* **345**, 760–765 (2014).
2. Romero, R. *et al*. The preterm parturition syndrome. *BJOG* **113**(Suppl 3), 17–42 (2006).
3. Howson, C. P., Kinney, M. V., McDougall, L. & Lawn, J. E. Born too soon: preterm birth matters. *Reprod. Health* **10**(Suppl 1), S1 (2013).
4. Blencowe, H. *et al*. National, regional, and worldwide estimates of preterm birth rates in the year 2010 with time trends since 1990 for selected countries: a systematic analysis and implications. *Lancet* **379**, 2162–2172 (2012).
5. Muglia, L. J. & Katz, M. The enigma of spontaneous preterm birth. *N. Engl. J. Med.* **362**, 529–535 (2010).
6. Romero, R. *et al*. The role of infection in preterm labour and delivery. *Paediatr. Perinat. Epidemiol.* **15**(Suppl 2), 41–56 (2001).
7. Goldenberg, R. L., Culhane, J. F., Iams, J. D. & Romero, R. Epidemiology and causes of preterm birth. *Lancet* **371**, 75–84 (2008).
8. Goldenberg, R. L., Hauth, J. C. & Andrews, W. W. Intrauterine infection and preterm delivery. *N. Engl. J. Med.* **342**, 1500–1507 (2000).
9. Relman, D. A., Loutit, J. S., Schmidt, T. M., Falkow, S. & Tompkins, L. S. The agent of bacillary angiomatosis. *An approach to the identification of uncultured pathogens. N. Engl. J. Med.* **323**, 1573–1580 (1990).
10. Carroll, S. G. *et al*. Preterm prelabour amniorrhexis: intrauterine infection and interval between membrane rupture and delivery. *Arch. Dis. Child Fetal Neonatal Ed.* **72**, F43–46 (1995).
11. Gomez, R. *et al*. The fetal inflammatory response syndrome. *Am. J. Obstet. Gynecol.* **179**, 194–202 (1998).

12. Oka, A., Belliveau, M. J., Rosenberg, P. A. & Volpe, J. J. Vulnerability of oligodendroglia to glutamate: pharmacology, mechanisms, and prevention. *J. Neurosci.* **13**, 1441–1453 (1993).
13. Alexander, J. M., Gilstrap, L. C., Cox, S. M., McIntire, D. M. & Leveno, K. J. Clinical chorioamnionitis and the prognosis for very low birth weight infants. *Obstet. Gynecol.* **91**, 725–729 (1998).
14. Kannan, S. *et al*. Dendrimer-based postnatal therapy for neuroinflammation and cerebral palsy in a rabbit model. *Sci. Transl. Med.* **4**, 130ra146 (2012).
15. Been, J. V., Lievense, S., Zimmermann, L. J., Kramer, B. W. & Wolfs, T. G. Chorioamnionitis as a risk factor for necrotizing enterocolitis: a systematic review and meta-analysis. *J. Pediatr.* **162**, 236–242.e232 (2013).
16. Goldenberg, R. L. The management of preterm labor. *Obstet. Gynecol.* **100**, 1020–1037 (2002).
17. Hartling, L., Liang, Y. & Lacaze-Masmonteil, T. Chorioamnionitis as a risk factor for bronchopulmonary dysplasia: a systematic review and meta-analysis. *Arch. Dis. Child Fetal Neonatal Ed.* **97**, F8–F17 (2012).
18. Shatrov, J. G. *et al*. Chorioamnionitis and cerebral palsy: a meta-analysis. *Obstet. Gynecol.* **116**, 387–392 (2010).
19. Tita, T. & Andrews, W. W. Diagnosis and management of clinical chorioamnionitis. *Clin. Perinatol.* **37**, 339–354 (2010).
20. Lencki, S. G., Maciulla, M. B. & Eglinton, G. S. Maternal and umbilical cord serum interleukin levels in preterm labor with clinical chorioamnionitis. *Am. J. Obstet. Gynecol.* **170**, 1345–1351 (1994).
21. Buhimschi, A. *et al*. Advances in medical diagnosis of intra-amniotic infection. *Expert Opin. Med. Diagn.* **7**, 5–16 (2013).
22. DiGiulio, D. B. *et al*. Microbial prevalence, diversity and abundance in amniotic fluid during preterm labor: a molecular and culture-based investigation. *PLoS One* **3**, e3056 (2008).
23. Han, Y. W., Shen, T., Chung, P., Buhimschi, I. A. & Buhimschi, C. S. Uncultivated bacteria as etiologic agents of intra-amniotic inflammation leading to preterm birth. *J. Clin. Microbiol.* **47**, 38–47 (2009).
24. DiGiulio, D. B. *et al*. Prevalence and diversity of microbes in the amniotic fluid, the fetal inflammatory response, and pregnancy outcome in women with preterm pre-labor rupture of membranes. *Am. J. Reprod. Immunol.* **64**, 38–57 (2010).
25. Wang, X. *et al*. Comparative microbial analysis of paired amniotic fluid and cord blood from pregnancies complicated by preterm birth and early-onset neonatal sepsis. *PLoS One* **8**, e56131 (2013).
26. Combs, C. A. *et al*. Amniotic fluid infection, inflammation, and colonization in preterm labor with intact membranes. *Am. J. Obstet. Gynecol.* 210, 125.e121–125.e115 (2014).
27. Rodriguez, N., Fernandez, C., Zamora, Y., Berdasquera, D. & Rivera, J. A. Detection of *Ureaplasma urealyticum* and *Ureaplasma parvum* in amniotic fluid: association with pregnancy outcomes. *J. Matern. Fetal Neonatal Med.* **24**, 47–50 (2011).
28. Gomez, R. *et al*. The value of amniotic fluid interleukin-6, white blood cell count, and gram stain in the diagnosis of microbial invasion of the amniotic cavity in patients at term. *Am. J. Reprod. Immunol.* **32**, 200–210 (1994).
29. Romero, R. *et al*. Microbial invasion of the amniotic cavity during term labor. Prevalence and clinical significance. *J. Reprod. Med.* **38**, 543–548 (1993).
30. Gosalbes, M. J. *et al*. Meconium microbiota types dominated by lactic acid or enteric bacteria are differentially associated with maternal eczema and respiratory problems in infants. *Clin. Exp. Allergy* **43**, 198–211 (2013).
31. Jimenez, E. *et al*. Isolation of commensal bacteria from umbilical cord blood of healthy neonates born by cesarean section. *Curr. Microbiol.* **51**, 270–274 (2005).
32. Gardella, C. *et al*. Identification and sequencing of bacterial rDNAs in culture-negative amniotic fluid from women in premature labor. *Am. J. Perinatol.* **21**, 319–323 (2004).
33. Blanc,W. A. Pathology of the placenta, membranes, and umbilical cord in bacterial, fungal, and viral infections in man. *Monogr. Pathol.* 67–132 (1981).
34. Said, H. S. *et al*. Dysbiosis of salivary microbiota in inflammatory bowel disease and its association with oral immunological biomarkers. *DNA Res.* **21**, 15–25 (2014).
35. Kim, S. W. *et al*. Robustness of gut microbiota of healthy adults in response to probiotic intervention revealed by high-throughput pyrosequencing. *DNA Res.* **20**, 241–253 (2013).
36. Yoneda, N. *et al*. Polymicrobial amniotic fluid infection with *Mycoplasma*/*Ureaplasma* and other bacteria induces severe intra-amniotic inflammation associated with poor perinatal prognosis in preterm labor. *Am. J. Reprod. Immunol.* **75**, 112–125 (2016).
37. Aagaard, K. *et al*. The placenta harbors a unique microbiome. *Sci. Transl. Med.* **6**, 237ra265 (2014).
38. Prince, L. *et al*. The placental membrane microbiome is altered among subjects with spontaneous preterm birth with and without chorioamnionitis. *Am. J. Obstet. Gynecol.* **214,** 627.e621–627.e616 (2016).
39. Waites, B., Schelonka, R. L., Xiao, L., Grigsby, P. L. & Novy, M. J. Congenital and opportunistic infections: *Ureaplasma* species and *Mycoplasma hominis*. *Semin. Fetal Neonatal Med.* **14**, 190–199 (2009).
40. Catlin, B. W. *Gardnerella vaginalis*: characteristics, clinical considerations, and controversies. *Clin. Microbiol. Rev.* **5**, 213–237 (1992).
41. Fredricks, D. N., Fiedler, T. L. & Marrazzo, J. M. Molecular identification of bacteria associated with bacterial vaginosis. *N. Engl. J. Med.* **353**, 1899–1911 (2005).
42. Aagaard, K. *et al*. A metagenomic approach to characterization of the vaginal microbiome signature in pregnancy. *PLoS One* **7**, e36466 (2012).
43. Saez-Llorens, X. & McCracken, G. H. Jr. Bacterial meningitis in children. *Lancet* **361**, 2139–2148 (2003).
44. Devi, U., Bora, R., Das, J. K., Malik, V. & Mahanta, J. *Sneathia* species in a case of neonatal meningitis from Northeast India. *Oxf. Med. Case Reports* **2014**, 112–114 (2014).
45. Pereyre, S. *et al*. Life on arginine for *Mycoplasma hominis*: clues from its minimal genome and comparison with other human urogenital mycoplasmas. *PLoS Genet.* **5**, e1000677 (2009).
46. Uchida, K. *et al*. Yanagihara, Effects of *Ureaplasma parvum* lipoprotein multiple-banded antigen on pregnancy outcome in mice. *J. Reprod. Immunol.* **100**, 118–127 (2013).
47. Salter, S. J. *et al*. Walker, Reagent and laboratory contamination can critically impact sequence-based microbiome analyses. *BMC Biol.* **12**, 87 (2014).
48. Berry, C. The bacterium, *Lysinibacillus sphaericus*, as an insect pathogen. *J. Invertebr. Pathol.* **109**, 1–10 (2012).
49. Yousten, A., Benfield, E. F., Campbell, R. P., Foss, S. S. & Genthner, F. J. Fate of *Bacillus sphaericus* 2362 spores following ingestion by nontarget invertebrates. *J. Invertebr. Pathol.* **58**, 427–435 (1991).
50. Yousten, A., Genthner, F. J. & Benfield, E. F. Fate of *Bacillus sphaericus* and *Bacillus thuringiensis* serovar israelensis in the aquatic environment. *J. Am. Mosq. Control Assoc.* **8**, 143–148 (1992).
51. Hadapad, B., Hire, R. S., Vijayalakshmi, N. & Dongre, T. K. UV protectants for the biopesticide based on *Bacillus sphaericus* Neide and their role in protecting the binary toxins from UV radiation. *J. Invertebr. Pathol.* **100**, 147–152 (2009).
52. Romero, R. *et al*. A comparative study of the diagnostic performance of amniotic fluid glucose, white blood cell count, interleukin-6, and gram stain in the detection of microbial invasion in patients with preterm premature rupture of membranes. *Am. J. Obstet. Gynecol.* **169**, 839–851 (1993).
53. Oludag, T. *et al*. Value of maternal procalcitonin levels for predicting subclinical intra-amniotic infection in preterm premature rupture of membranes. *J. Obstet. Gynaecol. Res.* **40**, 954–960 (2014).
54. Thornburg, L., Queenan, R., Brandt-Griffith, B. & Pressman, E. K. Procalcitonin for prediction of chorioamnionitis in preterm premature rupture of membranes. *J. Matern. Fetal Neonatal Med.* **29**, 2056–2061 (2016).
55. Dulay, T. *et al*. Compartmentalization of acute phase reactants Interleukin-6, C-Reactive Protein and Procalcitonin as biomarkers of intra-amniotic infection and chorioamnionitis. *Cytokine* **76**, 236–243 (2015).

56. Le Ray, I. *et al.* Changes in maternal blood inflammatory markers as a predictor of chorioamnionitis: a prospective multicenter study. *Am. J. Reprod. Immunol.* **73**, 79–90 (2015).
57. Hindson, M. *et al.* Tewari, Absolute quantification by droplet digital PCR versus analog real-time PCR. *Nat. Methods* **10**, 1003–1005 (2013).
58. Sze, A., Abbasi, M., Hogg, J. C. & Sin, D. D. A comparison between droplet digital and quantitative PCR in the analysis of bacterial 16S load in lung tissue samples from control and COPD GOLD 2. *PLoS One* **9**, e110351 (2014).
59. Ueno, T. *et al.* Eukaryote-Made Thermostable DNA Polymerase Enables Rapid PCR-Based Detection of Mycoplasma, Ureaplasma and Other Bacteria in the Amniotic Fluid of Preterm Labor Cases. *PLoS One* **10**, e0129032 (2015).
60. Chorionic villus sampling and amniocentesis: recommendations for prenatal counseling. Centers for Disease Control and Prevention. *MMWR Recommendations and Reports* **44**, 1–12 (1995).
61. Mujezinovic, F. & Alfirevic, Z. Procedure-related complications of amniocentesis and chorionic villous sampling: a systematic review. *Obstet. Gynecol.* **110**, 687–694 (2007).
62. Alfirevic, Z., Sundberg, K. & Brigham, S. Amniocentesis and chorionic villus sampling for prenatal diagnosis. *Cochrane Database Syst Rev*. Cd003252 (2003).
63. Odibo, O. *et al.* Revisiting the fetal loss rate after second-trimester genetic amniocentesis: a single center's 16-year experience. *Obstet. Gynecol.* **111**, 589–595 (2008).
64. Edgar, R. C. Search and clustering orders of magnitude faster than BLAST. *Bioinformatics* **26**, 2460–2461 (2010).
65. Lozupone, C., Hamady, M. & Knight, R. UniFrac—an online tool for comparing microbial community diversity in a phylogenetic context. *BMC Bioinformatics* **7**, 371 (2006).

Acknowledgements

We would like to extend our sincere gratitude to Masafumi Onodera, Toru Uchiyama, Chie Shindo, Yoko Takahashi, Kazuhiko Nakabayashi, Koji Okamura, Keiko Hayashi, Hiromi Kamura, Toshiyuki Yoshizato, Hirotsugu Obama, Satoshi Fukagawa, Sachiko Yuki, Takako Suwabe, Hami Urushiyama, Seiiku-Biobank, and all hospital physicians, midwives, and laboratory staff for their invaluable help with the present study. We would like to thank Editage (www.editage.com) for English language editing and Publication Support. This work was supported in part by NCCHD (26–13), AMED (17ek0109278h0001), Scientific Research (B) (no. 26293365) to K. Hata, a Grant-in-Aid for Young Scientists (B) (no. 227790536), Challenging Exploratory Research (no. 26670731), Scientific Research (B) (no. 26293362, 26293365), Scientific Research (C) (no. 23592470), and funds from the Central Research Institute of Fukuoka University (141011); the Centre for Advanced Molecular Medicine, Fukuoka University, the Ministry of Education, Culture, Sports, Science and Technology (Tokyo, Japan), a Grant-in-Aid from the Kakihara Science and Technology Foundation (Fukuoka, Japan), and Princess Takamatsu Cancer Research Fund to S. Miyamoto.

Author Contributions

D.U. designed the study, enrolled subjects, developed the extraction and amplification protocols, conducted data acquisition; analysed the data, and wrote and edited the manuscript. S.M. and K.H. designed the study, obtained funding, enrolled subjects, developed the extraction and amplification protocols, and wrote and edited the manuscript. W.S., M.H. and E.O. conducted data acquisition, analysed the data, and wrote and edited the manuscript. M.N. designed the study, enrolled subjects, and conducted data acquisition. R.A., C.K., M.K., A.S., F.Y., M.M., and K.N. conducted data acquisition. S.Y. and S.S. interpreted the analysed data, and wrote and edited the manuscript.

Additional Information

Supplementary information accompanies this paper at doi:10.1038/s41598-017-11699-8

Competing Interests: The authors declare that they have no competing interests.

Publisher's note: Springer Nature remains neutral with regard to jurisdictional claims in published maps and institutional affiliations.

日衛誌（Jpn. J. Hyg.），71，195–199（2016）

総　説

ミニ特集　発達期環境に起因する疾患素因の形成―DOHaD の視点から―

生殖と発生異常にかかわるエピゲノム変化と環境の影響

河合　智子，秦　健一郎

国立研究開発法人国立成育医療研究センター研究所周産期病態研究部

Reproductive/Developmental Abnormalities Induced by Epigenetic Aberrations and Possible Environmental Causes

Tomoko KAWAI and Kenichiro HATA

Department of Maternal-Fetal Biology, National Research Institute for Child Health and Development

Abstract　Foetal environmental factors, including maternal nutrition, hormonal disturbance, and chemical exposure, affect foetal growth and can cause birth defects. Recent studies have shown the link of poor foetal growth with increased risks of coronary heart disease, type II diabetes, kidney disease, and brain disorders in adulthood. Epigenetic modifications, such as DNA methylation and histone modifications, are involved in tissue- and developmental stage-specific gene expression and silencing, and they can be transmitted stably through mitotic cell division, thereby inducing long-term changes in gene regulation. Developmental programming during the foetal period, therefore, could affect adult health through epigenetic mechanisms. In fact, many studies using animal models have demonstrated that nutrient manipulation during pregnancy induces epigenetic alterations at specific loci or globally in the offspring. In this review, we summarize our findings that elucidate the effects of *in utero* environments on the human placental epigenome.

Key words: epigenetics（エピジェネティクス），Developmental Origin of Health and Disease（DOHaD），infertility（不妊・不育症），Small for Gestational Age（SGA 児）

1. はじめに

生殖や発生異常では，染色体検査を行っても明らかな異常（ゲノムの異常）が見つからないことが稀ではない。その理由として，これらが多因子性疾患であること，あるいは従来技術では同定できないような微細な染色体構造異常や点変異が関与していること，等が推測される。一方，近年エピジェネティックな因子の生殖・発生への関与が明らかにされつつあり，これらの遺伝子機能欠失モデルマウスでは多くの場合，生殖や発生の重篤な表現型が観察される。加えて，一部のヒト先天奇形症候群でも，モデルマウスと同様の症状や分子生物学的変化が観察される。これらの状況証拠から，ヒトの生殖細胞，胎児，胎盤の発生・分化・発育には，エピジェネティックな機構による遺伝子発現制御が必須であること，そして，前述の「ゲノムの異常が見つからないヒト生殖・発生異常症例」の一部には，未知のエピジェネティックな異常を伴う症例が存在すること，が推測される。

さらに，環境の影響を受けて起こり得る胎児や生殖細胞のエピゲノム変化もわかってきた。少なくともモデル生物では，胚培養などの人為的操作や妊娠母獣の食餌などの影響により，初期胚や胎児にエピゲノム変化が生じ，出生後も遺残して遺伝子発現に影響する事が示されている。また一部のモデル系では，生殖細胞を介した（世代間の）エピゲノム変化の伝達も報告されている。これらのメカニズムは，「受精時，胎芽期，胎児期の子宮内及び乳幼児期の望ましくない環境がエピゲノム変化を起こ

受付 2016 年 4 月 1 日，受理 2016 年 6 月 21 日
Reprint requests to: Kenichiro HATA
Department of Maternal-Fetal Biology, National Research Institute for Child Health and Development, 2-10-1 Okura, Setagaya, Tokyo 157-8535, Japan
TEL: +81(3)3416-0181, FAX: +81(3)3417-2864
E-mail: hata-k@ncchd.go.jp

し，それが疾病素因となり，出生後の環境との相互作用によって疾病が発症する。生活習慣病等の多因子疾患はこの 2 段階を経て発症する。」（日本 DOHaD 研究会ホームページより引用）という DOHaD（Developmental Origin of Health and Disease）学説の有力な分子病態の一つと考えられる。本総説では，生殖や発生にかかわるエピゲノム変化と環境の影響に関する最近の知見を概説すると共に，ヒト胎盤で観察されるエピゲノム変化を，我々の知見を交えてお示しする。

2. 生殖と発生にかかわるエピジェネティックな遺伝子調節の基盤

哺乳類の正常な発生には卵子と精子が必要で，決して単為発生しない。卵子と精子の有するジェネティックな情報（遺伝子の配列）は同一であっても，エピジェネティックな情報（インプリンティング遺伝子領域の DNA メチル化状態など）は異なるため，卵子と精子の遺伝情報が等価ではない。一方で，大部分のゲノム領域では，受精直後に精子由来のメチル化は速やかに消去され（能動的脱メチル化），卵子由来のメチル化はそれに遅れ，DNA 複製依存的に維持されずに失われていく（受動的脱メチル化）。親由来の DNA メチル化修飾情報はこのように大部分が一度消去され，その後胚盤胞期まで低メチル化状態にあり，着床後，複数の DNA メチル化酵素（DNMTs）によってメチル化状態が再構築され，発生段階特異的かつ組織特異的なメチル化修飾（エピゲノム）が確立されていく。雄性生殖細胞系列では，胎児期にメチル化修飾が行われ，出生前の精原細胞ですでにゲノム全体が高度にメチル化されているのに対し，雌性生殖細胞系列では，出生後の卵母細胞成長期にメチル化修飾が入る（図 1）。特にヒトでは，卵子の解析は倫理的・手技的に困難であり，精子の解析が進んでいるが，精子（配偶子）形成に必要な遺伝子のプロモーターはバイバレントな修飾（正と負の調節修飾が同時に起こっている状態）を受け，かつ，高メチル化修飾（>60% methylation）されている特徴を持つ。成熟精子ゲノムにはこのような，発現活性型の高メチル化プロモーターがプロタミン遺伝子や piRNA クラスターなどの，成熟精子形成過程に必須な遺伝子に見出された。これらの領域はプロタミンに置換されることなく，成熟精子でもヒストンヌクレオソームに位置する（1）。少なくとも精子において

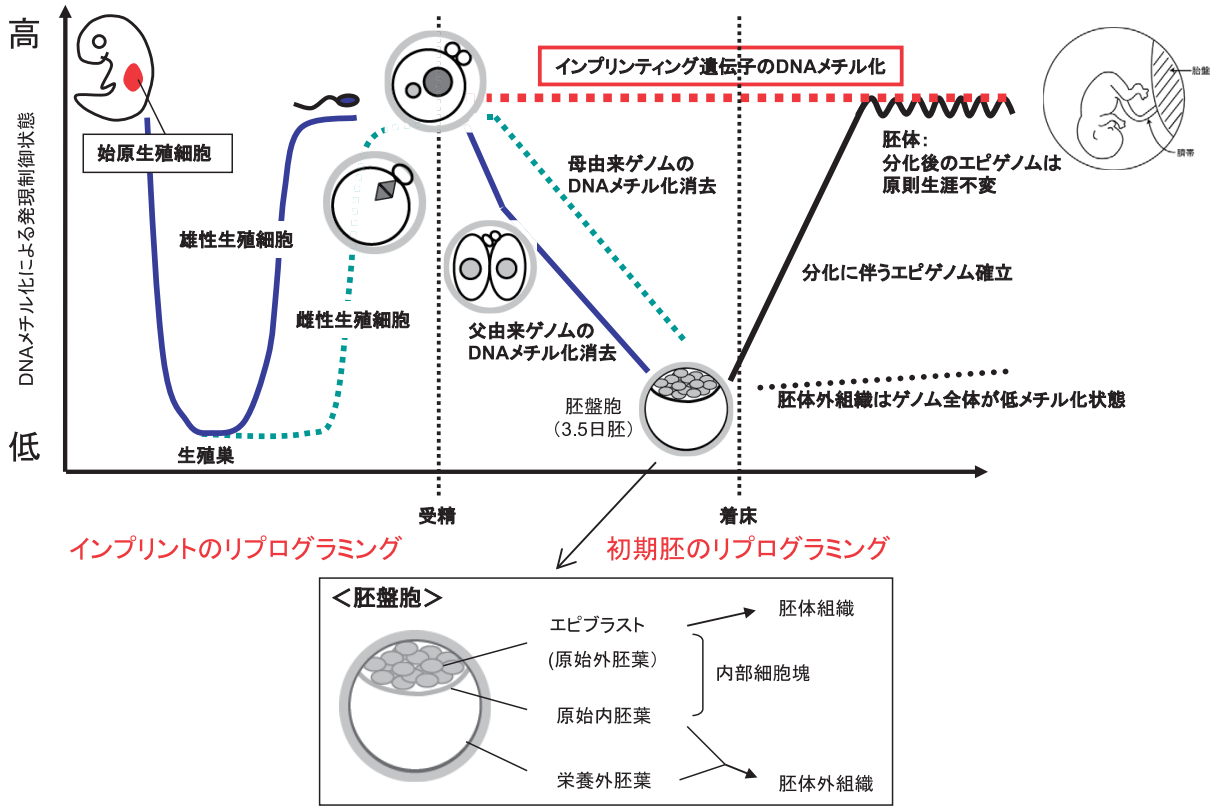

図 1　発生過程の組織特異的遺伝子のエピジェネティックな制御。受精後，着床までの間に，精子由来・卵子由来の両親のエピゲノム情報は消去され，着床後時期特異的ならびに組織特異的なメチル化修飾が再び胚ゲノムに入る。精子由来，卵子由来のインプリント領域のメチル化は脱メチル化から逃れる機構を備えており，両親のインプリント領域のメチル化修飾は胎児に遺残する。この精子由来・卵子由来のインプリント領域のメチル化は，両親の生殖細胞の分化の過程で確立されている。両親の生殖細胞は，胎児期の始原生殖細胞において自身の両親からのメチル化修飾が消去され，インプリント領域を含む精子ゲノム，卵子ゲノム特異的なメチル化修飾が生殖細胞の分化に伴い書き直される。

は，胎児期のエピゲノム修飾獲得が鍵となり，その修飾状態が生涯にわたり維持され，妊孕能，胚発生分化能に関与している可能性が示唆される。

3. 不妊症や不育症で報告されているエピゲノム異常

これまでに，原因不明と診断された不妊を呈す様々な疾患の精子ゲノムにおいてインプリント領域の DNA メチル化異常が報告されている。インプリンティング遺伝子は，DNA メチル化により制御され，厳密な片親アレル発現を保持する。これらのエピジェネティックな制御は，前述の発生初期のゲノム全体の DNA メチル化消去と再構築から免れているため，配偶子のエピゲノム（DNA メチル化）異常が胚発生を左右し，不妊や発育異常の直接の原因となりうる。

特に，精子ゲノムの *H19* インプリント領域低メチル化は自然流産，不育症，乏精子症，精子無力症の患者で認められている（2–5）。他に，乏精子症，精子無力症の精子では *PEG1/MEST* の高メチル化も報告されている（4–7）。これら乏精子症や精子無力症のメチル化異常は，全ての精子で生じているのではなく，正常なメチル化パターンを持った精子と異常パターンの精子がモザイク状に存在することも示された。さらに，乏無力精子症の精子ゲノム *H19* 低メチル化は，母由来アレルの低メチル化に起因することも認められている（5）。

非インプリント領域においても，不妊を呈するヒト精子ゲノムにおいて，葉酸代謝関連酵素遺伝子のメチル化異常や（8），生殖細胞特異的な piRNA 機構に関与する遺伝子のメチル化異常が検出されている（9）。特定の遺伝子に対するエピゲノム異常にとどまらず，不妊症例では本来精子特異的に高メチル化が認められる領域が広く DNA メチル化異常を起こしていることも認められている（10）。

動物実験では，これらのメチル化異常誘導因子の一つとして，父親の葉酸摂取不足が指摘されている。雄マウスの葉酸不足は，精子形成や精子の数・受精能・胚形成には変化を及ぼさないものの，着床後の流産率を高め，解剖学的異常を呈する胎仔の出生率を高めた。この雄マウスの精子では，ヒストンのメチル化修飾が全体的に減少しており，かつ，発生にかかわる遺伝子近傍の DNA メチル化修飾に変化が認められた（11）。このモデル系では，胎仔期から離乳まで葉酸欠乏状態に曝しており，胎仔期の葉酸不足がこの雄マウスの精子エピゲノム異常にクリティカルである可能性も示唆される。

4. 精子エピゲノム確立に寄与する環境

胎児期環境の攪乱が，生殖細胞のインプリンティング遺伝子インプリント機構の異常を介して生殖機能や次世代の発生に影響を及ぼすことが動物実験で確認されている。高分子樹脂として汎用され，広く環境中に存在する合成エストロゲンのビスフェノール A（BPA）に新生仔期に曝露すると，ラットの精子ゲノムあるいはその精子が受精した胚で，*H19* インプリント領域の低メチル化と遺伝子発現異常が認められ，最終的に流産する（12）。防カビ剤成分のビンクロゾリンに胎仔期に曝露すると，精子エピジェネティック異常と精子形成細胞のアポトーシスが 3 世代後まで遺残することが認められている（13, 14）。ビンクロゾリンによる世代を超えたエピジェネティクス異常はいくつかのインプリント領域でも生じている一方で，世代を超えるごとに徐々に正常化しているとの報告もある（15）。

胎児期ではなく成人期の環境が，精子エピゲノミクス異常を介して次世代に影響する現象もモデル生物において分子機構の解明とともに報告されている。雄の食事内容が精子エピゲノム調節異常を介して次世代の肥満を呈するメカニズムがショウジョウバエで明らかにされ，標的となるのは代謝にかかわる遺伝子のヒストンの抑制マーク（H3K27me3, H3K9me3）の修飾異常であることが解明された（16）。

5. 子宮内環境に影響を受けるエピゲノム

我々は，胎生期の環境がエピゲノミクス制御に深く関与する例として，胎盤エピゲノムが母体の妊娠中の体重増加量によって左右される現象を見出した（17）。SGA 児（Small for Gestational Age）では予想通り，AGA 児（Appropriate for Gestational Age）と比較して胎盤の DNA メチル化状態の乱れが観察された。驚いたことに，AGA 児であっても，妊娠期体重増加量が不適切なほど（痩せすぎていたり太り過ぎていたりすると），個々の症例で DNA メチル化の外れ値を示す領域の数が増えた（DNA メチル化が乱れていた）（図 2）。共通の異常を示す遺伝子は見つからなかったが，これらのメチル化外れ値領域は，転写因子プロモーターに多く認められることから，実際に遺伝子発現を乱している可能性が示唆された。これらの転写因子の中には，HOX genes や SOX genes，FOX genes がいくつか認められた。これらの遺伝子群は，発生時期・組織特異的に発現し，それ以外ではエピジェネティックに抑制されていることが知られている（18）。ヒトの発生過程においても，ヒストンの抑制マークとそこにある DNA 領域のメチル化制御が，エピゲノム異常感受性の強い場所として，修飾変化を受ける可能性が示唆された。

6. おわりに

以上のように，受精前や胎児期の環境が，胎児ゲノムの様々な領域にエピジェネティック変化を引き起こし，出生後も長期にわたり遺残して成人期の疾患素因となる可能性は，様々なモデルで示されている。ヒトでも，不

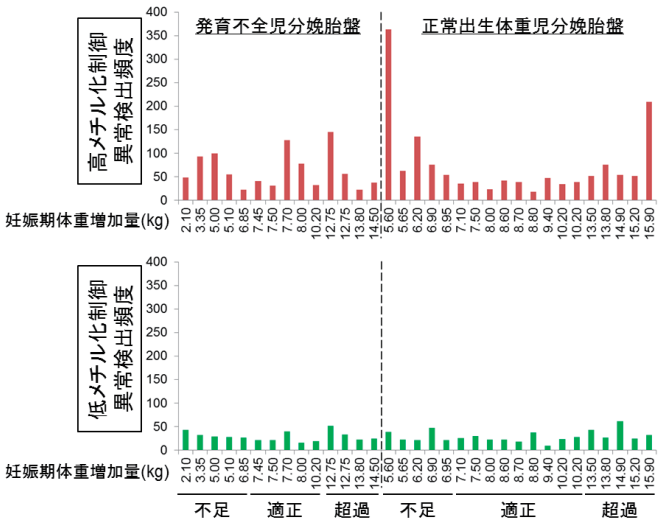

有意と考えられるDNAメチル化変化が観察された遺伝子の例
胚性幹細胞においてH3K27me3修飾を受けている遺伝子（赤字）
胚性幹細胞においてH3K9me3修飾を受けている遺伝子（青字）

category	Subject	Gene Symbol	# of hyper-methylated outliers in pTSS	average Δβ of outliers
児:正常_適正増加	N_adequate_5	ZNF649	6	0.19
児:正常_超過増加	N_excessive_1	GBX2	3	0.25
	N_excessive_1	ZNF350	8	0.30
	N_excessive_2	ZFP37	4	0.44
	N_excessive_5	ZHX2	8	0.15
	N_excessive_5	CDKN1C	4	0.28
	N_excessive_5	PAX6	2	0.23
児:正常_不足増加	N_insufficient_1	KCNH8	4	0.24
	N_insufficient_1	FOXL2	10	0.21
	N_insufficient_1	F2R	3	0.20
	N_insufficient_1	SOX7	3	0.18
	N_insufficient_1	NFIB	2	0.37
	N_insufficient_1	HMX2	2	0.23
	N_insufficient_2	TFCP2	5	0.19
	N_insufficient_3	PROX1	3	0.15
	N_insufficient_3	FOXC1	8	0.19
	N_insufficient_3	FOXB1	2	0.17
	N_insufficient_5	ETV1	6	0.11
	N_insufficient_5	ZNF426	2	0.17
児:発育不全	FGR_adequate_1	PER1	6	0.16
	FGR_adequate_3	ZNF619	4	0.27
	FGR_adequate_3	ZKSCAN4	3	0.25
	FGR_adequate_3	PGBD1	7	0.21
	FGR_adequate_3	HOXB7	4	0.23
	FGR_adequate_4	ESR1	3	0.17
	FGR_adequate_4	MGA	3	0.17
	FGR_excessive_1	RFX8	3	0.33
	FGR_excessive_1	ZNF483	2	0.20
	FGR_excessive_1	ZNF254	3	0.21
	FGR_excessive_2	ZNF577	6	0.43
	FGR_excessive_3	ZNF655	2	0.35
	FGR_insufficient_1	ZNF562	8	0.36
	FGR_insufficient_1	ZNF805	2	0.30
	FGR_insufficient_2	ZNF583	6	0.27
	FGR_insufficient_3	ZNF354C	7	0.27
	FGR_insufficient_3	ETV1	6	0.16
	FGR_insufficient_4	ZIK1	2	0.42

図 2　妊娠中の母体体重増加量に影響を受ける胎盤の DNA メチル化。胚発生と同時期に形成される胚体外組織である胎盤も，子宮内環境の要因の一つである妊娠期母体体重変化量の違いによって，抑制修飾を受けるヒストンヌクレオソーム領域に特徴的に DNA メチル化変化を受ける可能性が示唆された。

妊症・不育症・胎児発育異常等の疾患には，明らかに様々なエピゲノム異常が関与していることが推測され，一部の疾患では実際に証明されている。更に，一見正常であっても，隠れたエピゲノム変化が存在する可能性が我々のデータからは示唆された。短期的には，配偶子や初期胚のエピゲノム診断法を確立すれば，エピゲノム異常の観点から配偶子や胚の品質評価が可能となり，不妊症や不育症のリスク因子の一部を軽減できると期待できる。今後はさらに，これらのエピゲノム異常と長期予後との分子疫学的な検証が待たれる。

利益相反なし

文　　献

（1）Hammoud SS, Low DH, Yi C, Carrell DT, Guccione E, Cairns BR. Chromatin and transcription transitions of mammalian adult germline stem cells and spermatogenesis. Cell Stem Cell 2014;15(2):239–253.
（2）Ankolkar M, Patil A, Warke H, Salvi V, Kedia Mokashi N, Pathak S, et al. Methylation analysis of idiopathic recurrent spontaneous miscarriage cases reveals aberrant imprinting at H19 ICR in normozoospermic individuals. Fertil Steril 2012;98(5):1186–1192.
（3）Boissonnas CC, Abdalaoui HE, Haelewyn V, Fauque P, Dupont JM, Gut I, et al. Specific epigenetic alterations of IGF2-H19 locus in spermatozoa from infertile men. Eur J Hum Genet 2010;18(1):73–80.
（4）Poplinski A, Tüttelmann F, Kanber D, Horsthemke B, Gromoll J. Idiopathic male infertility is strongly associated with aberrant methylation of MEST and IGF2/H19 ICR1. Int J Androl 2010;33(4):642–649.
（5）Laurentino S, Beygo J, Nordhoff V, Kliesch S, Wistuba J, Borgmann J, et al. Epigenetic germline mosaicism in infertile men. Hum Mol Genet 2015;24(5):1295–1304.
（6）Marques CJ, Costa P, Vaz B, Carvalho F, Fernandes S, Barros A, et al. Abnormal methylation of imprinted genes in human sperm is associated with oligozoospermia. Mol Hum Reprod 2008;14(2):67–74.
（7）Hammoud SS, Purwar J, Pflueger C, Cairns BR, Carrell DT. Alterations in sperm DNA methylation patterns at imprinted loci in two classes of infertility. Fertil Steril 2010;94(5):1728–1733.
（8）Wu W, Shen O, Qin Y, Niu X, Lu C, Xia Y, et al. Idiopathic male infertility is strongly associated with aberrant promoter methylation of methylenetetrahydrofolate reductase

(MTHFR). PLoS One 2010;5(11):e13884.
（9）Heyn H, Ferreira HJ, Bassas L, Bonache S, Sayols S, Sandoval J, et al., Epigenetic disruption of the PIWI pathway in human spermatogenic disorders. PLoS One 2012; 7(10):e47892.
（10）Urdinguio RG, Bayón GF, Dmitrijeva M, Toraño EG, Bravo C, Fraga MF, et al. Aberrant DNA methylation patterns of spermatozoa in men with unexplained infertility. Hum Reprod 2015;30(5):1014–1028.
（11）Lambrot R, Xu C, Saint-Phar S, Chountalos G, Cohen T, Paquet M, et al. Low paternal dietary folate alters the mouse sperm epigenome and is associated with negative pregnancy outcomes. Nat Commun 2013;4:2889.
（12）Doshi T, D'souza C, Vanage G. Aberrant DNA methylation at Igf2–H19 imprinting control region in spermatozoa upon neonatal exposure to bisphenol A and its association with post implantation loss. Mol Biol Rep 2013;40(8):4747–4757.
（13）Anway MD, Cupp AS, Uzumcu M, Skinner MK. Epigenetic transgenerational actions of endocrine disruptors and male fertility. Science 2005;308(5727):1466–1469.
（14）Guerrero-Bosagna C, Covert TR, Haque MM, Settles M, Nilsson EE, Anway MD, et al. Epigenetic transgenerational inheritance of vinclozolin induced mouse adult onset disease and associated sperm epigenome biomarkers. Reprod Toxicol 2012;34(4):694–707.
（15）Stouder C, Paoloni-Giacobino A. Transgenerational effects of the endocrine disruptor vinclozolin on the methylation pattern of imprinted genes in the mouse sperm. Reproduction 2010;139(2):373–379.
（16）Öst A, Lempradl A, Casas E, Weigert M, Tiko T, Deniz M, et al., Paternal diet defines offspring chromatin state and intergenerational obesity. Cell 2014;159(6):1352–1364.
（17）Kawai T, Yamada T, Abe K, Okamura K, Kamura H, Akaishi R, et al. Increased epigenetic alterations at the promoters of transcriptional regulators following inadequate maternal gestational weight gain. Sci Rep 2015;5:14224.
（18）Schwartz YB, Pirrotta V. A new world of Polycombs: unexpected partnerships and emerging functions. Nat Rev Genet 2013;14(12):853–864.

Original Article

Gynecologic and Obstetric Investigation

Gynecol Obstet Invest
DOI: 10.1159/000441780

Received: November 25, 2014
Accepted after revision: October 15, 2015
Published online: November 26, 2015

Novel Nonsense Mutation in the *NLRP7* Gene Associated with Recurrent Hydatidiform Mole

Yuki Ito[a, c] Kayoko Maehara[a] Eisuke Kaneki[d] Kentaro Matsuoka[b] Naoko Sugahara[a] Tomoko Miyata[a] Hiromi Kamura[a] Yuko Yamaguchi[a] Ayako Kono[a] Kazuhiko Nakabayashi[a] Ohsuke Migita[a] Ken Higashimoto[e] Hidenobu Soejima[e] Aikou Okamoto[c] Hitomi Nakamura[f] Tadashi Kimura[f] Norio Wake[d] Takeshi Taniguchi[g] Kenichiro Hata[a]

[a]Department of Maternal-Fetal Biology, National Research Institute for Child Health and Development, [b]Department of Pathology, National Center for Child Health and Development, and [c]Department of Obstetrics and Gynecology, The Jikei University School of Medicine, Tokyo, [d]Department of Obstetrics and Gynecology, Graduate School of Medical Science, Kyushu University, Fukuoka, [e]Division of Molecular Genetics and Epigenetics, Department of Biomolecular Sciences, Faculty of Medicine, Saga University, Saga, [f]Department of Obstetrics and Gynecology, Osaka University Graduate School of Medicine, and [g]Taniguchi Hospital, Osaka, Japan

Key Words
Recurrent hydatidiform mole · DNA methylation · *NLRP7* · Genomic imprinting

Abstract
Aim: This study aimed to clarify the genetic and epigenetic features of recurrent hydatidiform mole (RHM) in Japanese patients. ***Methods:*** Four Japanese isolated RHM cases were analyzed using whole-exome sequencing. Villi from RHMs were collected by laser microdissection for genotyping and DNA methylation assay of differentially methylated regions (DMRs). Single nucleotide polymorphisms of *PEG3* and *H19* DMRs were used to confirm the parental origin of the variants. ***Results:*** A novel homozygous nonsense mutation in *NLRP7* (c.584G>A; p.W195X) was identified in 1 patient. Genotyping of one of her molar tissue revealed that it was biparental but not androgenetic in origin. Despite the fact that the RHM is biparental, maternally methylated DMRs of *PEG3*, *SNRPN* and *PEG10* showed complete loss of DNA methylation. A paternally methylated DMR of *H19* retained normal methylation. ***Conclusions:*** This is the first Japanese case of RHM with a novel homozygous nonsense *NLRP7* mutation and a specific loss of maternal DNA methylation of DMRs. Notably, the mutation was identified in an isolated case of an ethnic background that has not previously been studied in this context. Our data underscore the involvement of *NLRP7* in RHM pathophysiology and confirm that DNA methylation of specific regions is critical.

Y. Ito and K. Maehara contributed equally to this work.

0378–7346/15/0000–0000$39.50/0

E-Mail karger@karger.com
www.karger.com/goi

Kenichiro Hata, MD, PhD
Director, Department of Maternal-Fetal Biology
National Research Institute for Child Health and Development
2-10-1 Setagaya-ku, Tokyo 157-8535 (Japan)
E-Mail hata-k@ncchd.go.jp

Introduction

Complete hydatidiform mole (CHM) is an abnormal pregnancy that typically arises from an androgenote (diploid conception without maternal chromosomes) and predominantly gives rise to the development of only trophoblastic tissues [1, 2]. Recent studies of rare familial cases with recurrent molar pregnancies have shown that mutations of *NLRP7* and *KHDC3L (C6orf221)* are associated with recurrent hydatidiform moles (RHMs) [3, 4]. However, more than 20% of RHM cases have no mutations in these genes [5], and the mechanism underlying the occurrence of molar pregnancy associated with *NLRP7* and *KHDC3L (C6orf221)* mutation remains unknown. To clarify the genetic etiology of RHMs, further comprehensive genetic screening in various ethnic backgrounds is important.

In Japan, the incidence of CHM has become as low as that in western countries. The incidence of CHM per 1,000 live births was 0.49 in 2,000, with a recurrence rate of 1.3% [6, 7]. Nonetheless, a genetic and epigenetic analysis of RHM in Japan has not been performed previously.

CHM conceptions exhibit abnormal genomic imprinting. Although some villi of RHM possess normal biparental alleles, they exhibit loss of maternal DNA methylation of differentially methylated regions (DMRs) within imprinted loci, and thus have aberrant genomic imprinting [8, 9]. Because the histopathological findings of diploid biparental RHM are identical to those of diploid androgenetic CHM, diploid biparental RHM cannot be distinguished from typical CHM without a genetic and epigenetic diagnosis. To clarify the molecular mechanisms of RHM, we performed comprehensive genetic and epigenetic analyses of isolated Japanese RHM cases and in doing so, we identified a novel nonsense *NLRP7* mutation. The RHM tissue contained biparental alleles and showed a loss of maternal DNA methylation of imprinted genes. This evidence strongly supports the role for *NLRP7* in maternal DNA methylation of imprinted genes and the involvement of *NLRP7* in RHM.

Materials and Methods

Study Participants and Samples

Patients with RHM (n = 5) and CHM (n = 9) were included in this study. The profiles of the 5 RHM patients are shown in table 1. Each sample was histopathologically diagnosed as CHM or partial hydatidiform mole and previously genetically diagnosed as an androgenote or a triploid, with the exception of Patients 1, 2, 4 and 5 [10]. All the villi of the 9 CHM conceptions were androgenote. None of the CHM patients had a family history of the condition. Genomic DNA was extracted from peripheral blood cells and molar tissues. This study was approved by the Institutional Review Board Committee at the National Center for Child Health and Development, Tokyo, Japan (approval number 234), and written informed consent was obtained from all patients.

Table 1. Profiles of 5 patients with RHM

Patient ID	Pathological diagnosis	Genetic diagnosis	Familial history
1	5 CHM	This study	No
2	2 CHM	No samples	No
3	PHM, NP, SA, CHM	Triploid[1]	No
4	CHM, PHM	No samples	No
5	SA, PHM, NP, PHM	No samples	No

PHM = Partial hydatidiform mole; NP = normal pregnancy; SA = spontaneous abortion.

[1] Genetic diagnosis of the first molar pregnancy (PHM).

Whole-Exome Sequencing

The whole-exome library was prepared from the peripheral blood cells of 4 RHM patients (Patients 1–4 in table 1) by using Agilent SureSelect Human All Exon V3 capture reagent (Agilent Technologies, Inc., Santa Clara, Calif., USA), and sequenced using the Illumina HiSeq1000 platform. Data analysis procedures are described in the online supplementary materials and methods (for all online suppl. material, see www.karger.com/doi/10.1159/000441780).

NLRP7 Mutation Analysis

The mutations were confirmed by direct sequencing [11]. Ten coding exons and 1 non-coding exon of *NLRP7* were amplified using primers and PCR conditions that were previously described [12].

Genotyping of Molar Tissue

The molar tissue of Patient 1 was genotyped. The villi were selectively laser microdissected using an LMD7000 (Leica Microsystems GmbH, Wetzlar, Germany), and genomic DNA was extracted using the QIAamp DNA FFPE Tissue Kit (Qiagen, Hilden, Germany). The refSNP(rs) numbers of the 8 genotyped loci are shown in online supplementary table S1.

DNA Methylation Assay

The villi of a CHM from a patient with RHM (Patient 1), an androgenetic CHM and normal placenta were examined for *PEG3*, *SNRPN*, *PEG10* and *H19* gene methylation by bisulfite sequencing [13]. Bisulfite conversion was performed using the EpiTect Bisulfite kit (Qiagen, Hilden, Germany) with primers listed in online supplementary table S2.

Results

RHM is most likely caused by genetic factors, and 2 candidate genes have been previously reported [3, 4]. To search for additional mutations in genes that have not

Table 2. SNVs detected by whole-exome sequencing

Chromosome[1]	Position	Gene	Location	SNV	Protein alteration	RefSNP	Allele frequency in HGVB	Patient 1	Patient 2	Patient 3	Patient 4
1	52828383	*CC2D1B*[1]	Exon 3	c.G105A	p.M35I	rs183845075	0.02	G/G	G/G	G/G	A/A
3	10452493	*ATP2B2*[1]	Exon 3	c.C206T	p.P69L	N/A	N/A	T/T	C/C	C/C	C/C
3	16254129	*GALNT15*[1]	Exon 6	c.C1251A	p.H417Q	rs185944497	0.008	A/A	C/C	C/C	C/C
9	140007466	*DPP7*[1]	Exon 7	c.C809T	p.A270V	rs181036640	0.013	T/T	C/C	C/C	C/C
11	69063476	*MYEOV*[1]	Exon 3	c.C559T	p.R187W	rs116926312	0.044	C/C	C/C	C/C	T/T
13	41835028	*MTRF1*[1]	Exon 2	c.T16C	p.C6R	N/A	0.009	T/T	C/C	T/T	T/T
16	30735148	*SRCAP*[1]	Exon 25	c.C4403T	p.S1468L	rs75035256	0.019	T/T	C/T	C/C	C/C
17	27030713	*PROCA1*[1]	Exon 4	c.G874A	p.E292K	rs3744637	0.043	C/C	C/C	C/C	A/A
19	55451603	*NLRP7*	Exon 4	c.G584A	p.W195X	N/A	N/A	A/A	G/G	G/G	G/G
21	38439597	*PIGP*[1]	Exon 4	c.G239A	p.S80N	rs114319840	0.004	A/A	G/G	G/G	G/G

HGVB = Human Genetic Variation Browser; N/A = not available.
[1] Except for *NLRP7*, the 10 SNVs detected have no particular reported/predicted pathogenic features in the reproduction system.

Table 3. Summary of the SNVs found in *ZFP57*, *NLRP7* and *NLRP2* in 4 patients with RHM by whole-exome sequencing

Chromosome	Position	Gene	Location	SNV	Protein	RefSNP	Patient 1	Patient 2	Patient 3	Patient 4
6	29644668	*ZFP57*	Exon 14	c.G113>A	p.R38Q	rs142917604	G/G	G/G	G/A	A/A
19	55441902	*NLRP7*	Exon 9	c.A2775>G	p.A925A	rs269950	G/G	G/G	G/G	A/G
19	55441995	*NLRP7*	Exon 9	c.T2682>C	p.Y894Y	rs269951	G/G	G/G	G/G	A/G
19	55451050	*NLRP7*	Exon 4	c.G1137>A	p.K379K	rs10418277	A/A	G/G	G/G	G/G
19	55451232	*NLRP7*	Exon 4	c.G955>A	p.V319I	rs775882	A/A	G/G	G/G	G/G
19	55451603	*NLRP7*	Exon 4	c.G584>A	p.W195X	N/A	A/A	G/G	G/G	G/G
19	55451797	*NLRP7*	Exon 4	c.G390>A	p.Q130Q	rs775883	A/A	G/G	G/G	G/G
19	55485899	*NLRP2*	Exon 4	c.G312>A	p.K104K	rs2217659	G/G	A/A	G/G	A/A
19	55494881	*NLRP2*	Exon 7	c.C1815>G	p.L605L	rs11672113	G/G	C/C	G/G	C/C
19	55512137	*NLRP2*	Exon 14	c.C3060>A	p.I1020I	rs12768	A/A	C/A	A/A	A/A
19	55512232	*NLRP2*	Exon 14	c.C3155>A	p.A1052E	rs1043673	C/C	C/C	A/A	C/C

N/A = Not available.
[1] A novel homozygous nonsense mutation of *NLRP7* (c.584G>A; p.W195X) was found in Patient 1. Other SNVs are all commonly known SNPs with RefSNP(rs) numbers.

been previously associated with RHM, we performed whole-exome sequencing using peripheral blood cells from 4 RHM patients (Patients 1–4 in table 1). Quality filtering in the patients resulted in a set of 176,663 single nucleotide variations (SNVs) in coding regions. We excluded all non-coding SNVs and SNVs with more than 5% frequency in the 1000 Genomes database (http://www.1000genomes.org/, May 5, 2013) or the Human Genetic Variation Browser (http://www.genome.med.kyoto-u.ac.jp/SnpDB/). The remaining 10 SNVs (table 2) contained no particular potential pathogenic genes involved in the reproduction process except for an *NLRP7* mutation, as described later.

Next, we focused on *NLRP7*, *NLRP2*, *ZFP57* and *KHDC3L (C6orf221)*, which were previously reported as candidate genes for RHM or were associated with DNA methylation defects [3, 4, 14, 15]. Based on the minor allele frequency information of the 1000 Genomes database and other reports [3, 5, 9, 12, 16], the homozygous nonsense mutation of *NLRP7* (c.584G>A; p.W195X) identified in Patient 1 is considered a mutation, which was not previously reported (table 3). Other SNVs found in *ZFP57*, *NLRP7* and *NLRP2* are common variants. Sanger sequencing of genomic DNA from 5 RHM patients (Patients 1–5 in table 1), 9 patients with typical androgenetic CHM and 86 controls confirmed that the *NLRP7* muta-

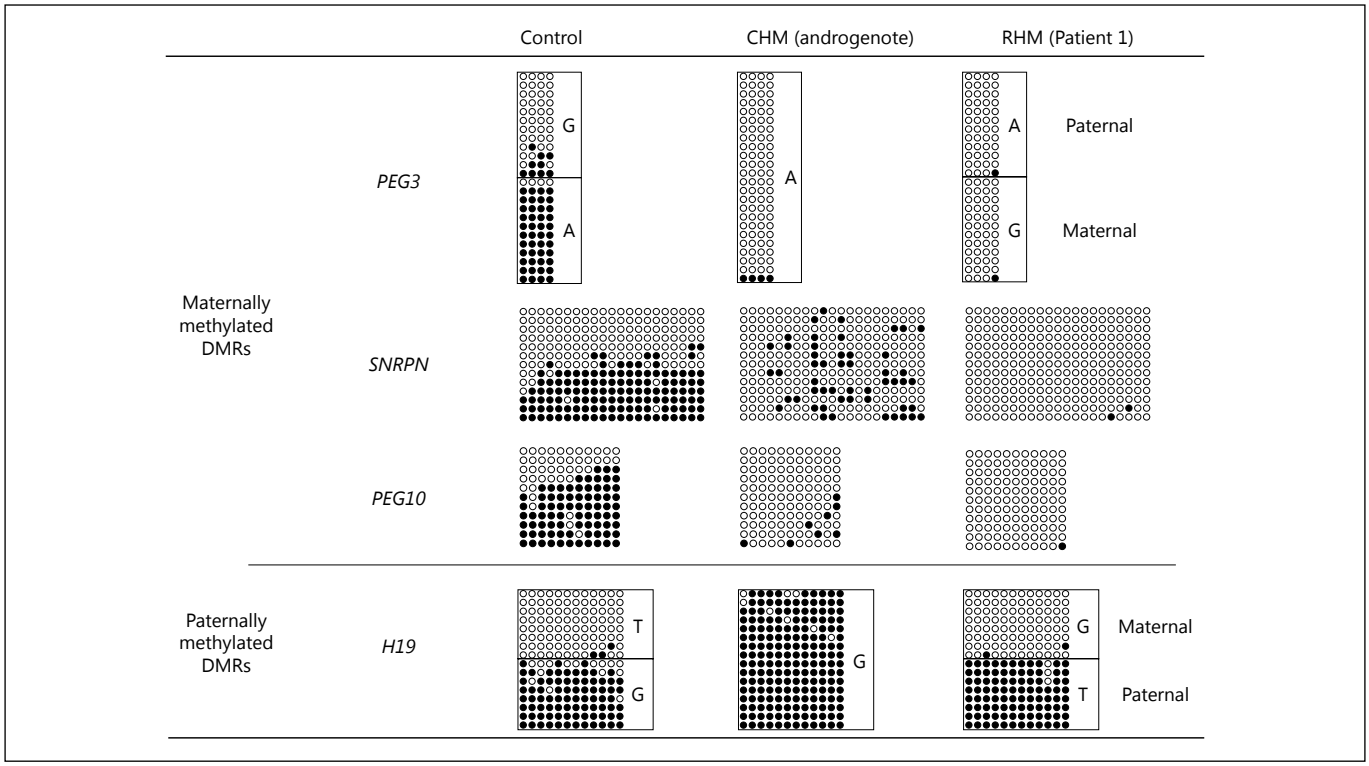

Fig. 1. DNA methylation assay of DMRs. Bisulfite sequencing was performed for 3 maternal DMRs (*PEG3*, *SNRPN* and *PEG10*) and 1 paternal DMR *(H19)*. Each line indicates a single clone, and each circle denotes a CpG; filled and open circles represent methylated and unmethylated cytosine residues, respectively. Allele-specific methylation was definitively diagnosed by SNPs in *PEG3* and *H19* DMRs. All maternally methylated DMRs (*PEG3*, *SNRPN* and *PEG10*) showed loss of DNA methylation in the villi of RHM (Patient 1). In contrast, paternal methylation of the *H19* DMR was maintained normally, even in the villi of RHM. Methylation defects were observed only in maternally methylated DMRs.

tion (c.584G>A; p.W195X) was observed only in 1 RHM (Patient 1; online suppl. table S3, fig. S1).

Previous reports have shown that the origin of a subset of RHM is not androgenic but biparental [12–14]. To precisely confirm the genotype of the villi of RHM Patient 1, the villi were selectively collected by laser microdissection, and a small amount of genomic DNA was obtained. Since the extracted DNA was fragmented and of low quality, analysis of polymorphic DNA markers was inconclusive. We then performed a comprehensive SNP analysis of the biological parents to confirm the origin of the villi of RHM Patient 1. Eight loci in which each parent (Patient 1 and her husband) possesses the opposite major or minor homozygous allele were genotyped, and all showed heterozygous genotypes in the villi (online suppl. table S1). These results clearly show that the villi of RHM Patient 1 contain both parental alleles and thus it is not androgenic, but biparental.

To clarify epigenetic abnormalities in the villi of Patient 1 RHM, DNA methylation analysis of DMRs of imprinted genes was performed using bisulfite sequencing (fig. 1). Three maternally methylated DMRs in *PEG3*, *SNRPN* and *PEG10* and a paternally methylated DMR in *H19* were analyzed. SNPs of *PEG3* and *H19* were used to distinguish between paternal and maternal alleles, enabling specific estimations of allele-specific DNA methylation defects of DMRs. The villi of RHM Patient 1 showed a loss of methylation in all the analyzed maternal DMRs and retained completely normal methylation in the paternal DMR.

Discussion

It is currently not possible to distinguish diploid biparental RHM from typical diploid androgenetic CHM with conventional pathological criteria. In fact, the RHM of Patient 1 and control CHM are histopathologically identical and were both p57KIP2-negative upon immunohistochemical analysis (online suppl. fig. S2). Though striking features of RHM are being revealed with genetic and epi-

genetic analyses [3, 8, 17–19], there is no clear mechanistic understanding as to why certain candidate genes are associated with the condition. Furthermore, no candidate genes have been identified in approximately 20% of all cases [5]. Thus, there is a clear need to explore genetic mutations and epigenetic aberrations in different genetic backgrounds. Additionally, whole-exome sequencing is a potentially promising approach to identifying unknown genetic factors [20]; however, to our knowledge, this is the first report of whole-exome sequencing in RHM patients.

To clarify the features of these Japanese isolated RHM cases, we performed comprehensive genetic and epigenetic analyses. We successfully detected a novel pathogenic homozygous nonsense *NLRP7* mutation (c.584G>A; p.W195X). Since we could not obtain genomic DNA to confirm the mutation in the parents of Patient 1, the parental origin of the mutation is unknown. The approximate 1-Mb region around the *NLRP7* mutation (c.584G>A) shows copy neutral loss of heterozygosity (data not shown). Although the parents of the Patient 1 do not appear to be consanguineous, we speculate that the *NLRP7* region of Patient 1 most likely has alleles identical by descent.

The examination of DNA methylation abnormalities is indispensable for a definitive diagnosis of epigenetic mutations specifically observed in diploid biparental RHMs. In this study, the parental origin of the *PEG3* and *H19* DMRs were definitively confirmed by SNP analysis. The villi of RHM Patient 1 clearly showed complete loss of DNA methylation of maternally methylated DMRs (*PEG3*, *SNRPN* and *PEG10*) but retained methylation of a paternally methylated DMR *(H19)*. Although the villi of the RHM were genetically normal, they showed abnormal DNA methylation and their DNA methylation profile was quite similar to that in a typical androgenetic CHM. This is in contrast to previous studies, in which patterns including hypermethylation of *H19* DMR [21] and retention of methylation at *PEG10* DMR were observed [12]. These differences are likely due to the multifactorial nature in which the DNA methylation machinery is regulated; this would account for the variable methylation changes within DMRs, as we previously reported in our study of *Dnmt3L* knockout mice [22].

RHM patients with *NLRP7* mutations are most likely to have failed in the establishment of methylation of maternal DMRs during oogenesis. The p.W195X mutation in Patient 1 is located upstream of the known nonsense mutations in RHM patients [5]. It is, therefore, expected that RHM from Patient 1 would exhibit the typical phenotype, and indeed this patient had 5 molar pregnancies. Some reported missense mutations could be hypomorphic and show stochastic effects on the methylation of DMRs [9, 12]. If DMR methylation defects are partial, they may cause ordinary abortion or may be sufficiently mild so as to allow normal pregnancy rather than cause molar pregnancy [21]. In fact, patients with *NLRP7* missense mutations have a mixed reproductive history of molar pregnancy and abortion or normal pregnancy [23]. Thus, some unexplained cases of infertility might be attributed to such stochastic epigenetic aberrations.

The NLR family proteins have roles in inflammation and apoptosis [24]. *NLRP7* is involved in the secretion of IL-1β [25–27], but there is no direct evidence that perturbations to the NLRP7-IL-1β axis cause loss of DNA methylation and molar pregnancy. Since *NLRP7* is present in oocytes [16] and preimplantation embryos [28], it could be involved in the hypomethylation of DMRs observed in the villi of RHMs. However, because *NLRP7* has no ortholog in mice [24], evaluation of its function in oogenesis and early embryogenesis is challenging. Therefore, identification of genetic and/or epigenetic mutations in isolated cases and in different genetic backgrounds remains an important aspect of studies designed to unravel the mechanisms underlying RHM pathogenesis.

In conclusion, we have, for the first time, identified a novel nonsense homozygous mutation of *NLRP7* in a Japanese RHM patient. Our study is the first to report an isolated RHM case in a previously unreported ethnic background. This comprehensive genetic and epigenetic analysis approach can facilitate the definitive molecular diagnosis of diploid biparental RHM in isolated cases and can be performed using fragmented DNA extracted from formaldehyde-fixed and paraffin-embedded tissue samples. *NLRP7* mutations cause abnormal DNA methylation in DMRs [21]. However, the mechanisms underlying region-specific DNA methylation remain unknown. Further analysis of RHM will shed light on the unknown etiology of infertility and the mechanisms that control region-specific DNA methylation.

Acknowledgments

This research has been conducted using the National Central Biobank Network (NCBN), Japan.

Funding Sources

This study was supported by a grant from the Ministry of Health, Labor and Welfare, Japan (H26-082, H26-001, H25-001), the CREST Program of the Japan Science and Technology Agency (JST), a grant from the Ministry of Education, Culture, Sports, Sci-

ence and Technology (MEXT), Japan (grant numbers: 26670734, 26293365), and a grant from the National Center for Child Health and Development (NCCHD), Japan (26-13). The study sponsors had no involvement in study design, in the collection, analysis and interpretation of data, in the writing of the report and in the decision to submit the report for publication.

Disclosure Statement

None to declare.

References

1 Kajii T, Ohama K: Androgenetic origin of hydatidiform mole. Nature 1977;268:633–634.
2 Sánchez-Ferrer ML, Hernández-Martínez F, Machado-Linde F, Ferri B, Carbonel P, Nieto-Diaz A: Uterine rupture in twin pregnancy with normal fetus and complete hydatidiform mole. Gynecol Obstet Invest 2014;77:127–133.
3 Murdoch S, Djuric U, Mazhar B, Seoud M, Khan R, Kuick R, Bagga R, Kircheisen R, Ao A, Ratti B, Hanash S, Rouleau GA, Slim R: Mutations in NALP7 cause recurrent hydatidiform moles and reproductive wastage in humans. Nat Genet 2006;38:300–302.
4 Parry DA, Logan CV, Hayward BE, Shires M, Landolsi H, Diggle C, Carr I, Rittore C, Touitou I, Philibert L, Fisher RA, Fallahian M, Huntriss JD, Picton HM, Malik S, Taylor GR, Johnson CA, Bonthron DT, Sheridan EG: Mutations causing familial biparental hydatidiform mole implicate c6orf221 as a possible regulator of genomic imprinting in the human oocyte. Am J Hum Genet 2011;89:451–458.
5 Nguyen NM, Slim R: Genetics and epigenetics of recurrent hydatidiform moles: basic science and genetic counselling. Curr Obstet Gynecol Rep 2014;3:55–64.
6 Matsui H, Iitsuka Y, Suzuka K, Seki K, Sekiya S: Subsequent pregnancy outcome in patients with spontaneous resolution of HCG after evacuation of hydatidiform mole: comparison between complete and partial mole. Hum Reprod 2001;16:1274–1277.
7 Matsui H, Iitsuka Y, Yamazawa K, Tanaka N, Seki K, Sekiya S: Changes in the incidence of molar pregnancies. A population-based study in Chiba prefecture and Japan between 1974 and 2000. Hum Reprod 2003;18:172–175.
8 Judson H, Hayward BE, Sheridan E, Bonthron DT: A global disorder of imprinting in the human female germ line. Nature 2002;416:539–542.
9 Kou YC, Shao L, Peng HH, Rosetta R, del Gaudio D, Wagner AF, Al-Hussaini TK, Van den Veyver IB: A recurrent intragenic genomic duplication, other novel mutations in NLRP7 and imprinting defects in recurrent biparental hydatidiform moles. Mol Hum Reprod 2008;14:33–40.
10 Kaneki E, Kobayashi H, Hirakawa T, Matsuda T, Kato H, Wake N: Incidence of postmolar gestational trophoblastic disease in androgenetic moles and the morphological features associated with low risk postmolar gestational trophoblastic disease. Cancer Sci 2010;101:1717–1721.
11 Li C, Qiao B, Zhan Y, Peng W, Chen ZJ, Sun L, Zhang J, Zhao L, Gao Q: Association between genetic variations in MTNR1A and MTNR1B genes and gestational diabetes mellitus in Han Chinese women. Gynecol Obstet Invest 2013;76:221–227.
12 Hayward BE, De Vos M, Talati N, Abdollahi MR, Taylor GR, Meyer E, Williams D, Maher ER, Setna F, Nazir K, Hussaini S, Jafri H, Rashid Y, Sheridan E, Bonthron DT: Genetic and epigenetic analysis of recurrent hydatidiform mole. Hum Mutat 2009;30:E629–E639.
13 Clark SJ, Harrison J, Paul CL, Frommer M: High sensitivity mapping of methylated cytosines. Nucleic Acids Res 1994;22:2990–2997.
14 Meyer E, Lim D, Pasha S, Tee LJ, Rahman F, Yates JR, Woods CG, Reik W, Maher ER: Germline mutation in NLRP2 (NALP2) in a familial imprinting disorder (Beckwith-Wiedemann Syndrome). PLoS Genet 2009;5:e1000423.
15 Li X, Ito M, Zhou F, Youngson N, Zuo X, Leder P, Ferguson-Smith AC: A maternal-zygotic effect gene, zfp57, maintains both maternal and paternal imprints. Dev Cell 2008;15:547–557.
16 Wang CM, Dixon PH, Decordova S, Hodges MD, Sebire NJ, Ozalp S, Fallahian M, Sensi A, Ashrafi F, Repiska V, Zhao J, Xiang Y, Savage PM, Seckl MJ, Fisher RA: Identification of 13 novel NLRP7 mutations in 20 families with recurrent hydatidiform mole; missense mutations cluster in the leucine-rich region. J Med Genet 2009;46:569–575.
17 Moglabey YB, Kircheisen R, Seoud M, El Mogharbel N, Van den Veyver I, Slim R: Genetic mapping of a maternal locus responsible for familial hydatidiform moles. Hum Mol Genet 1999;8:667–671.
18 Helwani MN, Seoud M, Zahed L, Zaatari G, Khalil A, Slim R: A familial case of recurrent hydatidiform molar pregnancies with biparental genomic contribution. Hum Genet 1999;105:112–115.
19 Fisher RA, Khatoon R, Paradinas FJ, Roberts AP, Newlands ES: Repetitive complete hydatidiform mole can be biparental in origin and either male or female. Hum Reprod 2000;15:594–598.
20 Rabbani B, Tekin M, Mahdieh N: The promise of whole-exome sequencing in medical genetics. J Hum Genet 2014;59:5–15.
21 El-Maarri O, Seoud M, Coullin P, Herbiniaux U, Oldenburg J, Rouleau G, Slim R: Maternal alleles acquiring paternal methylation patterns in biparental complete hydatidiform moles. Hum Mol Genet 2003;12:1405–1413.
22 Henckel A, Nakabayashi K, Sanz LA, Feil R, Hata K, Arnaud P: Histone methylation is mechanistically linked to DNA methylation at imprinting control regions in mammals. Hum Mol Genet 2009;18:3375–3383.
23 Deveault C, Qian JH, Chebaro W, Ao A, Gilbert L, Mehio A, Khan R, Tan SL, Wischmeijer A, Coullin P, Xie X, Slim R: NLRP7 mutations in women with diploid androgenetic and triploid moles: a proposed mechanism for mole formation. Hum Mol Genet 2009;18:888–897.
24 Tian X, Pascal G, Monget P: Evolution and functional divergence of NLRP genes in mammalian reproductive systems. BMC Evol Biol 2009;9:202.
25 Kinoshita T, Wang Y, Hasegawa M, Imamura R, Suda T: PYPAF3, a PYRIN-containing APAF-1-like protein, is a feedback regulator of caspase-1-dependent interleukin-1beta secretion. J Biol Chem 2005;280:21720–21725.
26 Messaed C, Akoury E, Djuric U, Zeng J, Saleh M, Gilbert L, Seoud M, Qureshi S, Slim R: NLRP7, a nucleotide oligomerization domain-like receptor protein, is required for normal cytokine secretion and co-localizes with Golgi and the microtubule-organizing center. J Biol Chem 2011;286:43313–43323.
27 Khare S, Dorfleutner A, Bryan NB, Yun C, Radian AD, de Almeida L, Rojanasakul Y, Stehlik C: An NLRP7-containing inflammasome mediates recognition of microbial lipopeptides in human macrophages. Immunity 2012;36:464–476.
28 Zhang P, Dixon M, Zucchelli M, Hambiliki F, Levkov L, Hovatta O, Kere J: Expression analysis of the NLRP gene family suggests a role in human preimplantation development. PLoS One 2008;3:e2755.

Research article

Journal of Applied Toxicology

Received: 22 January 2015, Revised: 13 February 2015, Accepted: 17 February 2015 Published online in Wiley Online Library: 30 March 2015

(wileyonlinelibrary.com) DOI 10.1002/jat.3149

Augmenting effects of gestational arsenite exposure of C3H mice on the hepatic tumors of the F_2 male offspring via the F_1 male offspring

Keiko Nohara[a]*, Kazuyuki Okamura[a], Takehiro Suzuki[a], Hikari Murai[a], Takaaki Ito[b], Keiko Shinjo[c], Shota Takumi[d], Takehiro Michikawa[a], Yutaka Kondo[c] and Kenichiro Hata[e]

ABSTRACT: Gestational exposure can affect the F_2 generation through exposure of F_1 germline cells. Previous studies reported that arsenite exposure of only F_0 females during their pregnancy increases hepatic tumors in the F_1 males in C3H mice, whose males are predisposed spontaneously to develop hepatic tumors later in life. The present study addressed the effects of gestational arsenite exposure on tumorigenesis of the F_2 males in C3H mice. Expression analysis of several genes in the normal livers at 53 and 80 weeks of age clearly showed significant changes in the F_2 males obtained by crossing gestational arsenite-exposed F_1 (arsenite-F_1) males and females compared to the control F_2 males. Some of the changes were shown to occur in a late-onset manner. Then the tumor incidence was assessed at 75–82 weeks of age in the F_2 males obtained by reciprocal crossing between the control and arsenite-F_1 males and females. The results demonstrated that the F_2 males born to arsenite-F_1 males developed tumors at a significantly higher rate than the F_2 males born to the control F_1 males, irrespective of exposure of F_1 females. Gene expressions of hepatocellular carcinoma markers β-catenin (CTNNB1) and interleukin-1 receptor antagonist in the tumors were significantly upregulated in the F_2 males born to arsenite-F_1 males compared to those born to the control F_1 males. These results show that arsenite exposure of only F_0 pregnant mice causes late-onset changes and augments tumors in the livers of the F_2 males by affecting the F_1 male offspring. Copyright © 2015 John Wiley & Sons, Ltd.

Keywords: arsenic; gestational exposure; hepatic tumor; transgenerational; gene expression

Introduction

Gestation is known to be vulnerable to a variety of environmental conditions, including chemical exposure and nutritional imbalances, and the adverse effects of environmental conditions in this period can lead to a number of adult-onset diseases in the F_1 offspring and in subsequent multiple generations (Aiken and Ozanne, 2014; Guerrero-Bosagna and Skinner, 2012; Perera and Herbstman, 2011). A possible causative route of the effects on the F_2 and subsequent generations by gestational chemical exposure is through direct exposure of germline cells in the F_1 fetuses and the responsible germ cells can be those of male, female, or both (Aiken and Ozanne, 2014; Guerrero-Bosagna and Skinner, 2012; Perera and Herbstman, 2011).

Naturally occurring inorganic arsenic, which is known as a human carcinogen, is causing serious health problems, including cancer, in many areas in the world (Hughes *et al*., 2011). Although animal models are pivotal to elucidate the mechanism of arsenic toxicity, it has been difficult to verify the carcinogenicity of arsenic in rodents (Rossman *et al*., 2002). Pioneering studies by Waalkes and colleagues showed that exposure of pregnant C3H mice (F_0) from gestational day (GD) 8–18 to inorganic arsenite results in an increase in tumors in the liver and adrenal gland of their F_1 male offspring at 74 weeks of age (Waalkes *et al*., 2003). As male C3H mice are predisposed to spontaneously develop hepatic tumors in adulthood (Köhle *et al*., 2008; Maronpot *et al*., 1995), the finding by Waalkes and colleagues supports the notion that arsenic acts in combination with other tumor promoting factors or dispositions (Klein *et al*., 2007). The results obtained by Waalkes *et al*. (2003) also indicate that gestation is a vulnerable period for arsenic carcinogenicity. Epidemiological studies have reported that gestational exposure to arsenite is associated with increased cancers in adulthood (Smith *et al*., 2006; Yuan *et al*., 2010). These findings on the sensitivity of gestational period against arsenic imply the possibility that gestational arsenic exposure may also affect F_1 germline cells and have an impact on late-onset tumorigenesis in the F_2 and subsequent generations, while those issues have not been addressed.

*Correspondence to: Keiko Nohara, Center for Environmental Health Sciences, National Institute for Environmental Studies, Tsukuba 305-8506, Japan.
E-mail: keikon@nies.go.jp

[a]Center for Environmental Health Sciences, National Institute for Environmental Studies, Tsukuba, Japan

[b]Department of Pathology and Experimental Medicine, Kumamoto University Graduate School of Medical Sciences, Kumamoto, Japan

[c]Department of Epigenomics, Nagoya City University Graduate School of Medical Sciences, Nagoya, Japan

[d]Department of Public Health and Environmental Medicine, The Jikei University School of Medicine, Tokyo, Japan

[e]Department of Maternal-Fetal Biology, National Research Institute for Child Health and Development, Tokyo, Japan

We previously investigated the causal factors of hepatic tumor augmentation in the F_1 male offspring by gestational arsenite exposure in the experimental model reported by Waalkes *et al.* (2003) Nohara *et al.*, 2012). The results showed several characteristic changes, such as late-onset gene expression changes in the normal livers and an increase in hepatic tumors, particularly those having a C to A somatic mutation at codon 61 in oncogene Ha-*ras*, in the F_1 offspring by gestational arsenite exposure (Nohara *et al.*, 2012). In the present study, we addressed the effects of gestational arsenite exposure on the F_2 males of C3H mice by investigating gene expression changes in the normal livers, the hepatic tumor incidence, and the incidence of Ha-*ras* mutation at codon 61 in the tumors. In the assessment of tumor incidence, we performed a reciprocal crossing experiment between the control and arsenite-F_1 males and females to clarify the F_1 sex responsible for the tumor augmentation in the F_2 males. We also measured gene expression of several human hepatocellular carcinoma markers in the tumors of the F_2 males for confirmation of the tumor augmenting effects of gestational arsenite exposure.

The results of the present study made the novel findings on the tumor augmenting effects of gestational arsenite exposure on the F_2 generation.

Materials and methods

Design of Animal Experiments

Pregnant C3H/HeN mice (F_0) were purchased from CLEA Japan (Tokyo, Japan) and given free access to a standard diet (CA-1; CLEA Japan) and tap water (control mice) or tap water containing 85 ppm sodium arsenite (Sigma, St. Louis, MO, USA) from day 8 to 18 of gestation as described previously (Nohara *et al.*, 2012). Throughout the experiments, arsenite was only given to F_0 pregnant mice and not to F_1 or F_2 mice. To assess the tumor incidence and the F_1 sex responsible for the F_2 tumor augmentation, we did a reciprocal crossing experiment among the control F_1 males and females and arsenite-F_1 males and females, which originated from 22 control F_0 females and 29 arsenite-F_0 females. Male and female mice were mated at 10 weeks of age. The resulting F_2 males were reared until 75–82 weeks (17.5–19 months) of age and used for the assessment. Hepatic tumors were examined macroscopically (Nohara *et al.*, 2012) and some were subjected to histological analysis as described below.

The animals were handled in accordance with the National Institute for Environmental Studies guidelines for animal experiments.

Histological Analysis

Sections prepared from paraffin-embedded liver tissues were stained with hematoxylin and eosin as previously described (Nohara *et al.*, 2012). The histology of the liver neoplasms was classified as hepatocellular adenoma or hepatocellular carcinoma. Briefly, hepatocellular adenoma is characterized by a well-circumscribed lesion composed of well-differentiated hepatocytes, and hepatocellular carcinoma is characterized by an abnormal growth pattern and both cytological and nuclear atypia (Harada *et al.*, 1999).

cDNA Preparation and Real-Time Polymerase Chain Reaction

Total RNA of individual livers was prepared with an RNeasy Mini Kit (Qiagen, Valencia, CA, USA). After checking the quality of the RNA by electrophoresis, reverse transcription reactions were performed with an AMV Reverse Transcriptase XL (TaKaRa Bio, Shiga, Japan) using 100 ng of total RNA. Quantitative real-time polymerase chain reaction (PCR) analysis was performed on a LightCycler 480 instrument, version 1.5 (Roche Diagnostics, Basel, Switzerland) as described previously (Nohara *et al.*, 2006). The primer sequences and annealing temperatures used for real-time PCR are shown in Table 1.

Ha-*ras* Mutation

Ha-*ras* mutations at codon 61 were analyzed by the pyrosequencing method (Ogino *et al.*, 2005). The DNA region containing the sequence coding codon 61 in the Ha-*ras* gene was amplified by PCR using the biotinylated primers (5′-cggaaacaggtggtcattgat-3′ and biotin-5′-tgatggcaaatacacagaggaag-3′) and a PyroMark PCR kit (Qiagen). Amplification was achieved by heating at 95 °C for 5 min, cycling at 95 °C for 30 s, 55 °C for 30 s and 72 °C for 45 s, and was followed by extension at 72 °C for 10 min after the final cycle. The biotinylated PCR product was captured on streptavidin-coated beads (GE Healthcare Bio-Science, Little Chalfont, UK), denatured and washed. The sequence primer for codon 61 (5′-ggacatcttagacacagca-3′) was annealed to the biotinylated PCR product and pyrosequencing analysis was performed by using a

Table 1. Primers for real-time polymerase chain reaction analysis

Gene	Forward primer 5′-3′	Reverse primer 5′-3′	Annealing temp. (°C)
Creld2	gcagacagcagaaggcaaa	tgcccgtcacaaatcctc	60
Slc25a30	gaacgcccagaagatgaaac	ctgttctgtgcttgcattcg	60
Ell3	ccagaaacgcctggacaa	cttgaggctagaggcagagc	64
Fabp4	cagcctttctcacctggaag	ttgtggcaaagcccactc	60
Gpat-1	agcaagtcctgcgctatcat	ctcgtgtgggtgattgtgac	64
Afp	cccaaccttcctgtctcagt	tggctctcctcgatgtgttt	64
Il-1rn	tgcacaacactagaggctga	agtgatcaggcagttggtga	64
Ctnnb1	ccctgagacgctagatgagg	tgtcagctcaggaattgcac	64
Cpb	agactgttccaaaaacagtgga	gatgctctttcctcctgtgc	64
rRNA	tgcgaatggctcattaaatcagtt	ccgtcggcatgtattagctctag	64

Journal of Applied Toxicology

PyroMark Q96 ID system (Qiagen) and PyroMark Q96 ID Software 2.5 (Qiagen) according to the manufacturer's instructions.

Western Blotting

Tissues were homogenized in ice-cold lysis buffer (1% Triton X-100, 0.1% sodium dodecyl sulfate [SDS], 0.5% deoxycholic acid, 1 mM EDTA, 1 mM EGTA, 2.5 mM sodium pyrophosphate, 1 mM β-glycerophosphate, 1 mM sodium orthovanadate, 1 mM phenylmethylsulfonyl fluoride, 50 mM Tris–HCl [pH 7.5] and 150 mM NaCl) with a pellet mixer and then with a Bioruptor UCD-200TM (Cosmo Bio, Tokyo, Japan). The supernatant was boiled with the same volume of × 2 SDS sample buffer (100 mM Tris–HCl [pH 6.8], 4% SDS, 20% glycerol, 200 mM DTT, 0.002% bromophenol blue), and subjected to SDS-polyacrylamide gel electrophoresis. The first antibodies used were anti-p44/42 MAPK (Cell Signaling Technology, Danvers, MA, USA; 9102), anti-phospho-p44/42 MAPK (Cell Signaling Technology; 9101) and anti-β-actin (Sigma; A5441). The second antibodies were horseradish peroxidase-conjugated anti-rabbit IgG (Sigma) and antimouse IgG (Sigma). The membranes were developed using the ECL Prime Western Blotting Detection System (GE Healthcare) and the images were captured using a VersaDoc imaging system (Bio Rad, Hercules, CA, USA).

Statistical Analysis

The difference in the tumor incidence between the two groups was analyzed by a chi-squared test. The difference in gene expression between the two groups was analyzed by Student's *t*-test. Those analyses were conducted with Stata11 (Stata Corporation, College Station, TX, USA).

Results

Late-Onset Gene Expression Changes Detected in the Normal Liver of the F_2 Generation

Analyses of mouse livers with Affymetrix GeneChips in our previous study showed that expression of two genes, *Creld2* and *Slc25a30*, was upregulated more than twofold and expression of another two genes, *Fabp4* and *Ell3*, was downregulated more than twofold in the normal livers of arsenite-F_1 males in comparison with those of the control males at 74 weeks of age (Nohara *et al.*, 2012). The expression changes of these genes were found to occur in an adult-onset manner (Nohara *et al.*, 2012). To examine whether arsenite exposure of F_0 pregnant mice has any effect on the F_2 offspring, we measured the expression of these four genes in the normal livers of the control F_2 males and the F_2 males obtained by crossing arsenite-F_1 males and females (arsenite-F_2) at 53 weeks and 80 weeks of age.

The results of the measurements showed significant downregulation of *Creld2* from 53 weeks of age and late-onset downregulation of *Slc25a30* at 80 weeks of age in arsenite-F_2 males in comparison with the control F_2 males. On the other hand, those genes were upregulated in arsenite-F_1 males in comparison with the control F_1 males at 49 and/or 74 weeks of age. Thus, direction of the changes by gestational arsenite exposure in the arsenite-F_1 and arsenite-F_2 males was the opposite (Fig. 1). Expression of *Ell3* was significantly upregulated in arsenite-F_2 males in comparison

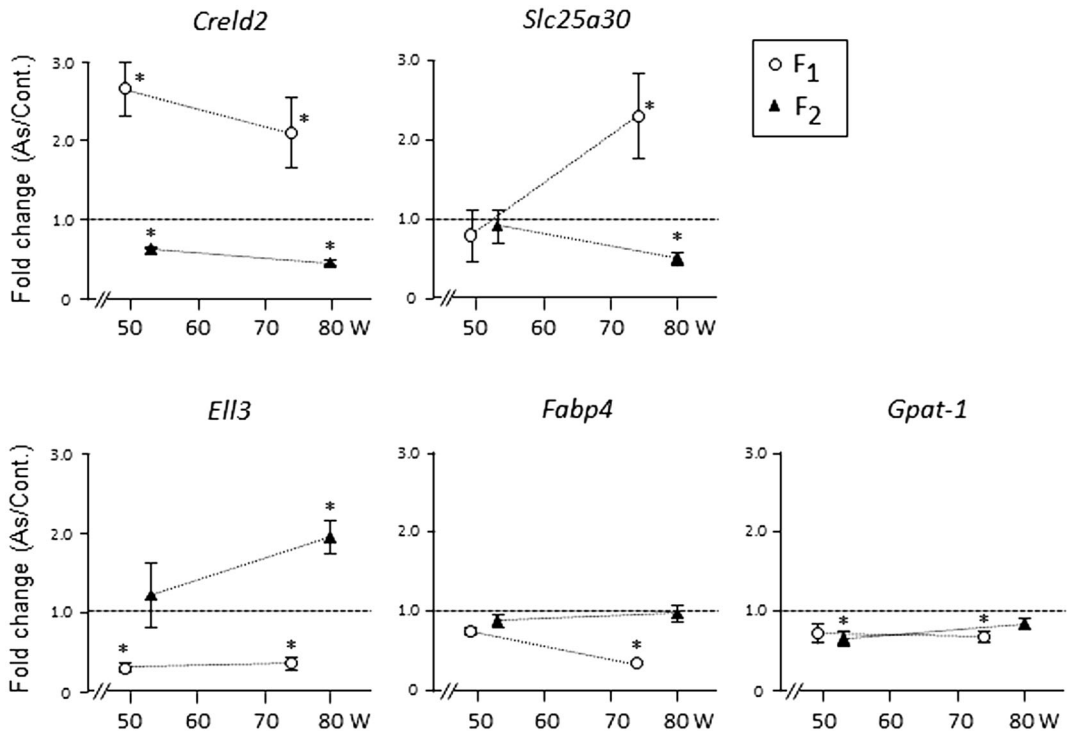

Figure 1. The changes in hepatic gene expression in the arsenite-F_1 males and arsenite-F_2 males in comparison with their control males. The expressions of five genes in the livers of the control F_2 males and arsenite-F_2 males were measured by real-time polymerase chain reaction at 53 weeks of age ($n = 4$ in each group) and 80 weeks of age ($n = 6$ in each group) and normalized to expression of *Cpb*. For the gene expressions in the F_1 generation, data obtained at 49 weeks of age ($n = 4$ in each group) and 74 weeks of age ($n = 8$ in each group) in our previous study (Nohara *et al.*, 2012) were used. The graphs show the ratios of the expression in the arsenite-exposed group normalized to the expression in the control group. The error bar shows the standard error. *Significant difference ($P < 0.05$) between the offspring of the control females and the offspring of the arsenite-exposed females.

with the control F_2 males also in a late-onset manner. The effect of gestational arsenite exposure on *Ell3* expression in the F_2 males was again the opposite of its effect in the F_1 males. Downregulation of *Fabp4*, which was detected in the arsenite-F_1 males, was not detected in the F_2 generation (Fig. 1).

In our previous study, we also observed downregulation of a lipid metabolism-related gene *Gpat-1* at 74 weeks of age in the normal livers of arsenite-F_1 males in comparison with the control males (Nohara *et al.*, 2012). This gene was downregulated in arsenite-F_2 males in comparison with the control F_2 males at 53 weeks of age (Fig. 1).

These changes in gene expression clearly showed significant effects of gestational arsenite exposure on the F_2 males, and the effects on the F_1 and the F_2 were varied.

Increased Hepatic Tumors in the F_2 Males Born to the Arsenite-F_1 Males

We performed the reciprocal crossing experiment with the control and arsenite-F_1 males and females as shown in Fig. 2 to assess the effects of gestational arsenite exposure on tumorigenesis in the F_2 males and determine the F_1 sex responsible for the F_2 tumor augmentation.

The tumor incidences in each F_2 group were 33.8% in CC, 34.3% in CA, 49.2% in AC and 43.6% in AA (Fig. 2A). Comparison of the tumor incidence between the F_2 male offspring of arsenite-F_1 males (AC and AA) and the control F_1 males (CC and CA) showed a significantly higher tumor incidence in the F_2 offspring of arsenite-F_1 males (45.9% in AC and AA vs 34.1% in CC and CA) (Fig. 2B). On the other hand, the tumor incidence of the F_2 male offspring of arsenite-F_1 females (39.9% in CA and AA) and the control F_1 females (41.1% in CC and AC) were not different (Fig. 2B). These results showed that the tumor-augmenting effect of gestational arsenite exposure is transmitted to the F_2 males via the F_1 male offspring, but not via the F_1 female offspring.

Pathological examination of tumor tissues from the control F_2 and arsenite-F_2 males (10 samples from each group) showed that hepatocellular adenoma was the predominant histological tumor type (Fig. 3). This finding was consistent with the observation of the hepatic tumors of the control mice and arsenite-F_1 mice in our previous study (Nohara *et al.*, 2012).

Ha-*ras* Mutation in the Tumors of the F_2 Generation

Our previous study showed that gestational arsenite exposure particularly increased the percentage of hepatic tumors containing

A)

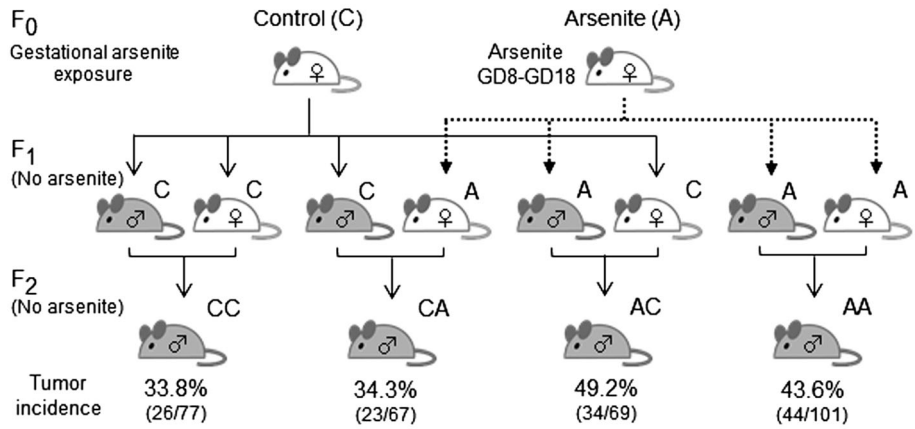

B)

Comparison to assess the F_1 sex responsible for the F_2 tumor augmentation

	Tumor incidence		p value
F_2 group	Offspring of control F_1 male (CC, CA)	Offspring of arsenite-F_1 male (AC, AA)	
	34.1% (49/144)	45.9% (78/170)	0.033
F_2 group	Offspring of control F_1 female (CC, AC)	Offspring of arsenite-F_1 female (CA, AA)	
	41.1% (60/146)	39.9% (67/168)	0.827

Figure 2. Increase in the tumor incidence in the F_2 male offspring born to arsenite-F_1 males but not to arsenite-F_1 females. (A) The F_2 males were obtained by reciprocally crossing the control and arsenite-F_1 males and females as shown in the figure. The F_2 mice were macroscopically examined for hepatic tumors at 75–82 weeks of age I n an age-matched manner. Small lesions (≤1 mm in diameter) were omitted. The number in parenthesis is that of mice bearing hepatic tumors/the number of mice investigated. (B) The difference between the tumor incidences in the two groups was analyzed by chi-squared test. GD, gestational day.

Journal of AppliedToxicology

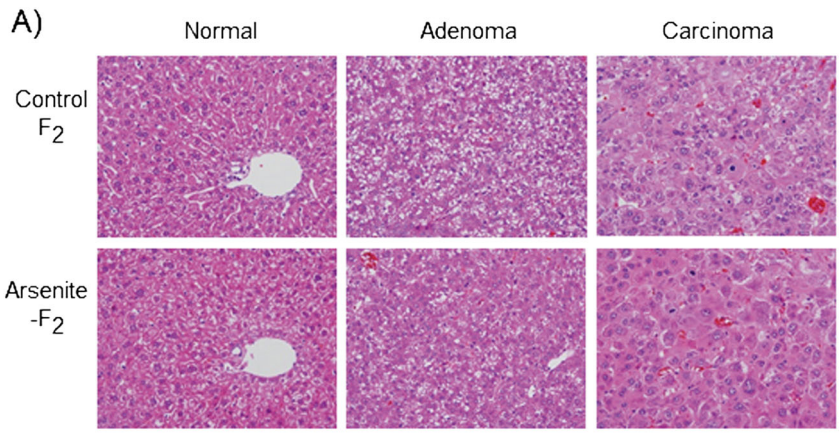

B)

Occurrence of hepatocellular adenoma and hepatocellular carcinoma

	Number of tumors	
	Adenoma	Carcinoma
Control F_2 (n=10)	8	2
Arsenite-F_2 (n=10)	7	3

Figure 3. Histological analysis of the hepatic tumors of the control and arsenite-F_2 males. (A) Representative sections of hepatocellular adenoma and hepatocellular carcinoma of the control F_2 males and arsenite-F_2 males. (B) Occurrence of hepatocellular adenoma and hepatocellular carcinoma.

the Ha-*ras* C61A somatic mutation in the F_1 males (Nohara *et al.*, 2012). Ha-*ras* mutation is thought to be involved in carcinogenesis by activating several signaling pathways, including the RAF/MEK/ERK cascade (Pylayeva-Gupta *et al.*, 2011). The investigation in the present study confirmed that the Ha-*ras* mutations increase the activating phosphorylated forms of ERKs, ERK1 (p44 MAPK) and ERK2 (p42 MAPK) in the tumor tissues harboring codon 61 Ha-*ras* mutations in both the control F_2 males and arsenite-F_2 males (Fig. 4A). p44/p42 MAPK was shown to be hypophosphorylated in the non-tumor tissues of tumor-bearing livers, which do not contain mutated Ha-*ras* (Fig. 4B).

On the other hand, Ha-*ras* C61A mutation or the total Ha-*ras* mutations in codon 61 in the tumor tissues was shown not to be increased in the F_2 males born to arsenite-F_1 males (AC and AA) in comparison with the F_2 males born to the control males (CC and CA) (Table 2). Thus, the existence of Ha-*ras* mutations seems not to be the major causation of the increased hepatic tumor incidence in the F_2 males born to arsenite-F_1 males.

Upregulation of Cancer Related Genes in the Tumor Tissues of F_2 Males Born to the Arsenite-F_1 Males

In an effort to establish early diagnostic markers for detecting human hepatocellular carcinoma, increases in several serum proteins, including α-fetoprotein, β-catenin (CTNNB1) and interleukin-1 receptor antagonist (IL1-RN), were shown to be closely associated with hepatocellular carcinoma (Sun *et al.*, 2008). The expression of those genes was shown to be higher in the tumor tissues compared to the normal tissues or the non-tumor tissues of tumor-bearing livers, while the expression of *Afp* is varied widely among samples (Fig. 5). The expressions of *Ctnnb1* and *Il1rn* genes were significantly higher in the F_2 males born to arsenite-F_1 males (AC and AA) than those born to the control males (CC and CA) (Fig. 5).

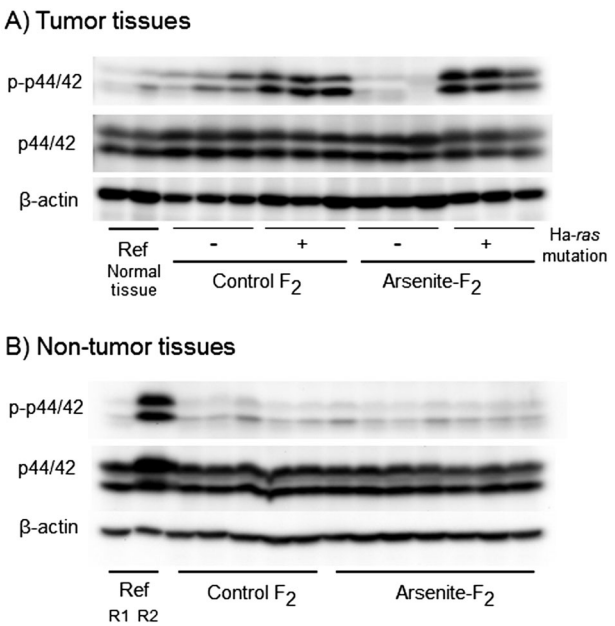

Figure 4. p44/42 MAP kinases activation as a result of Ha-*ras* mutation in the hepatic tumors of C3H males. Western blots of hepatic tumor tissues (A) and non-tumor tissues in the tumor-bearing livers (B) of the control F_2 and arsenite-F_2 males were prepared as described in the Materials and methods section. Labels in (B) are R1, normal tissue and R2, tumor tissue with a Ha-*ras* mutation.

Interestingly, when the gene expression was assessed separately in tumor tissues with and without Ha-*ras* mutation, the expression of *Il-1rn* seemed to be upregulated by Ha-*ras* mutation (Fig. 5).

Table 2. Spectra of Ha-*ras* codon 61 mutations in the hepatic tumors of the F_2 males

F_2 group (*n*)		Ha-*ras* codon 61 type (%)			
		CAA wild-type	AAA	CTA	CGA
CC	(29)	31	41	7	7
CA	(33)	61	18	3	3
AC	(34)	38	35	3	3
AA	(49)	39	45	6	6

The hepatic tumor tissues were obtained in the reciprocal crossing experiment (Fig. 2) and analyzed for mutations in Ha-*ras* codon 61 by a pyrosequencing method.

Discussion

The earliest studies carried out primarily in the middle 1900s reported that maternal exposure or germ cell exposure to radiation and some carcinogenic chemicals transgenerationally affect the susceptibility of the progeny to cancer (Tomatis, 1994). The transgenerational effects of radiation, chemicals and nutritional imbalances on cancers and other disorders have been reported to be transmitted paternally, maternally, or both paternally and maternally (Aiken and Ozanne, 2014; Anway *et al.*, 2005; Barber *et al.*, 2002; Mohamed *et al.*, 2010; Tomatis, 1994). The individual molecular mechanisms of the transmission are yet to be clarified.

The present study showed that gestational arsenite exposure of pregnant C3H mice from GD8 to GD18 increases the incidence of hepatic tumors in the F_2 males born to arsenite-F_1 males (AC and AA in Fig. 2) compared to the F_2 males born to the control males (CC and CA in Fig. 2), irrespective of exposure of the F_1 females. These results showed that tumor augmenting effects by gestational arsenite exposure is transmitted to the F_2 males through the F_1 males. We also detected significant late-onset changes in gene expression in the normal livers of arsenite-F_2 (AA F_2) males compared to those of the control F_2 males (Fig. 1), indicating that transient gestational arsenite exposure of pregnant females causes a significant impact on the F_2 generation. Furthermore, the cancer-related genes *Ctnnb1* and *Il1rn* were shown to be upregulated in the hepatic tumors of the F_2 males born to arsenite-F_1 males (AC and AA) compared to those born to the control males (CC and CA) (Fig. 5). These results show the augmenting effects of gestational arsenite exposure on the hepatic tumors of the F_2 male offspring.

The F_1 male fetuses in the present study were exposed from GD8 to GD18, when the primordial germ cells appear and differentiate into the sperm precursor cells (Sasaki and Matsui, 2008). The epigenetic profile of the primordial germ cells undergoes dynamic alterations, including imprint erasure, during the development stage, and disruption of the epigenetic profile during this stage has been implicated in transgenerational effects of F_0 gestational exposure (Aiken and Ozanne, 2014; Guerrero-Bosagna and Skinner, 2012; Perera and Herbstman, 2011). A previous study (Devesa *et al.*, 2006) reported the concentrations of inorganic arsenic and methylated arsenic at GD18 in the fetus organs, including

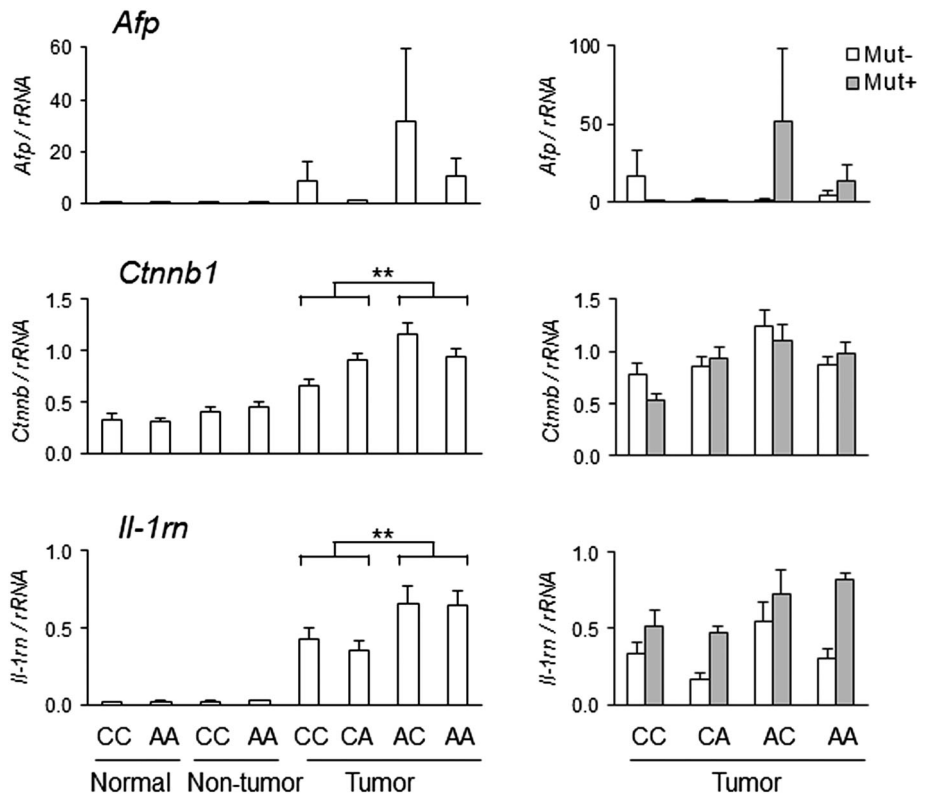

Figure 5. Expression of cancer-related genes in the hepatic tissues in the F_2 mice. The expressions of *Afp*, *Ctnnb* and *Il-1rn* were measured by real-time PCR for the normal livers ($n = 6$), non-tumor tissues from tumor-bearing livers ($n = 6$) and tumor tissues ($n = 9$–11) from the F_2 males and normalized to the expression of rRNA. The difference in the gene expressions in the tumor tissues between the F_2 males born to the control F_1 males (CC and CA) and those born to arsenite-F_1 males (CA and AA) was analyzed by Student's *t*-test. $^{**}P < 0.01$.

Journal of AppliedToxicology

the liver and blood in the same gestational arsenite exposure model of C3H mice we used. The study showed that fetus organs are directly exposed upon gestational arsenite exposure. As arsenic has been reported to induce epigenetic changes, particularly DNA methylation changes (Reichard and Puga, 2010; Ren *et al.*, 2011; Suzuki *et al.*, 2013), the gestational arsenite exposure may alter the phenotype of the F_2 generation by affecting the epigenetic profile of genes, possibly including imprinted genes, in the F_1 male germ cells.

Arsenic has been thought to be a weak mutagen or not a mutagen based on the results of assays using bacteria and mammalian cells *in vitro* (reviewed by Rossman, 2003). Our recent study using *gpt* delta transgenic mice clarified that arsenite exposure greatly increases the incidence of G:C to T:A transversion *in vivo* (Takumi *et al.*, 2014). Thus, mutation in the proliferating and differentiating primordial germ cells might be another possible causation of the F_2 effect by arsenite exposure of F_0 pregnant mice.

In the present study, we found that gestational arsenite exposure significantly affects hepatic expression of *Creld2*, *Slc25a30* and *Ell3* even in the F_2 generation, but the effect of the exposure was the opposite of its effect on the F_1 generation (Fig. 1). The difference seems to be attributable to the fact that exposure of the F_1 and F_2 mice occurred in a different manner, e.g., the fetal liver is directly exposed in the F_1 and F_2 is exposed at the germ cell stage. On the other hand, *Gpat-1* was significantly downregulated in the liver of the F_2 generation, as was also observed in the F_1 generation (Nohara *et al.*, 2012) (Fig. 1). *Gpat-1* is one of the target genes of sterol regulatory element-binding protein 1, a member of the central transcription factors that control intracellular cholesterol and fatty acid levels (Raghow *et al.*, 2008; Wendel *et al.*, 2010). Lipid accumulation in the liver has been implicated in hepatic carcinogenesis through an increase in oxidative stress (Ziech *et al.*, 2011). The change in *Gpat-1* expression in the liver of the F_1 and F_2 mice may indicate involvement of lipid metabolism changes in the increase in hepatic tumors.

We previously found a higher proportion of C61A Ha-*ras* mutation in the hepatic tumors of arsenite-F_1 males (Nohara *et al.*, 2012). In the present study, we confirmed that Ha-*ras* mutation increases activated forms of ERKs in the hepatic tumors of C3H mice (Fig. 4). However, the percentage of Ha-*ras* mutation in the tumors was not increased in the F_2 males born to arsenite-F_1 males (Table 2), which indicated that the tumor increase in the exposed F_2 males could not be attributed to the increase in Ha-*ras* codon 61 mutation 1.

In summary, we demonstrated the novel finding that gestational arsenite exposure of F_0 pregnant mice increases hepatic tumor incidence in the F_2 male offspring through the impact on the F_1 males. Further studies will be required to identify the factors that cause tumor augmentation in the liver of the F_2 generation by arsenite exposure of F_0 pregnant mice and to explore changes in the F_1 male germ cells that induce such tumor-augmenting factors in the liver of the F_2 generation.

Acknowledgments

We wish to thank Dr. A. Furuyama, Dr. Y. Aoki, Dr. H. Nitta (National Institute for Environmental Studies) and Dr. Kayo Ueda (Kyoto University) for their useful discussions, M. Owada and F. Ishitsuka for their excellent technical assistance and S. Itaki, Y. Yamazaki and S. Umehara for their helpful secretarial assistance. The authors also wish to thank the staff of the Animal Care Company (Tokyo, Japan) for their excellent assistance in the maintenance of mice. This study was partly supported by the National Institute for Environmental Studies (1115AA082; 1315AT001 KN), and Grant-in-Aid for Scientific Research (B) (no. 23390166, 26293154, KN) from the Ministry of Education, Culture, Sports, Science and Technology of Japan.

References

Aiken CE, Ozanne SE. 2014. Transgenerational developmental programming. *Hum. Reprod. Update* **20**: 63–75.

Anway MD, Cupp AS, Uzumcu M, Skinner MK. 2005. Epigenetic transgenerational actions of endocrine disruptors and male fertility. *Science* **308**: 1466–1469.

Barber R, Plumb MA, Boulton E, Roux I, Dubrova Y. 2002. Elevated mutation rates in the germ line of first- and second-generation offspring of irradiated male mice. *Proc. Natl. Acad. Sci. U. S. A.* **99**: 6877–6882.

Devesa V, Adair BM, Liu J, Waalkes MP, Diwan BA, Styblo M, Thomas DJ. 2006. Arsenicals in maternal and fetal mouse tissues after gestational exposure to arsenite. *Toxicology* **224**: 147–155.

Guerrero-Bosagna C, Skinner MK. 2012. Environmentally induced epigenetic transgenerational inheritance of phenotype and disease. *Mol. Cell. Endocrinol.* **354**: 3–8.

Harada T, Enomoto A, Boorman GA, Maronpot RR. 1999. Liver and gallbladder. In *Pathology of the Mouse*, Maronpot RR, Boorman GA, Gaul BW (eds). Cache River Express: St. Louis, MO; 119–183.

Hughes MF, Beck BD, Chen Y, Lewis AS, Thomas DJ. 2011. Arsenic exposure and toxicology: a historical perspective. *Toxicol. Sci.* **123**: 305–332.

Klein CB, Leszczynska J, Hickey C, Rossman TG. 2007. Further evidence against a direct genotoxic mode of action for arsenic-induced cancer. *Toxicol. Appl. Pharmacol.* **222**: 289–297.

Köhle C, Schwarz M, Bock KW. 2008. Promotion of hepatocarcinogenesis in humans and animal models. *Arch. Toxicol.* **82**: 623–631.

Maronpot RR, Fox T, Malarkey DE, Goldsworthy TL. 1995. Mutations in the ras proto-oncogene: clues to etiology and molecular pathogenesis of mouse liver tumors. *Toxicology* **101**: 125–156.

Mohamed el-SA, Song WH, Oh SA, Park YJ, You YA, Lee S, Choi JY, Kim YJ, Jo I, Pang MG. 2010. The transgenerational impact of benzo(a)pyrene on murine male fertility. *Hum. Reprod.* **25**: 2427–2433.

Nohara K, Ao K, Miyamoto Y, Ito T, Suzuki T, Toyoshiba H, Tohyama C. 2006. Comparison of the 2,3,7,8-tetrachlorodibenzo-p-dioxin (TCDD)-induced CYP1A1 gene expression profile in lymphocytes from mice, rats, and humans: most potent induction in humans. *Toxicology* **225**: 204–213.

Nohara K, Tateishi Y, Suzuki T, Okamura K, Murai H, Takumi S, Maekawa F, Nishimura N, Kobori M, Ito T. 2012. Late-onset increases in oxidative stress and other tumorigenic activities and tumors with a Ha-ras mutation in the liver of adult male C3H mice gestationally exposed to arsenic. *Toxicol. Sci.* **129**: 293–304.

Ogino S, Kawasaki T, Brahmandam M, Yan L, Cantor M, Namgyal C, Mino-Kenudson M, Lauwers GY, Loda M, Fuchs CS. 2005. Sensitive sequencing method for KRAS mutation detection by pyrosequencing. *J. Mol. Diagn.* **7**: 413–421.

Perera F, Herbstman J. 2011. Prenatal environmental exposures, epigenetics, and disease. *Reprod. Toxicol.* **31**: 363–373.

Pylayeva-Gupta Y, Grabocka E, Bar-Sagi D. 2011. RAS oncogenes: weaving a tumorigenic web. *Nat. Rev. Cancer* **11**: 761–774.

Raghow R, Yellaturu C, Deng X, Park EA, Elam MB. 2008. SREBPs: the crossroads of physiological and pathological lipid homeostasis. *Trends Endocrinol. Metab.* **19**: 65–73.

Reichard JF, Puga A. 2010. Effects of arsenic exposure on DNA methylation and epigenetic gene regulation. *Epigenomics* **2**: 87–104.

Ren X, McHale CM, Skibola CF, Smith AH, Smith MT, Zhang L. 2011. An emerging role for epigenetic dysregulation in arsenic toxicity and carcinogenesis. *Environ. Health Perspect.* **119**: 11–19.

Rossman TG. 2003. Mechanism of arsenic carcinogenesis: an integrated approach. *Mutat. Res.* **533**: 37–65.

Rossman TG, Uddin AN, Burns FJ, Bosland MC. 2002. Arsenite cocarcinogenesis: An animal model derived from genetic toxicology studies. *Environ. Health Perspect.* **110**: S749–S752.

Sasaki H, Matsui Y. 2008. Epigenetic events in mammalian germ-cell development: reprogramming and beyond. *Nat. Rev.* **9**: 129–140.

Smith AH, Marshall G, Yuan Y, Ferreccio C, Steinmaus C. 2006. Increased mortality from lung cancer and bronchiectasis in young adults after exposure to arsenic in utero and in early childhood. *Environ. Health Perspect.* **114**: 1293–1296.

Sun H, Chua MS, Yang D, Tsalenko A, Peter BJ, So S. 2008. Antibody arrays identify potential diagnostic markers of hepatocellular carcinoma. *Biomark. Insights* **3**: 1–18.

Suzuki T, Yamashita S, Ushijima T, Takumi S, Sano T, Michikawa T, Nohara K. 2013. Genome-wide analysis of DNA methylation changes induced by gestational arsenic exposure in liver tumors. *Cancer Sci.* **104**: 1575–1585.

Takumi S, Aoki Y, Sano T, Suzuki T, Nohmi T, Nohara K. 2014. *In vivo* mutagenicity of arsenite in the livers of *gpt* dalta transgenic mice. *Mutation Res.* **760**: 42–47.

Tomatis L. 1994. Transgenerational carcinogenesis: A review of the experimental and epidemiological evidence. *Jpn. J. Cancer Res.* **85**: 443–454.

Waalkes MP, Ward JM, Liu J, Diwan BA. 2003. Transplacental carcinogenicity of inorganic arsenic in the drinking water: induction of hepatic, ovarian, pulmonary, and adrenal tumors in mice. *Toxicol. Appl. Pharmacol.* **186**: 7–17.

Wendel AA, Li LO, Li Y, Cline GW, Shulman GI, Coleman RA. 2010. Glycerol-3-phosphate acyltransferase 1 deficiency in ob/ob mice diminishes hepatic steatosis but does not protect against insulin resistance or obesity. *Diabetes* **59**: 1321–1329.

Yuan Y, Marshall G, Ferreccio C, Steinmaus C, Liaw J, Bates M, Smith AH. 2010. Kidney cancer mortality: fifty-year latency patterns related to arsenic exposure. *Epidemiology* **21**: 103–108.

Ziech D, Franco R, Pappa A, Panayiotidis MI. 2011. Reactive oxygen species (ROS)-induced genetic and epigenetic alterations in human carcinogenesis. *Mutat. Res.* **711**: 167–173.

SCIENTIFIC REPORTS

OPEN

Increased epigenetic alterations at the promoters of transcriptional regulators following inadequate maternal gestational weight gain

Received: 11 February 2015
Accepted: 20 August 2015
Published: 29 September 2015

Tomoko Kawai[1], Takahiro Yamada[4], Kosei Abe[1], Kohji Okamura[2], Hiromi Kamura[1], Rina Akaishi[4], Hisanori Minakami[4], Kazuhiko Nakabayashi[3,*] & Kenichiro Hata[1,*]

Epigenetic modifications are thought to serve as a memory of exposure to *in utero* environments. However, few human studies have investigated the associations between maternal nutritional conditions during pregnancy and epigenetic alterations in offspring. In this study, we report genome-wide methylation profiles for 33 postpartum placentas from pregnancies of normal and foetal growth restriction with various extents of maternal gestational weight gain. Epigenetic alterations accumulate in the placenta under adverse *in utero* environments, as shown by application of Smirnov-Grubbs' outlier test. Moreover, hypermethylation occurs frequently at the promoter regions of transcriptional regulator genes, including polycomb targets and zinc-finger genes, as shown by annotations of the genomic and functional features of loci with altered DNA methylation. Aberrant epigenetic modifications at such developmental regulator loci, if occurring in foetuses as well, will elevate the risk of developing various diseases, including metabolic and mental disorders, later in life.

Foetal environmental factors, including maternal nutrition, hormonal disturbance, and chemical exposure, affect foetal growth and can cause birth defects. Recent studies have linked poor foetal growth to increased risks of coronary heart disease[1], type II diabetes[2,3], kidney disease[1,4], and brain disorders[5] in adulthood. Barker first proposed that nutritional conditions *in utero* may be responsible, at least in part, for the developmental programming of the foetus and placenta, potentially predisposing the individual to adult metabolic disease[6]. The concept that the foetal environment affects health later in life has been defined as the developmental origins of health and disease (DOHaD)[7], in which epigenetic modifications are thought to serve as a memory of exposure to *in utero* environments[8,9]. Epigenetic modifications, such as DNA methylation and histone modifications, are involved in tissue- and developmental stage-specific gene expression and silencing, and they can be transmitted in a stable manner through mitotic cell division, thereby inducing long-term changes in gene regulation. Developmental programming during the foetal period, therefore, could affect adult health through epigenetic mechanisms. In fact, many studies using animal models have demonstrated that nutrient manipulation during pregnancy induces epigenetic alterations at specific loci or globally in the offspring[10]. On the other hand, human studies showing associations of *in utero* conditions and epigenetic alterations have been relatively limited[11].

The predominant form of DNA methylation is methylation of cytosine in the context of CpG. The diploid human genome contains more than 10^8 cytosines, of which more than 10^7 are present in the context

[1]Department of Maternal-Fetal Biology, National Research Institute for Child Health and Development, Tokyo 157-8535, Japan. [2]Department of Systems BioMedicine, National Research Institute for Child Health and Development, Tokyo 157-8535, Japan. [3]Division of Developmental Genomics, National Research Institute for Child Health and Development, Tokyo 157-8535, Japan. [4]Department of Obstetrics and Gynecology, Hokkaido University Graduate School of Medicine, Sapporo 060-8638, Japan. *These authors contributed equally to this work. Correspondence and requests for materials should be addressed to T.K. (email: kawai-tm@ncchd.go.jp) or K.N. (email: nakabaya-k@ncchd.go.jp) or K.H. (email: hata-k@ncchd.go.jp)

of CpGs[12]. The genome-wide DNA methylation pattern in various types of cells in the body is bimodal, with the majority of CpG sites being highly methylated (>85%), while CpG islands (CGIs) are largely unmethylated (<10%). After fertilisation of the oocyte by sperm, the paternal genome becomes actively demethylated in the zygote, and the maternal genome undergoes passive demethylation until the early blastocyst stage[13]. DNA methylation patterns are re-established in a lineage-specific manner[14,15]. The genome in cells of the placenta remains relatively hypomethylated compared to that in somatic tissues. A genome-wide DNA methylation analysis of promoter regions in human placental tissues collected during the first, second, and third trimesters revealed that there is a significant increase in the average methylation level in autosomes from the second-trimester placenta to the full-term placenta[16]. Interindividual variations in DNA methylation levels have also been shown to increase during gestation[16]. Foetal environmental factors, such as maternal weight, maternal alcohol intake, maternal smoking, and maternal psychological stress, have recently been shown to affect DNA methylation in the human placenta[11,17,18]. However, compared to the number of studies that have examined the DNA methylation levels at repetitive sequences, such as long interspersed nuclear elements (LINEs) and short interspersed nuclear elements (SINEs), and at certain imprinted loci[19–21], studies evaluating the alterations in DNA methylation on the genome-wide scale in relation to the foetal environment have been limited[18,21–24].

Maternal gestational weight gain (GWG) influences the foetal nutritional environment during gestation. The Japan Ministry of Health, Labour, and Welfare recommends that women with a prepregnancy body mass index (BMI) between 18.5 and 25 should gain about 7–12 kg body weight during the gestational period. Excessive GWG has been reported to be associated with increased neonatal obesity during infancy and adulthood[25–27]. On the other hand, insufficient GWG is related to increased risk of low birth weight[28,29], which is known to be associated with metabolic syndrome, including impaired glucose tolerance, insulin resistance, and coronary heart disease, during adulthood[1–4]. Foetal growth restriction (FGR), which may be caused by foetal, placental, and/or maternal factors[30], is defined as a foetus that has not reached its growth potential (below the 10th percentile for gestational age).

In this study, we elucidate the effects of *in utero* environments on the human placental epigenome. To this end, we examine a collection of postpartum placentas using array-based genome-wide DNA methylation analysis and evaluate DNA methylation levels in placental tissues in relation to GWG and birth weight. We demonstrate that inadequate GWG perturbs the placental epigenome variably among subjects, and that such epigenetic alterations occur preferentially at the CGI promoters of genes encoding transcriptional factors. Therefore, our results demonstrate that epigenetic alterations accumulate in the placenta under adverse *in utero* environments, supporting the importance of appropriate *in utero* conditions and maternal health in foetal development.

Results

Alterations in placental DNA methylation were associated with FGR and GWG. We subjected placentas from 14 births exhibiting FGR and 19 births within the normal range of birth weight (Table 1) to genome-wide DNA methylation analysis, and assessed whether the FGR placentas contained CpG sites that were differentially methylated compared with the placentas with a birth weight within normal range. Wilcoxon rank-sum tests[31] did not detect any CpG sites as significantly differentially methylated between two groups (significance level = Benjamini–Hochberg [BH] adjusted p-value of 0.05). Comparisons of FGR and normal placentas within subgroups depending on maternal GWG (insufficient, adequate, and excessive) also did not detect any differentially methylated CpG sites in the FGR placentas (Supplementary Fig. 1). Next, we assessed whether placentas from subjects with excessive or insufficient maternal GWG contained CpG sites that were differentially methylated compared with those in placentas from subjects with adequate GWG. Four comparisons (i.e., insufficient versus adequate and excessive versus adequate within FGR and normal categories) did not detect any significantly differentially methylated CpG sites between two subgroups (Supplementary Fig. 1). These results suggested that no specific CpG sites showed consistent changes in DNA methylation associated with the FGR phenotype or inadequate maternal GWG in this study.

Next, we considered the possibility that the FGR phenotype and/or inadequate GWG may affect the placental epigenome in different ways among individual subjects rather than showing similar effects for all individuals within a group. To evaluate this possibility, we searched for CpG sites whose methylation level differed significantly in one placenta (as compared with all of the other placenta samples) by performing Smirnov-Grubbs' outlier test with Bonferroni multiple test corrections (significant level = 0.1) for each placenta. We detected 2,983 and 1,416 CpG sites as hyper- and hypomethylated outliers, respectively, among the 33 subjects. To reduce the numbers of outliers that could have been detected spuriously due to SNPs at/near the target CpG sites, we excluded the CpG sites whose corresponding probes are annotated to contain known SNPs as described in the Methods. When 89,678 probes were regarded as potentially SNP-containing based on the Illumina probe annotation, 2,521 (85%) and 977 (69%) CpG sites remained as hyper- and hypomethylated outliers, respectively (Fig. 1 and Supplementary Tables 1 and 2).

We subjected these remaining outliers to further data analyses. Hypomethylated outliers coincided with SNP-containing probes more often than hypermethylated outliers (439/1,416 (31%) versus 462/2,983 (15%)). The mean (standard deviation [SD]) β values of the 2,521 hyper- and the 977 hypomethylated outliers were 0.24 (0.13) and 0.56 (0.19), respectively. The mean (SD) $\Delta\beta$ values ($\Delta\beta$ = the β value of the

	FGR			Normal		
	adequate	insufficient	excessive	adequate	insufficient	excessive
	(n = 5)	(n = 5)	(n = 4)	(n = 9)	(n = 5)	(n = 5)
BMI of pre-pregnancy (kg/m^2)	20.3 ± 2.0	18.7 ± 1.1	19.6 ± 1.0	20.1 ± 1.9	19.7 ± 2.2	19.8 ± 1.1
BMI at delivery (kg/m^2)	23.7 ± 2.5	20.4 ± 1.4[a]	25.2 ± 1.6	23.5 ± 1.7	22.3 ± 1.9	25.5 ± 1.2[d]
B.W. of pre-pregnancy (kg)	49.0 ± 5.3	49.4 ± 5.9	46.5 ± 1.7	51.0 ± 5.4	48.0 ± 7.0	50.6 ± 3.6
B.W. at delivery (kg)	57.2 ± 5.7	53.9 ± ± 6.5	60.0 ± 2.2	59.7 ± 4.8	54.3 ± 6.5	65.3 ± 3.9[d]
Gestational weight gain (kg)	8.2 ± 1.2	4.5 ± 1.8[a]	13.5 ± 0.9[b]	8.7 ± 1.1	6.3 ± 0.7[c]	14.7 ± 1.0[d]
B.W. of newborn (g)	1984 ± 296[e]	1702 ± 282[f]	1860 ± 535[g]	2937 ± 297	3010 ± 483	3452 ± 200
B.W./B.H. of newborn (cm/g)	45.4 ± 5.2[e]	40.9 ± 5.5[f]	43.8 ± 7.7[g]	61.3 ± 4.0	62.5 ± 7.9	68.3 ± 3.6[d]
Placental weight (P.W.) (g)	417.0 ± 47.9[e]	351.0 ± 83.2[f]	487.5 ± 24.0[b,g]	631.7 ± 189.2	639.0 ± 132.9	652.0 ± 97.8
B.W. of newborn/P.W.	4.8 ± 0.5	5.0 ± 1.1	3.8 ± 1.1[g]	4.9 ± 1.2	4.8 ± 1.0	5.4 ± 0.7
Gestational weeks	37.0 ± 1.4	35.8 ± 1.3[f]	36.3 ± 3.0	38.0 ± 1.7	39.6 ± 1.7	39.6 ± 1.1
Ratio of C. section to vaginal delivery	3 to 2	2 to 3	2 to 2	2 to 7	1 to 4	1 to 4
Ratio of male to female newborns	3 to 2	2 to 3	0 to 4	6 to 3	1 to 4	3 to 2
Age at delivery	31.4 ± 3.6	28.6 ± 2.4	26.8 ± 4.0	32.0 ± 7.1	31.4 ± 7.6	32.6 ± 5.9

Table 1. Characteritics of mothers, newborns, and placentas enrolled in this study. BMI, body mass index; B. W., body weight; B. H., body height. [a]$p < 0.05$ in the t-test between FGR_insufficient and FGR_adequate. [b]$p < 0.05$ in the t-test between FGR_excess and FGR_adequate. [c]$p < 0.05$ in the t-test between Normal_insufficient and Normal_adequate. [d]$p < 0.05$ in the t-test between Normal_excess and Normal_adequate. [e]$p < 0.05$ in the t-test between FGR_adequate and Normal_adequate. [f]$p < 0.05$ in the t-test between FGR_insufficient and Normal_insufficient. [g]$p < 0.05$ in the t-test between FGR_excess and Normal_excess.

outlier–the mean β value of the other samples) of hyper- and hypomethylated outliers were 0.18 (0.11) and –0.27 (0.12), respectively.

While the numbers of outliers in the "normal_adequate" category were low and relatively consistent among subjects (ranging from 46 to 74), those in the other five categories were higher, exhibiting statistical significance (Tukey's multiple comparison test p-value < 0.001; Fig. 1B) and diverse among the subjects (ranging from 44 to 421). In normal subjects, the greater the insufficiency or excessiveness of maternal GWG, the higher the number of methylation outliers, as represented by the U-shaped appearance of the bar plots for the number of outliers in normal subjects sorted according to weight gained during pregnancy (Fig. 1C). In FGR subjects, all three subcategories (FGR_insufficient, FGR_adequate, and FGR_excessive) contained significantly higher numbers of outliers than the "normal_adequate" category (Fig. 1B). The numbers of outliers in FGR_insufficient and FGR_excessive categories were also significantly higher than those in FGR_adequate (Fig. 1B). The numbers of outliers were neither associated with C-section nor correlated with gestational weeks (Supplementary Table 4). These results suggested that both FGR and inadequate GWG conditions affected the placental epigenome independently and additively.

Next, we examined the numbers of hyper- and hypomethylated outliers in each subject (Fig. 1E,G). While the numbers of hypomethylated outliers were not much different among subjects (Fig. 1F), the numbers of hypermethylated outliers were significantly higher in subjects in the other five categories compared to subjects in the "normal_adequate" category ($P < 0.001$; Fig. 1D). Therefore, only hypermethylated outliers occurred with FGR pregnancies and normal pregnancies with inadequate GWG. Because of the nature of the Smirnov-Grubbs' outlier test, the identified methylation outliers were all specific to individuals (deviated only in one sample among the cohort). Our results demonstrate that the adverse pregnancy conditions, FGR and inadequate GWG, affected the placental epigenome variably among individuals.

Contrasting genomic features of hyper- and hypomethylated outliers. We subsequently annotated the genomic features of 2,521 hyper- and 977 hypomethylated outliers (Fig. 2). Among these outliers, 2,107 (84%) and 758 (78%) CpG sites were located in genic regions (in 1,001 and 606 genes, respectively). Hypermethylated outliers were found to be predominantly located in CGIs or their shores/shelves (94% in total) and proximal to the transcriptional start sites (defined as "pTSS" hereafter; i.e., TSS1500, TSS200, the 5′ untranslated region [UTR], and the first exon categories; 77%). In contrast, hypomethylated outliers were most frequently located outside of CGIs, shores, and shelves (open sea,

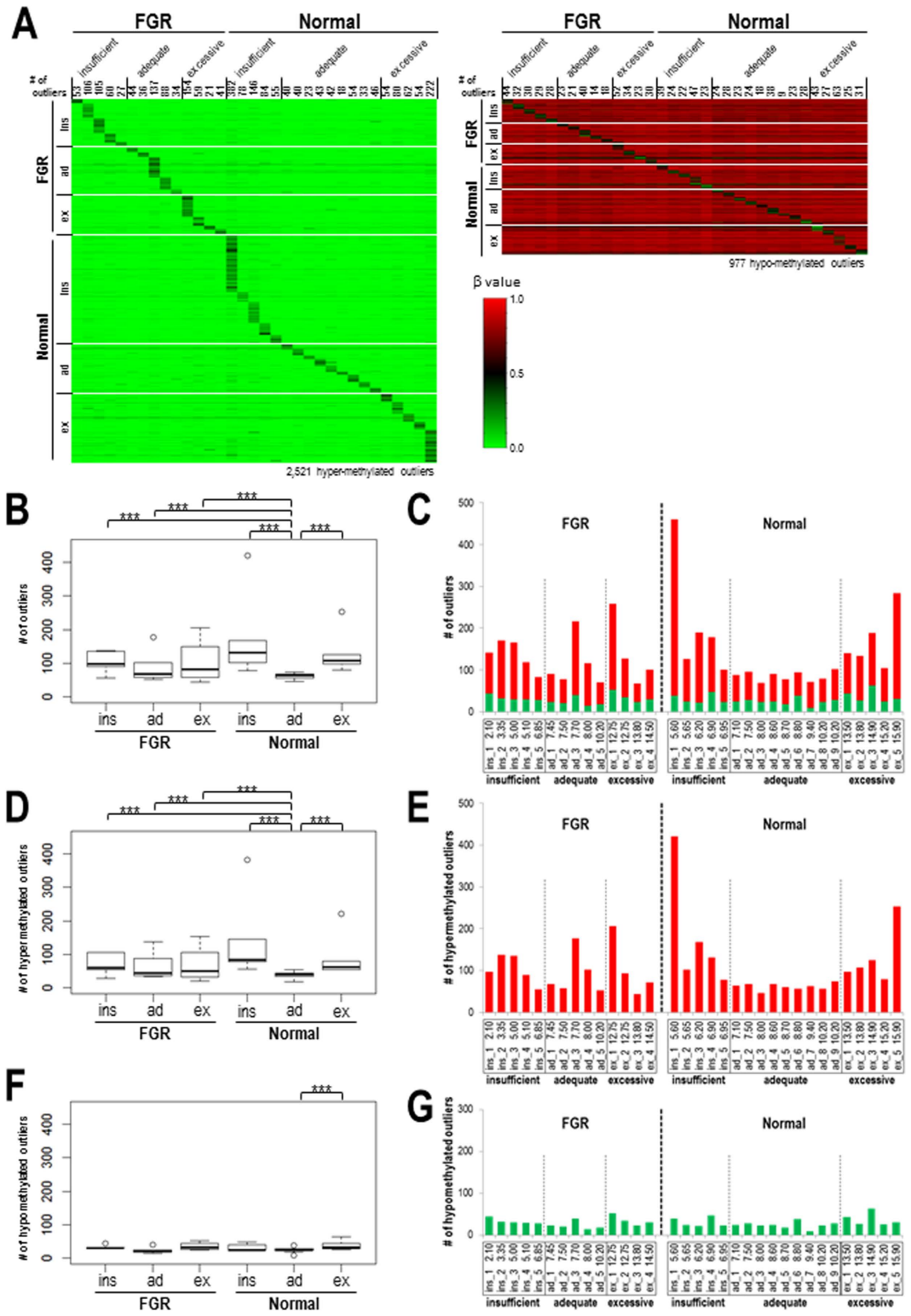

Figure 1. (**A**) Heatmap visualisation of the β value of methylation outliers detected by Smirnov-Grubbs' outlier tests. The numbers of outliers detected in each placenta are indicated above the heatmap. The colour scale represents the β value from 0 to 1. The left and right panels represent hypermethylated and hypomethylated outliers, respectively (**B,D,F**). Box plots showing the distribution of the numbers of outliers in each of six placental categories (***, Tukey's multiple comparison test P-value < 0.001). ins, insufficient; ad, adequate; ex, excessive (**C,E,F**). Bar plots for the numbers of outliers in FGR and normal subjects sorted according to weight gained during pregnancy. Plots for all outliers (**B,C**), hypermethylated outliers only (**D,E**), and hypomethylated outliers only (**F,G**) are shown. Red and green bars represent the numbers of hyper- and hypomethylated outliers, respectively (**C,E,F**).

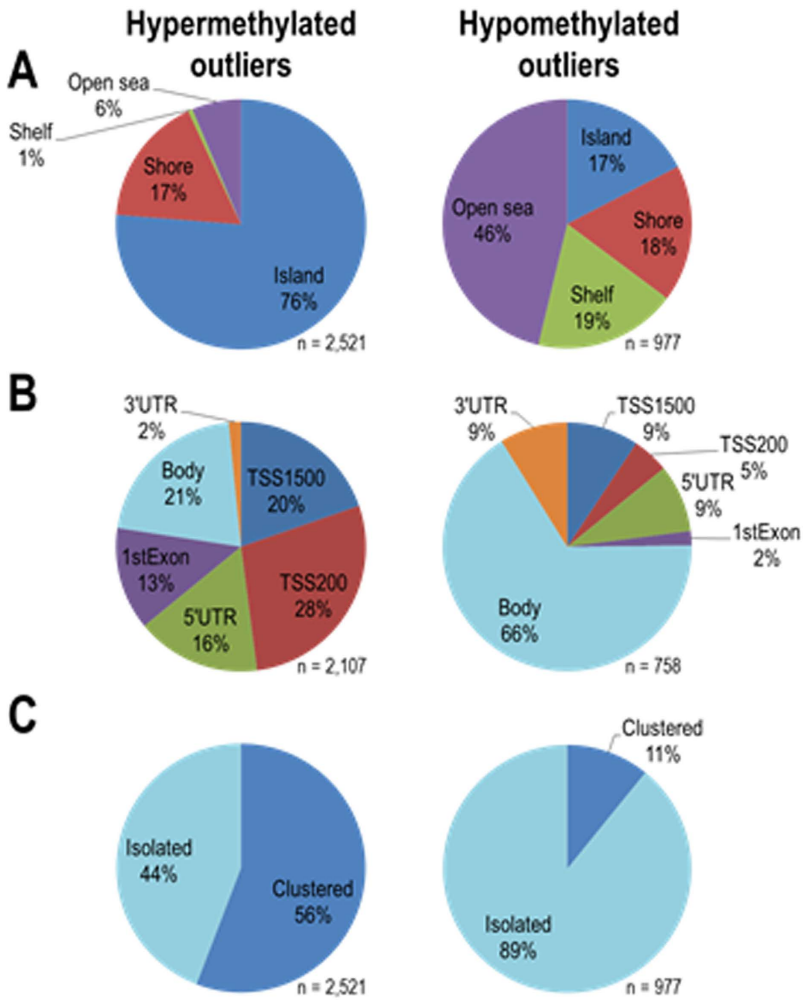

Figure 2. Genomic features of 2,521 hyper- and 977 hypomethylated outliers. Distribution of outliers in relation to CGIs and their shores and shelves (**A**) and to gene feature groups (**B**). Six gene feature categories, i.e., TSS1500, TSS200, the 5′UTR, the first exon, the gene body, and the 3′UTR, are regarded as genic regions, in which 2,107 (84%) and 758 (78%) CpG sites were located. The ratio of clustered and isolated outliers is shown (**C**).

46%) and in gene bodies (66%) (Fig. 2A,B). Hypermethylated outliers tended to be detected consecutively at two or more adjacent probes ("clustered"; 56%), while hypomethylated outliers did not (11%; Fig. 2C). These results implied that hypermethylated outliers tended to be clustered within CGI promoters.

We therefore scrutinised the extent of hypermethylation and the positional distribution relative to the TSS of hypermethylated outliers by visualising β and $\Delta\beta$ values on the Integrative Genomics Viewer (IGV, www.broadinstitute.org/igv/home). Indeed, we found that hypermethylated outliers were often distributed in a promoter-wide manner (i.e., located consecutively and clustered around the TSS) with relatively large methylation differences, as exemplified by *FOXC1*, *FOXL2*, and *HOXB7* loci (Fig. 3). The methylation statuses in the outlier sample and a control (Normal_adequate_7) at these promoter regions were validated to be hypermethylated and unmethylated, respectively, by targeted bisulfite sequencing analyses (Fig. 3). The appearance of both of heavily methylated and unmethylated clones in individual outlier samples may indicate the mosaic composition of normal and epimutated cells in these placentas.

The observation that hypermethylated outliers were often clustered at CGI promoters suggested that placental hypermethylation events do not occur in a purely random manner in terms of genomic location, but instead occur due to dysfunction of certain intrinsic mechanisms regulating the epigenetic status of CGI promoters under adverse *in utero* environments.

Hypermethylated outliers were frequently associated with genes encoding transcriptional regulators. In order to search for functional characteristics of genes containing hypermethylated outliers, we performed gene ontology (GO) analysis; 1,001 genes hosting hypermethylated outliers (as well as 606 genes hosting hypomethylated outliers for comparison) were analysed using the Database for Annotation, Visualization, and Integrated Discovery (DAVID) v6.7. The 606 genes hosting hypomethylated

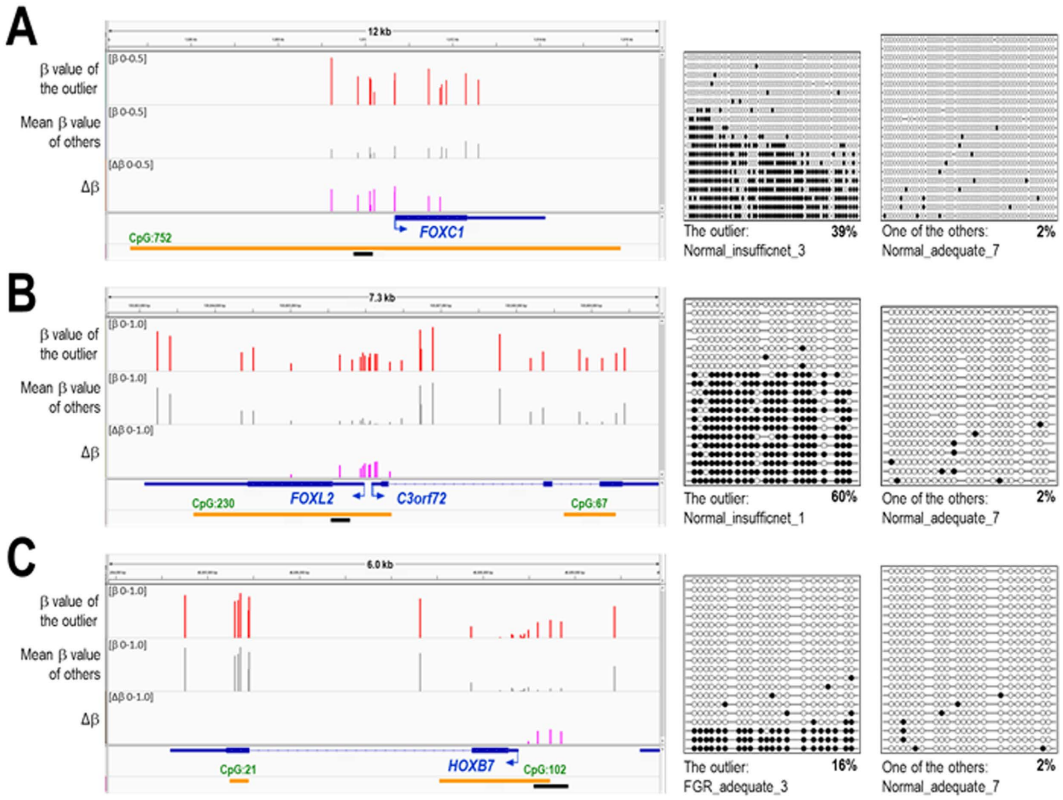

Figure 3. Examples of promoter-wide hypermethylation at *FOXC1* (**A**), *FOXL2* (**B**), and *HOXB7* (**C**) loci. The β value of the outlier, the mean of the β values of samples other than the outlier, and the Δβ are shown together with Refseq gene and UCSC-defined CGIs using IGV at the left side in each panel. The data range of 0 to 0.5 (or 0 to 1.0) is shown for β and Δβ values. The outlier samples for the three loci are Normal_insufficient_3 (**A**), Normal_insufficient_1 (**B**), and FGR_adequate_3 (**C**). DNA methylation status of these promoter regions were validated by targeted bisulfite sequencing (BS). The black horizontal bar at the bottom in each panel shows the interval of the bisulfite-PCR amplicon. The BS results for the outlier sample and a control (Normal_adequate_7) are shown at the right side in each panel. Open and closed circles represent unmethylated and methylated CpG sites, respectively. Each row of circles corresponds to an individual clone sequenced. The overall methylation rate (%) is shown underneath each panel of the BS results.

Gene ontology term (Biological Process)	Gene count	Fold enrichment	*p*-value	Benjamini's adjusted *p*-value
GO:0006355 regulation of transcription, DNA-dependent	157	1.70	6.73E-12	1.96E-08
GO:0030182 neuron differentiation	60	2.63	1.29E-11	1.88E-08
GO:0051252 regulation of RNA metabolic process	157	1.66	3.85E-11	3.74E-08
GO:0045449 regulation of transcription	199	1.47	2.39E-09	1.74E-06
GO:0007409 axonogenesis	31	3.08	6.61E-08	3.85E-05

Table 2. Top 5 gene ontology (GO) Biological Process terms significantly enriched among the 1,001 genes hosting 2,521 hypermethylated outliers.

outliers were found to be weakly enriched with only one term, "cytoskeletal protein binding", in the Molecular Function (MF) category (Benjamini's corrected $Pc = 0.0025$). However, the 1,001 genes hosting hypermethylated outliers were highly enriched with terms related to transcriptional regulators and neuronal differentiation in the Biological Process (BP) and MF categories (e.g., BP terms "regulation of transcription, DNA-dependent" [$Pc = 1.96 \times 10^{-8}$] and "neuronal differentiation" [$Pc = 3.16 \times 10^{-8}$]; Table 2 and Supplementary Table 3). We subsequently performed GO analysis for subgroups of genes:

409 genes hosting highly deviated ($\Delta\beta > 0.2$) hypermethylated outliers, 709 genes hosting hypermethylated outliers in the pTSS, and 317 genes hosting two or more clustered hypermethylated outliers. These subgroups of genes were also found to be significantly enriched with terms related to transcriptional regulators (Supplementary Table 3). These results supported our observation that hypermethylated outliers are often distributed in a promoter-wide manner and that the genes hosting such outliers are significantly enriched with genes encoding transcriptional regulators. We further performed GO analysis for the 163 genes hosting highly deviated ($\Delta\beta > 0.2$) and clustered hypermethylated outliers in the pTSS. Among those, 36 genes were assigned to the category "GO:0006355~regulation of transcription, DNA-dependent" with a statistical significance [$Pc = 0.0038$] and showed a higher fold enrichment value to the term than that of the entire (1,001) genes (2.25 versus 1.70, Supplementary Table 3). Importantly, in 35 out of the 36 genes encoding transcriptional regulators (97%), promoter hypermethylation was detected in the placentas from cases of inadequate GWG or FGR (Table 3).

Discussion

In this study, we demonstrated the possibility that inadequate maternal GWG enhances aberrant DNA methylation in the placenta. We initially failed to identify specific loci whose methylation was commonly altered across all subjects in each of the GWG categories. We subsequently used Smirnov-Grubbs' outlier tests, which detect the most significantly deviated outlier among subjects, for each of the CpG probes and found that hypermethylated loci accumulated in normal pregnancies with inadequate GWG and in FGR pregnancies. The results suggested that the epigenetically affected loci due to adverse *in utero* environments were variable among the subjects examined in this study. It should be noted that the relatively small number of the enrolled subjects (partly due to exclusion of the subjects with certain types of pregnancy complications) with various layers of heterogeneities (e.g., genetic, phenotypic, and environmental) may account for a primary cause of the absence of commonly epigenetically affected loci and the variation of affected loci among the individuals studied. While many animal studies have clearly demonstrated direct associations between *in utero* nutritional conditions during foetal development and epigenetic alterations (at certain loci or globally)[10], evidence from studies in human populations has been limited. Unlike the homogeneous genetic backgrounds of animal models and the well-controlled environmental and experimental conditions that can be easily achieved in animal studies, individuals in human studies are genetically heterogeneous and have not been exposed to identical environments throughout their lives. These unavoidable genetic and environmental heterogeneities in human subjects very likely give rise to individual variations in epigenetically affected loci, even when the subjects were exposed to similar nutritional environments for a certain period. Provided that epimutations could occur not only at common loci but at variable loci among subjects, Smirnov-Grubbs' outlier test is effective in evaluating the extent of the accumulation of the latter type of epimutations under certain disease and/or malnutrition conditions and may be applicable to a wide range of epigenetic studies in human populations.

FGR is idiopathic in most cases and is generally thought to be caused by foetal, placental, maternal, and/or environmental factors[30]. Therefore, the hypermethylation events observed with significantly high frequencies in placentas from FGR births in this study may also be explained by various factors. Unidentified genetic factors, such as foetal and/or placental chromosomal abnormalities and mutations at certain genes, if they exist, could affect the epigenomes of both the foetus and placenta, regardless of *in utero* conditions. Maternal and environmental factors deteriorating *in utero* conditions and contributing to the FGR phenotype may not have been identified in some subjects enrolled in this study. On the other hand, in normal pregnancy cases with inadequate GWG, since the body weights of the babies were within the normal range, the foetuses (and the placentas) were considered to be genetically normal. Under this assumption, promoter hypermethylation observed with higher frequencies in placentas with inadequate GWG than in those with adequate GWG can be regarded as environmentally induced epigenetic alterations.

Multiple independent studies have shown that genetic variants can cause variations in DNA methylation levels, defined as sequence-dependent allele-specific DNA methylation (ASM)[32]. A recent methylC-Seq study of the mouse genome revealed that sequence-dependent ASMs typically exist as isolated CpG sites in intergenic and intronic regions, but are relatively depleted from proximal promoters[33]. Moreover, sequence-dependent ASMs are influenced by defined sequences nearby and they appear to have little effect on gene expression. The genomic features of hypomethylated outliers in our study were similar to those of sequence-dependent ASMs. On the other hand, the characteristics of the hypermethylated outliers, being clustered (56%) in the pTSS (77%), were distinct from those of sequence-dependent ASMs. It is generally challenging to distinguish whether differentially methylated regions among genetically heterogeneous human populations are epimutations or sequence-dependent ASMs. However, considering the above-mentioned genomic features of the hypermethylated outliers as well as their enrichment in the promoter regions of transcriptional regulator genes (which will be discussed in detail in the next paragraph), at least a portion of these outliers likely represent genuine epigenetic alterations rather than sequence-dependent changes in DNA methylation.

We initially considered that placental epimutations may have occurred randomly under aberrant *in utero* environments; our data subsequently revealed that hypermethylated outliers were not found completely randomly in terms of genomic location, but tend to be frequent at the promoters of genes

Subject	Gene Symbol	Gene Name	# of hyper-methylated outliers in pTSS	average Δβ of outliers
N_adequate_5	*ZNF649***	zinc finger protein 649	6	0.19
N_excessive_1	*GBX2**	gastrulation brain homeobox 2	3	0.25
N_excessive_1	*ZNF350***	zinc finger protein 350	8	0.30
N_excessive_2	*ZFP37***	zinc finger protein 37 homolog	4	0.44
N_excessive_5	*ZHX2**	zinc fingers and homeoboxes 2	8	0.15
N_excessive_5	*CDKN1C**	cyclin-dependent kinase inhibitor 1C	4#	0.28
N_excessive_5	*PAX6**	paired box 6	2	0.23
N_insufficient_1	*KCNH8**	potassium voltage-gated channel, subfamily H, member 8	4	0.24
N_insufficient_1	*FOXL2**	forkhead box L2	10	0.21
N_insufficient_1	*F2R**	coagulation factor II (thrombin) receptor	3	0.20
N_insufficient_1	*SOX7**	SRY (sex determining region Y)-box 7	3	0.18
N_insufficient_1	*NFIB**	nuclear factor I/B	2	0.37
N_insufficient_1	*HMX2**	H6 family homeobox 2	2	0.23
N_insufficient_2	*TFCP2**	transcription factor CP2	5	0.19
N_insufficient_3	*PROX1**	prospero homeobox 1	3	0.15
N_insufficient_3	*FOXC1**	forkhead box C1	8	0.19
N_insufficient_3	*FOXB1**	forkhead box B1	2	0.17
N_insufficient_5	*ETV1*	ets variant 1	6	0.11
N_insufficient_5	*ZNF426***	zinc finger protein 426	2	0.17
FGR_adequate_1	*PER1*	period homolog 1	6	0.16
FGR_adequate_3	*ZNF619***	zinc finger protein 619	4	0.27
FGR_adequate_3	*ZKSCAN4***	zinc finger with KRAB and SCAN domains 4	3	0.25
FGR_adequate_3	*PGBD1*	piggyBac transposable element derived 1	7	0.21
FGR_adequate_3	*HOXB7**	homeobox B7	4	0.23
FGR_adequate_4	*ESR1**	estrogen receptor 1	3#	0.17
FGR_adequate_4	*MGA*	MAX gene associated	3	0.17
FGR_excessive_1	*RFX8**	hypothetical protein LOC731220	3	0.33
FGR_excessive_1	*ZNF483***	zinc finger protein 483	2	0.20
FGR_excessive_1	*ZNF254***	zinc finger protein 254	3#	0.21
FGR_excessive_2	*ZNF577***	zinc finger protein 577	6#	0.43
FGR_excessive_3	*ZNF655***	zinc finger protein 655	2	0.35
FGR_insufficient_1	*ZNF562***	zinc finger protein 562	8	0.36
FGR_insufficient_1	*ZNF805***	zinc finger protein 805	2	0.30
FGR_insufficient_2	*ZNF583***	zinc finger protein 583	6	0.27
FGR_insufficient_3	*ZNF354C***	zinc finger protein 354C	7	0.27
FGR_insufficient_3	*ETV1*	ets variant 1	6	0.16
FGR_insufficient_4	*ZIK1***	zinc finger protein interacting with K protein 1	2	0.42

Table 3. The list of 36 genes assigned with transcription factor-related gene ontology terms among the 163 genes hosting highly-deviated and clustered hypermethylated outliers in pTSS. *Polycomb repressive complex 2 (PRC2) target genes in mouse or human embryonic stem cell lines (16/36, 44%). The 653 mouse PRC2-targets identified in Ref.36 and the ChIP-seq dataset of the PRC2 components (EZH2 and SUZ12) for a human ES cell line (H1-hESC) produced by the Encyclopedia of DNA Elements (ENCODE) Consortium were refered to search for PRC2-targets among the 36 genes. **Zinc-finger genes (15/36, 42%). #indicates gene body probes nearby (<1 kb) the pTSS region.

encoding transcription factors. Considering that the promoter regions of genes encoding developmental regulators, such as homeobox proteins and other developmental transcription factors, have been reported to be mostly devoid of sequence-dependent ASMs[33], the hypermethylated outliers located at the promoter regions of such genes identified in this study (Table 3) most likely represent epigenetic alterations due to aberrant *in utero* environments. In a recent genome-wide DNA methylation study using reduced representation bisulphite sequencing (RRBS) in a murine model of FGR, genes hosting differentially methylated regions in the placenta upon maternal calorie restriction are significantly enriched ($P < 0.05$) with GO terms such as homeobox and transcription factor activity, among others[34]. Notably, our own annotations for the 131 genes hosting hypermethylated regions in the placenta upon maternal gestational calorie restriction[34] using DAVID revealed that these genes were moderately enriched with genes assigned with the GO Molecular Function term "DNA binding" (17 out of the 131 genes were assigned this term). Therefore, although the statistical method used for detecting differentially methylated regions is different from that in our study, some aspects of this murine study were consistent with our findings demonstrating the enrichment of placental epimutations in transcriptional regulator genes.

Our findings also suggested the possibility that certain epigenetic regulatory systems are susceptible to the disruptive effects of aberrant *in utero* environments. In fact, a careful analysis of the 36 genes assigned with GO terms related to transcriptional regulation (Table 3) revealed that polycomb group repressive complexes (PRCs)[35] represent a primary candidate of such regulatory mechanisms. We found that seven out of the 36 genes (i.e., *HOXB7*, *GBX2*, *HMX2*, *SOX7*, *F2R*, *FOXL2*, and *FOXC1*) were included in the 653 PRC2 targets in mouse embryonic stem cells, as identified by a ChIP-on-chip analysis[36]. Further annotations of the 36 genes using the ChIP-seq data for EZH2 and SUZ12, which are components of PRC2[35], from a human ES cell line (H1-hESC) produced by the Encyclopedia of DNA Elements (ENCODE) Consortium (http://genome.ucsc.edu/ENCODE/) identified additional eight PRC2 targets (Table 3). Consistent with our observations, epigenetic variation between twin-twin transfusion syndrome children, wherein twin foetuses occasionally exhibit striking growth differences, is most prominent at the CpG sites within the target regions of PRCs[37]. Furthermore, Wilhelm-Benartzi *et al.* reported significant associations of placental LINE-1 and AluYb8 methylation levels with birth weight percentile and significant differences in the methylation levels of these repetitive elements upon maternal alcohol or tobacco use during pregnancy[21]. Interestingly, the authors also revealed the positive association of increased placental AluYb8 methylation with the average methylation levels of CpG sites in polycomb group target genes. Therefore, evidence from these previous reports and our current findings suggest the possibility that PRCs occasionally fail to recognise their targets with a stochastic nature in the placenta under improper *in utero* environments, leading to epigenetic switching from PRC marks (H3K27me3) to DNA methylation. Another striking feature of these 36 genes was that 15 (42%) were zinc-finger genes (Table 3). Zinc-finger genes are often silenced through H3K9me3-mediated gene silencing coupled with promoter DNA methylation in toxicant-induced carcinogenesis, suggesting the existence of an unknown epigenetic mechanism through which many zinc-finger genes are coregulated[38]. This hypothetical regulatory mechanism may also be susceptible to the effects of adverse *in utero* environments.

In addition to the enrichment of GO terms related to transcriptional regulation, the genes hosting hypermethylated outliers were also found to be enriched with the GO term "neuron differentiation" (Supplementary Table 3).This seemingly unexpected observation is consistent with those of previous studies. In an array-based expression study that identified 7,519 genes exhibiting differential expression between human placentas sampled during the first and third trimesters, both up- and downregulated genes in the third trimester were found to be enriched with genes involved in human neurogenesis[39]. The authors of the study have suggested that the brain and placenta possibly share common developmental routes. In the above-mentioned RRBS study of the murine model of intrauterine malnutrition[34], GO terms found to be enriched in genes hosting altered placental DNA methylation upon maternal caloric restriction were shown to contain neuron-related terms[34]. Additionally, several neural factors, such as BDNF[40], NGF[41], and serotonin[42], have been shown to be secreted from the placenta. Among these factors, BDNF has also been shown to potentiate placental development and play an important role in cytotrophoblast differentiation[43,44]. Furthermore, placental BDNF expression has been reported to be significantly correlated with neonatal birth weight[40] and to be decreased upon maternal malnutrition in rats[45]. Because of the functional significance of a subset of genes in both the placenta and brain, it is tempting to speculate that the foetuses may have gained epigenetic alteration patterns that are similar to those observed in the placenta in pregnancies with inadequate GWG. Hypermethylation at the promoter regions of genes encoding developmental regulators (PRC2 targets) and neuronal regulators at early embryonic stages would reduce their expression levels when these genes are expressed in a spatio-temporal manner, and such aberrant expression of critical developmental regulators may elevate the risk of developing various diseases, including metabolic and mental disorders, later in life.

In this study, we demonstrated that loci with alterations in the placental DNA methylation under inadequate GWG were not common among subjects but were instead distributed in an individual-specific manner. Furthermore, such epigenetic alterations under the adverse pregnancy condition were found to occur preferentially at the CGI promoters of genes encoding transcriptional factors. Our novel findings support the necessity of large-scale epigenomic studies of placental tissues and samples (e.g., cord blood) from newborns for pregnancies under normal and malnutrition conditions, together with follow-up

studies when the newborns reach adulthood in order to elucidate the epigenetic mechanisms underlying developmental programming in humans and their roles in health and disease in later life.

Materials and Methods

Study design. The present study was approved by the Ethics Committee of the National Center of Child Health and Development (NCCHD), Japan and by the Human Study Committee of the Hokkaido University Hospital, Japan. Informed consent was obtained from all subjects. Pregnant Japanese women who did not have pregnancy complications of gestational diabetes, pre-eclampsia, or pregnancy-induced hypertension were enrolled. All enrolled subjects did not smoke or drink alcohol, and did not exhibit hypertension or proteinuria during pregnancy. Subjects ($n = 33$) were categorised into six categories according to GWG and newborn birth weight: FGR_adequate, FGR_insufficient, FGR_excessive, normal_adequate, normal_insufficient, and normal_excessive, consisting of 5, 5, 4, 9, 5, and 5 placentas, respectively. Prepregnancy BMIs were similar among all groups. The characteristics of each group are shown in Table 1. BMI, body weight, GWG, and additional clinical information (maternal complication, gestational week, delivery method, and newborn's gender) for each of the subjects are provided as Supplementary Table 4. Although the Institute of Medicine of the United States recommends that pregnant women whose prepregnancy BMI is in the normal range (18.5–24.9) should gain 11.3–15.9 kg during pregnancy, we defined adequate GWG as gaining 7–12 kg in this study in accordance with the recommendations of the Japan Ministry of Health, Labour, and Welfare[46]. This difference is also consistent with the different average BMIs of Japanese and US women (21.14 ± 3.28[47] versus 27.05 ± 0.35[48], respectively).

Genomic DNA extraction and DNA methylation profiling. Full-term placental samples were obtained from normal caesarean sections or vaginal deliveries. Chorionic villous tissue was obtained from the foetal side of the placenta. Genomic DNA was purified from the tissue using a QIAamp DNA Mini kit (Qiagen, Valencia, CA, USA). Genomic DNA (1.5 μg) was bisulphite converted using an EpiTect Plus DNA Bisulfite Kit (Qiagen). After determining the concentration of bisulphited DNA, 300 ng of bisulphite DNA from each sample was subjected to Illumina Infinium HumanMethylation450 BeadChip analysis using the manufacturer's standard protocol.

Data processing. To calculate the DNA methylation levels of more than 480,000 CpG sites assayed on the HumanMethylation450 BeadChip (Illumina), the signal intensity data (.idat files), produced by the Illumina iSCAN system, were processed using Illumina GenomeStudio Methylation Analysis Module v1.9.0 with background subtraction and control normalisation options. The methylation levels were calculated as β values ranging from 0 (completely unmethylated) to 1 (completely methylated; β value = intensity of the methylated allele/[intensity of the unmethylated allele + intensity of the methylated allele + 100]). The obtained data have been deposited in NCBI's Gene Expression Omnibus and are accessible through GEO accession number GSE62733. From 485,577 probes on the BeadChip array, the following probes were excluded: the probes on sex chromosomes, the probes for 65 random SNPs (which assay highly-polymorphic SNPs rather than DNA methylation), and the probes whose detection *p*-value was higher than 0.01 or whose β value was missing in one or more samples. The β values (methylation levels) of the remaining 449,848 probes were corrected by an Empirical Bayes method, ComBat[49], to remove the array-batch effect, and subjected to statistical tests.

To detect differentially methylated CpG sites between groups, the Illumina Methylation Analyzer (IMA)[31] was run using the Wilcoxon rank-sum test for inference of differences between categorical groups. The BH procedure was used for multiple testing corrections, and the cut-off for the adjusted *p*-values was set to 0.05. Smirnov-Grubbs' outlier test with Bonferroni multiple test corrections was performed using the R Package 'outliers' (http://cran.r-project.org/web/packages/outliers/outliers.pdf) and custom R scripts to detect outlying CpG sites, and the cut-off for the corrected *p*-values was set to 0.1.

The Illumina-provided probe annotation, HumanMethylation450_15017482_v.1.1.csv, was used to sort out the outlying CpG sites whose β value could possibly have been affected by sequence variation within the corresponding probe sequence. This table lists 89,678 probes as SNP-containing in its "probe_SNPs" and "probe_SNPs_10" columns based on the information of NCBI dbSNP Build 131. The refSNP information registered in dbSNP Build 142 was also tested for the same purpose of SNP filtering (Supplementary Fig. 2).

When a single CpG site was assigned to multiple gene symbols or gene features in the Illumina probe annotation, only the lead-off gene symbol or feature was used for gene ontology and genome feature annotations.

Targeted bisulfite sequencing. Bisulfite sequencing analysis was performed as described previously[50] using bisulfite-PCR primers designed by the MethPrimer website[51]. The forward and reverse primer sequences, and the genomic interval (hg19) of the amplicon are: 5′-GAGAGGTTGGGGTAATTTTAG-3′, 5′-AAAAACTTCTAAACTTTTAAACATCC-3′ and chr6:1609671-1610171 (501bp) for the *FOXC1* locus; 5′-GGGGTAGTTGGTTATTATGATAAAGT-3′, 5′-ACTCCCCATAACCAAAAACTAAACT-3′, and chr3:138665547-138665794 (248 bp) for the *FOXL2* locus; 5′-AGTTTTGTGGATTGGGGTTG-3′,

5′-ACACCTAAAAAAACTTACTCCATCTC-3′, and chr17:46688533-46688920 (388 bp) for the *HOXB7* locus. The obtained sequence data were analysed using the QUMA website[52].

References

1. Abitbol, C. & Rodriguez, M. The long-term renal and cardiovascular consequences of prematurity. *Nat. Rev. Nephrol*. **8,** 265–274 (2012).
2. Sandovici, I., Hammerle, C., Ozanne, S. & Constância, M. Developmental and environmental epigenetic programming of the endocrine pancreas: consequences for type 2 diabetes. *Cell Mol. Life Sci.* **70,** 1575–1595 (2013).
3. Berends, L. & Ozanne, S. Early determinants of type-2 diabetes. *Best Pract. Res. Clin. Endocrinol. Metab*. **26,** 569–580 (2012).
4. Luyckx, V. *et al.* Effect of fetal and child health on kidney development and long-term risk of hypertension and kidney disease. *Lancet* **382,** 273–283 (2013).
5. Reynolds, R. Glucocorticoid excess and the developmental origins of disease: two decades of testing the hypothesis—2012 Curt Richter Award Winner. *Psychoneuroendocrinology* **38,** 1–11 (2013).
6. Barker, D., Eriksson, J., Forsén, T. & Osmond, C. Fetal origins of adult disease: strength of effects and biological basis. *Int. J. Epidemiol.* **31,** 1235–1239 (2002).
7. Barker, D. The origins of the developmental origins theory. *J. Intern. Med.* **261,** 412–417 (2007).
8. Christian, L. R. & Sheela, S. Mechanisms affecting neuroendocrine and epigenetic regulation of body weight and onset of puberty: potential implications in the child born small for gestational age (SGA). *Rev. Endocr. Metab. Disord.* **13,** 129–140 (2012).
9. Gabory, A., Attig, L. & Junien, C. Developmental programming and epigenetics. *Am. J. Clin. Nutr.* **94,** 1943S–1952S (2011).
10. Seki, Y., Williams, L., Vuguin, P. M. & Charron, M. J. Minireview: Epigenetic programming of diabetes and obesity: animal models. *Endocrinology* **153,** 1031–1038 (2012).
11. Hogg, K., Price, E., Hanna, C. & Robinson, W. Prenatal and perinatal environmental influences on the human fetal and placental epigenome. *Clin. Pharmacol. Ther.* **92,** 716–726 (2012).
12. Rakyan, V., Down, T., Balding, D. & Beck, S. Epigenome-wide association studies for common human diseases. *Nat. Rev. Genet.* **12,** 529–541 (2011).
13. Smallwood, S. *et al.* Dynamic CpG island methylation landscape in oocytes and preimplantation embryos. *Nat. Genet.* **43,** 811–814 (2011).
14. Smith, Z. *et al.* A unique regulatory phase of DNA methylation in the early mammalian embryo. *Nature* **484,** 339–344 (2012).
15. Cantone, I. & Fisher, A. Epigenetic programming and reprogramming during development. *Nat. Struct. Mol. Biol.* **20,** 282–289 (2013).
16. Novakovic, B. *et al.* Evidence for widespread changes in promoter methylation profile in human placenta in response to increasing gestational age and environmental/stochastic factors. *BMC Genomics* **12,** 529 (2011).
17. Novakovic, B. & Saffery, R. The ever growing complexity of placental epigenetics—role in adverse pregnancy outcomes and fetal programming. *Placenta* **33,** 959–970 (2012).
18. Banister, C. E. *et al.* Infant growth restriction is associated with distinct patterns of DNA methylation in human placentae. *Epigenetics* **6,** 920–927 (2011).
19. Sandovici, I., Hoelle, K., Angiolini, E. & Constância, M. Placental adaptations to the maternal-fetal environment: implications for fetal growth and developmental programming. *Reprod. Biomed. Online* **25,** 68–89 (2012).
20. Michels, K. B., Harris, H. R. & Barault, L. Birthweight, maternal weight trajectories and global DNA methylation of LINE-1 repetitive elements. *PLoS One* **6,** e25254 (2011).
21. Wilhelm-Benartzi, C. S. *et al. In utero* exposures, infant growth, and DNA methylation of repetitive elements and developmentally related genes in human placenta. *Environ. Health. Perspect.* **120,** 296–302 (2012).
22. Suter, M. *et al.* Maternal tobacco use modestly alters correlated epigenome-wide placental DNA methylation and gene expression. *Epigenetics* **6,** 1284–1294 (2011).
23. Ruchat, S. M. *et al.* Gestational diabetes mellitus epigenetically affects genes predominantly involved in metabolic diseases. *Epigenetics* **8,** 935–943 (2013).
24. The, A. L. *et al.* The effect of genotype and *in utero* environment on interindividual variation in neonate DNA methylomes. *Genome Res.* **24,** 1064–1074 (2014).
25. Josefson, J., Hoffmann, J. & Metzger, B. Excessive weight gain in women with a normal pre-pregnancy BMI is associated with increased neonatal adiposity. *Pediatr. Obes*. **8,** e33–e36 (2013).
26. Schack-Nielsen, L., Michaelsen, K., Gamborg, M., Mortensen, E. & Sørensen, T. Gestational weight gain in relation to offspring body mass index and obesity from infancy through adulthood. *Int. J. Obes. (Lond)* **34,** 67–74 (2010).
27. Ensenauer, R. *et al.* Effects of suboptimal or excessive gestational weight gain on childhood overweight and abdominal adiposity: results from a retrospective cohort study. *Int. J. Obes. (Lond)* **37,** 505–512 (2013).
28. Simas, T. *et al.* Prepregnancy weight, gestational weight gain, and risk of growth affected neonates. *J. Womens Health (Larchmt)* **21,** 410–417 (2012).
29. Drehmer, M., Duncan, B., Kac, G. & Schmidt, M. Association of second and third trimester weight gain in pregnancy with maternal and fetal outcomes. *PLoS One* **8,** e54704 (2013).
30. Divon, M. Y. Fetal growth restriction: Causes and risk factors. (http://www.uptodate.com/contents/fetal-growth-restriction-causes-and-risk-factors) (2014) (Date of access:30/01/2015).
31. Wang, D. *et al.* IMA: an R package for high-throughput analysis of Illumina's 450K Infinium methylation data. *Bioinformatics* **28,** 729–730 (2012).
32. Tycko, B. Allele-specific DNA methylation: beyond imprinting. *Hum. Mol. Genet*. **19,** R210–R220 (2010).
33. Xie, W. *et al.* Base-resolution analyses of sequence and parent-of-origin dependent DNA methylation in the mouse genome. *Cell* **148,** 816–831 (2012).
34. Chen, P. Y. *et al.* Intrauterine calorie restriction affects placental DNA methylation and gene expression. *Physiol Genomics* **45,** 565–576 (2013).
35. Schwartz, Y. & Pirrotta, V. A new world of Polycombs: unexpected partnerships and emerging functions. *Nat. Rev. Genet.* **14,** 853–864 (2013).
36. Lee, T. I. *et al.* Control of developmental regulators by Polycomb in human embryonic stem cells. *Cell* **125,** 301–313 (2006).
37. Marsit, C. J. *et al.* Developmental genes targeted for epigenetic variation between twin-twin transfusion syndrome children. *Clin. Epigenetics* **5,** 18 (2013).
38. Severson, P. L., Tokar, E. J., Vrba, L., Waalkes, M. P. & Futscher, B. W. Coordinate H3K9 and DNA methylation silencing of ZNFs in toxicant-induced malignant transformation. *Epigenetics* **8,** 1080–1088 (2013).
39. Sitras, V., Fenton, C., Paulssen, R., Vårtun, Å. & Acharya, G. Differences in gene expression between first and third trimester human placenta: a microarray study. *PLoS One* **7,** e33294 (2012).
40. Dhobale, M., Pisal, H., Mehendale, S. & Joshi, S. Differential expression of human placental neurotrophic factors in preterm and term deliveries. *Int. J. Dev. Neurosci.* **31,** 719–723 (2013).

41. Toti, P. *et al.* Human placenta and fetal membranes express nerve growth factor mRNA and protein. *J. Endocrinol. Invest.* **29,** 337–341 (2006).
42. Bonnin, A. *et al.* A transient placental source of serotonin for the fetal forebrain. *Nature* **472,** 347–350 (2011).
43. Kawamura, K. *et al.* Brain-derived neurotrophic factor promotes implantation and subsequent placental development by stimulating trophoblast cell growth and survival. *Endocrinology* **150,** 3774–3782 (2009).
44. Kawamura, K. *et al.* Brain-derived neurotrophic factor/tyrosine kinase B signaling regulates human trophoblast growth in an *in vivo* animal model of ectopic pregnancy. *Endocrinology* **152,** 1090–1100 (2011).
45. Mayeur, S. *et al.* Placental BDNF/TrkB signaling system is modulated by fetal growth disturbances in rat and human. *Placenta* **31,** 785–791 (2010).
46. Japan Ministry of Health, Labour and Welfare. Chart of optimum weight gain during gestational period. (http://www.mhlw.go.jp/houdou/2006/02/dl/h0201-3a4.pdf) (2006) (Date of access:30/01/2015).
47. Japan Ministry of Health, Labour and Welfare. Japan National Health and Nutrition Survey of 2010. (http://ghdx.healthdata.org/record/japan-national-health-and-nutrition-survey-2010) (2012) (Date of access:30/01/2015).
48. Ogden, C. L. *et al.* Mean body weight, height, and body mass index, UnitedStates1960–2002. (www.cdc.gov/nchs/data/ad/ad347.pdf) (2004) (Date of access:30/01/2015).
49. Sun, Z. *et al.* Batch effect correction for genome-wide methylation data with Illumina Infinium platform. *BMC Med. Genomics* **4,** 84 (2011).
50. Miyata, K. *et al.* DNA methylation analysis of human myoblasts during *in vitro* myogenic differentiation: *de novo* methylation of promoters of muscle-related genes and its involvement in transcriptional down-regulation. *Hum Mol Genet.* **24,** 410–423 (2015).
51. Li L. C. & Dahiya R. MethPrimer: designing primers for methylation PCRs. *Bioinformatics* **18,** 1427–1431 (2002)
52. Kumaki, Y., Oda, M. & Okano, M. QUMA: quantification tool for methylation analysis. *Nucleic Acids Res.* **36,** W170–W175 (2008).

Acknowledgments

This study was supported by Grants from the MHLW of Japan (H26-082, H26-Itaku-001, H25-Jisedai-Ippan-001), KAKENHI (24890299, 26670734, 26293365), Grants from the NCCHD of Japan (24-3, 26-13), and a CREST Program of JST (Epigenomic analysis of the human placenta and endometrium constituting the fetal-maternal interface).

Author Contributions

T.K. designed the project. T.Y., R.A., H.M. and K.H. contributed materials. T.K. and H.K. obtained the experimental data. T.K., K.A., K.O. and K.N. analysed the data. T.K. and K.N. wrote the manuscript. K.N. and K.H. cosupervised the project.

Additional Information

Supplementary information accompanies this paper at http://www.nature.com/srep

Competing financial interests: The authors declare no competing financial interests.

How to cite this article: Kawai, T. *et al.* Increased epigenetic alterations at the promoters of transcriptional regulators following inadequate maternal gestational weight gain. *Sci. Rep.* **5**, 14224; doi: 10.1038/srep14224 (2015).

平成29年度厚生労働科学研究費補助金（化学物質リスク研究事業）

「発達期における統合的な遅発性神経毒性試験法の開発」

（研究課題番号：H28-化学-一般-003）

平成 29 年度　第 1 回班会議　議事次第

日時：平成 29 年 7 月 13 日（木）13 時 30 分～18 時 40 分（13:00 開場）

場所：八重洲倶楽部　第 7 会議室（〒104-0028　東京都中央区八重洲 2-1）

http://www.yaechika.com/access.php

議事次第：

13:30-13:40 開会の挨拶

研究代表者　諫田泰成

13:40-13:50 本研究班に対するコメント

厚生労働省医薬食品局審査管理課化学物質安全対策室

13:50-14:10 本研究班の概要

国立医薬品食品衛生研究所　諫田泰成

14:10-14:30 海外動向

国立医薬品食品衛生研究所　諫田泰成

14:30-15:00 情報提供

住友化学　斎藤幸一

15:00-15:30 研究進捗状況①

国立医薬品食品衛生研究所　諫田泰成

15:30-16:00 研究進捗状況②

国立医薬品食品衛生研究所　山崎大樹

16:00-16:20 休憩

16:20-16:50 研究進捗状況③

産業医科大学　上野晋

16:50-17:20 研究進捗状況④

豊橋技術科学大学　吉田祥子

17:20-17:50 研究進捗状況⑤

国立成育医療研究センター研究所　秦健一郎

17:50-18:30 まとめと今後の予定

18:30-18:40 閉会の挨拶

研究代表者　諫田泰成

連絡先:
国立医薬品食品衛生研究所・薬理部第二室
Tel:　03-3700-1141　内 319
E-mail:（山崎）daiju-y@nihs.go.jp;（野崎）a.nozaki@nihs.go.jp

以上

平成29年度厚生労働科学研究費補助金（化学物質リスク研究事業）

「発達期における統合的な遅発性神経毒性試験法の開発」

（研究課題番号：H28-化学-一般-003）

平成 29 年度　第 2 回班会議　議事次第

日時：平成 29 年 11 月 7 日（木）13 時 00 分～18 時 00 分（12:45 開場）

場所：八重洲倶楽部　第 5 会議室（〒104-0028　東京都中央区八重洲 2-1）

http://www.yaechika.com/access.php

議事次第：

13:00-13:10　開会の挨拶

研究代表者　諫田泰成

13:10-13:20　本研究班に対するコメント（予定）

厚生労働省医薬食品局審査管理課化学物質安全対策室

13:20-13:40　本研究班の概要

国立医薬品食品衛生研究所　諫田泰成

13:40-14:00　海外動向

国立医薬品食品衛生研究所　諫田泰成

14:00-14:30　iPS 細胞の神経分化能を指標とした発達神経毒性評価法の開発

国立医薬品食品衛生研究所　諫田泰成

14:30-15:00　多点電極システムを用いたラット海馬神経細胞ネットワーク評価系の開発

国立医薬品食品衛生研究所　山崎大樹

15:00-15:20　休憩

15:20-15:50　シナプス形成期の神経回路活動性で評価する化学物質の発達神経毒性

産業医科大学　上野晋

15:50-16:20　バルプロ酸で誘発された小脳過形成における分子的変異

豊橋技術科学大学　吉田祥子

16:20-16:50　既存の毒性データおよびヒトデータとの検証

国立成育医療研究センター研究所　秦健一郎

16:50-17:30　まとめと今後の予定

17:30-17:40　閉会の挨拶

研究代表者　諫田泰成

連絡先：

国立医薬品食品衛生研究所・薬理部第二室

Tel:　03-3700-1141　内 347

E-mail:（山崎）daiju-y@nihs.go.jp;（野崎）a.nozaki@nihs.go.jp

以上